Development of Advanced Ophthalmic Formulations: Polymeric Nanoparticles and 3D-Printed Contact Lens-like Patches for Treating Bacterial Keratitis

THESIS

Submitted in partial fulfillment

of the requirements for the degree of

DOCTOR OF PHILOSOPHY

By

CH SAI SANJAY

ID. No. 2019PHXF0047H

Under the Supervision of

Prof. Swati Biswas

BIRLA INSTITUTE OF TECHNOLOGY AND SCIENCE, PILANI

2024

BIRLA INSTITUTE OF TECHNOLOGY AND SCIENCE, PILANI

CERTIFICATE

This is to certify that the thesis titled "**Development of Advanced Ophthalmic Formulations: Polymeric Nanoparticles and 3D-Printed Contact Lens-like Patches for Treating Bacterial Keratitis**," submitted by **CH SAI SANJAY**, ID No. **2019PHXF0047H**, for an award of a Ph.D. from the Institute, embodies original work done by him under my supervision.

Signature of the Supervisor:

Name in capital letters: SWATI BISWAS

Designation **:** Professor

Date **:** 20th March, 2024

DECLARATION

I declare that this thesis has been composed solely by myself and that it has not been submitted, in whole or in part, in any previous application for a degree. The content of the thesis is original and is the outcome of my research work. Any relevant material taken from the open literature has been referred to and cited, as per established ethical norms and practices.

CH SAI SANJAY

Acknowledgment

The satisfaction, which accompanies the successful completion of any task, is incomplete without the mention of the names of those people who made it possible in time with their blessings, guidance, support, instrumental help, and/or revitalizing tasks.

First and foremost, I would like to thank the almighty Supreme Soul for providing me with the patience and strength to undertake this research.

I would like to express my heartfelt gratitude to all those who have contributed to the successful completion of this thesis. I extend my deepest gratitude to my thesis supervisor, Prof. Swati Biswas for her unwavering guidance, invaluable insights, and constant encouragement throughout this research journey. Your expertise and support have been instrumental in shaping the direction and quality of this work. Your profound knowledge, insightful feedback, and constructive criticism have been instrumental in refining the research methodology and elevating the overall quality of this thesis. I am immensely grateful for the countless hours you invested in guiding me through the intricate challenges, always offering your unwavering support and encouragement. Your belief in my potential and unwavering confidence in my capabilities motivated me to strive for excellence. I consider myself fortunate to have had the privilege of learning from such an accomplished and inspiring individual, and I am genuinely grateful for your pivotal role in shaping me as a scholar and researcher.

I am deeply grateful to my mentor, Prof. Balaram Ghosh, whose unparalleled guidance and unwavering support have been the cornerstone of my academic journey. Your profound expertise, patience, and enthusiasm for the subject matter have continuously inspired and motivated me to pursue excellence. Throughout the research process, you have consistently provided valuable insights, pushing me to explore new avenues of thought and encouraging me to embrace challenges as opportunities for growth. Your mentorship extended beyond the

realms of academia, as you generously shared your wisdom, offering invaluable career advice and cultivating essential skills that will undoubtedly shape my future endeavors. I am truly fortunate to have had such an exceptional mentor who not only believed in my potential but also invested wholeheartedly in my professional development. You have always created a friendly conducive environment in the laboratory and made my time memorable at BITS-Pilani. My thesis would not have reached its fruition without your mentorship, and for that, I extend my deepest appreciation and gratitude.

I am wholeheartedly thankful to Prof. Balaram Ghosh, Department of Pharmacy, BITS-Pilani, Hyderabad campus who acted as a Doctoral Advisory Committee (DAC) member for his detailed constructive comments and support throughout this work.

I wish to express my warm and sincere thanks to Prof. Onkar Kulkarni, Department of Pharmacy, BITS-Pilani, Hyderabad campus who acted as a Doctoral Advisory Committee (DAC) member for his suggestions and invaluable time to review my dissertation report.

I wish to express my gratitude to Prof. Ahmed Kamal, Prof. D. Sriram, Prof. P. Yogeeswari, Prof. Punna Rao Ravi, Prof. K V G Chandra Sekhar, Prof. Onkar Prakash Kulkarni, Prof. Arti Dhar, Dr. Akash Chaurasiya, Dr. Nirmal Jain, Dr. Srinivas Prasad K, Dr. Abhijeet Rajendra Joshi, and Dr. Yuvraj Singh for giving me unrestricted access to use instruments and facilities in laboratories.

I also expressed my profound gratitude to Prof. Sajeli Begum, Professor, and Head of the Department of Pharmacy, for her support and for extending the facilities to work at the institute.

It is my duty to express my sincere thanks to the Chancellor, BITS-Pilani for providing the necessary infrastructural support to carry out my research work. I am sincerely thankful to Prof. G. Sundar, Director; Prof. V. Ramgopal Rao, Vice-Chancellor; Col Soumyabrata Chakraborty (Retd), Registrar; Prof. Venkata Vamsi Krishna Venuganti, Dean, Academic - Graduate

Studies and Research; and Prof. P. Yogeeswari, Dean, General Administration for facilitating my research work at the institute.

I would like to thank the central analytical laboratory of BITS-Pilani, Hyderabad Campus for providing me with a scientific platform to excel in my career.

I am fortunate to have met nice colleagues and lab mates in BITS where I got an opportunity to work with them during various occasions. I am grateful to Mrs. Soniya, Mr. Milan, Mr. Asif, Mrs. Sri Ganga, Mr. Nageswara Rao, Mr. Praful, Ms. Varshini, Mr. Ganesh, Mrs. Sravani, Mr. Tarun, Mr. Sanjeev, Ms. Darakshan begum, Ms. Nikitha, and Ms. Himaja. Thanks, all of you for your remembrance and for being a source of happiness.

I express my sincere thanks to seniors Dr. Himanshu Bhatt, Dr. Soniya Kumbham, and Dr. Yamini Bobde, who were very supportive, their attention and timely concern for my Ph.D. gave me a lot of enthusiasm.

I am thankful to Mrs. Sarita, Mrs. Rekha, Mrs. Sunita, Mr. Rajesh, Mr. Upalaiah, Mr. Mallesh, Mr. Kumar, Mr. Narsimha, and Mr. Tirumalaiah for their kind co-operation during the lab in the entire tenure of my Ph.D.

I am indebted to ICMR, and DST for providing me with a scholarship and necessary financial support to pursue my Ph.D. work without any hindrance.

I would like to thank everybody who was important for the successful completion of this research work that I may have inadvertently failed to mention.

I owe my loving thanks to my father Mr. Venkateswara rao, my mother Mrs. Varalakshmi, my brother Mr. Sandeep, and my sister-in-law Mrs. Pavithra. Without their encouragement and understanding it would have been impossible for me to finish this work.

My special gratitude to my brother Mr. Sandeep for his unconditional support throughout my Ph.D. degree that made the completion of thesis possible.

CH SAI SANJAY

ABSTRACT

Bacterial keratitis is a sight threatening ocular infection caused by Gram-negative and Gram-positive bacteria that require immediate treatment. The existing therapy fluoroquinolone eyedrops have numerous drawbacks such as lacrimal drainage, and poor bioavailability of drugs at the site of action. So, there is an immediate need for novel drug delivery systems to carry the payload to the site of action and increase the corneal residence time. One of the approaches is nano drug carriers synthesized with mucoadhesive polymers. These nanocarriers have unique properties such as the polymers used in these systems interact with mucin and increase the corneal residence time and being nanosized, particles can penetrate the cornea and deliver the payload. Apart from these characteristics, nanocarriers can be tuned for favorable drug release profiles, and has high surface area to volume ratio.

First, fluoroquinolone antibiotic moxifloxacin (Mox), being highly water-soluble, suffers from poor corneal penetration leading to unsatisfactory therapeutic outcomes in BK. Here, we prepared Mox-loaded co-polymeric nanoparticles (NPs) by entrapping the drug in co-polymeric NPs constituted by the self-assembly of a water-soluble copolymer, poly (ethylene glycol)-*b*-p(hydroxypropyl) methacrylamide (mPH). The polymer (mPH) was prepared using a radical polymerization technique at different mPEG: HPMA ratios of 1:70/100/150. The polymer/nanoparticles were characterized by GPC, CAC, DLS, SEM, XRD, DSC, FTIR, % DL, % EE, and release studies. The *ex vivo* muco-adhesiveness and corneal permeation ability were judged using a texture analyzer and Franz Diffusion Cells. *In vitro* cellular uptake, cytotoxicity, and safety assessment were performed using HCE cells in monolayers, spheroids, and multilayers in transwells. The DOE-optimized colloidal solution of Mox-mPH NPs (1:150) displayed a particle size of ~116 nm, superior drug loading (8.3 %), entrapment (83.2 %), robust mucoadhesion *ex vivo*, and ocular retention *in vivo* (~ 6 h) (judged by *in vivo* image analysis). The non-irritant formulation, Mox-mPH NPs (1:150) (proven by HET-CAM test)

exhibited intense antimicrobial activity against *P. aeruginosa, S. pneumoniae, and S. aureus in vitro* analyzed by live-dead cells assay, zone of inhibition studies, and by determining the minimum inhibitory and bactericidal concentrations. The polymeric nanoparticles, mPH (1:150), decreased the opacity and the bacterial load compared to the other treatment groups. The studies warrant the safe and effective topical application of the Mox-mPH NPs solution in bacterial keratitis.

Second, A mucoadhesive self-assembling polymeric system was developed to carry moxifloxacin (M) for treating bacterial keratitis (BK). Chitosan-PLGA (C) conjugate was synthesized, and poloxamers (F68/127) were mixed in different proportions (1: 5/10) to prepare moxifloxacin (M)-encapsulated mixed micelles (M@CF68/127(5/10)Ms), including M@CF68(5)Ms, M@CF68(10)Ms, M@CF127(5)Ms, and M@CF127(10)Ms. The corneal penetration and mucoadhesiveness were determined biochemically, *in vitro* using human corneal epithelial (HCE) cells in monolayers and spheroids, *ex vivo* using goat cornea, and *in vivo* via live-animal imaging. The antibacterial efficacy was studied on planktonic biofilms of *P aeruginosa* and *S aureus* (*in vitro*) and Bk-induced mice (*in vivo*). Both M@CF68(10)Ms and M@CF127(10)Ms demonstrated high cellular uptake, corneal retention, muco-adhesiveness, and antibacterial effect, with M@CF127(10)Ms exhibiting superior therapeutic effects in *P aeruginosa* and *S aureus*-infected BK mouse model by reducing the corneal bacterial load and preventing corneal damage. Therefore, the newly developed nanomedicine is promising for clinical translation in treating BK.

Third, A mucoadhesive polyelectrolyte complex (PEC) nanoparticles were developed for ocular moxifloxacin (Mox) delivery in Bacterial Keratitis (BK). Gelatin (G), cationized gelatin (CG), a cationic polymer, and sodium alginate (Alg) were used as an anionic polymer to form G/CG-Alg NPs loaded with moxifloxacin. Mox@CG-Alg NPs were characterized for physicochemical parameters, including particle size by DLS and SEM analysis, DSC, XRD,

encapsulation efficiency, drug loading, mucoadhesive study by texture analyzer, mucin turbidity, and viscosity assessments. The corneal uptake and toxicity of the formulation were analyzed in Human Corneal Epithelial (HCE) Cell line and by HET-CAM assay. The results indicated that the CG-Alg NPs, with optimal size (217.2 ± 4 nm) and polydispersity (0.22 ± 0.05), were taken up by the HCE cells and spheroids, displayed mucoadhesiveness and trans-corneal permeation, and sustained the release of the loaded Mox. The anti-bacterial efficacy studied on planktonic bacteria/biofilms of *P. aeruginosa* and *S. aureus* indicated that the Mox@CG-Alg NPs displayed low MIC, higher zone of bacterial growth inhibition, and cell death compared to free Mox. A significant reduction of bacterial load was observed in the BK-induced mouse model.

Fourth, Delivery of therapeutic agents through contact lens (CLS) is a promising strategy to achieve significant bioavailability with negligible eye drainage. The present study investigates the preparation and three-dimensional (3D) printing of mucoadhesive Gelatin Methacryloyl (GelMA)/ Chitosan Methacryloyl (ChiMA) hydrogels to fabricate them as contact lens-like patches (CLP) loaded with antimicrobial peptide, S100A12 (AMP) for treating bacterial keratitis (BK). The effect of viscosity and mechanical properties of bioinks on printability was determined with rheological and shear rates. The 3D printed CLP were crosslinked using Irgacure 2959 under UV light and exhibited significant swelling properties. AMP-loaded CLP have demonstrated sustained release with enhanced trans corneal permeation. AMP-loaded CLP have displayed significant antibacterial and antibiofilm efficacy against *Pseudomonas aeruginosa in vitro* experiments. The results from the *in vivo* experiment conducted on *P. aeruginosa*-infected BK rabbit model after the treatment with AMP-loaded CLP have shown a significant decrease in bacterial load when plated for CFU. As a whole, the newly developed delivery system can overcome the current treatment challenges of multidrug resistance (MDR) in bacteria, as AMPs do not pose such a risk. This treatment strategy could achieve high

bioavailability of AMPs and offer biofilm-disrupting ability in BK with the potential to use as personalized medicine.

Table of Contents

List of Tables

List of Figures

LIST OF ABBREVIATIONS AND SYMBOLS

ACN	Acetonitrile
AMP	Anti-microbial peptide
ALG	Alginate
CCD	Central composite design
CDCl3	Deuterated chloroform
ChiMA	Chitosan Methacryloyl
CG	Cationized gelatin
DAPI	4′,6-Diamidino-2-phenylindole dihydrochloride
DL	Drug loading
DLS	Dynamic light scattering
DMEM	Dulbecco's Modified Eagle Medium
DMSO	Dimethyl sulphoxide
DIPEA	N,N-Diisopropylethylamine
DOE	Design of experiment
DSC	Differential scanning calorimetry
EE	Encapsulation efficiency
EDC	N-(3Dimethylaminopropyl)-N′-ethylcarbodiimide hydrochloride
FITC	Fluorescein isothiocyanate
FTIR	Fourier transform infrared spectroscopy
GPC	Gel Permeation Chromatography
GelMA	Gelatin Methacryloyl

H & E	Hematoxylin and eosin
HPLC	High performance liquid chromatography
1H NMR	Proton Nuclear Magnetic Resonance
IC50	Half maximal inhibitory concentration
IVIS	*In vivo* imaging system
mPEG	Methoxy polyethylene glycol
MIC	Minimum Inhibitory Concentration
MBC	Minimum Bactericidal Concentration
MTT	3-(4,5-dimethylthiazol-2-yl)-2,5-di-phenyltetrazolium bromide
MWCO	Molecular weight cut-off
mg	Milligram
min	Minute
mL	Millilitre
mm	Millimetre
mmol	Millimole
NHS	N-hydroxysuccinimide
nm	Nanometre
PBS	Phosphate Buffer Saline
PLGA	Poly(lactic-co-glycolic acid)
PDI	Polydispersity Index
PI	Propidium iodide
RT	Room temperature
SD	Standard deviation
SEM	Scanning electron microscope
TEA	Triethylamine

THF	Tetrahydrofuran
XRD	X-Ray Diffraction
µg	Microgram
µL	Microlitre
µM	Micromolar
ZOI	Zone of Inhibition

Chapter 1

Introduction

1.1. Infectious Keratitis

The human eye has a special anatomy that makes it vulnerable to many infection-causing pathogens in addition to being exposed to the environment. An infection of the cornea known as infectious keratitis is sometimes called an infected corneal ulcer or opacity. When pathogenic bacteria penetrate the corneal stroma, they first induce inflammation in the cornea, which leads to the eventual death of these structures (Ansari et al., 2013; Wong et al., 2012a). There are mainly two types of infectious keratitis a) Microbial Keratitis, which is caused by bacteria, parasites, and fungus b) Viral keratitis, caused by the herpes virus (Durand et al., 2021; Ung, Bispo et al., 2019). Infectious keratitis is the fifth major cause of overall blindness accounting for 3.5 % (36 million) of the world's population as of 2015, and it is the most common cause of non-trachomatous corneal opacification (Ung, Acharya, et al., 2019). Despite the data being underreported, from around 1.6 million instances in 1990 to 1.3 million cases in 2015, infectious keratitis cases leading to corneal blindness have reduced, and during the same period, the cases related to visual impairment have reduced from 3.3 million to 2.9 million (Flaxman et al., 2017; Grimes et al., 1992; Ung, Acharya, et al., 2019). Acanthamoeba keratitis is a corneal infection mainly caused by a parasite called Acanthamoeba. They are common, free-living micro-organisms that may be found in various environments, including air, soil, fresh/tap water, medical devices, clinical tools, clinical equipment, air ducts, and conditioners (de Jonckheere, 1991). The primary risk factors for Acanthamoeba keratitis include prolonged contact lens wear, ocular trauma, and exposure to contaminated water/soil (Marciano-Cabral & Cabral, 2003). Fungi cause fungal keratitis or mycotic keratitis, and they represent more than 50% of all microbial keratitis that are culture positive, particularly in tropical and sub-tropical regions (Nath et al., 2011; Xie et al., 2006). Two kinds of fungi are primarily accountable to fungal keratitis, and they are classified as filamentous fungi, including pathogens such as *Fusarium, Aspergillus*, *Curvularia*, and *Scedosporium apiospermum.* The other fungi type is

yeast fungi, which include pathogens such as Candida albicans, and other candida species. These are known to be most commonly associated with fungal keratitis (Thomas & Kaliamurthy, 2013). Substantial risk factors such as contact lens use, ocular surface diseases, and extensive use of corticosteroids lead to fungal keratitis. On the other hand, when there is an underlying ocular condition such as inadequate tear secretion, improper eye closure, and systemic illness such as diabetes mellitus and immunosuppression prone to keratitis related to *C. albicans* and some other related species (Thomas, 2003).

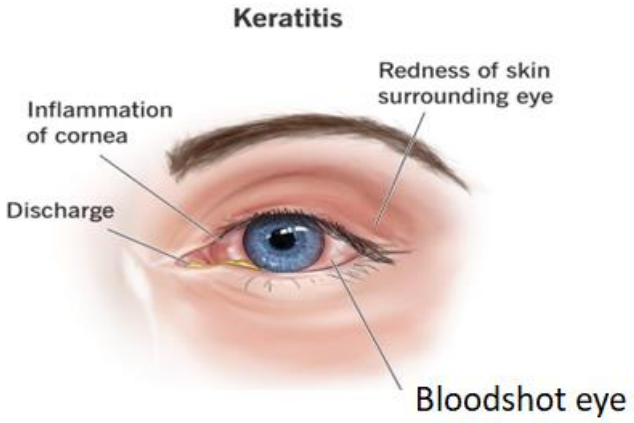

Figure 1.1. Illustration of eye infected with bacterial keratitis and its symptoms (*Keratitis: Types, Symptoms & Treatment*, n.d.).

1.2. Bacterial Keratitis

Bacterial Keratitis (BK) is the leading cause of ocular infections leading to ocular blindness globally and is majorly caused by bacteria (Teweldemedhin et al., 2017a). Early-stage treatment is necessary to avoid severe loss of ocular vision, and deleting the antimicrobial therapy may lead to recovery of only 50% of vision (C. N. Ezisi et al., 2018a). Both Gram-positive and Gram-negative bacteria are responsible for the pathogenesis of BK. Despite having a similar inner cytoplasmic membrane, the gram-positive bacteria is composed of peptidoglycan layers distributed with acids such as teichoic and lipoteichoic acids; gram-negative bacteria is composed of thin peptidoglycan middle layer and lipopolysaccharide outer

membrane, which is believed to be responsible for the pathogenesis of the infection (Fleiszig et al., 2020a; Silhavy et al., 2010). The bacteria such as *Staphylococcus aureus* and *Streptococcus pneumoniae* are the most common pathogens with Gram-positive responsible for BK, whereas *Pseudomonas aeruginosa* is the most common pathogen with Gram-negative strain (Ajayi et al., 2011; C. N. Ezisi et al., 2018b; Plotkowski et al., 1991). The adherence of the bacteria to the damaged corneal epithelial cells and stroma is primarily due to the presence of fibrillae in Gram-positive and fimbriae and glycocalyx in gram-negative bacteria. The strong adherence quality of *Pseudomonas aeruginosa* is also due to the organ pili mainly consisting of calcium and magnesium. The biofilm is a complex ability of bacteria that has a group of different colonies and adhere to the surface; this adherence quality helps the bacteria to remain on contact lens and epithelial lesions causing BK (Fleiszig et al., 1994; Stern et al., 1985; Vermeltfoort et al., 2008). The many other factors prone to cause BK are the use of contact lenses, enucleation, corneal damage, intraocular inflammation, age, undernourishment, and keratoconjunctivitis (Ting, Ho, et al., 2021a; Zheng et al., 2021). Contact lens wear is one of the significant risk factors. Due to its complex pathogenesis and hypothesis of possible mechanisms such as superficial injury to the contact lens wear and it is also believed that degradation of protective components at the ocular surface caused due to the low exchange of tears during blinking, tear deflation under the contact lens which results in the adherence of bacteria to the corneal surface, variations of tear fluid biochemistry and some other factors included with contact lens wear are using lens overnight, poor hygienic conditions such as the use of expired contact lens/solutions/case (Fleiszig et al., 2020b; Stapleton et al., 2017; Zimmerman et al., 2016).

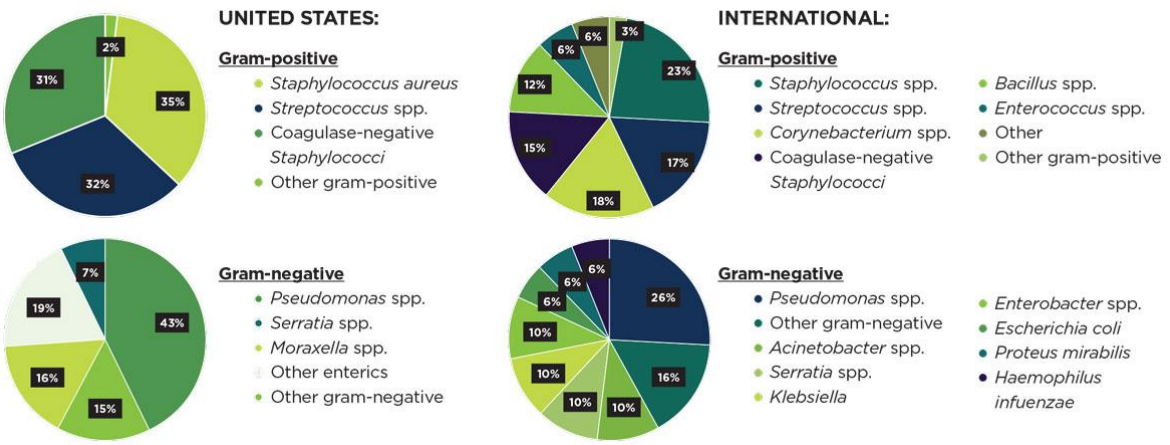

Figure 1.2. Most Gram-positive and Gram-negative bacterial strains are responsible for BK worldwide (*Hot Topics in Bacterial Keratitis*, n.d.)

1.3. Pathogenesis in Bacterial keratitis

The pathogenesis of these bacteria starts with invasion and is followed by corneal necrosis. The host defense of the corneal stroma is compromised by the several exotoxins and proteases released by the bacteria resulting in the degradation of the corneal membrane and damaging the extracellular matrix, leading to cell death. Due to the continuous multiplication of the bacteria in the cornea, the exotoxins such as proteases, lipases, and coagulases are produced by the bacteria resulting in uninterrupted stromal carnage. The unique structural arrangement of gram-negative bacteria develops stromal rings in the cornea upon releasing the lipopolysaccharides an endotoxin released by these bacteria. These stromal rings contain polymorphonuclear leukocytes in corneal cells and get attracted by C-pathway, thereby alternating the cell path (Al-Mujaini et al., 2009a; Cameron, 1995; Karp et al., 2003; Lakhundi et al., 2017). Therefore, factors such as contact lens wear, LASIK surgery, enucleation, keratoconjunctivitis, and diabetes are responsible for the impairment of corneal epithelium and are the significant risk factors for the BK (Leonardi & Secchi, 2003; R et al., 2011). Bacteria have structures for adhesion on their surface called pili or fimbriae that identify certain

carbohydrates on the host cell's surface. Epithelial glycoproteins on the cornea mediate pilus binding activity, and the amino sugar sialic acid restricts the pilus binding to mice corneal epithelial cells.

Furthermore, mice are protected from *Pseudomonas* corneal infection by an anti-flagellar antibody similar to the infecting strain. Additionally, the glycocalyx may play a role in bacterial adherence by generating slime aggregates resistant to phagocytosis, allowing bacteria to stick to cells. *Pseudomonas aeruginosa* is a gram-negative organism that is a frequent cause of contact lens-associated bacterial keratitis(Fleiszig & Evans, 2021a).

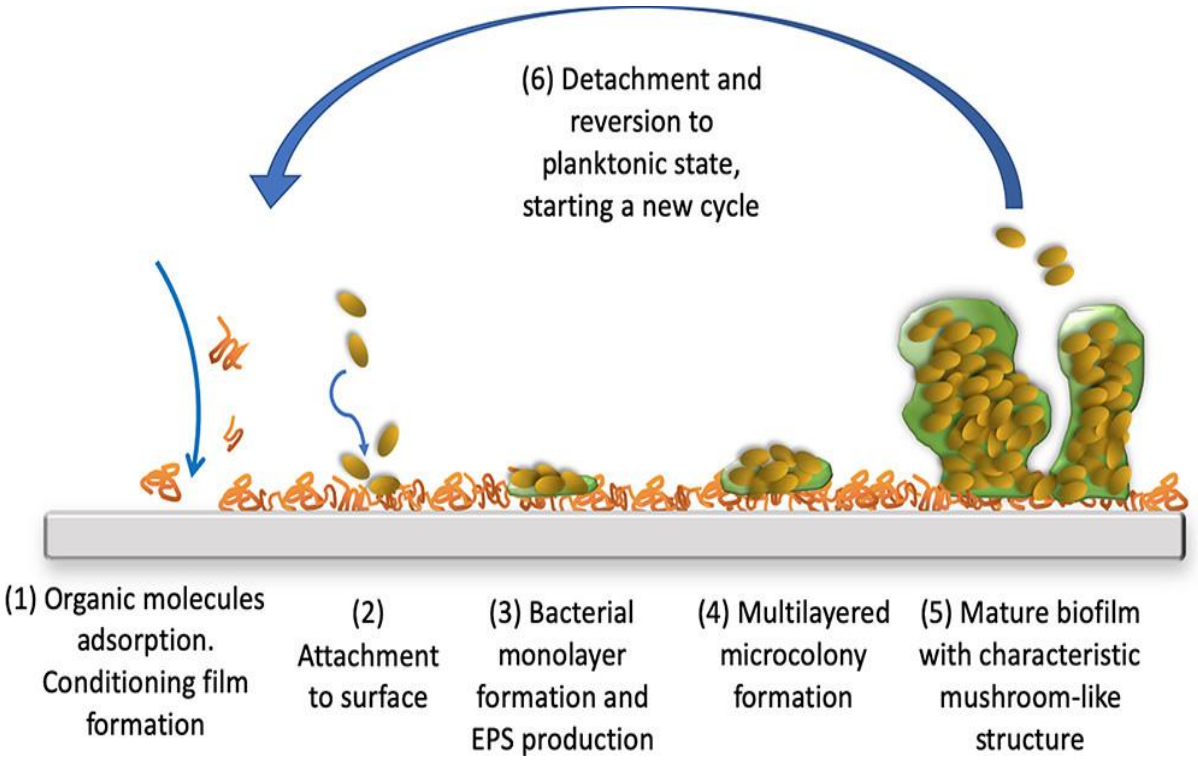

Figure 1.3. Biofilm formation steps (Ghilini et al., 2019)

Destructive enzymes produced by *P. aeruginosa*, such as lipase, protease, and exotoxins, result in ulceration of corneal stroma with a yellow-white appearance. The ulcer often extends peripherally and deeply, resulting in a diffusive grey; ground glass appearance developed by the corneal epithelium. The glycocalyx of bacteria protects it from phagocytic engulfment.

Bacterial keratitis develops due to compromise of defense mechanisms of the eye. The tear film covers the cornea from infection by inhibiting the growth of microorganisms. This antimicrobial activity is associated with lactoferrin, lysozyme, and beta-lysin. The ocular virulence of *P. Aeruginosa* is reduced by the presence of IgA in tear fluid (Song et al., 2021). Microbial Surface Components recognizing adhesive matrix molecules, such as collagen fibrinogen, have also been found to facilitate bacterial adhesion to extracellular matrix components elastin in *S. aureus*(Song et al., 2021). Rhem et al. demonstrated that collagen-binding adhesion is a virulence factor for *S. aureus* keratitis (Foster, 2019). Jett & Gilmore studied the effect of S. Aureus as a parasite on Host human corneal epithelial cells. They studied fibronectin-binding protein as an epithelial adhesin, which has similar structures with other gram +ve cell surface molecules such as signal sequences (Jett & Gilmore, 2002).

1.4. Mechanism of Biofilm formation

As individual organisms, bacteria are more susceptible to environmental conditions. Recent microbiological research emphasized that maximum pathogens stay in specialized groups referred to as biofilms rather than as individual organisms (Aung et al., 2016). Unicellular organisms collectively shape a network and are connected to a surface and encapsulated in an exopolysaccharide matrix (Mah & O'Toole, 2001). EPSs are the fundamental components that regulate biofilms' physicochemical and biological features and are primarily responsible for their structural and functional integrity. The microorganisms are embedded in a three-dimensional, gel-like, and typically charged biofilm matrix formed by the Eps (Flemming & Wingender, 2001). Biofilms are extremely organized but heterogeneous microenvironments with chemical gradients of critical parameters like oxygen, pH, and nutrients. The biofilm's geometry and subsequent bacterial density are determined by nutrition availability and the presence or absence of fluid shear during growth (Liu et al., 2019). The formation of a biofilm begins with attaching to a living or non-living surface accompanied by multiplication and

attachment inside a secreted matrix. This matrix provides antibiotic resistance and protects the bacteria embedded in the matrix.

A lack of antibiotic response will be observed in infections having a biofilm phase. Chronic infections are more susceptible to developing biofilms (Aung et al., 2016). Surface hydrophobicity may influence bacterial adherence, an early step in biofilm formation, and the subsequent establishment of a sessile biofilm that attaches the bacteria to the lens surface. Once a biofilm is developed, the bacteria undergo phenotypic changes that necessitate considerably greater antibiotic doses to prevent multiplication. (Girard 2010). The minimum inhibitory concentration (MIC) is the standard laboratory method for determining planktonic bacterial antibiotic sensitivity. The MIC does not accurately predict the antibiotics needed to treat a bacterial biofilm. The minimum biofilm eradication concentration (MBEC) is a parameter that can be used to assess a biofilm (Aung et al., 2016).

1.5. Challenges of ocular drug delivery

Drug delivery to the posterior segments of the eye is the most challenging due to its complex structure and is essential for treating many corneal-related infections and disorders (Gaudana et al., 2010; V. H. L. Lee & Robinson, 1986a). To achieve good therapeutic efficacy of BK, the drug instilled should penetrate the corneal epithelium, and an adequate amount should be present at the site of action. The traditional method of delivering antimicrobials to the cornea is installing eye drops. Despite having easy administration by the patients, eye drops have poor bioavailability due to the nasolacrimal drainage, thereby washing away the drug and leading to low corneal permeability. Frequent administration is required to maintain the therapeutic levels, affects the patient's compliance, and leads to overdosage, which may cause corneal tissue damage (Baranowski et al., 2014a; Schlech, 2005). Apart from these limitations, the present frontline treatment for BK is antibiotics. Due to repeated and routine use of antibiotics,

antibacterial resistance has emerged as a major challenge in treating BK, as the bacterial strains develop resistance through genetic mutations and gene transfer (Egrilmez & Yildirim-Theveny, 2020b; Grandi et al., 2019; Ting, Ho, et al., 2021b).

1.6. Anatomical challenges of the eye

The major anatomical challenges of the drug delivery to the eye are the low bioavailability of the drug at the anterior segments, such as the cornea, conjunctiva, and nasolacrimal drainage. Many factors affect the low bioavailability of the drug after the topical administration, including loss of drug due to ocular drainage, blinking of the eye, and tear film.

Nasolacrimal drainage

Nasolacrimal drainage is the predominant factor for the drugs' low bioavailability and poor residence time. The anatomical disadvantage of the tear film is only about 3 µL of tear fluid can be incorporated at once. After the installation of the eye drops, this volume was destabilized, leading to an increase in tear fluid and thereby passing through the nasolacrimal duct (*Determination of Tear Volume and Tear Flow - PubMed*, n.d.; Hillery et al., 2016). Due to these limitations, most of the drugs got eliminated immediately after administering eye drops, with only 5% reaching the targeted site of action. The tear film also acts as a defense mechanism to the eye, filled with mucin, which eliminates the pathogens and clears the ocular surface by forming a hydrophilic layer as it leads to major drug loss (I. Ahmed, 2003; *Duane's Ophthalmology | WorldCat.Org*, n.d.; Jeon, 2003).

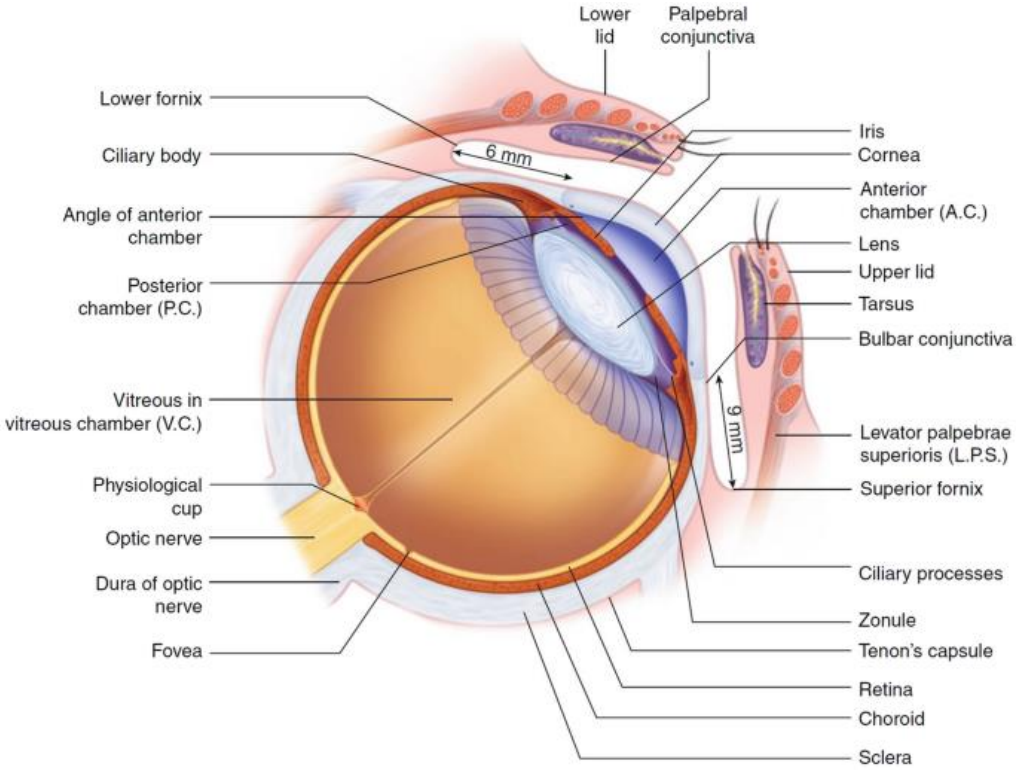

Figure 1.4. The anatomy of the eye (Prada et al., 2019)

Conjunctiva

Conjunctiva covers 1/3rd of the anterior segment of the eye, comprising two layers: epithelium and stroma. The conjunctiva epithelium is structurally continuous with corneal epithelium and comprises 5-15 layers of epithelial cells. These cells are connected by tight junctions at apical sides, acting as a major permeability barrier and restricting the molecules less than 20KDa to permeate(Hosoya et al., 2005; Huang et al., 1989).

Corneal epithelium

The corneal epithelium is the major diffusion barrier for drug absorption. It is the anterior eye segment; the corneal epithelial cells form the tight junctions in the intracellular space and are located only at the apical side of the eye, acting as a drug diffusion barrier. These tight junctions comprise two transmembrane proteins, claudin, and occludin, affecting the paracellular

transport mechanism, which makes it practically impossible for molecules larger than 5KDa to permeate through the cornea (Ban et al., 2003; Huang et al., 1989; Mannermaa et al., 2006a).

1.7. Conventional treatment of Bacterial keratitis:

Most marketed ophthalmic preparations are conventional dosage forms such as eye drops because of their patient compliance and ease of installation (C. Le Bourlais et al., 1998). In topical eye drops, less than 5% of the drug only can reach the posterior segment of the eye due to the loss of drug by several protective mechanisms of the eye such as nasolacrimal drainage, blinking that always washes the ocular surface, several ocular barriers result in reduced ocular bioavailability (Gaudana et al., 2009). Due to membrane receptors and transporters, hydrophilic drugs that do not permeate the lipophilic ocular barriers can be delivered through receptor-mediated drug delivery systems (Katragadda et al., 2008).

The conventional treatment for bacterial keratitis is Tobramycin (14 mg/mL) 1 drop every hour, alternating with fortified cefazolin (50 mg/mL) or vancomycin (50 mg/mL) 1 drop every hour (*Bacterial Keratitis Treatment & Management: Medical Care, Surgical Care, Consultations*, n.d.). Toxicity and instability are the major problems associated with fortified antibiotics. The broad-spectrum antibiotics that can destroy both Gram-Negative and Gram-Positive bacteria can be considered the frontline treatment for BK. Earlier, the use of fortified antibiotics as a combination therapy (cefazolin + tobramycin) was followed and later was replaced by fluoroquinolone monotherapy (M.-S. Hanet et al., 2012; McLeod et al., 1995). Fluoroquinolones such as second-generation (ciprofloxacin, ofloxacin), third-generation (levofloxacin), and fourth-generation (gatifloxacin, moxifloxacin) are available for the treatment of BK. Second- and third-generation fluoroquinolones are commercially available and have been approved by the US Food and Drug Administration (FDA) (Egrilmez & Yildirim-Theveny, 2020c; KING et al., 2000). Whereas the fourth generation Fluoroquinolones (Gatifloxacin and Moxifloxacin) are extensively used as the off-label treatment due to their

superiority over the other generations, demonstrating better bactericidal efficacy against both Gram -ve and Gram +ve bacteria and have greater aqueous humor penetration than the other generation molecules (Egrilmez & Yildirim-Theveny, 2020a; Sharma & Taniguchi, 2017). The mechanism of Action (MoA) of fluoroquinolones involves targeting and inhibiting the DNA gyrase and topoisomerase IV. At lethal doses, the fluoroquinolones inhibit the supercoiling within the cell, thereby impairing DNA replication and leading to cell death (Drlica, 1999; Redgrave et al., 2014). Although fluoroquinolones are considered broad-spectrum antibiotics, their preferential targets are DNA gyrase for Gram -ve and topoisomerase IV for Gram +ve bacteria (Drlica et al., 2008; Redgrave et al., 2014). The antibiotics currently used in treating BK, along with the mechanism of action and their dosage, are listed in **Table 1.1.**

Table 1.1. The antibiotics currently used for treating BK include concentration, dosage, and mechanism of action.

Drug	Concentration	Dosage	Mechanism of Action
Fortified Antibiotics			
Tobramycin/Gentamycin	0.3-1.5% solution	Combination of Tobramycin/gentamycin +	Protein synthesis inhibition
Cefazolin/Ceftazidime	5% solution	Cefazolin, 1 drop for every 15min, followed by every 30min-1h. Reduce the frequency.	Bacterial cell wall synthesis inhibition
Vancomycin	1-5% solution	Depending upon the response 1 drop every hour and taper depending upon the response	Protein synthesis inhibition
Fluoroquinolones			
Second Generation			
Ciprofloxacin	0.3% solution	**Day 1-2:**1-2 drops, for every 2h, **Day 2-4:** 1-2 drops for every 4h and taper upon the response.	Inhibition of DNA gyrase and topoisomerase IV
Ofloxacin			
Third Generation			
Levofloxacin	0.5-1.5% solution	**Day 1-3:**1-2 drops, for every 30min till 2h, and 1-2 drops for every 4h.	Inhibition of DNA gyrase and topoisomerase IV
Fourth Generation			
Moxifloxacin		**Day 4:**1-2 drops for every 4h, Taper upon the response 1 drop, twice a day for 5 days	Inhibition of DNA gyrase and topoisomerase IV
Gatifloxacin	0.5% solution		
Gemifloxacin			

1.8 Moxifloxacin

Moxifloxacin is a fourth-generation fluoroquinolone antibiotic with a methoxy group in the C-8 position and a bulky C-7 side chain. It has a broad spectrum of activity against Gram-positive

and Gram-negative bacteria. Compared to 3rd generation fluoroquinolones Ciprofloxacin, moxifloxacin has better activity. From the *in vitro* studies, the Minimum Inhibition Concentration (MIC) inhibiting 90% of strains for moxifloxacin was found to be less than 0.5 µg/mL for Gram-positive and Gram-negative bacteria.

Physicochemical properties of Moxifloxacin

Moxifloxacin (C21H24FN3O4, mol weight: 401.4 g/mol) comes under the Quinolone family that comprises 4-oxo-1,4-dihydroquinoline-3-carboxylic acid containing a cyclopropyl, fluoro, and a methoxy substituent. It is soluble in water and has a log P value 2.9 with UV absorption maxima at 294 nm. The chemical structure of Moxifloxacin is shown in Figure ("National Center for Biotechnology Information, PubChem Compound Database; CID= 152946)

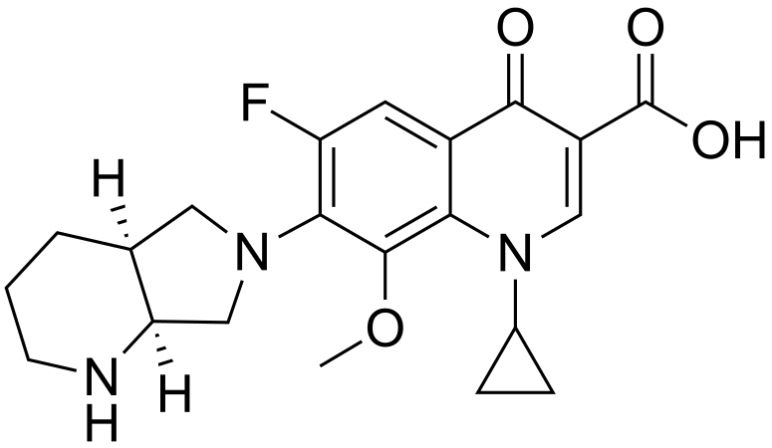

Figure 1.5. Chemical structure of Moxifloxacin

1.9 Mucus and its role on the ocular surface

Mucin is the biological fluid and the major component of mucus, secreted by goblet cells present at epithelial surfaces of all human organs such as the eye, gastro-intestinal and respiratory tracts. Mucin is a high molecular mass glycol protein comprised of amino acids and polysaccharides chains, which are linked to the protein core, and the hydroxyl groups of the serine and threonine residues on the protein backbone and glycoproteins are negatively charged

at physiological pH (Khanvilkar et al., 2001). Mucin maintains mucus's structural integrity and function(Cone, 2009; Lundin et al., 2005; Popov, 2020). The mucin on the ocular surfaces can be categorized as cell surface and secreted mucin. Tear fluid is mainly concentrated with secreted mucin, and cell surface mucins are immobilized as a layer comprising of glycocalyx present on the epithelial surface and act as a physical barrier on the ocular surface and thereby obstructing the drug permeation across the cornea, whereas secreted mucin may interfere with the components of eye drops without forming any barrier (Argüeso et al., 2009a; Ruponen & Urtti, 2015). Mucins are negatively charged and can bind with cationic substances, and upon hydration, the mucus layer forms a gel layer with rheological properties (Greaves & Wilson, 1993a). Various mucin expressions are widely expressed at different segments of the eye as MUC1, with a molecular weight of (120000-300000 Da), is the most expressed cell surface mucin and is expressed on an apical layer of corneal, conjunctival epithelium, and lacrimal gland and duct epithelia and can be able to bind to the pathogens such as *Pseudomonas aeruginosa* and can activate the clearance mechanism of ectodomain into the tear fluid (Lillehoj et al., 2001a). MUC4 (MW 900000 Da) on the surface of the conjunctival epithelium. These cell surface mucins prevent the adhesion of pathogens on the corneal surface, thereby known as anti-adhesives (Gipson & Argüeso, 2003; Inatomi et al., 1996; Lillehoj et al., 2001b; Paulsen et al., 2003).

Theories of Mucoadhesion of polymers on the ocular surface

The mucoadhesion of the ocular delivery systems will be affected by different factors due to the complex and physio-chemical properties of the tear film. Many theories have been proposed to explain mucoadhesion, such as wetting, adsorption, diffusion, and electronics. The selection of the polymer to achieve mucoadhesion must contain characteristics to permeate through the depth of the mucus layer to form a strong bond. The polymeric chains must be mobile and capable of initiating immediate contact with the mucus layer, flexible enough to diffuse through

the mucus layer, and also could be able to form hydrogen, hydrophobic and electrostatic interactions (Lam et al., 2021; Mikos & Peppas, 1990; Mizrahi & Domb, 2008).

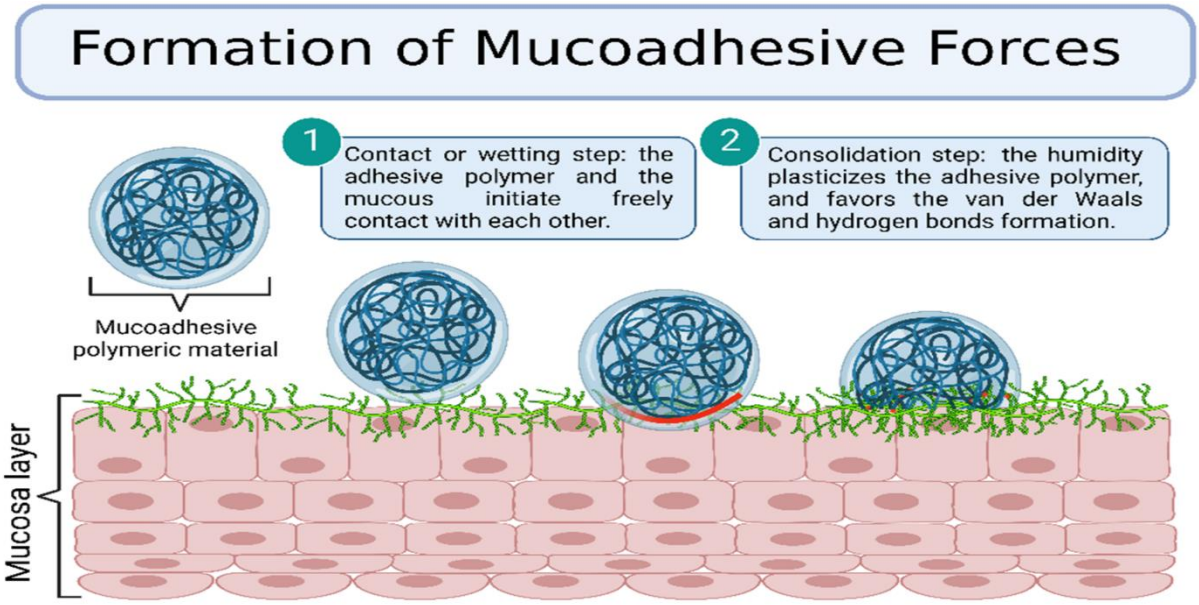

Figure 1.6. Mucoadhesive force formation by polymeric materials (de Lima et al., 2022)

The *Wetting theory* describes the polymer/ delivery systems, which tend to swell upon interacting and can spread over the mucus layer; polymeric agents achieve this by penetrating through the substrate's surface irregularities and producing adhesive anchors. The spreading of the polymers is achieved by overcoming the surface tension at the interface. The affinity of a liquid for an interface can be measured with the help of contact angle. The lower the contact angle, it is considered greater the affinity, and it can be determined by using the formula:

$S_{AB} = \gamma_B - \gamma_A - \gamma_{AB}$, where γ_A- surface tension of the liquid, γ_B- surface tension of the liquid, and γ_{AB}- interfacial energy between solid and liquid (Roy et al., 2012; Shaikh et al., 2011a).

In *Adsorption theory*, the main forces responsible for the interaction of adhesives the hydrogen bonding and Vander Waal's forces, and there is also an assumption by chemisorption theory that interaction between the polymer and mucus may also occur due to the strong covalent bonding.

The interdiffusion of polymeric chains through the mucus/adhesive interface is described by *diffusion theory*. The diffusion of the polymers depends upon their chain length and concentration gradient. The adhesive bond formation relies on the depth of interpenetration of polymer chains and the contact time.

In *electronic theory*, electron transfer occurs upon contacting the adhering surfaces. This happens due to the differences in the electronic structure and would result in the formation of a double layer of the electrical interface due to attractive forces. The electrolyte presence in the polymeric carrier increases a polymer's fluid uptake, which is essential in achieving significant interaction with the mucus.

The pH also has a significant effect on the mucus interaction of the polymer; upon decreasing the pH of the medium, the proton donating groups react with mucin molecules through hydrogen bonding, and with an increase in the pH, the repulsion takes place between the anions and results in polymer extension. The swelling pressure across the polymer increases with the number of available charged groups leading to the enlargement of the frame network of the polymer (Ahuja et al., 2008; Peppas et al., 2009; Peppas & Sahlin, 1996). Some other polymer-related factors that affect mucoadhesion are the hydrophilic nature of the polymer, which is capable of forming hydrogen bonds, molecular weight, functional groups (carboxyl, hydroxyl, amino, and sulfate groups), hydration and surface charge of the polymer (Khutoryanskiy, 2011; Peppas & Buri, 1985).

1.10 Mucoadhesive polymers

The polymers adhering to the mucus surface can be broadly categorized as anionic, cationic, Non-ionic polymers, and polymeric thiomers.

Anionic polymers

The anionic polymers related to the mucoadhesion properties can be subcategorized as cellulose derivates and acrylates.

Cellulose derivatives

Methyl cellulose was the first cellulose polymer to introduce in the 1950s (SWAN, 1945), and other cellulose ether derivatives have been raised over time due to the ability of carboxylic groups to form hydrogen bonds with the oligosaccharide chains of the mucin. Some cellulose-ethers (Hydroxypropyl methylcellulose and hydroxypropyl cellulose) interact with the components of the tear film and impart viscosity to the solution due to their wetting properties and thereby increasing the contact time on the corneal surface (Rossi et al., 2008).

Viscosifying polymers screened for ocular mucoadhesive capacity

Polymer	Charge	Mucoadhesive capacity
Poly(acrylic acid) (neutralized)	A	+++
Carbomer (neutralized)	A	+++
Hyaluronan	A	+++
Chitosan	C	++
Na carboxymethylcellulose	A	++(+)
Poly(galacturonic acid)	A	++
Na alginate	A	++(+)
Pectin	A	++(+)
Xanthan gum	A	+
Xyloglucan gum	A	+
Scleroglucan	A	+
Poloxamer	NI	+(+)
Hydroxypropylmethylcellulose	NI	+
Methylcellulose	NI	+
Poly(vinyl alcohol)	NI	+
Poly(vinyl pyrrolidone)	NI	+

Charge: A: anionic; C: cationic; NI: non-ionic.
Mucoadhesive capacity: +++: excellent; ++: good; +: poor/absent.

Figure 1.7. Summary of polymers with their mucoadhesive capacity and surface charge (Ludwig, 2005)

Acrylates

Polyacrylic acid and carbomers are the first polymers used as mucoadhesive polymers (Hui & Robinson, 1985). Polyacrylic acid mucoadhesive property is mainly due to the hydrogen bonding as hydrophobic interaction with mucin is poor (Sau-Hung Spence Leung & Robinson, 1987). The strongest interaction between anionic polymers and mucin occurs at an acidic pH, indicating that the mucoadhesive polymer in its protonated state is what causes the mucoadhesion (C. A. Le Bourlais et al., 2008). The swelling polymer's interaction with the mucin stabilizes a thick hydrogel structure on the eye surface(Greaves & Wilson, 1993b; Shaikh et al., 2011b).

Hyaluronan

Hyaluronan is present at the posterior segment of the eye and has been proposed as a viscosifying agent. Mucin stabilizes a thick layer of water by extending polymers adsorbed at the mucin/aqueous interface into the neighboring aqueous phase. The benefits of high viscosity between blinks and low viscosity during blinking are combined with sodium hyaluronate's non-Newtonian nature (Greaves & Wilson, 1993b; Laurent, 1987; C. A. Le Bourlais et al., 2008; Sintzel et al., 1996).

Cationic Polymers

Chitosan

The ability to make molecular attraction forces due to electrostatic interaction with negatively charged mucus membrane make cationic polymers superior (Lehr et al., 1992). Chitosan is a biodegradable, biocompatible, non-toxic polymer with antibacterial and wound-healing properties. Depending on the pH of the environment, the positively charged amino groups of chitosan engage ionically or establish secondary chemical interactions, such as hydrogen bonds, with the negatively charged sialic acid residues of mucins to provide mucoadhesive characteristics. At neutral or slightly alkaline pH, like in the tear film, chitosan's mucoadhesive

performance is noticeably greater (Felt et al., 1999; Greaves & Wilson, 1993b; Hassan & Gallo, 1990; Rossi et al., 2001). Chitosan was chosen as a viscosifier in artificial tear formulations due to its significant topical tolerance after application, bioadhesive qualities, hydrophilicity, and effective spreading of the whole cornea (Calonge, 2001; Felt et al., 2000).

Physico-chemical properties of chitosan

The molecular structure and pKa of chitosan make it less soluble and soluble in all the acidic solvents like acetic, tartaric, and citric acid at pH less than 6.2 (Nagpal et al., 2010). This solubility limitation is due to the crystalline arrangement of its structure that enhances the inter and intra-molecular hydrogen bonding. Due to amine groups on its structural backbone, chitosan exhibits a strong positive charge in an acidic medium. This positive charge interacts with counterions such as drugs, polymers, proteins, or other excipients. The chitosan's mechanical strength and barrier properties depend on its molecular weight. The mucoadhesive character of the chitosan is due to the polycationic surface and its interaction with the mucin layer containing residues of the sialic acids that result in the strong electrostatic interaction and lead to the generation of the mucoadhesive effect. Along with the mucoadhesive property, chitosan also exhibits antimicrobial efficacy (Chung et al., 2006).

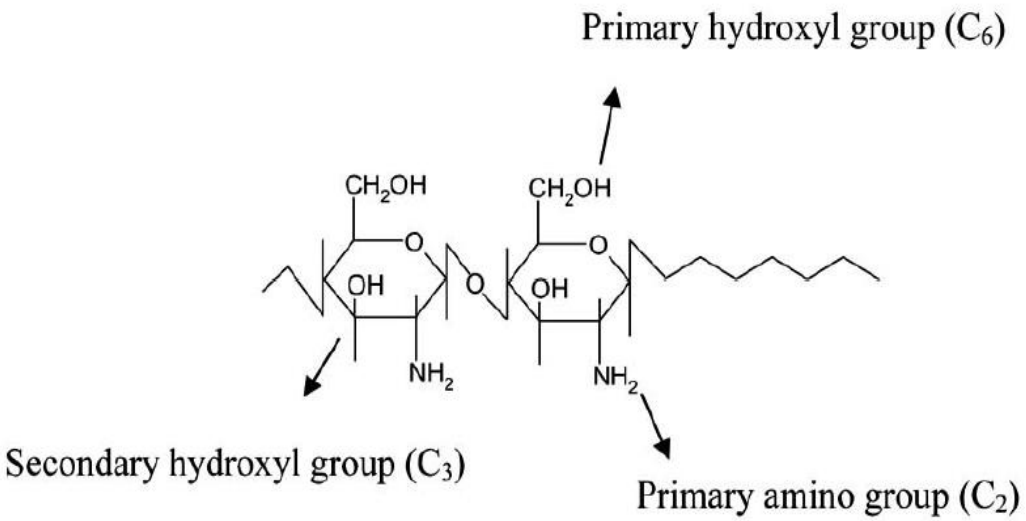

Figure 1.8. The chemical structure of chitosan represents its functional groups. Reproduced from (Wadhwa et al., 2010)

1.11. Thermoresponsive polymers

The stimuli that trigger drug release can vary depending on the nature or the type of induced energy; for ocular applications, the temperature is undoubtedly the most used, and injectable thermoresponsive polymers have been particularly recommended. These systems undergo a reversible transition (owing to reduced volume or phase transition to a solid or gel form) in the physiological temperature range because a critical temperature characterizes them. By avoiding the necessity for a surgical operation for the system's implantation, it would be feasible to introduce them into the body with little intrusion (A. Patel et al., 2013). The thermoresponsive polymers can be natural or semi-synthetic, and various therapeutic agents can be formulated at temperatures below the Low Critical Solution Temperature (LCST) and can be converted to high viscous liquids or hydrogels(Jeong et al., 1997; N. K. Singh & Lee, 2014).

Cellulose and its derivatives

Cellulose is composed of several polysaccharide β-(1,4)-linked d-glucose units that are insoluble in water. Various cellulose derivatives are produced via the alkylation of cellulose, which displays a sol-gel transition as the temperature rises. These cellulose derivatives typically include methyl cellulose (MC), carboxy methyl cellulose (CMC), and hydrophobic methyl cellulose (HPMC)(Bourges et al., 2002; Nadagouda & Varma, 2007).

These cellulose derivatives often have sol-gel transition temperatures that are significantly higher than physiological temperatures, making them unsuitable for ocular medication administration. The ocular applicability of this hydrogel is still debatable because of its

relatively high osmotic pressure, even if the addition of salts (such as NaCl) decreases the sol-gel transition temperature of MC to 32–34 °C (Chang et al., 2010; S. C. Joshi & Lam, 2006).

N-isopropylacrylamide Copolymers

PNIPAM is a synthetic, non-biodegradable polymer that exhibits a typical sol-gel transition in its aqueous solution at around 32 °C. This kind of thermosensitive hydrogel has received much attention from researchers working on various biological applications, such as drug delivery, tissue engineering, and wound healing (Haq et al., 2016; Y. Li et al., 2012).

Poloxamers

Poloxamers are hydrophobic propylene oxide (PPO) and two hydrophilic ethylene oxide (PEO) blocks that are combined to form an amphiphilic tri-block copolymer that may undergo a sol-gel transition when heated at varying ratios of PEO: PPO. Poloxamer 407 (F-127) and Poloxamer 188 (F-68) are two of these commercially available compounds that have been licensed by the Food and Drug Administration and are frequently employed as thermosensitive in situ gelling systems for drug delivery applications (D. Lin et al., 2019).

Physico-chemical properties of the poloxamers

The viscosity of the formulations increases upon the incorporation of soluble polymers into ophthalmic pharmaceutical formulations, increasing the drug's retention in the ocular globe. Poloxamers fall under the broad category of stimuli-responsive polymers. These particular polymers exhibit an active reaction to minute signals and environmental alterations, resulting in appreciable alterations in their microstructure. Like other surfactants, poloxamers exist separately as monomolecular micelles when distributed in a liquid at low concentrations. But when the system's poloxamer concentration rises, this causes the development of

multimolecular aggregates. The PPO group forms the central hydrophobic core in which, upon solubilization, the methyl groups react through van der Waals interactions. The solubility is achieved through the hydrogen bonding interactions of the ether oxygen groups of PEO in poloxamers. Due to these unique characteristic properties, poloxamers are readily solubilized in aqueous solutions, which are stable at acidic, alkalic, and ionic conditions. Poloxamers of two grades are mainly used as dosage forms, including poloxamers (188) F68 and (407) F127. The major difference in these grades is the ratio of PPO/PEO, which determines its hydrophobicity.

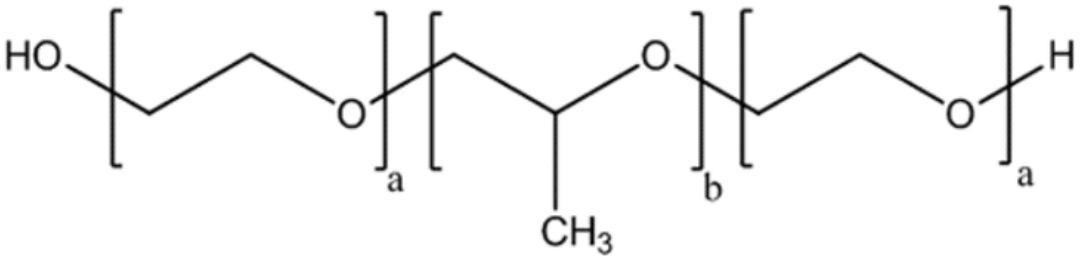

Figure 1.9. The chemical structure of poloxamer consists of PEO and PPO blocks.

Polyester

Polyesters are another class of thermosensitive polymers that are composed of mostly amphiphilic polyesters, including poly (ethylene glycol), poly(lactic acid-co-glycolic acid), and poly(ε-caprolactone) that are extensively used in the ocular drug delivery. Contrary to PNIPAM and poloxamers, which are not biodegradable, synthetic amphiphilic polyester is sensitive to esterase, which results in its good *in vivo* biodegradability. For the treatment of different eye illnesses, numerous therapeutic agents, including chemical drugs and peptides, have been encapsulated in thermosensitive polyester-based delivery systems (Ni et al., 2014; *Thermosensitive Polymeric Hydrogels as Drug Delivery Systems - PubMed*, n.d.; Tonda-Turo et al., 2018).

1.12. Nanoparticle drug delivery system for ocular drug delivery

Various drug delivery techniques, including emulsions, ointments, and suspensions, have been created to overcome the drawbacks of ocular drug administration and increase ocular bioavailability. Each dosage strategy has some restrictions, albeit to varying degrees. Finding a better ocular delivery route with high bioavailability and increased patient compliance is vital. The applications of nano-drug delivery systems were started in the early 1990s and have attracted much attention. It has numerous excellent qualities, like nanosized, biodegradable, and less irritant. In the interim, several nanomaterials can deliver various therapeutic active agents with diverse chemical properties. Emulsion polymerization, free radical polymerization, and interfacial polymerization create nanoscale carriers (K. C. Lee & Choo, 2014). Research indicates that the nano-controlled release method may significantly increase drug bioavailability, decrease drug adverse effects, prolong drug retention in local tissue, and reduce drug dose and dosing frequency, demonstrating its clear superiority in many areas.

Nanoparticles often used in ophthalmic drug delivery comprise lipids, proteins, and polymers of synthetic, semi-synthetic, or natural origin. The diameter of the nanoparticles ranges between 10-1000 nm. The common nanoparticles used for ocular delivery were polyethylene glycol, poly (lactide-co-glycolide), chitosan, and hyaluronic acid (Ideta et al., 2004).

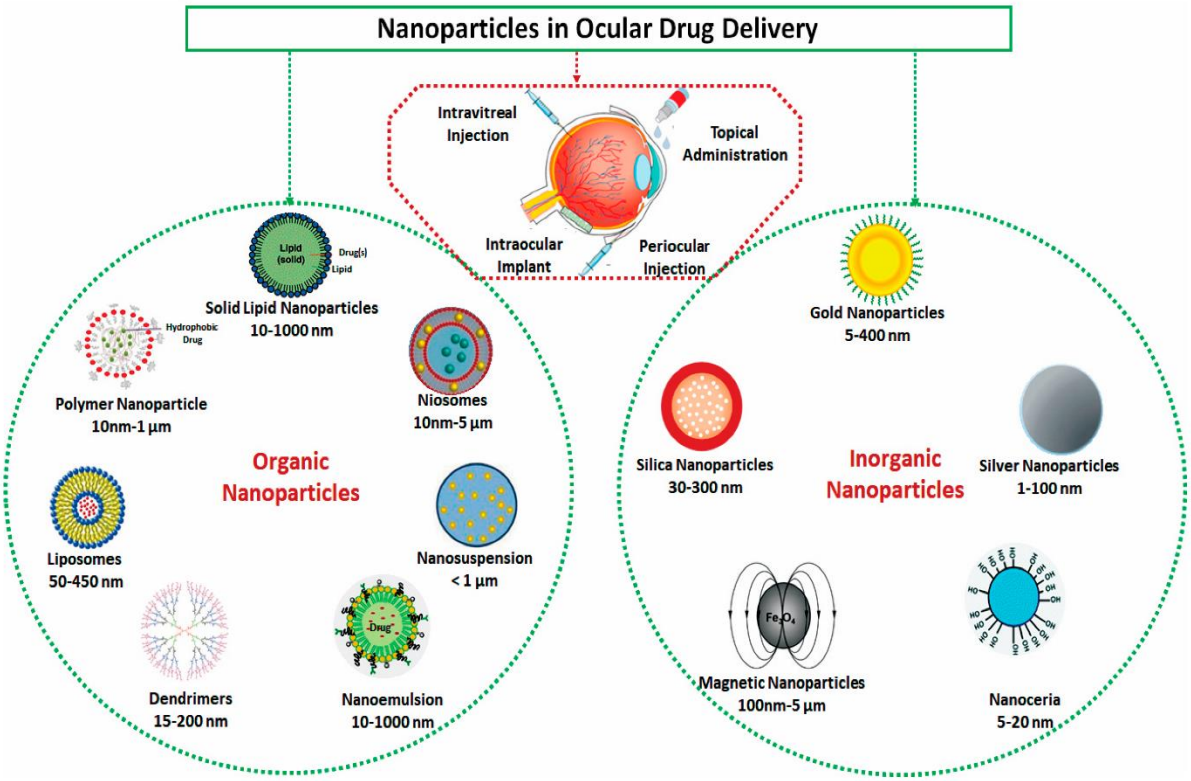

Figure 1.10. Schematic representation of various nanoparticles used in ocular delivery (Khiev et al., 2021)

Nano micelles in ocular drug delivery system

Nano micelles are the aqueous formulations most widely used as drug delivery systems. The formulation of nano micelles can increase the bioavailability of medications in the eye's tissues. This is because nano micelles have a high drug-loading capacity and water solubility caused by a hydrophilic coronary structure and are compact and simple to make. Both the anterior and posterior segments of the eye can receive ocular medication delivery via nano micelles (X. Wang et al., 2015). Nano micelles consist of a hydrophobic core and hydrophilic shell and are highly acceptable for passive delivery for mainly hydrophobic drugs. The size of polymeric micelles ranges from 10-200 nm. It is dependent on the self-assembly of amphiphilic molecules or block polymers. The micelles' self-assembly occurs over concentrations exceeding Critical Micelle Concentration (CMC) (Lu & Park, 2013). Low-molecular-weight surfactant-based

micelles have a greater CMC than polymeric micelles, reducing their stability and posing negative side effects. Because hydrophobic compounds may be solubilized and stabilized by polymeric micelles, this prolongs their retention, which enhances therapeutic results (Mandal et al., 2017a). Amphiphilic di-block (hydrophilic-hydrophobic) polymers, tri-block (hydrophilic-hydrophobic-hydrophilic) polymers, graft (hydrophilic-hydrophobic), and ionic (hydrophilic-ionic) copolymers make up the majority of the polymeric micelles utilized in drug administration. The main hydrophilic component of most of these systems is poly(ethylene glycol, or PEG). The hydrophilic part of the micelles can be mainly constructed using polymers of PEG, polyethylene oxide, poly(vinyl pyrrolidone), and a mixture of polyethylene oxide or polyelectrolytes (Štěpánek et al., 2001). The core forming blocks of polymers such as Poloxamers, Poly(L-amino acids), and Polyesters such as PLGA, Poly(D-Lactic acid) can be used as hydrophobic parts for the preparation of micelles (Kedar et al., 2010).

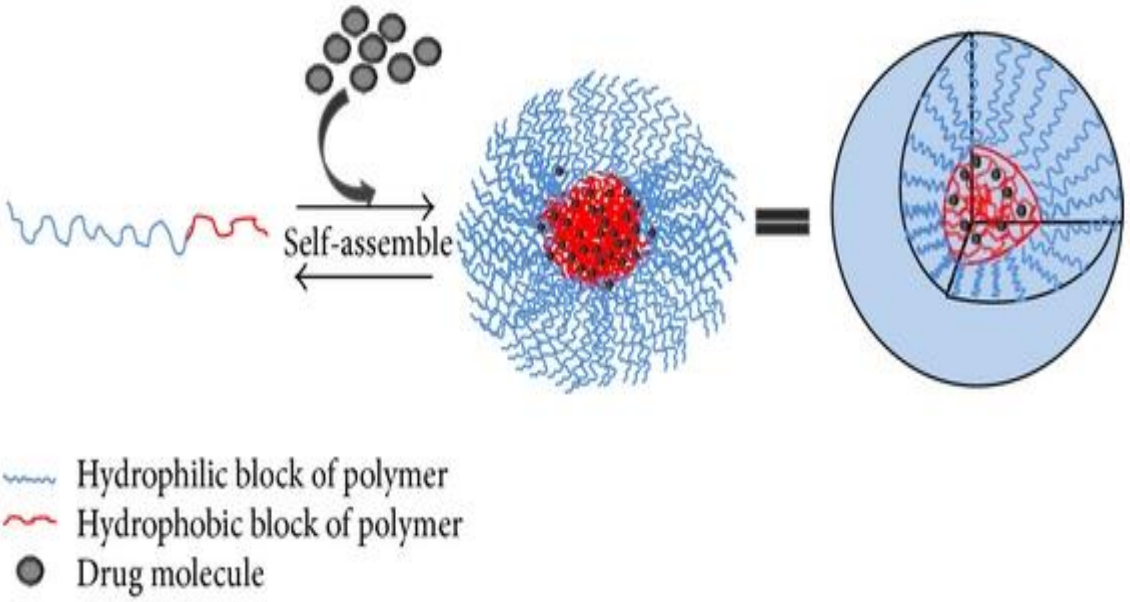

Figure 1.11. The drug loading and self-assembly of micelles in aqueous solution (Xu et al., 2013)

Table 1.2. Polymers used in the development of Ocular drug delivery reproduced from the(Mandal et al., 2017b)

Polymers	**Drug**
Pluronic F127	Ciprofloxacin
Poloxamer 407 (Pluronic F127) Poloxamer 188 (Pluronic F68)	Itraconazole
Methoxy poly(ethylene glycol)–poly(ε-caprolactone) (MPEG–PCL)	Diclofenac
Poly(butylene oxide)-poly(ethylene oxide)-poly(butylene oxide)	Fluconazole
Methoxy(polyethylene glycol)-block-polycaprolactone (MePEG-b-PCL)	Dexamethasone acetate
Methoxy poly(ethylene) glycol (MPEG)	Cyclosporine A (CsA)
N-isopropylacrylamide (NIPAAM)	Ketorolac
Polyoxyethylated nonionic surfactant Pluronic® F127 (F127) cationic polyelectrolyte chitosan (CH)	Dexamethasone

1.13. Ocular delivery pathways

After installing eye drops, a drug might reach the posterior segments of the eye through the corneal or the conjunctival-scleral pathway. The cornea constitutes 85-90% of hydrophilic stroma and is a rate-limiting barrier for many topically administered hydrophobic drugs (V. H. L. Lee & Robinson, 1986b). Due to their small particle size, polymeric micelles can pass through the cornea and a different conjunctival-scleral route following topical treatment. Since the conjunctival-scleral surface area is greater, such polymeric micelles can diffuse laterally and reach the eye's posterior portion (Di Tommaso et al., 2012).

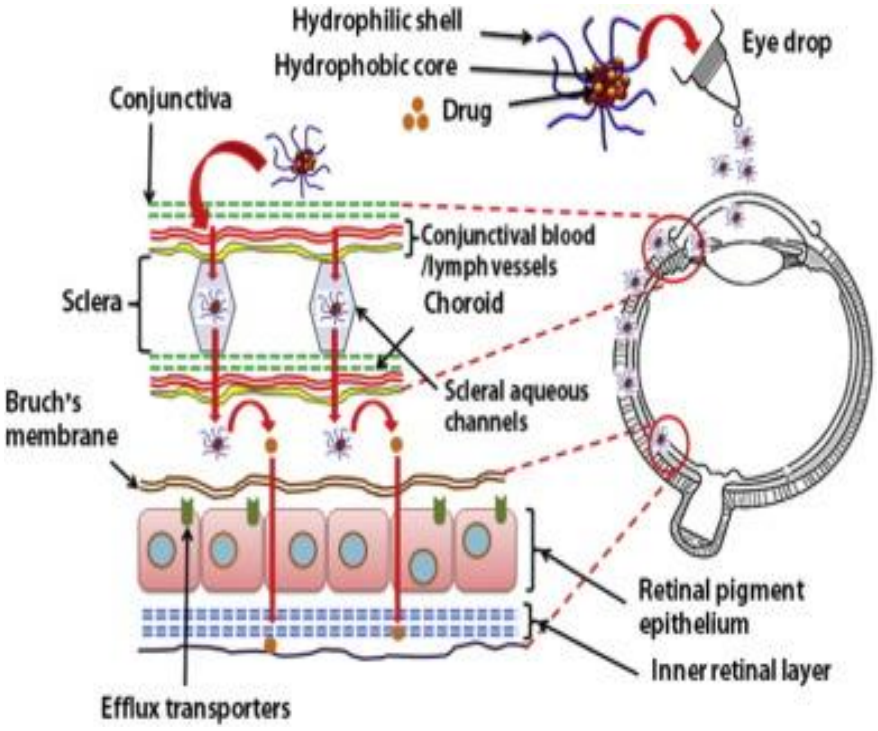

Figure 1.12. Ocular drug delivery pathways after topical administration (Mandal et al., 2017b)

The scleral transport of the micellar-drug complex through the aqueous pores/channels is aided by nano-sized micelles and their hydrophilic corona. The conjunctival blood circulation and lymphatics also reduce the likelihood of drugs washout into the systemic circulation via the scleral route. To create therapeutic concentrations in the posterior ocular tissues, RPE cells may

further gulp the polymeric micelle via endocytosis from the posterior segment (Allen et al., 1999; Luo et al., 2002).

Corneal permeation is an essential factor determining drug penetration efficiency through topical administration. The passage of hydrophilic or polar drugs of molecular size greater than the cornea restricts to 60-100 Da. In contrast, hydrophobic compounds solubilize in the lipid cell membranes of the cornea and pass through the corneal epithelium (Dey et al., 2005). The mechanism of permeation of compounds through the cornea is majorly occurring through transcellular and paracellular movement. Cell portioning or tissue portioning, channel diffusion, and carrier-mediated transport mechanisms are commonly involved in transcellular movement.

In contrast, paracellular movements involve diffusive and convective transport through tight junctions and intracellular spaces. Partitioning is the most important factor for hydrophobic compounds to cross cellular membranes. The diffusion mechanism depends on the concentrations of the solute and the membrane's permeability, surface area properties. Convective transport depends entirely upon the hydrostatic and osmotic gradients and the membrane barrier's hydraulic and reflective coefficients. The lateral movement of many topical ophthalmic drugs through a paracellular mechanism in the eye's anterior chamber is restricted due to the cellular arrangement of the corneal epithelium. Stroma being hydrophilic, it is a diffusional barrier to many lipophilic drugs. Paracellular transport through stroma can be achieved through stroma as no complex tight junctions are resent (Malhotra & Majumdar, 2001).

1.14. Contact lenses-like patches

Innovative ocular drug delivery methods have been developed to address the drawbacks associated with topical delivery and maintain adequate drug concentration for longer residence

times as contact lenses (Maulvi et al., 2016a; Zhang et al., 2020). The high residence time improves the bioavailability of the drug by up to 50%, ultimately lowering the dose, reducing the dosing frequency, and minimizing systemic drug absorption (Jain, 1988; C. C. Li & Chauhan, 2006). Although contact lenses are extensively used for correcting vision, there is an increasing interest in their usage as therapeutic delivery systems in several ocular disorders such as dry eye, controlled drug delivery, and in treating several ocular diseases (Maulvi et al., 2016a; Zhang et al., 2020). The critical constraints such as swelling property, storage modulus, transparency, and oxygen/ion permeability are essential for achieving the therapeutic efficacy of contact lenses. There are many methods to design therapeutic contact lenses, such as the soaking method, molecular imprinting, nanoparticles loaded contact lenses, and supercritical fluid technology (Maulvi et al., 2016b).

Hydrogels for designing contact lenses/patches

Hydrogels are natural or synthetic polymeric materials that swell with water and retain a unique three-dimensional structure (3D). Based on their source (natural/synthetic), nature of cross-linking, physical structure (homogenous/porosity), and degradability, hydrogels can be classified (Kopeĉek, 2009). Most hydrogel architectures have good biocompatibility due to their high-water content. Hydrating the hydrogel mainly depends on the hydrophilicity of the polymer and the number of crosslinks connected to the polymer chain into a 3D structure. Initial studies were carried out extensively on hydrophilic methacrylic acid esters such as glycol, diglycol, and triglycol esters. Hydrophilic esterification of methacrylic acid has produced hydrogels with excellent characteristics; recent studies have shown that (meth)acrylic acid's N-substituted amides represented a class of polymers whose properties could be easily altered by selecting the right substituent on the amide nitrogen (Šprincl et al., 1971, 1973; Ulbrich & Kopeček, 1976). Due to the excellent properties of hydrogels, such as their hydrophilicity, biocompatibility/biodegradability, tunable physical/chemical properties,

stimuli-responsive, biomedical applications, and clinical translational applications, hydrogels are most widely used in bioprinting applications (Y. Wang et al., 2022).

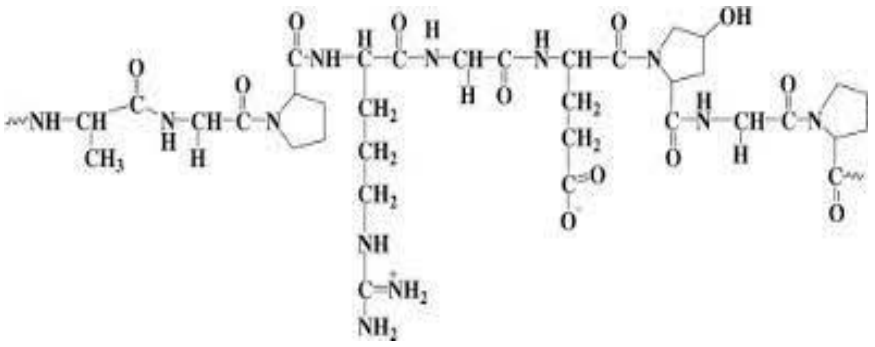

Figure 1.13. The chemical structure of Gelatin

1.15. 3D-Printing

Bioprinting is an additive bio-fabrication technique that prints the scaffolds automatically upon deposition of bioinks layer-by-layer. The technique creates scaffolds that resemble real tissue by carefully utilizing live cells, organic or synthetic biomaterials, crosslinkers, and other functional elements. 3D-Printing is widely used in ophthalmology for diverse purposes such as personalized contact lenses/patches, glasses, implants, and fabrication of preoperative eye models (Alqattan et al., 2018). Natural hydrogels are mostly considered for bioprinting as they have similar micro-cell environments. Collagen is widely used as a bioink due to its good biocompatibility and low immunogenicity. Since collagen exhibits low mechanical strength, it can be crosslinked (physically or chemically) with various other molecules such as fibrin, agarose, and alginate to improve collagen mechanical strength and alters its properties (J. M. Lee et al., 2021; Osidak et al., 2019; Stepanovska et al., 2021). Gelatin is the most widely used hydrogel for ocular applications due to its unique adhesive properties and is considered a good alternative for corneal engineering applications. Gelatin is non-toxic, biocompatible, and transparent. It mimics the extracellular matrix due to its compatibility in tuning viscoelastic mechanical properties (Khalili et al., 2021).

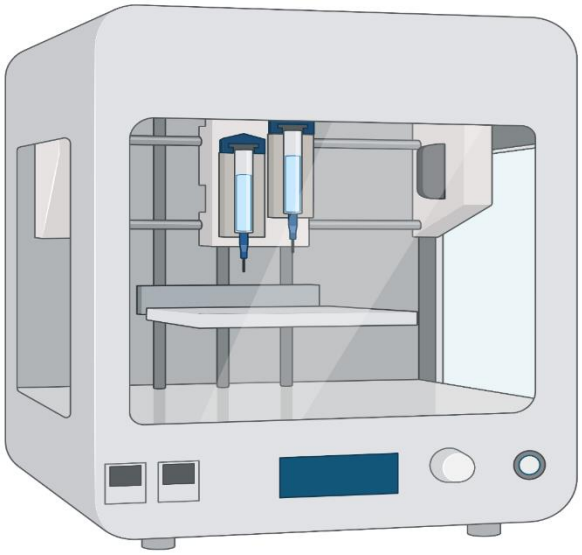

Figure 1.14. Illustration of 3D-Bioprinter.

In addition to natural bioinks, synthetic hydrogels were used extensively in bioprinting. For example, Gelatin Methacrylate (GelMA) is synthesized from water-soluble Gelatin, a photopolymerized hydrogel composed of natural ECM components. Gelatin is sensitive to temperature and transforms from sol-gel corresponding to the temperature. The thermal stability, mechanical stability, and biocompatibility of the Gelatin can be enhanced by crosslinking with methacryloyl (Ashammakhi et al., 2019).

1.16. Objectives

Our aim for the study is to develop nanomedicine for treating bacterial keratitis with superior efficacy compared to conventional therapy. We have adopted the strategy of developing mucoadhesive polymeric nanomedicine capable of incorporating a fluoroquinolone antibiotic drug to achieve the goal and develop a therapeutic agent eluting contact lenses using 3D printing technology. The following are the specific aims:

Objective 1. Hydroxypropyl methacrylamide-based copolymeric nanoparticles loaded with moxifloxacin as a mucoadhesive, cornea-penetrating nanomedicine with enhanced therapeutic benefits in bacterial keratitis.

Specific aims:

(i) To synthesize methoxy (polyethylene Glycol) and poly(N-2-hydroxypropyl methyl acrylamide) using the mPEG-ABCPA-mPEG macroinitiator and the monomer, 2-hydroxypropyl methacrylamide by free radical reaction

(ii) To prepare and optimize the Mox-loaded nanoparticles using the Design of experiments

(iii) To characterize the conjugate using GPC, CAC, SEM, FTIR, Particle size, Zeta analysis, DSC, XRD, and encapsulation efficiency.

(iv) To execute i*n-vitro* studies using Human Corneal Epithelial (HCE) cell lines, and ex vivo mucoadhesive studies using goat cornea

(v) To determine the *in vitro* bactericidal efficacy of the formulations against the Gram-positive and Gram-negative bacteria.

(vi) To determine the *in-vivo* therapeutic efficacy using mice models pre-infected with Bacterial keratitis.

Objective 2. Chitosan-poly(lactide-co-glycolide)/poloxamer mixed micelles as a mucoadhesive thermo-responsive moxifloxacin formulation to improve treatment efficacy in bacterial keratitis.

Specific aims:

(i) To synthesize Chitosan-poly(lactide-co-glycolide)/poloxamer mixed micelles.

(ii) To encapsulate moxifloxacin inside the synthesized mixed micelles.

(iii) To characterize the conjugate using ^{1}H NMR, CMC, SEM, GPC, FTIR, Zeta analysis, DSC, XRD, and encapsulation efficiency.

(iv) To execute i*n-vitro* studies using Human Corneal Epithelial (HCE) cell lines and ex vivo mucoadhesive studies using goat cornea.

(v) To determine the *in vitro* bacterial efficacy of the formulations against the Gram-positive and Gram-negative bacteria.

(vi) To determine the *in-vivo* therapeutic efficacy using mice models pre-infected with Bacterial keratitis.

Objective 3. Cationic Gelatin-Sodium alginate polyelectrolyte complex nanoparticles loaded with moxifloxacin optimized by Quality by Design approach for treating bacterial keratitis.

Specific aims:

(i) To synthesize Cationic Gelatin and sodium alginate polyelectrolyte complex nanoparticles.

(ii) To encapsulate moxifloxacin inside the synthesized nanoparticles.

(iii) To characterize the conjugate using ^{1}H NMR, SEM, GPC, FTIR, Zeta analysis, DSC, XRD, and encapsulation efficiency.

(iv) To execute i*n-vitro* studies using Human Corneal Epithelial (HCE) cell lines and ex vivo mucoadhesive studies using goat cornea.

(v) To determine the *in vitro* bacterial efficacy of the formulations against the Gram-positive and Gram-negative bacteria.

(vi) To determine the *in vivo* therapeutic efficacy using mice models pre-infected with Bacterial keratitis.

Objective 4. 3D-Printed Inherently antibacterial contact lens-like Patches Carrying Antimicrobial Peptide Payload for Treating Bacterial Keratitis.

Specific aims:

(i) To synthesize and characterize the GelMA/ChiMA-based bio-ink for 3D-Printing.

(ii) To optimize the bioprinting parameters and print AMP-loaded GelMA/ChiMA contact lens-like patches.

(iii) To execute i*n-vitro* studies using Human Corneal Epithelial (HCE) cell lines and carryout mucoadhesive studies using goat cornea.

(iv) To perform *in-vitro* bacterial studies on planktonic and biofilms of *Pseudomonas Aeruginosa.*

(v) To determine the *in-vivo* therapeutic efficacy using rabbit models pre-infected with Bacterial keratitis.

Chapter 2

Hydroxypropyl methacrylamide-based copolymeric nanoparticles loaded with moxifloxacin as a mucoadhesive, cornea-penetrating nanomedicine with enhanced therapeutic benefits in bacterial keratitis.

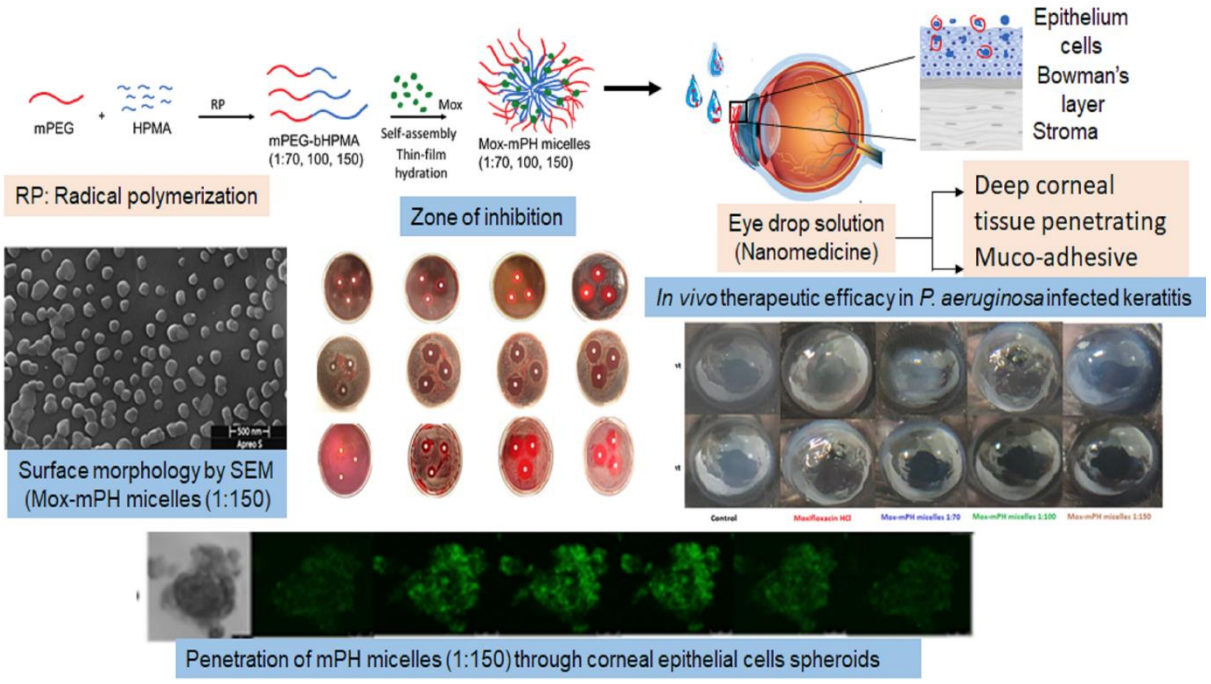

2.1 Introduction

A corneal infection, commonly referred to as keratitis, is a leading cause of visual impairment or unilateral blindness worldwide (Austin et al., 2017a; Bartimote et al., 2020; Hsiao et al., 2016). Microbial keratitis is a corneal infection caused by various pathogens, including bacteria, viruses, fungi, or parasites (Bharathi et al., 2003, 2007; Schaefer et al., 2001a; Wong et al., 2012b). Even though infectious agents are the prevalent cause of the initiation of the disease, however, several non-infectious causes, including ultraviolet exposure, eye trauma, or chemical exposure, can also lead to corneal damage (P. Singh et al., 2013; Taylor et al., 1989). Other conditions that increase the risk of microbial infections include diabetes mellitus, LASIK surgery, and immune suppression due to some pathogenic illness or the use of immunosuppressant drugs(Abud et al., 2017; Keratitis et al., 2000; Levitt et al., 2015). Contact lens wearers are the most vulnerable to corneal infection due to poor contact lens hygiene(Fleiszig, 2006). While contact lens-usage-related, BK is very common in wealthier countries, impure water, and unhygienic living cause the disease's initiation in developing countries (Eltis, 2011). Late diagnosis and improper treatment destroy the corneal layer, damaging the stroma, corneal scarring, and vision loss.

The type of bacteria causing bacterial keratitis (BK) varies greatly depending on the geographical locations and climates. *Staphylococci*, *Pseudomonas*, *Streptococci*, and *Serratia*, are the most common pathogens causing BK(Al-Mujaini et al., 2009b; Marquart & O'Callaghan, 2013). The infection is highly proliferative, starts with severe inflammation, and then quickly proceeds to corneal perforation, destruction of the corneal stroma, and loss of visual acuity(Mascarenhas et al., 2014). The broad-spectrum fluoroquinolone antibiotics, including moxifloxacin, gatifloxacin, and levofloxacin, are the drugs of choice (M. S. Hanet et al., 2012a; Thibodeaux et al., 2004). However, depending on the severity of the infection, other steroidal medicines, such as medroxyprogesterone, are included in the treatment regimen as an adjuvant

therapy to suppress the inflammation by inhibiting cytokines production and collagenase(Al-Shehri et al., 2009). Moreover, bacteria quickly develop resistance due to a sub-optimal therapeutic concentration of antimicrobial agents in the cornea (Goldstein et al., 1999a).

The conventional topically applied dosage forms intended to exert antibacterial effects, such as eye drop formulations, suffer from various drawbacks, including rapid clearance from the eyes due to blinking and nasolacrimal drainage, dilution with the tear fluid, enzymatic degradation, and low corneal penetration of the existing antimicrobial agents(Baranowski et al., 2014b; Cooper & Yang, 2019; P. B. Patel et al., 2010; Varela-Fernández et al., 2020). The nanomedicine-form of antibiotics has emerged recently and is beneficial compared to conventional therapy. Nanoparticles encapsulate drugs in the core, prevent enzymatic degradation, improve bioavailability, increase the drug's half-life, and promote nanomedicine-mediated corneal penetration and invasion in bacteria (Cholkar et al., 2012; Reimondez-Troitiño et al., 2015; Varela-Fernández et al., 2020). However, developing nanoparticle formulation of fluoroquinolone antibiotics is challenging due to the drug's extreme hydrophilicity(S. B. Singh et al., 2017). Here, we have prepared a topical eye drop formulation of moxifloxacin using an amphiphilic polymer of two hydrophilic blocks, mPEG and bHPMA. The polymeric NPs prepared by thin-film hydration technique were of nano-size, loaded moxifloxacin optimally, and exhibited sustained release. The nanoparticles were non-irritant, non-toxic to the corneal epithelial cells, penetrated the corneal tissue efficiently, were mucoadhesive, demonstrated longer corneal residence, and exerted promising antimicrobial effects.

2.2 Materials and methods

2.2.1 Materials

2-Hydroxypropyl methacrylamide (HPMA) was obtained from Sigma-Aldrich (USA). 4,4-azobis (4-cyano pentanoic acid) (ABCPA) was obtained from Sigma-Aldrich (Bangalore,

India). Methoxy PEG Succinimidyl Carboxymethyl Ester (mPEG, molecular weight 2000 Da) was procured from Jenkem Technology USA, USA. MSN Laboratories Pvt Ltd (Hyderabad) gave Moxifloxacin HCl as a gift sample. DCC and DMAP were procured from Sigma-Aldrich, Bangalore. Fluorescein isothiocyanate (FITC-NHS) and SYTO-9 was purchased from Thermo Scientific (USA). The dialysis membrane (MWCO 3500 Da and 12-14000 Da) was obtained from Spectrum Laboratories, Inc. (USA). All other organic solvents are bought from local vendors.

The human corneal epithelium, HCE cell line, was a gift from Dr. Sanhita Roy's lab at the L.V. Prasad Eye Institute, Hyderabad, India). Fetal bovine serum (FBS), Dulbecco's modified Eagle's medium F-12 (DMEM F-12), and penicillin/streptomycin solution were purchased from Himedia Laboratories (Mumbai, India). HCE cells were sub-cultured in DMEM F-12 media supplemented with 10% fetal bovine serum and 100 IU/mL of antibiotic penicillin/streptomycin. The cell-seeded flasks were kept in a sterile, humidified atmosphere at 37 °C and a 5 % CO_2 incubator.

All animal procedures were performed per the guidelines of CPCSEA (The Committee for Control and Supervision of Experiments on Animals), BITS-Pilani Hyderabad, India (BITS-Hyd/IAEC/2020/03). Mice (C57BL/6 and BALB/c) of approximately 18 g (5-6-week-old) were procured from the National Institute of Nutrition (NIN, Hyderabad). The animals were accustomed to the following conditions: Temperature. 19−25 °C, nocturnal−diurnal cycles for 1week, relative humidity. 50−60% with free access to food and water.

2.2.2 Methods

2.2.2.1 Synthesis of polymer and characterization

mPEG-poly(N-2-hydroxypropylmethacrylamide) block copolymer (mPEG-bHPMA) was synthesized by free radical polymerization reaction using mPEG-ABCPA-mPEG macroinitiator and the monomer, 2-hydroxypropyl methacrylamide following a previously

reported procedure with modification (Bobde et al., 2020b). The mPEG: HPMA feed ratios for the reaction were 1:70, 100, and 150 (**Table 2.1a**, **2.1b**, and **2.1c**). The reaction procedure was as follows: The macroinitiator and monomer at mol ratio 1:70, 100, and 150 (**Table 2.2**) were taken in a pyrex tube and dissolved in approximately 2-3ml Acetonitrile (ACN). The reaction mixture was purged thoroughly with nitrogen for 30 min, sealed, and kept in an oil bath (70 °C). The reaction was continued for 48 h under stirred conditions. The reaction mixture obtained was added dropwise into the cold diethyl ether. The precipitate was collected by centrifugation and dried under a vacuum.

Table 2.1. Calculations of the molar ratios of the reagents for the synthesis of the mPEG-bHPMA polymers

Table 2.1a. mPEG-bHPMA (1:70)

	Mol ratio	**Mol wt (Da)**	**Weight taken (mg)**	**No. of mol (mM)**
$mPEG_{2k}$-ABCPA-$mPEG_{2k}$	1	4244.28	127.03	0.0299
HPMA	70	143.18	300	2.0951

Table 2.1b. mPEG-bHPMA (1:100)

	Mol ratio	**Mol wt (Da)**	**Weight taken (mg)**	**No. of mol (mM)**
$mPEG_{2k}$-ABCPA-$mPEG_{2k}$	1	4244.28	148.167	0.03491
HPMA	100	143.18	500	3.4918

Table 2.1c. mPEG-bHPMA (1:150)

	Mol ratio	**Mol wt (Da)**	**Weight taken (mg)**	**No. of mol (mM)**
$mPEG_{2k}$-ABCPA-$mPEG_{2k}$	1	4244.28	148.167	0.03259
HPMA	150	143.18	700	4.8886

For Gel Permeation Chromatography (GPC) analysis, MilliQ water was used as solvent at a flow rate of 0.7 ml/min (injecting volume. 10µl). Samples were prepared by dissolving in DI water at a concentration of 2 mg/ml. The calibration was done using standards of shodex (the molecular weights ranging from 6300-530000 Da).

2.2.2.2 Preparation of mPH NPs

The NPs were formed by thin-film hydration technique following the previously reported procedure (Bobde et al., 2020b). Briefly, 10 mg of mPEG-bHPMA polymers, 1:70, 100, or 150, were dissolved in methanol: chloroform (1:1) mixture and were evaporated to obtain a thin film. The thin films were hydrated with 3 ml of PBS, pH 7.4, and vortexed at room temperature overnight.

To prepare Mox-mPH NPs, MOX (1 mL, 2mg/ml in methanol: chloroform mixture) and mPEG-bHPMA (1:70, 100, and 150) solutions (1 mL, 10 mg/mL) were mixed, evaporated using a rotary evaporator, hydrated with 3 ml phosphate buffer saline (PBS); pH 7.4 and vortexed at room temperature for overnight. The solution was dialyzed using cellulose ester membrane (MWCO. 6-8KDa) to remove the unloaded drug/unincorporated polymers. Mox-mPH NPs were collected and stored at 4 °C for further studies.

2.2.2.2.1 Preparation of C6-mPH NPs

C6 (1 mg, 1mg/ml in methanol) was mixed with the mPEG-bHPMA (1:70, 100 or 150) polymer solution (10 mg, 10 mg/mL chloroform: methanol solution (1:1)). The mixture was evaporated to obtain the thin film, hydrated in PBS, pH 7.4 (3 mL) by vortexing. The solution was dialyzed in a dialysis bag (6-8 KDa). The C6-loading in nanoparticles was determined using spectrofluorimetry at excitation and emission wavelengths of 457 nm and 501nm, respectively.

2.2.2.3 Synthesis of mPEG-bHPMA-FITC

mPEG-bHPMA (50 mg, 4.21 µmol) and FITC-NHS (2.05 mg, 4.21 µmol) were dissolved in pyridine (3 mL). DCC (1.5 mg) and DMAP (1 mg) were added to the reaction mixture. The reaction mixture was stirred at room temperature for 24 h. Pyridine was removed by a rotary evaporator, and the reaction mixture was diluted with water. The solution was dialyzed (MWCO. 3.5 KDa), and the dialysate was freeze-dried.

2.2.2.4 Formulation optimization/QbD approach

The factors that affect the formulation were identified with the preliminary experiments. The polymer amount (mg) and the rehydration (mL) volume were recognized as independent factors. The effect of the invariable factors on the variable factors, including the nanoparticle's particle size Zavg, % DL and % EE was determined by Central Composite Design (CCD) using the Design-Expert software. This design consists of five levels containing axial and center points. The independent variables, including the amount of polymer (5-10 mg) and the volume for rehydration (1-5mL), was studied at different levels coded as –α, −1, 0, 1, and + α where α =2n/4, n is the number of variables, and 0 corresponds to the central point. According to the CCD matrix generated by the Design-Expert software, 9 experiments were constructed. The effects of changes in independent factors on the variable factors were determined by creating nine different experiments. The data is shown in **Table 2.3.**

2.2.2.5 Morphology

Lyophilized powders of Mox-mPH NPs (1:70, 100, and 150) were spread on a holder attached to carbon tape. The powder was evenly distributed on tape and gold-coated for 30 min. Carbon tape containing samples was placed on a sample holder, and images were taken using a Field Emission Scanning Electron Microscope (Apreo Lo Vac, FEI, USA).

2.2.2.6. Entrapment Efficiency (EE) and Drug Loading (DL)

The Mox-mPH NPs (1:70, 100, and 150) were dispersed in the Phosphate Buffer Saline (PBS) and then diluted with methanol to break the nanoparticles. The drug concentration was

analyzed using a UV-Visible spectrometer (JASCO, Japan) at a wavelength of 290 nm. The % EE and % DL were calculated using the following equation:

$$\% \text{ DL} = \frac{\text{Amount of drug in NPs}}{\text{The initial amount of polymer and drug}} \text{ x } 100$$

$$\% \text{ EE} = \frac{\text{Amount of drug in NPs}}{\text{The initial amount of drug taken}} \text{ x } 100$$

2.2.2.7. Critical Aggregate Concentration (CAC)

CACs of mPEG-bHPMA polymers (1:70, 100, and 150) were determined by the pyrene incorporation method. Pyrene solution (50 µL, 10 mg/mL) was evaporated in glass vials. Polymer solutions in the water at varying concentrations (3.125-200 µg/mL) were added and incubated for 24 h at room temperature. The solutions were filtered, and the absorbance was recorded at an excitation/emission wavelength of 339/390 nm using a Spectramax™ M4 microplate reader.

2.2.2.8. Differential scanning calorimetry (DSC)

The polymer, Moxifloxacin HCl, and MOX-mPH NPs (1:150) were accurately weighed (3 mg) and loaded in the aluminum pans. The material was compressed and analyzed over a 30-300 °C temperature range at a heat exchange rate of 10 °C/min under the nitrogen atmosphere (flow rate of 20 ml/min). The thermal analysis was performed using differential scanning calorimetry (DSC 60, Shimadzu, Japan).

2.2.2.9. X-ray powder diffraction (XRD)

The polymer, Moxifloxacin HCl, and MOX-mPH NPs (1:150) were analyzed using a powder X-ray diffractometer (ULTIMA-IV, Rigaku, Japan). The instrument was equipped with a Cu anode (λ= 1.54 Å) operated at a voltage and current of 40 kV and 30 mA, respectively. Data were collected at 2θ from 5° to 70° at a scanning rate of 5 °/min.

2.2.2.10. Cell culture studies

2.2.2.10.1. MTT assay

The *in vitro* cytotoxicity of the HCE cells was determined by MTT assay. In brief, the cells were seeded in 96-well plates in DMEM-F12 complete growth media at a density of 2 x 10^4 cells/well and incubated at 37 º C for 24 h. Further, the polymeric NPs in serial dilutions of 3.25-50 µg/mL were added to the wells and incubated for 24 h. The control HCE cells were given no treatment. The next day, old media was discarded, followed by adding 100µL of MTT solutions (5 mg/mL). The cells were incubated with MTT solution for 4 h, and the solution was replaced by 150 µL of DMSO. After an additional 30 min incubation, the plate was read using a microplate reader (Spectramax™, Molecular Devices, US) at a 590 nm (reference wavelength. 620 nm). The following equation was used to calculate the percent cell viability:

% cell viability= $Abs_{sample}/Abs_{blank}X100$, where, Abs_{sample} = the absorbance of the cells treated with mPEG-bHPMA solution. $Abs_{control}$ = the averaged absorbance of the control cells. The study was carried out in triplicates and expressed as mean ± SD.

2.2.2.10.2. Cellular uptake in monolayer HCE cells

HCE cells, seeded on coverslips (5 X 10^4), were kept overnight, and the following day, the cells were treated with FITC-mPH NPs (5µg/ml FITC) in serum-free media for 1 h and 4 h. The cells were washed with PBS and stained with 100µL DAPI (6µg/mL) in PBS for 5 min. The cells were fixed using 4 % paraformaldehyde for 20 min at room temperature. The coverslips were mounted on slides using fluoromount-G and visualized under a confocal microscope (Leica Microsystems, Germany) using Ex/em wavelengths of DAPI and FITC at 358/461 and 491/516, respectively. The images were processed using *Image J* software.

For flow cytometry studies, HCE cells were seeded in 12-well plates at a density of 0.2 x10^6. The next day, the cells were treated with FITC-mPH NPs (FITC amount. 5 µg/mL) for 1 h and 4 h. The cells were then washed with PBS, trypsinized, centrifuged, and suspended in PBS to

analyze using flow cytometry (FACS ARIA III, BD Life Sciences). The viable cells were gated using forward and side scatter plots. Ten thousand viable cells were analyzed for fluorescence from each treatment group and plotted using IDEAS Application version 6.0 software.

2.2.2.10.3. Cellular uptake in HCE spheroids

HCE spheroids were prepared by the liquid overlay method (Bhatt et al., 2019). A sterilized agar solution (50 µL, 1.5 % w/v in DMEM F12 media) was added to each plate of a 96-well plate. The HCE cells (1 x 10^4,150 µL) were added to each well and centrifuged. The spheroids were used for further studies when the diameter reached 800 µm. The spheroids were incubated with the same FITC-mPH NPs solutions, gently washed, and visualized under a confocal microscope using the objective. 10X. The lens was focussed at various depths on the Z-axis from the cells' surface, and the micrographs were processed using *Image J* software.

2.2.2.10.4. Trans-epithelial Electrical resistance (TEER) measurement

The HCE cell line performed Transcorneal Permeation measurement of MOX-MPH NPs (1:70, 100, and 150). The HCE cells (1 × 10^6) were seeded onto the collagen-coated 12-well permeable inserts (Corning™) for ten days. The EVOM volt-ohm meter (Millicell®ERS-2, Millipore) was used to measure the TEER values. The cell layer was treated with formulations when the TEER value reached 170 Ω cm^2. The formulations (0.1ml, 2mg/mL Mox) were added to the apical chamber and kept for incubation for 5 min. The transepithelial voltage was measured at different intervals by touching the membrane surface with the electrode tip that uses alternating current.

2.2.2.11. Mucoadhesion using a texture analyzer

The mucoadhesive strength of mPH NPs (1:70, 100, and 150) was assessed by a Texture analyzer (Stable Micro Systems, Surrey, UK) using a goat intestinal membrane(Laulicht et al., 2012a). Freshly excised goat intestine from the slaughterhouse was cleaned and rinsed thoroughly with normal saline. The intestinal tissue was cut to the required size, and the basement membrane was fixed onto the basement probe and the stainless-steel probe on the

moving arm of the texture analyzer. The moving arm, at a speed of 0.5 mm/sec, touched the mPH nanoparticle solution (200 µL) placed on the luminal side of the membrane at a contact force of 5 g. A force (100 g) was applied to the mucous membrane and held for 120 sec. The probe moved up at a speed of 0.1 mm/sec. The force (expressed in grams) required to detach the probe from the membrane was noted as the mucoadhesive strength.

2.2.2.11.1. Falling liquid film method

The mucoadhesive property of the NPs was determined using the modified Falling liquid film method (Choy et al., 2008). The freshly excised goat eyeballs procured from the slaughterhouse were used to detach the cornea. The corneas with scleral rims were dissected and immediately placed in PBS solution, pH 7.4. The FITC-mPH NPs (~200 µL, FITC-normalized solutions, 3.3 mg/mL) were added at the cornea center towards the epithelial side and incubated for 30 mins. The corneas were placed on a falcon tube wall using double-sided tape at an angle of 45 °. The simulated tear fluid (STF), pH 7.4, flowed over the cornea at a 1 mL/min rate. The flow rate was controlled using a peristaltic pump. The difference between the fluorescence applied, and the fluorescence released in STF was a measure of adhered nanoparticles.

2.2.2.11.2. Mucin turbidity assay

The mucoadhesion potential of the mPH NPs was determined by measuring the turbidity of the mucin incubated with the nanoparticles (Han et al., 2020a). Briefly, mucin solution (1000 µL, 1 mg/mL) was incubated with mPH NPs (500 µL, 1mg/mL) at 37 °C under constant shaking (100 RPM). The absorbance of the solution was determined using a UV-Vis spectrophotometer (Jasco, Japan) at predetermined time intervals.

2.2.2.12. HET-CAM test

Fertilized hen's eggs collected from a hatchery farm were incubated horizontally at 37±0.5°C. The positioning ensures the embryo's development from the chorioallantoic membrane (CAM) (S. B. da Silva et al., 2016). On day 10, the eggs were illuminated, and the shell was cut out as

2X2 cm^2 using a drilling tool and a rotating cutting blade. The inner membrane, which is in direct contact with the CAM, was moistened with 0.5mL saline solution and removed carefully without damaging the blood vessels of the CAM. 0.5mL of test formulations were added to the CAM and observed for ocular tolerance/irritancy. Saline water was used as the negative control, and 1M NaOH as a positive control.

2.2.2.13. Drug diffusion studies

Ex-vivo permeability studies of free Moxifloxacin and Mox-mPEG-HPMA NPs (500 µg of moxifloxacin) were carried out using Franz diffusion cell through goat corneal tissue. The tissue was placed between the donor and receptor compartment, with an exposure area of 0.6399 cm^2. Different formulations equivalent to 500 µg of Mox were added to the donor compartment. The receptor compartment was filled with 5 ml of STF. The bath was maintained at 37 ± 1° C under continuous stirring. At predetermined time intervals, 300 µl of samples were withdrawn, and the same volume of fresh STF was added. The withdrawn samples were filtered using a syringe filter, diluted if necessary, and quantified for drug content by HPLC using the Phenomenex C18 column. The mobile phase used was a 1:1 mixture of methanol and 25 mM potassium phosphate buffer, pH 7.4. The flow rate was 1.0 mL/min (detection wavelength. 290 nm). The study was performed three times, and the graph was plotted for the percentage of drug diffused versus time (h).

2.2.2.14. Drug release study

Mox-mPH NPs (1000 µL, equivalent to 0.05% w/v of Mox) were placed in a dialysis bag (cellulose ester membrane, 3.5 kDa). The dialysis bag was dipped into 100 mL of STF (pH 7.4) at 37 °C under stirring conditions (300 RPM). 1 ml of STF was withdrawn at predetermined intervals and replaced with equal aliquots of fresh media. HPLC (Shimadzu, Japan) estimated the amount of drug released using the Phenomenex C18 column. The procedure was described in section 2.16. Cumulative drug release was calculated.

2.2.2.15. Viscosity and Phase transition studies

The viscosity of the mPH NPs of 1:70,100, and 150 were measured at different concentrations (0.5-3 % w/v) over a temperature range (25-40 °C) using Anton-Paar rheometer (MCR 302, Austria) using the temperature rampage application. Briefly, 0.5, 1, 1.5, 2, 2.5, and 3% (w/v) samples of all the polymer ratios were prepared, and each sample's viscosity was analyzed at different temperatures.

The Turbidimetry method carried out phase transition studies for the mPEG-bHPMA polymers (1:70, 100, and 150)(Henderson et al., 2009). The polymers' turbidity at different concentrations was determined by measuring the transmittance at a wavelength of 500 nm using Spectramax™, a microplate reader (Molecular Devices, USA). The mPEG-HPMA solutions were prepared at a concentration of 5, 10, 15, 20% (w/v) by dissolving in PBS (pH 7.4). The temperature was raised from 25-60 °C. The transmittance of the copolymer solutions was measured at a wavelength of 500 nm. The temperature corresponding to 50 % transmittance is indicated as the Lower Critical Solution Temperature (LCST).

2.2.2.16. Antibacterial study

Bacterial strains

LV Prasad Eye Institute and BITS-Pilani Hyderabad, India, provided *Streptococcus pneumoniae, Pseudomonas aeruginosa, and Staphylococcus aureus*. The strains (*Pseudomonas aeruginosa* and *Staphylococcus aureus*) were grown aerobically in Luria Bertani Broth, Miller (HIMEDIA, INDIA), and *Streptococcus pneumonia* was grown in Todd Hewitt Broth (HIMEDIA, INDIA) at 37 °C, and 85 % relative humidity. *P aeruginosa*, *S aureus*, and *S pneumonia* were incubated overnight at 37°C. The next day a subculture was incubated at 37°C (200 µL of overnight culture in 5 mL of LB broth) for 2hrs to get an OD_{600} of 0.2 for *p aeruginosa* and 0.6 for *S aureus* to get a CFU count of 10^8 CFU/mL and 10^9 CFU/mL respectively. *S pneumoniae* was cultured overnight to get an OD_{600} of 0.3 with a

bacterial count of 10^8 CFU/mL. All the bacteria were pelleted and resuspended in 1 mL LB, Todd Hewitt (*S pneumoniae*) broth, serially diluted with PBS, and pH 7.4 for further studies.

2.2.2.16.1. Minimum Inhibitory Concentration (MIC) determination

MIC was determined by the microtiter broth dilution method with some modifications (Malekinejad et al., 2012). Briefly, *P aeruginosa* and *S aureus* bacteria were diluted to (10^6 CFU/ mL in LB broth), and 100 µL of the bacteria were incubated at 37°C with Mox-mPH NPs (100 µL) of various concentrations (0-4 µg/ mL) in a 96 well plate. MIC was determined at different time points by observing visible turbidity and measuring the optical density of these cultured broths at 600nm. MIC was determined by MTT assay to compare with the microtiter broth dilution method (Malekinejad et al., 2012). Briefly, Mox-mPH NPs (100 µL) of different concentrations (0-4 µg/mL) were incubated with *P aeruginosa* and *S aureus* (10^6 CFU/ mL LB media) in a 96 well plate at 37°C for 12h. After the incubation, 50 µL MTT solution (5 mg/mL) was added to each well and incubated for 2 h. 80% MTT solution was removed from the plates, and dimethyl sulfoxide was added to each well to dissolve the MTT reagent. The optical density was checked at 590 nm using a microplate reader instrument (Spectramax M4, Molecular Devices, San Jose, USA), keeping reference absorption maxima at 620nm. The below-mentioned equation calculated the percentage of cell viability

$$\% \text{ cell viability} = \frac{Abs\ of\ sample}{Abs\ of\ control} \times 100$$

2.2.2.16.2. Zone of inhibition study

S pneumonia, *S aureus*, and *P aeruginosa* at a concentration (10^5 CFU/mL) were used to determine the inhibition zone following Mox treatment (5µg/mL). The sterile spreaders were used to spread the lawn of bacteria on nutrient agar plates. Mox, Mox-mPH NPs (1:70, 100, and 150) were soaked in sterile circular paper discs, put on the bacterial lawn, and incubated for 24 h. The untreated bacteria were considered as a negative control. The growth inhibition

zones were measured after 24 h of incubation, and the pictures were captured using a digital camera.

2.2.2.16.3. Live/Dead staining of bacteria by Fluorescence microscopy and flow cytometry

Planktonic bacteria (10^6 CFU, 1 mL) of both *P. aeruginosa* and *S. aureus* were incubated with 25 µg/mL of Mox in Mox-mPH NPs solutions (1:70, 1:100, and 1:150) for 10, 30, and 60-min at 37 °C (under shaking). Then, the bacteria were centrifuged at 6000 rpm for 10 min at 25°C. The bacteria were washed twice with sterile physiological saline solution (0.9 % w/v NaCl). The obtained pellet was dispersed in 200 µL of sterile PBS, pH 7.4, and stained using SYTO 9 and Propidium iodide (PI). The staining solution was prepared by mixing SYTO 9 and PI at 33.4 µM and 0.4 mM, respectively (Ou et al., 2019). The bacteria staining was performed by adding 3 µL and 5 µL of SYTO 9: PI (1:1) for *P. aeruginosa* and *S. aureus*, respectively, and kept in the dark for 10min. After the staining, the bacteria's images were captured using a fluorescence microscope (ex/em. 485/498) (Leica, DMi8, Germany).

For the flow cytometry study, both the bacteria were sub-cultured in fresh LB broth media and incubated at 37 °C. The suspension was centrifuged at 6000 rpm for 10 min when the solution's optical density at 600 nm reached 0.6. The cells were washed with PBS (1X, pH 7.4) and resuspended in 500 µL of PBS before adding 25 µg of Mox-mPH NPs (1:70, 1:100, and 1:150). The bacterial suspension was incubated for 10, 30, and 60-min at 37 °C (under shaking). The bacterial staining with PI and SYTO 9 was done as mentioned above. Untreated, unstained samples were used as a control, and 10,000 gated cells were analyzed using a flow cytometer (FACS ARIA III, BD Life Sciences, CA, USA) using FITC and PI lasers. The data was graphically represented in quadrant plots using BD FACSDiva Software.

2.2.2.17. *In vivo* imaging

The retention time of the Polymeric nanoparticles over the cornea was assessed in Balb/c mice. Coumarin 6 (C6)-loaded (4.15 µg C6/eye) mPH nanoparticle (1:70, 100, and 150) solutions of

20 µL were administered topically to both the mice' eyes. The animals were anesthetized using isoflurane before the administration. The fluorescence intensity signal was captured using IVIS LUMINA series III (Perkin Elmer). The Region of Interest (ROI) was measured at various time points (5 min post-administration-360 min) till the fluorescence signal disappeared (exposure time 30s) using Living Image version 4.5.5 software.

2.2.2.17.1. Assessment of therapeutic efficacy in a bacterial keratitis mouse model

An overnight culture of *P. aeruginosa* at 37 °C in LB broth was diluted to a 5 mL solution of OD_{600} of 0.2 (10^6 CFU/mL). The mice were anesthetized (Ketamine HCl of 150 µL) by the intraperitoneal route. Three 1 mm abrasions were made on the cornea using a 25-gauge needle. Then 5 µL of bacterial inoculum was added to both eyes. After the 12h of inoculation, mice with infected eyes (n=6/group) were divided into five groups: control, Mox solution (1 µg/µL), Mox-mPH NPs at Mox conc. 1 µg/µL). The formulations (5 µL) were administered topically to the right cornea at 12 h intervals for three cycles. The Control group received PBS, pH 7.4. Following the treatment, each mouse was scored for statistical comparison and photographed with a microlens-attached camera and graded accordingly: clear/slight opacity, 0, partially or fully covering the pupil; +1, slight opacity, covering the anterior segment; +2, dense opacity, partially or fully covering the pupil; +3, dense opacity, covering the anterior segment; +4, partial/ full corneal perforation.

2.2.2.17.2. Quantification of viable Bacteria

The eyes were enucleated and homogenized in 1 mL of sterile saline solution containing 0.25% BSA (0.9 % NaCl). 100 µL of the solution was diluted to 10 mL (1:10) in the same sterile solution. The diluted solution (15 µL) was plated in triplicate on pseudomonas isolation agar plates and incubated overnight at 37 °C. The bacterial colonies were counted and reported as the number of viable colonies using the following formula:

$$CFU = \frac{\textbf{No.of colonies}}{\textbf{10 x dilution factor}} \text{ X } 1000$$

2.2.3. Results

2.2.3.1. Physico-chemical characterization of nanoparticles

The GPC analysis indicated that the molecular weight (Mn) of the synthesized mPH-polymers was 11750, 16027, 22219 Da, indicative of the attachment of 66.95, 97.8, and 144 numbers of HPMA monomers/single PEG chain for the feed ratios of 1:70, 100, and 150, respectively (**Table 2.2, Figure 2.1**).

Table 2.2. Molecular weights of the synthesized polymers as determined by gel permeation chromatography.

Macroinitiator: HPMA mol ratio	Mw	Mn	Mp	PDI	No. of mols attached	%Yield
1:70	11750	6799	13444	1.863	66.95	81.2
1:100	16027	13701	14193	1.169	97.8	95.70
1:150	22219	17924	20472	1.239	144	88.84

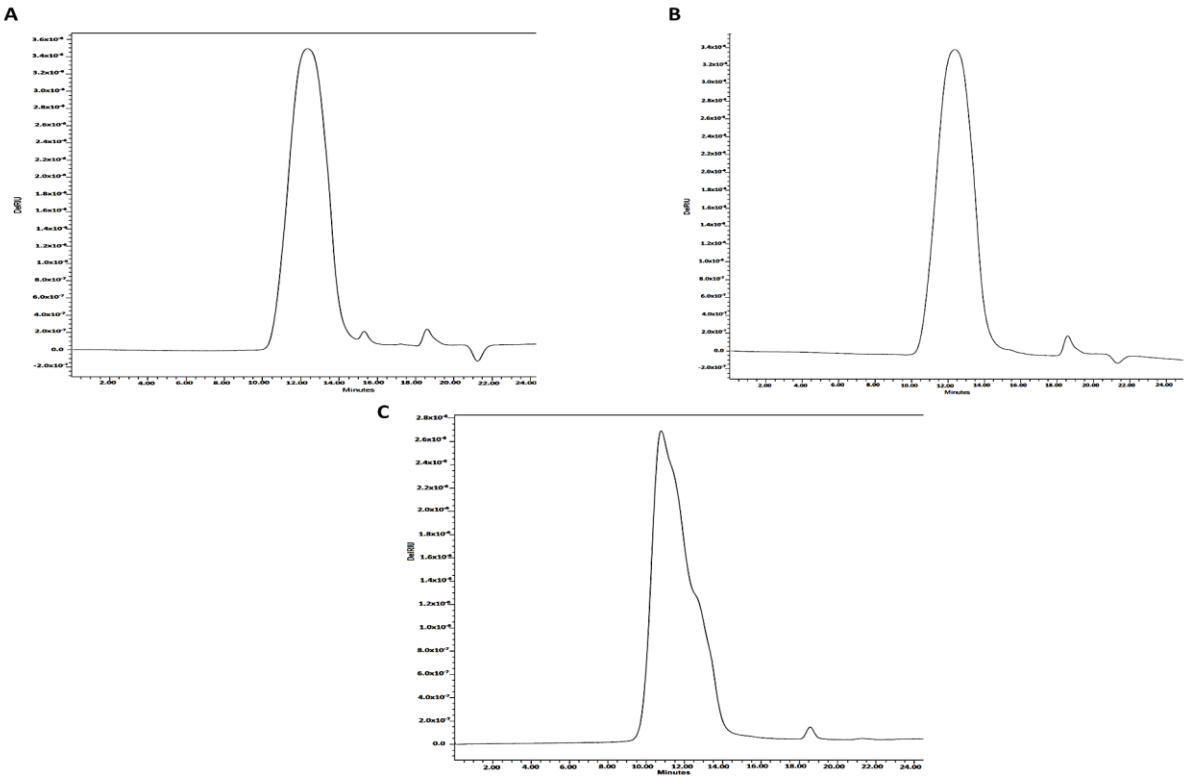

Figure 2.1. GPC chromatograms of the mPEG-HPMA polymer of mol ratios (**a**) 1:70, (**b**) 1:100, and (**c**) 1:150, respectively

mPH NPs (1:70, 100, 150) exhibited CACs of 1.544, 1.397, and 1.096 µM, respectively (**Figure 2.4**). The quadratic polynomial equations obtained from the results (Zavg, % DL, and % EE) of 9 experiments with the change of the polymer amount (1:70) and the rehydration volume (**Table 2.3**) are shown below:

Table 2.3. Central Composite Design with code values and Actual values

	Code value of factors		Actual value of factors		Observed values		
No.	**X1**	**X2**	**Amount of polymer**	**Rehydration Volume**	**Zavg**	**%DL**	**%EE**
1	0	0	10	3	256	5.21	63.2
2	-1	1	7.5	4.4	503.8	4.8	41.6
3	0	1.41421	10	5	371	6.08	66.8
4	-1	-1	7.5	1.58	293	4.3	51.5
5	-1.41421	0	5	3	283	0.8	21.2
6	0	-1.41421	10	1	231.6	1.3	14.7
7	1	-1	12.5	1.58	208.6	1.03	18.2
8	1	1	12.5	4.4	333	3.9	67.4
9	1.41421	0	15	3	361	5.21	56.1

$Zavg = +224 -18.0489 * A + 66.4802 * B + -21.475 * AB + 54.7062 * A^2 + 44.3562 * B^2$

$\%DL = 4.03769 + 0.255835 * A + 1.26374 * B$

$\%EE = 48.0769 + 5.23201 * A + 14.1226 * B + 14.775 * AB$

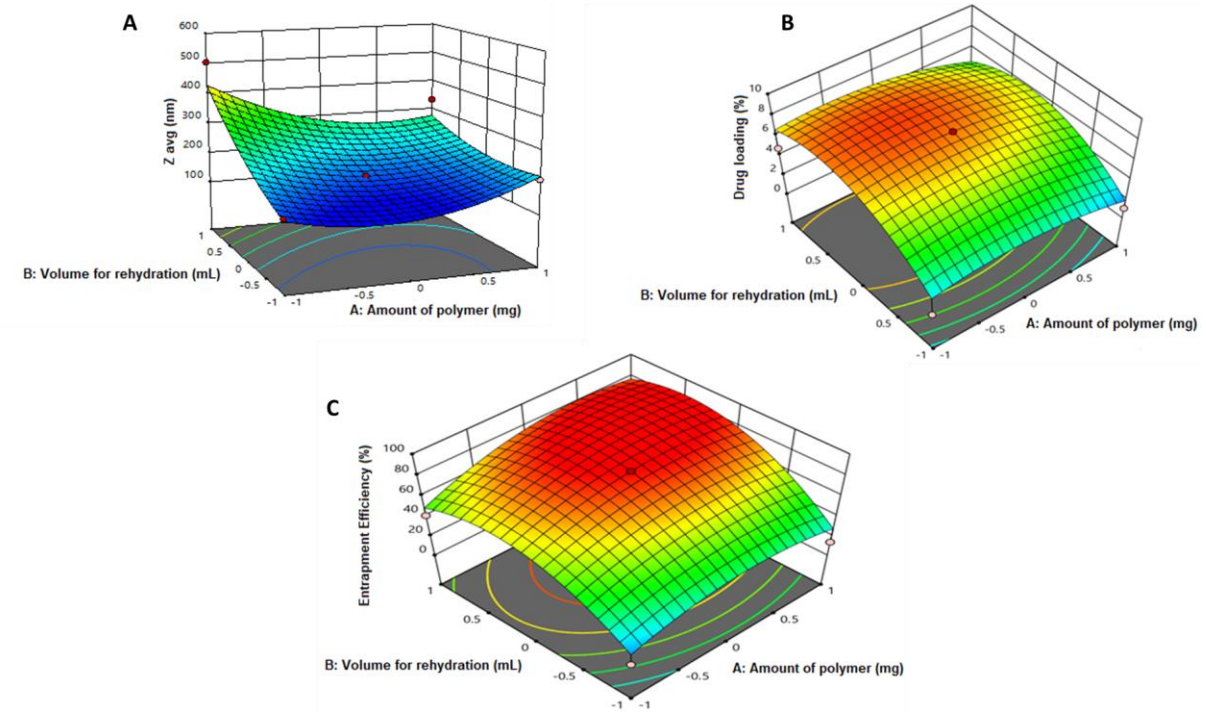

Figure 2.2. QbD analysis. The response surface plots for the effect of the amount of polymer and the volume for rehydration on the responses **(A)** Z avg, **(B)** % Drug Loading, and **(C)** % Entrapment Efficiency derived by Design-Expert software.

Here, X1 represents the amount of polymer, and X2 represents the volume of rehydration. The response surface analysis plotted in 3D graphs indicated the interaction and quadratic effect of two independent variables on the responses or dependent variables (Zavg, EE %, and DL %)) (**Figure 2.2**). The observed values of responses, Zavg, % DL, and % EE, ranged from 161-503.3 nm, 0.8-8.31, and 14.0-71.2, respectively, in the nine sets of experiments (**Table 2.4**). The predicted Zavg, % DL and % EE using the amount of polymer, 10 mg, and the rehydration volume, 3 mL, were 269.5 nm, 4.10, and 45.87, respectively. The optimum predicted formulation from the surface response plot is the amount of mPH polymer (1:70) 10 mg, the amount of drug 1 mg, and the rehydration volume 3 mL. The observed experimental values were 228.21 (Zavg), 4.31 (% DL), and 47.5 (% EE), respectively (**Table 2.4**). Mox-mPH NPs at mPEG to HPMA molar feed ratio of 1:70, 100, and 150 displayed particles size of 228 ±2.15,

251±1.96, and 116.2±2.24 nm, and drug loading of 4.31±1.21, 5.71±1.08, and 8.32±1.47, respectively (**Table 2.5**).

Table 2.4. Mean predicted and observed values of the optimized Mox-mPH NPs (1:70)

Analysis	Predicted Mean	Predicted Median	Observed	Std Dev	n	SE Pred	95% PI low	Data Mean	95% PI high
Zavg	269.501	269.501	228.21	58.6261	3	42.5133	168.973	228.21	370.029
Drug loading	4.10519	4.10519	4.31	1.61036	3	1.09065	1.67507	4.31667	6.53531
Entrapment Efficiency	45.8734	45.8734	47.5	14.4078	3	9.7868	23.7342	47.5733	68.0127

Table 2.5. Particle size, PDI, %DL and Zeta potential of the Mox-mPH NPs (1:70, 100, 150).

Macroinitiator: HPMA mol ratio	Particle Size (nm ± SE)	Polydispersity Index (± SE)	Zeta Potential (mV ± SE)	Drug Entrapment (% ± SE)	Drug Loading (% ± SE)
1:70	228±2.15	0.42± 0.11	-19.79±1.32	47.5±1.74	4.31±1.21
1:100	251.8±1.96	0.41±0.25	-19.93±2.34	62.9±1.55	5.71±1.08
1:150	116.2±2.24	0.39±0.18	-20.41±1.62	83.2±1.29	8.32±1.47

The nanoparticles displayed unimodal size distribution by DLS and spherical morphology by SEM studies (**Figure 2.3**).

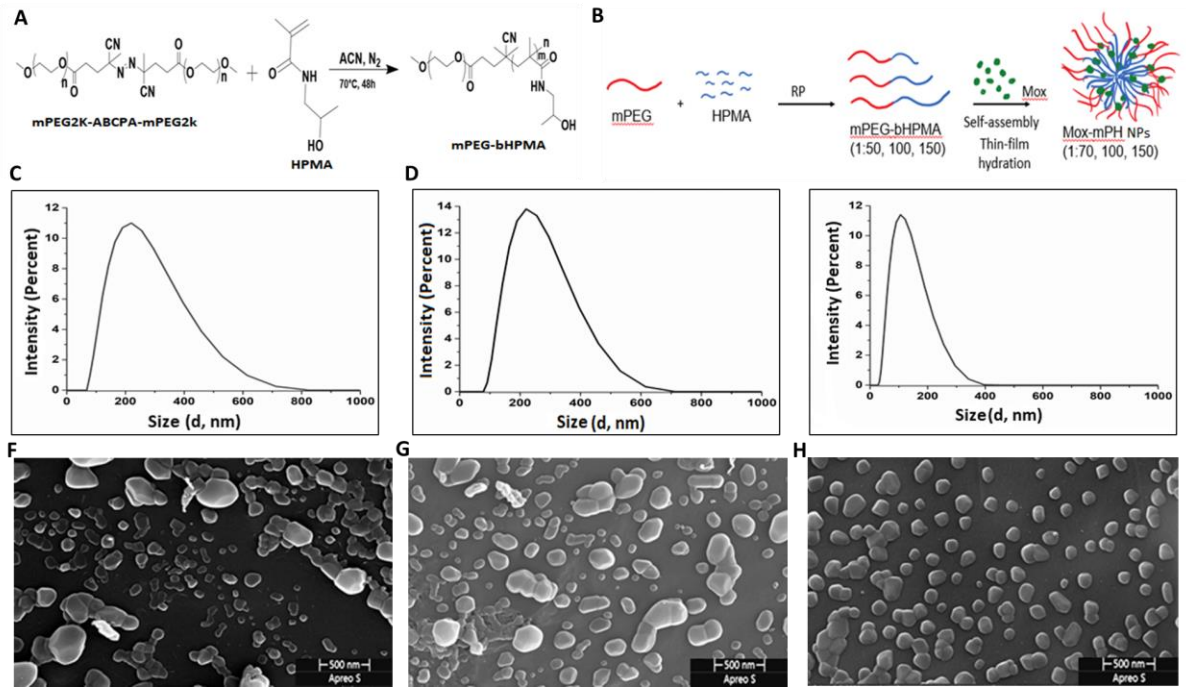

Figure 2.3. The general schemes for the synthesis of the polymer, mPEG-bHPMA (1:70, 100, 150) and the procedure for preparation of NPs (RP: Radical polymerization technique) (A, B); The particle size distribution of Mox-mPH NPs (1:70, 100, 150) (C, D, E, respectively) by DLS technique; scanning electron microscopy images of Mox-mPH NPs, 1:70 (F) 1:100 (G) and 1:150 (H). scale bar. 500 nm.

In XRD analysis, Mox displayed peaks at 12, 20, 25, 30, and 35 2ɵ, whereas no such peaks are observed in Mox-mPH NPs' diffractograms. In DSC analysis, Mox-mPH NPs did not display any characteristic peak, whereas the endothermic peak at 270 °C and 325 °C was observed for Mox and mPEG-bHPMA, respectively. In IR spectra, a signal at 1641 cm-1 indicated the presence of –NH groups in HPMA. The signs of –PEG moiety (at wavenumbers 1130 and 2929, representing C-O bending and –C-H stretching) and –COO (1465 cm^{-1}) were observed. In the drug release study, Mox-mPH NPs (1:150) released the drug most gradually, releasing 50.6 % Mox within 4 h compared to Mox-mPH-NPs of 1:70 (79%) and 1:100 (75.6 %). The Drug diffusion study measured Mox's permeation through goat cornea as ~90, 334, 399, and 428 µg/cm^2 for free Mox, Mox-mPH NPs of 1:70, 100, and 150, respectively. The highest

deviation of transepithelial electrical resistance (TEER) of up to 130.25 ±2.73 Ohm.cm^2 was observed following the treatment of multilayer HCE with Mox-mPH NPs (1:150) at 240 min compared to Mox-mPH NPs of 1:70 (101.09±3.51), and 1:100 (129.25±2.15), respectively (**Figure 2.4**).

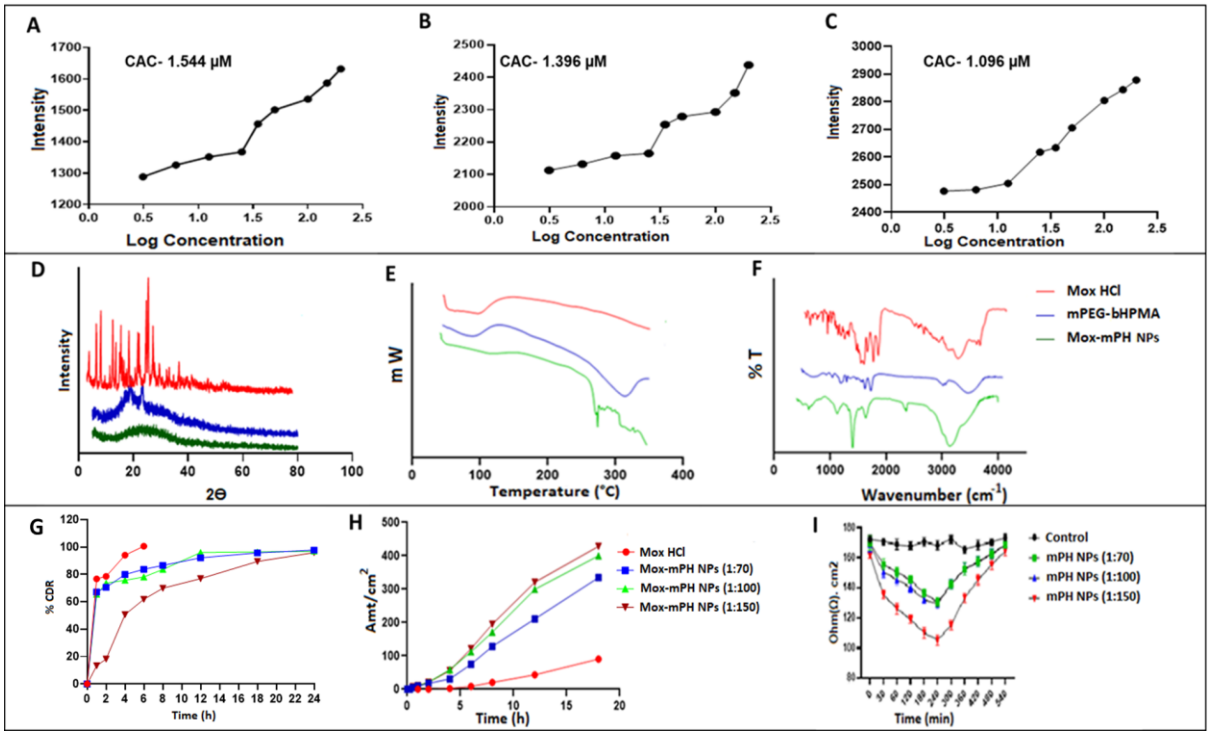

Figure 2.4. Critical aggregate concentrations of mPH NPs (1:70, 100,150) (A, B, and C, respectively); physicochemical characterization of mPEG-bHPMA, mPH NPs, and Mox-mPH NPs by XRD (D), DSC (E) FTIR (F); *in vitro* drug release study (G); e*x vivo* drug permeation through Franz diffusion cells (H); TEER study using HCE multilayer cells (I).

There was a concentration-dependent decrease in the viscosity of all three polymers with increased temperature. A slight variation in the transmittance of the polymers with an increase in the temperature was observed. However, transmittance decreases consistently with an increase in concentration (5-20 %) at the tested temperature range of 24-60 °C (**Figure 2.5**).

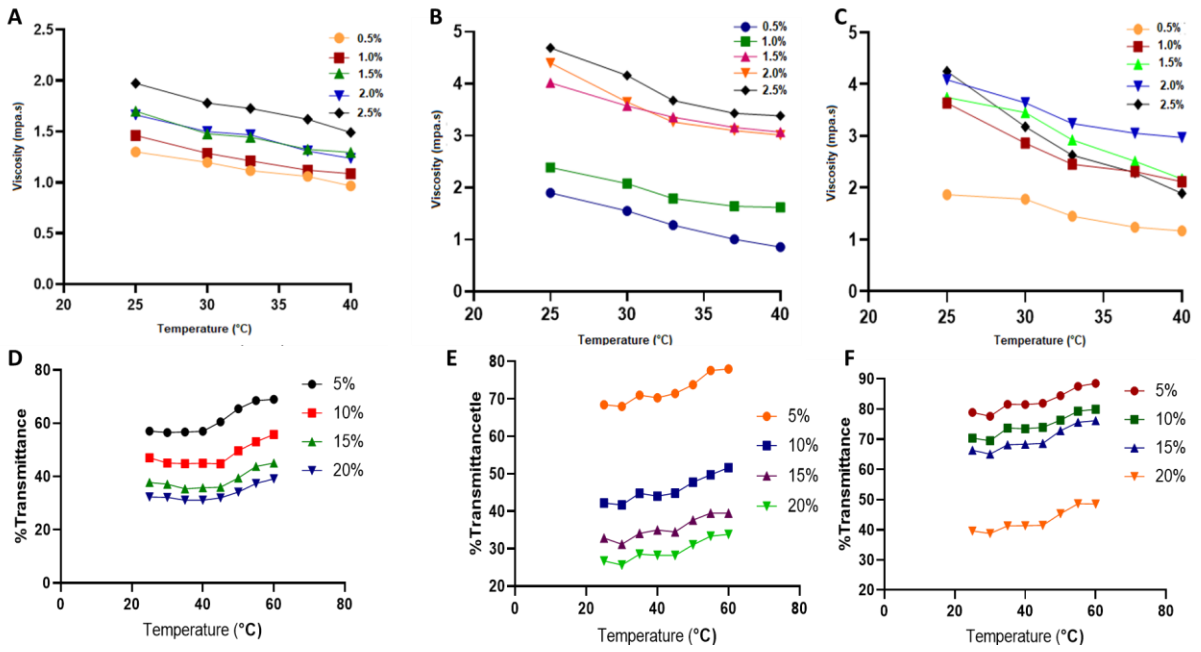

Figure 2.5. Temperature-dependent viscosity study of mPEG-bHPMA co-polymer of mol ratios (a) 1:70 (b) 1:100 (**c**) 1:150 at different concentrations 0.5, 1, 1.5, 2, 2.5 % (w/v). Phase transition studies of mPEG-HPMA co-polymer of mol ratios (**d**) 1:70, (**e**) 1:100, and (**f**) 1:150 at different concentrations 5, 10, 15, 20% (w/v).

The force required to remove the mPH NPs (1:70, 100, and 150) adhered to goat mucosa was found to be 10, 12, and 18 g/cm^2, respectively, as measured by the Texture analyzer. The free-falling liquid method indicated that the mPH NPs (1:70, 100, 150) adhered to the goat cornea following continuous STF rinsing for 60 min was 10, 22, and 30 % of the administered fluorescence, respectively. The incubation of mucin with mPH NPs (1:70, 100, 150) for 1 h caused a varying degree of turbidity with absorbance values of 0.2865, 0.3730, and 0.4109, respectively (**Figure 2.6**).

2.2.3.2. *In vitro* studies using HCE cells and in vitro antibacterial assay

The viability of HCE cells was compromised to ~80 % by MTT assay following nanoparticle treatment at the maximum concentration of the polymers (50 µg/mL) (**Figure 2.6**). HCE cells in monolayers and spheroid growth conditions took up a higher amount of mPH NPs of 1:150

than 1:70 and 100. The mPH NPs (1:150) penetrated efficiently till 100 µm, as observed by Z-stack analysis of spheroids.

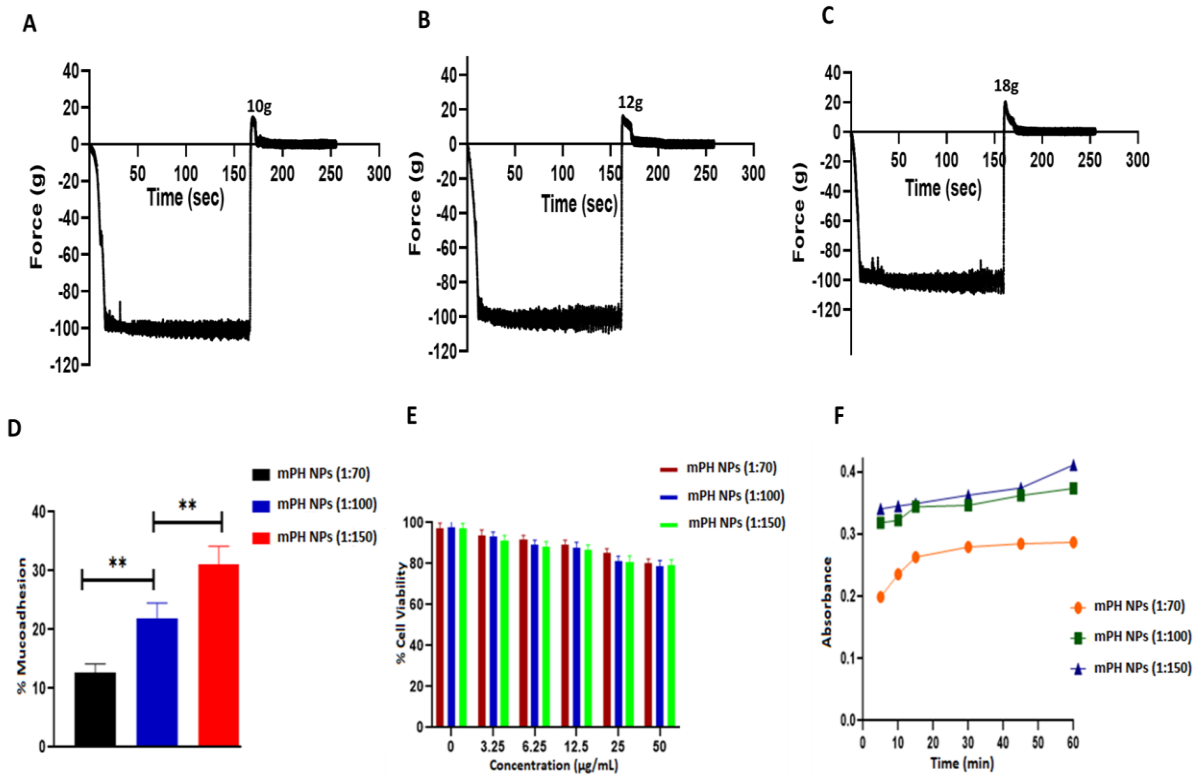

Figure 2.6. Determination of mucoadhesive strength by texture analyzer for mPH NPs, 1:70, 100, and 150, respectively (A, B, C); mucosal retainment of mPH NPs (Falling liquid method) (D); % cell viability of HCE cells treated with mPH NPs (E); analysis of turbidity by binding of mPH NPs with mucin over time by UV-Visible spectrophotometer (F).

The geometric mean fluorescence of cells treated with mPH NPs (1:70, 100, 150, FITC concentration. 5µg/mL) for 1 h was 711.3±147.6, 856.71±163.21, and 1549.47±183.27, which increased to 1678.84±159.34, 1899.51±178.29 and 2474.18±150.32 at 4 h of incubation, respectively **(Figure 2.7**).

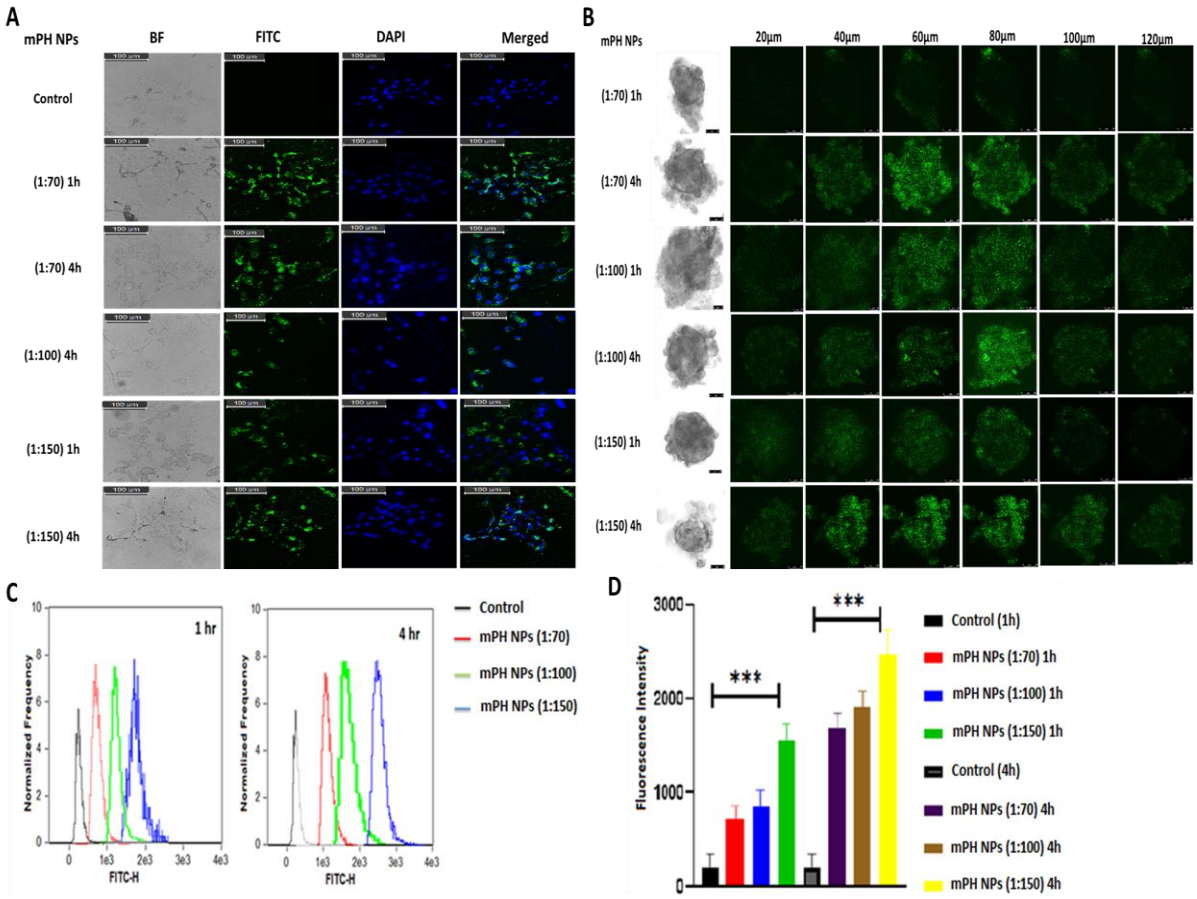

Figure 2.7. Cellular uptake of mPH NPs (1:70, 100, 150) by HCE cells in monolayers (A) and spheroids (B); histogram plot representing cellular uptake of mPH NPs by flow cytometry for 1-4 h (C), the bar graph plot representing the time dependency in cellular uptake quantitatively (D). The data represent the mean ± SD (n=3). *** represents $p<0.001$

HET-CAM test indicated that, unlike the positive control, Mox-mPH NPs did not show any hemorrhage sign despite slight bulging of the blood vessels (**Table 2.6**).

Table 2.6. Irritation scores of mPEG-HPMA NPs (1:70, 100, 150) on the HET-CAM test based on severity as follows: 0 - No reaction, 1 – Slight reaction, 2 – Moderate reaction, and 3 – Severe reaction

Severity	After 5 min
+ve control	3
-ve control	0
Mox-mPH NPs (1:70)	0
Mox-mPH NPs (1:100)	0
Mox-mPH NPs (1:150)	0

The Mox-mPH NPs (1:70) showed the MIC at the concentration of 0.5 µg/mL with MBC at 4 µg/mL against *P. aeruginosa* and *S aureus,* which is determined by measuring OD_{600} and by MTT assay. The Mox-mPH NPs (1:150) displayed the highest inhibition zone (22.3 ±0.1 mm, 26.0 ± 0.11 mm, and 23.3 ±0.17 mm) compared to other tested nanoparticles by controlling the growth of *P. aeruginosa*, *S. aureus,* and *S. Pneumoniae*, respectively (**Figure 2.8, Table 2.7**).

Table 2.7. Zone diameter (mm) for bacteria after treating with moxifloxacin and Mox-mPH NPs (1:70, 100, 150).

Formulation	Zone of Inhibition (mm)		
	Pseudomonas Aeruginosa	*Staphylococcus Aureus*	*Streptococci Pneumoniae*
Free Drug	11.1	13.0	7.3
Mox-mPH NPs 1:70	19.3	18.2	20.6
Mox-mPH NPs 1:100	20.1	22.6	21.2
Mox-mPH NPs 1:150	22.3	26.0	23.3

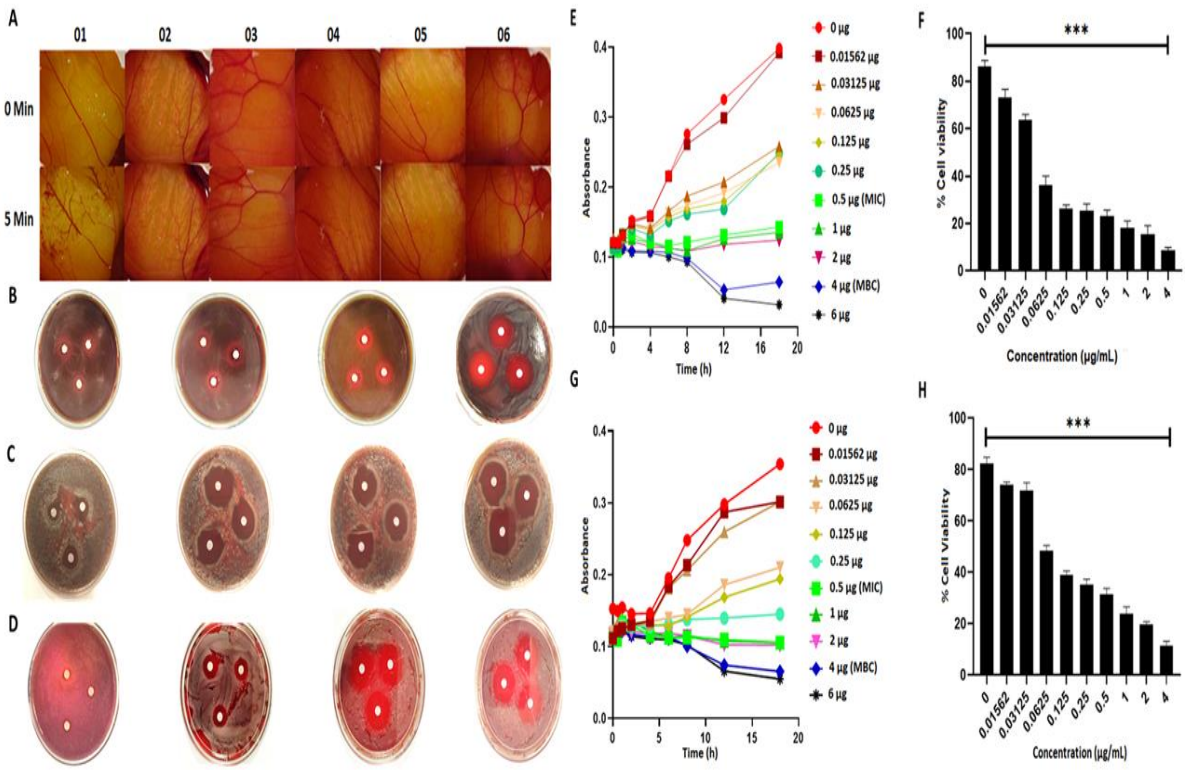

Figure 2.8. HET-CAM test. The photograph of CAM membrane exposed to free drug solution and formulations (01-06) indicates Control, free drug solution, Mox-mPH NPs of 1:70, 100, and 150 respectively (A); zone of inhibition of bacterial growth, *Pseudomonas aeruginosa*, (B); *Staphylococcus aureus* (C), and *Streptococci pneumoniae* (D) using Mox HCl aqueous solution, and Mox-mPH NPs, 1:70, 100, and 150 (left to right) at Mox HCl dose of 5 µg/mL; determination of minimum inhibitory concentration (MIC) of Mox-mPH NPs (1:70) by optical density measurement (OD_{600}) against *P. aeruginosa* and *S. aureus* (E, and G), respectively; determination of minimum bactericidal concentration (MBC) by MTT assay against *P. aeruginosa* (F) and *S. aureus* (H), the data are represented as n=3, P<0.001 as ***.

The fluorescence microscope images of bacterial cells treated with Mox-mPH NPs (1:100 and 150) indicated more red cells (PI labeled) than those treated with 1:70 NPs. The Mox-mPH NPs (1:70) displayed a higher population of SYTO-9 labeled cells than PI-labeled populations. The quantitative assessment of live-and-dead cell populations was performed by flow

cytometry, where Q1 and Q3 quadrants represent live cells, and the shifted cells in Q2 and Q4 quadrants represent the dying/dead cells population (**Figure 2.9**).

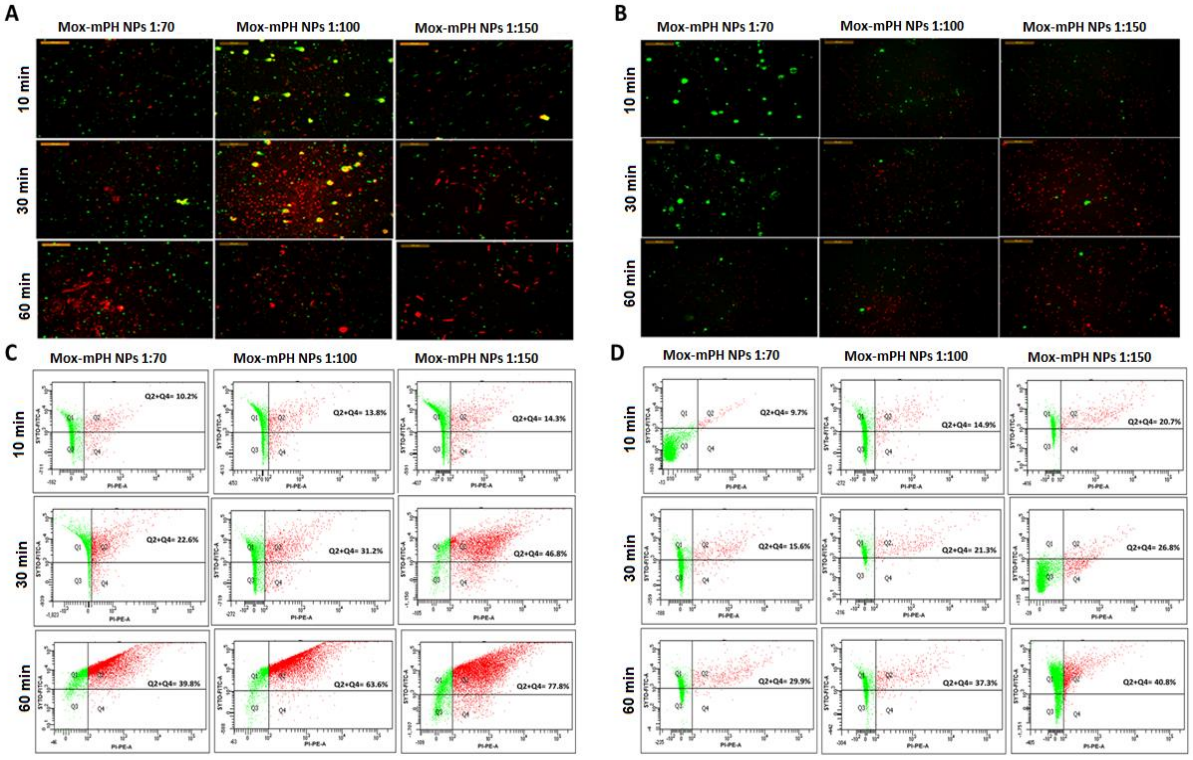

Figure 2.9. Live/dead assay of *P. aeruginosa* and *S. aureus* treated with Mox-mPH NPs (1:70, 100, 150). The fluorescence images of bacteria treated with Mox-mPH NPs for 10, 30, and 60 min, *P. aeruginosa* (A) and *S. aureus* (B), scale bar 100 µm; the flow cytometric quadratic dot plot diagram displaying the SYTO-9 and PI-stained cells populations. The cell populations in Q1, Q3, and Q2, Q4 quadrants represent live and dead cell populations, respectively (C, D). Overall, both bacteria had a time-dependent increase in the red cell population following Mox-mPH NPs treatment. Total Q2 and Q4 populations were estimated to be 39.8, 63.6, and 77.8% for Mox-mPH NPs of 1:70, 100, and 150, respectively, in *P. aeruginosa*. The values were 29.9, 37.3, and 40.8%, respectively, for *S. aureus*.

2.2.3.3. *In vivo* studies

The ocular fluorescence intensity, based on the region of interest, was $7.08e^{+009}$ AU, $1.5e^{+010}$ AU, and $2.08e^{+010}$ AU, 5 min after administering the mPH NPs, 1:50, 100, and 150,

respectively, which reduced to 5.48e^{+009} AU, 7.4e^{+009} AU, and 7.7e^{+009} AU after 30 min. mPH NPs, 1:150 showed the highest retention over the cornea till 360 min, the maximum tested time point with fluorescence intensity of 3.14e^{+009} AU. mPH NPs, 1:70 displayed signals till 240 min (3.14e^{+007} AU), whereas mpH NPs of mol ratio 1:100 showed detectable fluorescence signal (3.08e^{+009} AU) till 300 min (**Figure 2.10**).

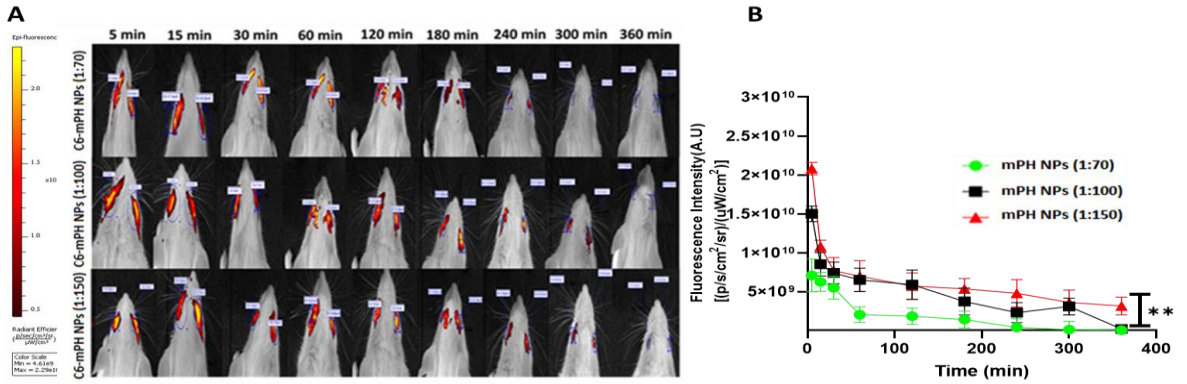

Figure 2.10. Real-time *in vivo* fluorescence imaging of mice administered mPH NPs (1:70, 100, 150) (fluorescently labeled) topically on eyes (A); graphical representation of mean ocular fluorescence intensity following treatment with formulations (B). Data are represented as mean ±SD (n=4, $p<0.01$ as **).

In the *in vivo* antimicrobial study, the cornea images taken using a camera attached to a macro lens indicated that all mice developed BK. The mean bacterial load (CFU) counts of the group treated with Mox-mPH NPs (1:70, 100, and 150) were 17450, 4150, and 2866/mL, with the mean clinical scores of +3, +1, and +1, respectively (**Figure 2.11**). Moxifloxacin HCl showed minimal effect with a CFU of 59650/mL and a clinical score of +4.

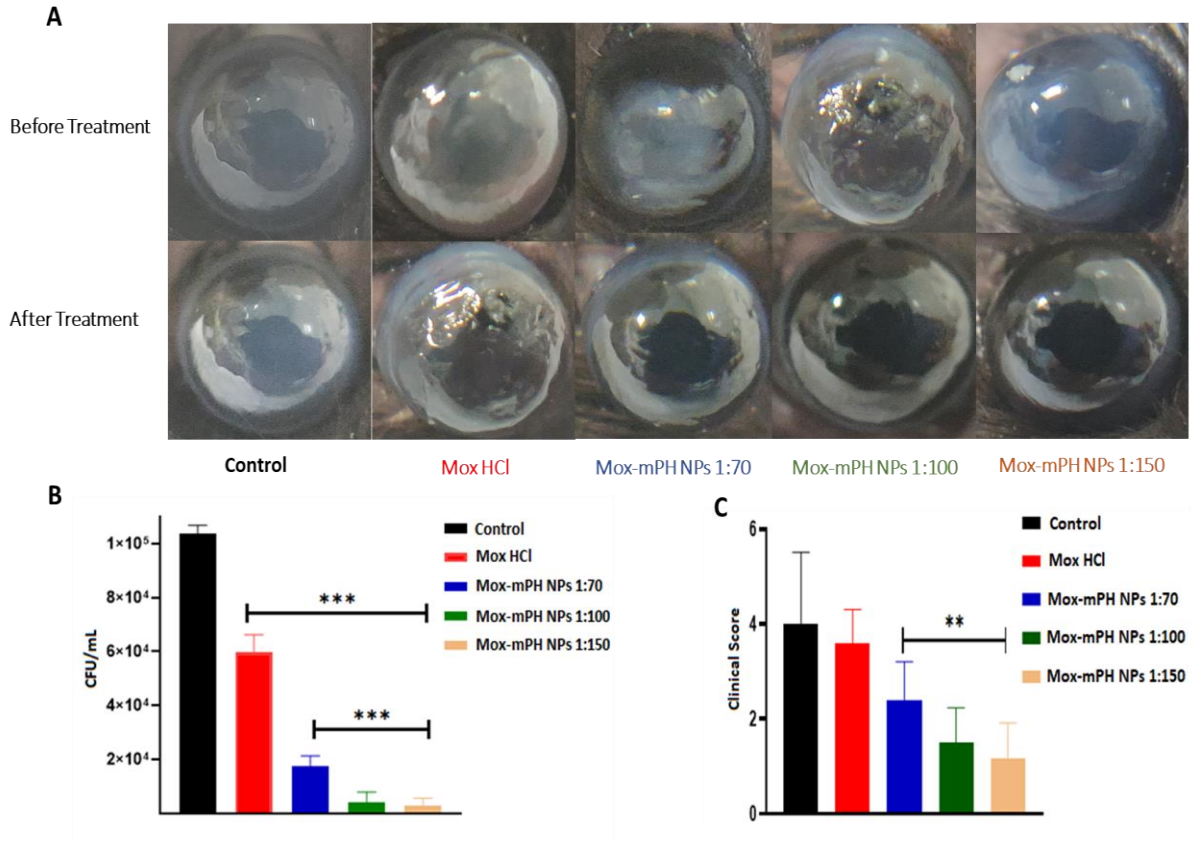

Figure 2.11. *In-vivo* therapeutic efficacy of Mox HCl-solution and Mox-mPH NPs (1:70, 1:100, 1:150) in *P. aeruginosa* infected bacterial keratitis. The images of the cornea before and after the treatment regimen; (A); bacterial load following treatment (B) the clinical score (0 to 5) based on the two criteria (transparent and perforated) (C) the data are represented as n=3, P<0.01 as **, and P<0.001 as ***.

2.2.4. Discussion

Various mol ratios of mPEG to HPMA monomers (1:70, 100, and 150) were taken to produce a reasonable hydrophobic and hydrophilic balance in the polymer mPEG-bHPMA. Since the polymeric blocks, mPEG, and HPMA are hydrophilic; the resultant nanoparticles have HLB to a higher side resulting in the efficient loading of the water-soluble drug moxifloxacin (**Table 2.5**). The hanging-free hydroxyl groups of HPMA are anticipated to offer non-covalent interactions with the secondary amine, ketone, ether, and acid groups of moxifloxacin. The poly(propylene) backbone in methacrylamide provided enough hydrophobicity for polymeric

self-assembly(Bobde et al., 2020a). The yields of monomers' attachment to mPEG were satisfactory, 95.6, 97.8, and 96 % for the feed ratios of 1:70, 100, and 150, respectively, as extrapolated from GPC analysis. mPH NPs (1:150) demonstrated the lowest CAC anticipating its ability to encapsulate the payload and carry it successfully without disassembling following dilution. The changes in two factors, the volume of rehydration and the polymer amount, significantly impacted the NPs characteristics with wide variations in the experimental formulations analyzed by CCD (**Table 2.3**). However, the low standard deviations between the predicted and observed variables of the optimized mPH NPs (1:70), mainly in % DL and % EE, indicated the robustness of CCD (**Table 2.4**). The optimized formula from CCD using the mPEG-HPMA (1:70) was applied to NPs preparation using other mPEG-bHPMA polymers of 1: 100 and 1:150. The particle size, drug loading, and drug encapsulation efficiency of prepared mPH NPs (1:50, 100, and 150) were satisfactory, mPH (1:150) was observed to have the smallest size, lowest polydispersity index, highest drug entrapment, and drug loading efficiencies.

The disappearance of Mox peaks in the Mox-mPH NPs XRD spectra indicated that the encapsulated Mox was in the amorphous form. The disappearance of the endothermic peak of Mox in mPH NPs (1:150) meant that the NPs encapsulated the drug in the core. The IR spectra of mPH NPs displayed the amalgamated peaks of mPEG-bHPMA and Mox, suggesting both the components' co-existence. The drug release study indicated that mPH NPs (1:150) released the loaded drug sustainably compared to other formulations. The permeation of Mox through goat cornea was maximum for mPH NPs (1:150) compared to the other tested nanoparticle formulations and free Mox as analyzed by the Franz diffusion technique. The low penetration of free Mox necessitates the development of advanced drug delivery systems for better penetration of the drug through ocular barriers and exertion of antibacterial action.

The toxicity of NPs has been assessed in three different experiments, including TEER studies, cell viability by MTT assay, and the HET-CAM test. The mPH NPs disturbed the membrane integrity to some extent, with nanoparticles 1:150 showing the highest perturbation. However, the multilayer epithelial cell layer returned to normalcy after a brief period without irreversible damage. Cell viability assay also suggested a similar outcome of no toxicity at the tested dose and incubation time. HET-CAM test did not exhibit blood clotting or hemorrhagic blood vessels as observed in the case of positive control, indicating the non-irritancy and overall non-toxicity of the polymeric nanoparticle systems (**Figure 2.8, Table 2.6**). The polymer blocks, HPMA and mPEG, have good water solubility and biocompatibility. Therefore, the toxicity evaluation proved the nanoparticle system safe for ocular application.

The NPs' adhesiveness to mucous membranes has been tested by various studies, including texture analyzer, falling liquid film method, mucin turbidity study, and *in vivo* image analysis. The mPH NPs, 1:150, adhered robustly to goat intestinal mucosa. The enhanced turbidity of mucin solution in the presence of nanoparticle solutions indicated their interaction with each other, resulting in aggregates' formation. The *in vivo* image analysis of mice treated with fluorescently labeled mPH NPs (1:70, 100, and 150) confirmed the highest muco-adhesivity of mPH NPs, 1:150. The strong interaction with mucous could be due to multiple hydroxyl groups in HPMA polymer that establish non-covalent interactions, including hydrogen bonding, electrostatic, and Vander Waals interactions with the mucin polysaccharides. The strong mucoadhesion is anticipated to result in higher penetration of the multiplayer cornea resulting in an antibacterial effect.

The time-dependent penetration efficiency of NPs through corneal epithelial cell layers was judged by uptake studies using corneal epithelial cells grown in monolayers and spheroids. The right shift of the nanoparticles-treated cells in the flow cytometry histogram plots compared to control cells indicated the nanoparticles' cellular association. The formulation with mPH NPs

(1:150) has shown high statistical significance of ***, $p<0.001$ compared to the other formulations. The Z-stack images are obtained by moving the objective in the z-axis between each captured image. The confocal micrographs of spheroid at various depths of fields (20-150 µm) indicated that the mPH NPs (1:150) penetrated the deepest in tissues than other nanoparticles. The higher penetration efficiency in mPH NPs (1:150) could be due to the enhanced hydrophobicity of the mPEG-bHPMA polymer (1:150). Methacrylate backbone could impart the optimum hydrophobicity required for penetration. In antibacterial studies, mPH NPs (1:150) exerted maximum antibacterial effect with the highest zone of inhibition. The antibacterial effect was twice and thrice as much as free Mox solution in *P. aeruginosa* and *S. Pneumoniae*, respectively. The live-dead cells assay was performed to validate the zone of inhibition studies. The largest number of dead cells population was observed under a fluorescence microscope following the treatment of bacteria with Mox-mPH NPs (1:150) compared to other treatments. The quantitative analysis was performed using flow cytometry, and the data corroborated the fluorescence microscopic observation.

Further, the therapeutic efficacy of the Mox solution and Mox-mPH NPs (1:70, 100, and 150) were analyzed in a mouse model of bacterial keratitis. The results indicated that the mPH NPs (1:150) reduced the clinical score significantly compared to free Mox solution and mPH NPs (1:70). The bacterial plate count method was used to assess the live bacterial load in the cornea. The results indicated that the live bacterial count in eyes decreased significantly in all the mice treated with Mox-mPH NPs than the control and the Mox-solution treated mice. The experiment used Mox eye drop, the conventional dosage form for topical administration, as a control. The high bacterial count (CFU/mL) indicated that the treatment regimen was ineffective for conventional Mox eye drop formulation. The free drug could not penetrate the ocular barrier and the bacterial cell wall. The Mox-mPH NPs nanomedicine stayed in the

cornea longer, penetrated well through the corneal barrier, and effectively reduced the bacterial load.

Nanomedicines have better efficacy than conventional drug delivery systems(Meng et al., 2019; Omerović & Vranić, 2020). The increased penetration of nanomedicines causes the accumulation of a high concentration of antimicrobial agents in the cornea, resulting in an enhanced therapeutic effect compared to topical eye drop formulations. The tested nanoparticle's fluoroquinolone formulation has demonstrated multiple benefits over conventional topical eye drop formulation. Hence, it has the potential for clinical translation for treating bacterial keratitis.

2.2.5. Conclusion

Bacterial keratitis is a sight-threatening corneal infection, if untreated, could lead to blindness. The fourth-generation fluoroquinolone antibiotic moxifloxacin significantly lowers the severity of infection. However, temporary corneal residence time and poor penetration limit its bacterial cell-killing efficiency. Here, we improved therapeutic efficacy by preparing a nanoparticle form of moxifloxacin using a block copolymer combining two hydrophilic segments, mPEG, and poly(HPMA), at different molar ratios (1:70,100 and 150). The polymer and the Mox-loaded polymeric NPs were physicochemically characterized, and formulation parameters were optimized. The Mox-mPH NPs demonstrated optimum drug loading, sustained drug release, mucoadhesion, corneal retention, and penetration. The *in vitro* studies using the bacterial strain *Pseudomonas aeruginosa*, *Staphylococcus aureus*, and *Streptococci pneumoniae* demonstrated superior antibacterial efficacy of Mox-mPH NPs than the free Mox. The mPH NPs (1:150) demonstrated the highest therapeutic benefit in the *in vitro* and *in vivo* studies than other nanoparticles and the conventional free Mox solution. Therefore, the newly

developed eye-compatible nanomedicine of moxifloxacin could be a promising treatment option that qualifies for further exploration in bacterial keratitis.

Chapter 3

Chitosan-poly(lactide-co-glycolide)/Poloxamer mixed micelles as a mucoadhesive thermo-responsive moxifloxacin formulation to improve treatment efficacy in bacterial keratitis

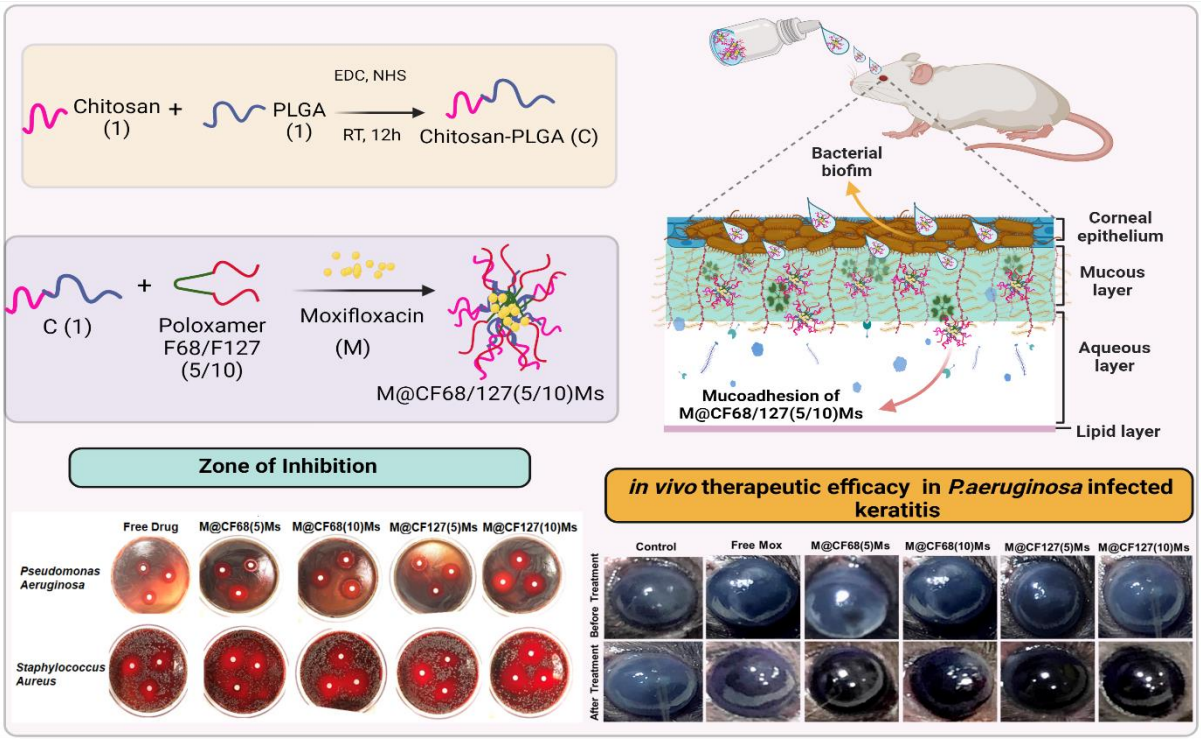

3.1 Introduction

Bacterial Keratitis (BK) is the leading cause of ocular infections leading to visual blindness globally (Teweldemedhin et al., 2017b). The factors prone to cause BK include unhygienic wearing of contact lenses, corneal damage, intraocular inflammation, age, undernourishment, and keratoconjunctivitis (H. Y. Lin et al., 2021; Schaefer et al., 2001b). Contact lens usage could cause superficial injury to the eye, low exchange of tears during blinking, and tear deflation under the contact lens, which results in the adherence of pathogenic bacteria to the corneal surface (Fleiszig et al., 2020c; Ting, Ho, et al., 2021c). Other factors associated with contact lens wear include using lenses overnight and poor hygienic conditions such as expired contact lenses, solutions, and infected cases (Dethorey et al., 2013; Sarwat et al., 2019). Early-stage treatment is necessary to avoid severe ocular vision loss by up to 50 % (Jones, 1981a; Wong et al., 2012b).

Both gram-positive and gram-negative bacteria are responsible for the pathogenesis of BK. *Pseudomonas aeruginosa* and *Staphylococcus aureus* are the most concerning pathogens(Argüeso et al., 2009b; C. Ezisi et al., 2018; Reichert & Stern, 1984). *P aeruginosa* is the most common isolate in corneal scrapings associated with contact lens use (Hilliam et al., 2020). Current therapy for BK is broad-spectrum antibiotics such as fluoroquinolones, including ciprofloxacin, moxifloxacin, and gatifloxacin, which act by inhibiting DNA synthesis in bacteria (M. S. Hanet et al., 2012b; Tsai et al., 2010). Conventional therapy includes the application of topical eye drops, which exert drawbacks, such as frequent drug administration due to lacrimal drainage, poor drug retention, and sub-optimal drug availability in deep layers of the cornea due to the difficulty in penetrating through the corneal tissue barriers and enzymatic degradation (Baranowski et al., 2014b; McKenzie et al., 2015; P. B. Patel et al., 2010; Varela-Fernández et al., 2020). Therefore, most drugs are eliminated immediately after administering the eye drops, with only 5% reaching the targeted site.

The tear film also acts as a defense mechanism for the eye, eliminating the pathogens by clearing the ocular surface and forming a hydrophilic layer, leading to drug loss (I. Ahmed & Patton, 1985). Therefore, to overcome the topical drug delivery limitations, a mucoadhesive approach is beneficial to increase the corneal retention time and eventual permeation of the drugs through the corneal epithelium. The mucoadhesive approach mainly involves the interaction of polymer chains and the mucin layer of the tear film. In this approach, the viscosity of polymer chains upon interaction with the mucus increases, resulting in an improvement of the residence time of the formulations on the cornea is prolonged without any irritation. The mucoadhesion of polymers may happen due to many theories, such as wetting theory, electrostatic theory, and diffusion theory (Bíró & Aigner, 2019; Shaikh et al., 2011c).

The researchers have done significant research on drug delivery systems such as micelles, nanosuspensions, nanoemulsions, liposomes, and dendrimers as an alternative to conventional therapy in treating ocular diseases of the eye's anterior segment. The development of novel drug delivery systems has significantly improved the absorption of topically applied drugs in the eye; also, ocular retention time and permeation through the cornea were improved. Especially, micelles offer a wide range of advantages as they enhance the solubility of poorly soluble drugs and improve their feasibility of being used as eye drops(Afarid et al., 2022; Onugwu et al., 2023; Vaneev et al., 2021). Micelles are composed of amphiphilic molecules that self-organize in an aqueous solution to form nanoparticles of size ranging from (10-1000 nm). Micelles can be prepared with a wide range of biocompatible and biodegradable polymers, eliminating toxicity and ocular irritation. Micelles provide high encapsulation of drugs with good corneal permeation. Their property of prolonged stability in the tear fluid can be used to increase the contact time with the cornea. All these advantages made nano micellar a popular ocular drug delivery system (Mandal et al., 2017c; Özsoy et al., 2019).

The second most abundant naturally occurring polycationic, linear polysaccharide chitosan (CS) exhibits strong mucoadhesion by forming hydrogens and ionic bonds between the chitosan amines and negatively charged sialic acid residues of mucin glycoproteins (Sogias et al., 2008a). Besides mucoadhesion, chitosan is biocompatible and exerts antibacterial and wound-healing properties (Anitha et al., 2011; Cheng et al., 2016; Eltis, 2011; Itoo et al., 2022a; J. Jung et al., 2020; L.-H. Li et al., 2010). Poly-(lactide-*co*-glycolide) (PLGA) is an anionic, biocompatible, and biodegradable polymer and is the most frequently used carrier for the delivery of drugs and other macromolecules (Chen et al., 2021; Kaur et al., 2020; Santos et al., 2017; Zeng et al., 2021). PLGA has found wide application in forming hydrophobic cores in polymeric micelles or nanoparticles that drives the self-assembly process in forming nano-spherical structures with low polydispersity. Poloxamers are thermoresponsive amphiphilic triblock copolymers composed of a central hydrophobic polypropylene oxide and two hydrophilic polyethylene oxide chains (Giuliano et al., 2018; Zarrintaj et al., 2020). Poloxamers of different grades impart various degrees of hydrophobicity based on the varying chain length.

In this study, we designed a mixed micellar delivery system using chitosan, PLGA, and poloxamers to treat bacterial keratitis (BK). Although the antibacterial activity of chitosan has been previously established, the employment of chitosan in the development of mixed micelles that encapsulate moxifloxacin, and the comprehensive assessment of the effectiveness of this micellar system against various bacterial strains, constitutes a novel scientific advancement. Here, we conjugated chitosan to PLGA at a chitosan: PLGA ratio of 1:1. The synthesized CS-PLGA (C) was mixed with poloxamer, either F68 or F127 at C: F68/F127 ratio of 1:5 or 10 to form nano mixed micelles (Ms) that encapsulated the fluoroquinolone antibiotic, moxifloxacin (M). The prepared mixed micelles, M@CF68(5)Ms, M@CF68(10)Ms, M@CF127(5)Ms, and M@CF127(10)Ms were thoroughly characterized physicochemically. The Ms, preferably M@CF68/127(10)Ms, showed strong mucoadhesion and long corneal retention time. Ms were

non-toxic to the corneal cells and penetrated the cornea effectively. The newly developed formulations enhanced the antimicrobial ability against P aeruginosa and S aureus and destroyed the biofilms compared to the moxifloxacin solution. The therapeutic efficacy was evaluated in P aeruginosa or S aureus-infected BK mice models. Our findings suggest that this newly developed mixed micellar drug delivery system may exhibit enhanced therapeutic efficacy for BK in clinical studies.

3.2 Materials and methods

3.2.1 Materials

Chitosan (Mw-15 KDa) was purchased from Polysciences, USA, *N*, *N*-dicyclohexylcarbodimide (DCC), dimethyl-4-aminopyridine (DMAP), N, N-Diisopropylethylamine (DIPEA), and poloxamers F68 and F127 were purchased from Sigma-Aldrich/Merck (Darmstadt, Germany). Polylactide Glycolide (PLGA 50:50) was procured from Poly-SciTech, USA. Moxifloxacin HCl was received as a gift sample by MSN Laboratories Pvt Ltd (Hyderabad, India). Fluorescein isothiocyanate (FITC-NHS), Coumarin 6, SYTO9, and PI were purchased from Thermo Scientific (USA). The MTT reagent was procured from Hychem laboratories (Hyderabad, India). All the solvents used in the study were purchased from SRL chemicals (Hyderabad, India). The dialysis membrane (MWCO 3500 Da and 12-14000 Da) was obtained from Spectrum Laboratories, Inc. (USA).

The human corneal epithelium, HCE cell line, was a gift from Dr. Sanhita Roy's lab at the L.V. Prasad Eye Institute, Hyderabad, India). Fetal bovine serum (FBS), Dulbecco's modified Eagle's medium F-12 (DMEM F-12), and penicillin/streptomycin solution were purchased from Himedia Laboratories (Mumbai, India). HCE cells were sub-cultured in DMEM F-12 media supplemented with 10% fetal bovine serum and 100 IU/mL of antibiotic penicillin/streptomycin. The cell-seeded flasks were kept in a sterile, humidified atmosphere at 37 °C and a 5 % CO_2 incubator.

All the animal experiments complied with the National Research Council's Guide for the Care and Use of Laboratory Animals (eighth edition). The study was conducted with approval from the Institutional Animal Ethics Committee of BITS-Pilani, Hyderabad, under protocol approval

number BITS-Hyd/IAEC/2020/51. Male mice (C57BL/6 and BALB/c) of approximately 18 g (5-6-week-old) were procured from the Sainath agencies, Hyderabad, India. The animals were accustomed to the following conditions: temperature, 19−25 °C, nocturnal−diurnal cycles for 1 week, and relative humidity of 50−60 % with free access to food and water.

3.2.1. Methods

3.2.2. Synthesis of CS-PLGA copolymer and characterization

CS (10 mg in 1mL of 1 % glacial acetic acid (GA)) was dissolved under continuous stirring for 3-4 h at 300 rpm. PLGA (30 mg) was activated by adding EDC and NHS in 0.5 mL of DMF upon continuous stirring at 400 rpm for 4-5 h (25 °C) in the presence of DIPEA. The activated PLGA solution was added dropwise to the CS solution along with the DIPEA. The reaction was stirred continuously overnight and evaporated (**Fig. 3.1A)**. The concentrate was dialyzed using cellulose ester dialysis membrane (MWCO- 12-14 KDa) against deionized (DI) water for 48 h. The resultant solution was lyophilized.

The chitosan, PLGA, and CS-PLGA structures were confirmed using ^{1}H NMR. The conjugate (4-5 mg/mL) and PLGA were dissolved in deuterated DMSO. Chitosan was dissolved in D_2O-containing acid, and spectra were recorded using a Bruker spectrometer (300 MHz Bruker, USA) operated at 300 MHz at 25 °C. The molecular weight of the chitosan, PLGA, and CS-PLGA was analyzed by GPC (Waters Corporations, USA), using ultrahydrogel™ linear (7.8 × 300 mm column) and refractive index as a detector. The analysis was performed under a flow rate of 1 mL/min (15 µL injection volume) using 1 % v/v glacial acetic acid as a solvent. The calibration curve determined the molecular weight using shodex standards having molecular weight ranges from 6300-530000 Da. The functional groups of the synthesized copolymer were analyzed by FTIR spectroscopy following the KBr pellet method, as previously reported (Kumari, Paul, Bobde, et al., 2020). The spectra were recorded over 400-4000 cm^{-1} using an FTIR (JASCO-4200, Japan).

3.2.3. Synthesis of FITC-labeled chitosan

CS was labeled by FITC at a 1:1 mol ratio. Briefly, CS was dissolved in 1 % v/v GA (2 mL), and FITC was dissolved in methanol (1 mL). The two solutions were mixed and kept for stirring at ambient temperature for 3 h. 0.5M NaOH (1 mL) was added to the reaction mixture to precipitate the CS-FITC. The obtained residue was washed with distilled water and separated by centrifugation. The CS-FITC was dissolved in 20 mL 0.1M acetic acid and dialyzed for 3 days in the dark with distilled water, and PLGA was conjugated as described in section 2.2.1.

3.2.4. Preparation of Mox-loaded Ms

The M@CF68/127(5/10)Ms were prepared by dialysis following the previously reported procedure (Kumari, Paul, Bhatt, et al., 2020). Briefly, PLGA was activated using EDC and NHS before reacting with CS. CS-PLGA copolymer solution (5 mg in 1000 µL acetic acid further diluted with 2.5 mL of DMF) and Mox solution (1 mg/mL in Milli-Q water) were mixed continuously for 15 min at room temperature. Pluronic F68 or Pluronic F127 (5 mL) in Milli-Q water was added dropwise under magnetic stirring. The stirring was continued overnight at room temperature. Two mixed micellar formulations were prepared at two ratios of CS-PLGA: poloxamers (for each poloxamer, F68 or F127), 1: 5 or 1: 10. The formulations prepared are as follows: Later, the solution mixture was subjected to dialysis against phosphate buffer saline, pH 7.4, using cellulose membrane (molecular weight cutoff (mcwo) 6-8 KDa) for 24 h to remove the organic solvents and aid in the micellar formation. The micellar solution thus obtained was centrifuged at 10,000 rpm for 20 min at 4 ˚C. The supernatant was collected and evaluated to determine the characteristic properties of the mixed micelles. The prepared mixed micelles, M@CF68(5)Ms, M@CF68(10)Ms, M@CF127(5)Ms, and M@CF127(10)Ms were lyophilized using mannitol as cryoprotectant. Coumarin 6 (C6) loaded polymeric micelles were prepared by following the procedure mentioned above, having the exception of replacing Mox with C6.

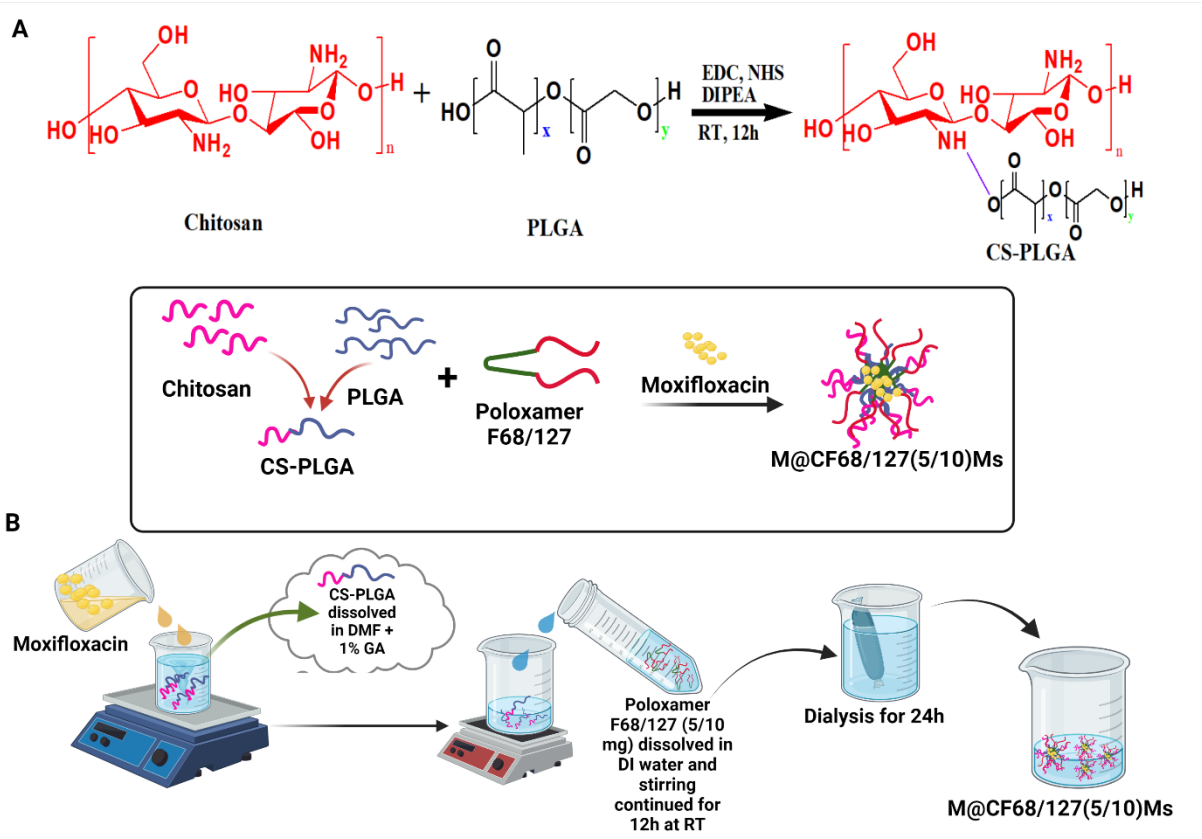

Figure 3.1. Synthetic scheme of CS-PLGA conjugate (A); Graphical presentation of preparation of mixed micelles (B).

3.2.5. Characterization of mixed micelles

The particle size and surface charge of the Mox-Ms were determined by the Dynamic Light Scattering (DLS) technique using the Zetasizer™ ZEN 3600 instrument (Malvern Instruments Ltd., UK). The mean size of the micelles was analyzed at a scattering angle of 90° at 25 °C. All the samples were analyzed in triplicates. The lyophilized Mox-Ms powders were spread on a holder attached to carbon tape to determine morphology. The powder was evenly distributed and gold-coated for 30 min. Carbon tapes containing samples were placed on a sample holder, and images were taken using a field emission scanning electron microscope (FESEM) (Apreo Lo Vac, FEI, USA).

3.2.6. Determination of Drug loading and Entrapment Efficiency

Mox loading in mixed micelles and the entrapment efficiency were determined by following the previously reported procedure (Kumbham et al., 2020). The mixed micelles were breached by diluting with methanol, and the amount of drug loaded was determined using a UV spectrophotometer (Jasco-UV 670, Japan) at 290 nm wavelength. The % DL and % EE were calculated using the following equations:

$$\% \text{ DL} = \frac{\text{Amount of drug in micelles}}{\text{The initial amount of polymer and drug}} \text{ x } 100$$

$$\% \text{ EE} = \frac{\text{Amount of drug in micelles}}{\text{The initial amount of drug taken}} \text{ x } 100$$

3.2.7. Determination of Critical Micelle Concentration (CMC)

3.2.7.1. By Pyrene incorporation method

The pyrene incorporation method was used to determine CMC following a previously published procedure (Kumbham et al., 2020). Pyrene solution (50 µL, 10 mg/mL chloroform solution) was taken in glass vials. The chloroform was evaporated under nitrogen gas, and then the mixed polymeric solutions CF68(5), CF68(10), CF127(5), and CF127(10) of different concentrations (3.125-200 µg/mL) were added and incubated for 24 h at 37 $^{\circ}$C. Finally, the solutions were filtered using a syringe filter (0.45 µM). 200 µL of each polymer concentration was taken in an amber-colored 96-well plate. Absorbance was recorded using a Spectramax™ M4 microplate reader at an excitation/emission wavelength of 339/390 nm.

3.2.7.2. By Surface tension method

The CMC of the polymers CF68(5), CF68(10), CF127(5), and CF127(10) were determined by surface tension method using a tensiometer (Biolin scientific (Theta Flow), Sweden). The pendant drop method was used, and polymers with various concentrations between 0.125-200 µg/mL were prepared and used for the analysis. The total volume of polymers containing 600 µL was kept

inside the sample holder, 200 µL was pipetted out as a drop, and the surface tension at each concentration was determined concentration at which no change in the surface tension value was considered as CMC.

3.2.8. DSC

Calorimetric studies were performed for the free drug and micelles using DSC 60, Shimadzu, Japan calorimeter following the previously reported procedure (Kumari, Paul, Bobde, et al., 2020). Briefly, the Mox and the Mox-Ms were accurately weighted (4-5 mg) and loaded in the aluminum pans. The pans were subjected to compression and analyzed over a 30-300 °C temperature under a nitrogen atmosphere at a flow rate of 20 mL/min with a heat exchange rate of 10 °C/min.

3.2.9. XRD

The structural properties of the Mox and formulations were analyzed using a powder X-ray diffractometer (ULTIMA-IV, Rigaku, Japan). The Mox and Mox-Ms were analyzed using the instrument equipped with a Cu anode (λ= 1.54 Å) operated at a voltage and current of 40 kV and 30 mA, respectively. Data were collected at 2θ from 5 ° to 70 ° at a scanning rate of 5 °/min.

3.2.10. Trans-corneal permeation study

Ex vivo permeability studies of Mox and Mox-Ms (500 µg of Mox) were carried out using a Franz diffusion cell through goat corneal tissue. The tissue was placed between the donor and receptor compartment, with an exposure area of 0.6399 cm^2. Different formulations equivalent to 500 µg of Mox were added to the donor compartment. The receptor compartment was filled with 5 mL of simulated tear fluid (STF), pH 7.4. The bath was maintained at 37 ± 1 °C under continuous stirring. At predetermined time intervals, 300 µL of samples were withdrawn, and the same volume of fresh STF was added. The withdrawn samples were filtered using a syringe filter, diluted if necessary, and quantified for drug content by HPLC at 290 nm. The study was performed three times, and the graph was plotted for the percentage of drug diffused versus time (h).

3.2.11. *In vitro* Drug release study

1 mL of Mox and Mox-Ms (equivalent to 500 µg Mox) was taken in a dialysis bag (MWCO 3.5 kDa). The dialysis bag was placed in a beaker containing 100 mL of STF, pH 7.4, with constant stirring (300 rpm) at 37 °C. At predetermined time points, 1 mL of aliquots were taken and replaced with the same volume of fresh STF. HPLC (Shimadzu, Japan) with Phenomenex C18 column was used to analyze the amount of drug released. In addition, cumulative drug release for up to 24 h was calculated.

3.2.12. Determination of contact angle

The contact angles for the formulations, CF68(5)Ms, CF68(10)Ms, CF127(5)Ms, and CF127(10)Ms, were determined using a tensiometer (Biolin Scientific theta flex, Sweden). The goat cornea was fixed at the bottom of the sample holder. Formulations of concentrations between 0.5-3 % w/v were prepared, and 600 µL was taken into the sample holder. 200 µL of the sample was dropped on the corneal tissue, and the angle at which the formulation spread on the cornea was determined.

3.2.13. Temperature-dependent viscosity studies

The viscosity of CF68/127(5/10)Ms has been studied at various temperatures (25-60 °C) at different concentrations (0.5-3 %w/v) and was determined by using an Anton-Paar rheometer (MCR 302, Austria)(Han et al., 2020b; Henderson et al., 2009).

3.2.14. Stability Studies

Mox-Ms was kept at room temperature (RT) and 4 °C for 30 days. The formulations were periodically tested for particle size analysis and drug loading, and the observations were plotted.

3.2.15. Mucoadhesive studies

3.2.15.1. Mucoadhesion using a texture analyzer

The texture analyzer (Stable Micro Systems, Surrey, UK) was used to determine the mucoadhesive strength of Ms, CF68/127(5/10)Ms by using a goat intestinal membrane (Laulicht et al., 2012b). Freshly excised goat intestine from the slaughterhouse was washed thoroughly with normal saline and cut into the required size. The basement membrane was fixed onto the basement probe and the stainless-steel probe on the moving arm of the texture analyzer. Moving arm at a speed of 0.5 mm/sec was allowed to touch the micelles solution located on the luminal side of the membrane with a contact force of 5 g. After applying a force of 100 g and holding for 120 sec, the probe moved up at a 0.1 mm/sec speed. The force (g) required to detach the probe from the membrane was plotted and considered the mucoadhesive strength.

3.2.15.2. Falling liquid film method

The falling liquid film method was also performed to determine the mucoadhesive property of the CF68/127(5/10)Ms (Choy et al., 2008). The freshly excised goat eyeballs procured from the slaughterhouse were used for this study. Corneas with scleral rims were dissected from freshly excised goat eyeballs procured from the slaughterhouse and placed in PBS of pH 7.4. The FITC-labeled micelles (~200 µL, 3.3 mg/mL) were added to the cornea at the center towards the epithelial side and incubated for 30 min. With the help of double-sided tape, the cornea was placed on the wall of a falcon tube at an angle of 45°. The simulated tear fluid (STF) of pH 7.4 was allowed to flow over the cornea at a rate of 1 mL/min, which was adjusted using a peristaltic pump. The difference between the fluorescently labeled formulation applied and the formulation collected in STF was used to measure the adhered micelles.

3.2.15.3. Mucin turbidity study

The mucoadhesion potential of the CF68/127(5/10)Ms was determined by measuring the turbidity of the mucin incubated with micelles. 1 mL of mucin solution (1 mg/mL) was incubated with 500 µL of Ms (1 mg/mL) at 37 °C under constant shaking (100 rpm). At specific time intervals, the absorbance of the solution was measured using a UV-Vis spectrophotometer (Jasco, Japan).

3.2.16. *In vitro* studies

3.2.16.1. Cell Culture

The human corneal epithelium (HCE) cell line was obtained as a gift from Dr. Sanhita Roy's lab at the L.V. Prasad Eye Institute, Hyderabad, India. Fetal bovine serum (FBS), Dulbecco's modified Eagle's medium F-12 (DMEM F-12), and penicillin/streptomycin solution were purchased from Himedia Laboratories (Mumbai, India). DMEM f-12 media containing fetal bovine serum (10 %) and penicillin/streptomycin (100 IU/mL) was used to sub-culture HCE cells and incubated at 37 °C with 5 % CO2 in a humidified sterile atmosphere.

3.2.16.2. Cytotoxicity by MTT assay

MTT assay was performed to determine the *in vitro* cytotoxicity of the HCE cells as per the previously published protocol (Kumari, Paul, Bobde, et al., 2020). In 96-well plates, HCE cells of 2 x 10^4 density/well were seeded in DMEM-F12 complete growth media and incubated at 37 °C for 24 h. The CF68/127(5/10)Ms solutions of various concentrations were added to wells and incubated for 24 h. No treatment was given to the control HCE cells. After 24 h, supernatant media was discarded and added with 100 µL of MTT solution (5 mg/ mL), incubated for 4 h, and then replacement of MTT solution with 150 µL of DMSO. After an additional incubation for 30 min, the absorbance of the well plate was analyzed using a microplate reader (Spectramax™, Molecular Devices, USA) at 590 nm (reference wavelength 620 nm). The following equation was used to calculate the percent cell viability:

% cell viability= Abs (sample) /Abs (blank) X 100, where Abs (sample) = the absorbance of the cells treated with drug-loaded polymeric micelles solution. Abs (control) = the average absorbance of the control cells. The study was carried out in triplicates and expressed as mean ± SD.

3.2.16.3. Cellular uptake by confocal microscopy and flow cytometry

3.2.16.4. By Confocal microscopy

HCE cells in monolayers and spheroids were treated with CS-FITC conjugated CF68/127(5/10)Ms (FITC-Ms) for 1 and 4 h according to the previously published procedure (Muddineti et al., 2017).

3.2.16.5. Cellular uptake in HCE monolayer cells

Briefly, for cellular uptake in monolayer cells, HCE cells at a density of $5X10^4$ were seeded on coverslips and kept incubation for overnight. The next day, the cells were treated with FITC-Ms (5 µg/mL of FITC) in serum-free media and incubated for 1 and 4 h, followed by washing the cells with PBS and stained with 100 µL DAPI (6 µg/mL) in PBS for 5 min. Cells were treated with 4 % paraformaldehyde for 20 min at room temperature and allowed for fixation. With the aid of fluoromount-G, the coverslips were mounted on slides and visualized under a confocal microscope (Leica Microsystems, Germany) at Ex/em wavelengths of DAPI (358/461 nm) and FITC (491/516 nm), respectively. The images were processed using *Image J* software.

3.2.16.7. Cellular uptake in HCE spheroid cells

The liquid overlay method was used to prepare HCE spheroids. 50 µL of sterile agar solution (1.5 % w/v in DMEM F12 media) was added to the wells of the 12-well plate. 150 µL of HCE cells of 1 x 10^4 /well density were added to each well and kept in shaking. The spheroids were used for further studies after reaching the diameter of 800 µm. The spheroids were incubated with the FITC-Ms solution. Z-stacking Images were taken by focussing the lens at various depths on the Z-axis from the surface of cells, and images were processed by *Image J* software.

3.2.16.8. By Flow cytometry

For flow cytometry studies, HCE cells at a density of 0.2 $x10^6$ /well were seeded in 12-well plates and kept at incubation overnight, followed by treating the cells with FITC-Ms (FITC -5 µg/mL) for 1 and 4 h. After washing the cells with PBS, trypsinized, centrifuged, and suspended in PBS, pH 7.4. Flow cytometry (FACS ARIA III, BD Life Sciences) assessed the micellar uptake of the

viable cells, and the cells were gated using a forward and side scatters plot. 10,000 viable cells were analyzed for fluorescence from each treatment group, and results were plotted using FlowJo software version 10.7.2.

3.2.16.9. Trans-epithelial Electrical resistance (TEER) measurement

Transcorneal penetration efficiency of Mox-Ms was performed by using the HCE cell line. The HCE cells at a density of ($1x10^6$ /well) were seeded onto the collagen-coated 12-well permeable inserts (Corning™, USA) for ten days. The TEER values were determined by the EVOM volt-ohm meter (Millicell®ERS-2, Millipore). After reaching the TEER value of 170 Ω $cm^{2,}$ the cell layers were treated with 0.1 mL of Mox-Ms formulations by adding to the apical chamber and kept at incubation for 5 min. At predetermined intervals, the transepithelial voltage was measured by touching the membrane surface with the electrode tip that uses alternating current.

3.2.17. HET-CAM test

Fertilized hen's eggs were obtained from a hatchery farm and incubated at 37 ± 0.5 °C. Eggs were positioned in such a way to ensure the development of the embryo away from the chorioallantoic membrane (CAM). The eggs were illuminated on day 10, and a 2X2 cm^2 shell was broken out using a drilling instrument, and a spinning cutting blade (M. M. Silva et al., 2017) 0.5 mL of saline solution was added to moist the inner membrane, which is closely attached to the CAM, and removed carefully without disrupting the blood vessels of the CAM. The redness was observed as ocular irritancy after treating the CAM with 0.5 mL of test formulations, CF68/127(5/10)Ms. Saline and 1M NaOH were used as the positive and negative controls, respectively.

3.2.18. Antibacterial studies

Bacterial strains

Pseudomonas aeruginosa and *Staphylococcus aureus* were obtained from LV Prasad Eye Institute and BITS-Pilani Hyderabad, India. Bacterial strains (*Pseudomonas aeruginosa* and

Staphylococcus aureus) were cultured in Luria Bertani (LB) Broth, Miller (HIMEDIA, INDIA) at 37 °C, and 85 % relative humidity aerobically. Strains were incubated, and subculturing was given to attain a bacterial concentration at an OD@600 nm of 0.2 for *Pseudomonas aeruginosa* (10^8 CFU/mL) and 0.6 for *Staphylococcus aureus* (10^9 CFU/mL) incubated at 37 °C (200 µL of overnight culture in 5 mL of LB broth). Serially diluted bacteria (PBS/LB broth) were used for further studies.

Biofilm Culture

P aeruginosa and *S aureus* (10^6 CFU/mL) in LB Broth were incubated on coverslips in a 12-well plate at 37 °C and 85 % relative humidity for 2 days. The next day, coverslips were removed and washed with PBS, pH 7.4, and utilized for further studies.

3.2.18.1. Determination of Minimum Inhibitory/Bactericidal Concentration (MIC/MBC)

The microtiter broth dilution method was used to determine the MIC per the previously published procedure (Ch et al., 2021a). Briefly, *P aeruginosa* and *S aureus* bacteria were adjusted to a 10^6 CFU/ mL density in LB broth. 100 µL of the bacteria were added to each well of 96 well plates and treated with 100 µL of various concentrations (0-4 µg/ mL) of M@CF68/127(5)Ms, followed by incubation at 37 °C for up to 12 h. Each well's visual turbidity and optical density were observed at different time points by measuring the absorbance at 600 nm.

MTT assay was used to determine the MBC to compare with the microtiter broth dilution method. Briefly, 100 µL of micelles formulations of varying concentrations (0-4 µg/mL) were added to *P aeruginosa* and *S aureus* (10^6 CFU/ mL in LB media) in a 96-well plate and incubated at 37 °C for 12 h followed by adding 50 µL of the MTT solution (5 mg/mL) and further incubated for 2 h. After incubation, the MTT solution was removed, and dimethyl sulfoxide was added to each well to dissolve the MTT reagent. The optical density was measured at 590 nm using a microplate reader instrument (Spectramax M4, Molecular Devices, San Jose, USA), keeping reference

absorption maxima at 620 nm. The below-mentioned equation was used for calculating the percentage of cell viability.

% cell viability = (Abs of sample)/(Abs of control) x 100

3.2.18.2. Zone of inhibition study

P aeruginosa and *S aureus* density were adjusted to 10^6 CFU/mL and spread over the solidified nutrient agar plates with sterile spreaders. Sterile circular paper discs were soaked in polymeric micelles solutions, placed on bacteria-inoculated agar plates, and incubated for 24 h. The diameters of the growth inhibition zones were measured after 24 h of incubation, and the pictures were captured using a digital camera.

3.2.18.3. Penetration study of Biofilms

The penetration study of biofilms was studied using a confocal microscope with some modifications (Wu et al., 2015). For uptake study in bacterial biofilms, bacteria *P aeruginosa* and *S aureus* (10^6 CFU/mL) were seeded on coverslips and incubated at 37 °C for 2 days. The following day, the biofilms were treated with FITC-Ms (5 µg/ml FITC) in serum-free media for 1 and 4 h. Later, the cells were washed with PBS and stained with 100 µL DAPI (6 µg/mL) in PBS for 5 min. Finally, the coverslips were mounted on slides using Fluoromount-G and visualized under a confocal microscope (Leica Microsystems, Germany) using Ex/em wavelengths of DAPI (358/461 nm), and FITC (491/516 nm), respectively. The images were processed using *Image J* software.

3.2.18.4. Live/Dead staining of bacteria by Fluorescence microscopy and flow cytometry

P aeruginosa and *S aureus* bacteria of 10^6 CFU/mL density were treated with 25 µg/mL of Mox-Ms (M@CF68/127(5/10)Ms) and kept at incubation for 10, 30, and 60 min at 37 °C followed by centrifugation of the bacteria at 6000 rpm for 10 min at 25 °C. The bacterial pellet was washed twice with sterile physiological saline solution (0.9 % w/v NaCl) and dispersed in 200 µL of pH 7.4 sterile PBS. 3 mL of the staining mixture of SYTO 9 and propidium iodide (PI) (1:1) in

concentrations of 33.4 µM and 0.4 mM, respectively, and kept in the dark for 10 min. After 10 min, the bacteria's images were captured using a fluorescence microscope (ex/em. 485/498 nm) (Leica, DMi8, Germany).

Freshly sub-cultured bacteria in LB broth media were used for flow cytometry studies. After adjusting the bacterial density, bacteria were centrifuged at 6000 rpm for 10 min, followed by washing with PBS (1X, pH 7.4) and resuspended in 500 µL of PBS. 25 µg/mL of Mox-Ms solutions were added to the bacterial suspension and incubated for 10, 30, and 60 min at 37 °C (under shaking). The staining with SYTO 9 and PI was done as mentioned above, untreated bacterial suspensions were used as a control, and 10,000 gated cells were analyzed using a flow cytometer (FACS ARIA III, BD Life Sciences, CA, USA) using FITC and PI lasers. The data was graphically represented in quadrant plots using BD FACSDiva Software.

3.2.18.5. Live/Dead Assay on bacterial biofilms by confocal microscopy

Biofilms of *P aeruginosa* and *S aureus* were incubated with 25 µg/mL of Mox-Ms for 1 and 4 h at 37 °C. The biofilms were washed twice with sterile physiological saline solution (0.9 % w/v NaCl) and stained using SYTO 9 and PI. The staining solution was prepared by mixing SYTO 9 and PI at 33.4 µM and 0.4 mM concentrations (Ou et al., 2019). The bacteria staining was performed by adding 3 µL and 5 µL of SYTO 9: PI (1:1) in the dark for 10 min. After the staining, the bacteria's biofilm 3D images were generated and captured using a confocal microscope (ex/em. 485/498 nm) (Leica, DMi8, Germany)(Ong et al., 2019).

3.2.19. *In vivo* studies

3.2.19.1. Mucoadhesive retention study by *in vivo* imaging

The retention time of the polymeric micelles over the cornea was assessed in Balb/c mice. Coumarin 6 (C6) (4.15 µg C6/eye) loaded C6@CF68/127(5/10)Ms, 20 µL was instilled topically to both the mice's eyes which were pre-anesthetized with isoflurane. The fluorescence intensity

signal was captured using IVIS LUMINA series III (Perkin Elmer). The Region of Interest (ROI) was measured at various time points (5 min post-administration-360 min) till the fluorescence signal disappeared (exposure time 30 s) using Living Image version 4.5.5 software.

3.2.19.2. Assessment of therapeutic efficacy in a bacterial keratitis mouse model

An overnight culture of *P aeruginosa* (C57) and *S aureus* (Balb/c) at 37 °C in LB broth was adjusted to OD@600nm of 0.2 (10^6 CFU/mL). The mice were anesthetized by the intraperitoneal injection of 150 µL of ketamine HCl. Three abrasions of 1 mm depth were made over the cornea with the help of a 25-gauge needle, and 5 µL of bacterial inoculum was added to both eyes. Following 12 h of inoculation, mice with infected eyes (n=6/ group) were divided into five groups: Control, Mox solution (5 µg/µL), Mox-Ms at Mox concentration of 5 µg/µL. Treatment was given in three cycles. 15 µL of formulations were applied topically to the right cornea at 12 h intervals. PBS of pH 7.4 was administered to the control group. After the treatment, each mouse was scored for statistical comparison and photographed with a micro lens-attached camera and graded accordingly: 0, +1, +2, +3, +4, and +5 (clear/slight opacity; partially or fully covering the pupil; slight opacity, covering the anterior segment; dense opacity, partially or fully covering the pupil; dense opacity, covering the anterior segment; partial/ full corneal perforation respectively.

3.2.19.3. Quantification of viable Bacteria

The eyes were surgically removed and homogenized with 1 mL of sterile saline solution containing 0.25 % BSA (0.9 % NaCl). 100 µL of 1:10 dilution was prepared with the same sterile solution. 15 µL of the diluted solution was plated on solidified nutrient agar plates and incubated overnight at 37 °C. The bacterial colonies were counted and reported as the number of viable colonies using the following formula:

$$\text{CFU} = \frac{\textbf{No.of colonies}}{\textbf{10 x dilution factor}} \text{ X } 1000$$

3.2.19.4. Histopathology

Following the treatment with formulations, the cornea was collected from the bacterial keratitis-induced mice models and cross-sectioned and fixed onto the slides at a 5 µm thickness. H&E staining was done on tissues according to the manufacturer's protocol, and staining was done on the sections with Harris's hematoxylin-eosin (H & E) reagent. The sections were observed under the light microscope for histological studies (Muddineti et al., 2017).

3.3. Results and Discussion

3.3.1. Physicochemical characterization, drug release, and mucoadhesion studies of mixed micelles

The CS-PLGA conjugation was confirmed by ^{1}H NMR (**Fig. 3.2**). The -*R-CO-NH* showed a signal at δ5.34 ppm, -C*H*$_3$ was present at δ1.45, δ1.48, and δ1.91 ppm. The (C*H*$_2$-O) groups of CS-PLGA are present at δ2.20 and δ2.57 ppm. Next, FTIR spectroscopy (**Fig. 3.4**) confirmed the presence of functional groups. The amide bond formation between the CS and PLGA was observed at peaks 3300 cm^{-1}, representing the presence of the N-H group, and 1620 cm$^{-1,}$ representing the C=O group. The Mn value of the CS-PLGA conjugate determined by the GPC analysis was around 60 kDa, with a PDI of 1.7, indicating 0.977 mols of CS attached to the PLGA (**Fig. 3.3, Table 3.1**).

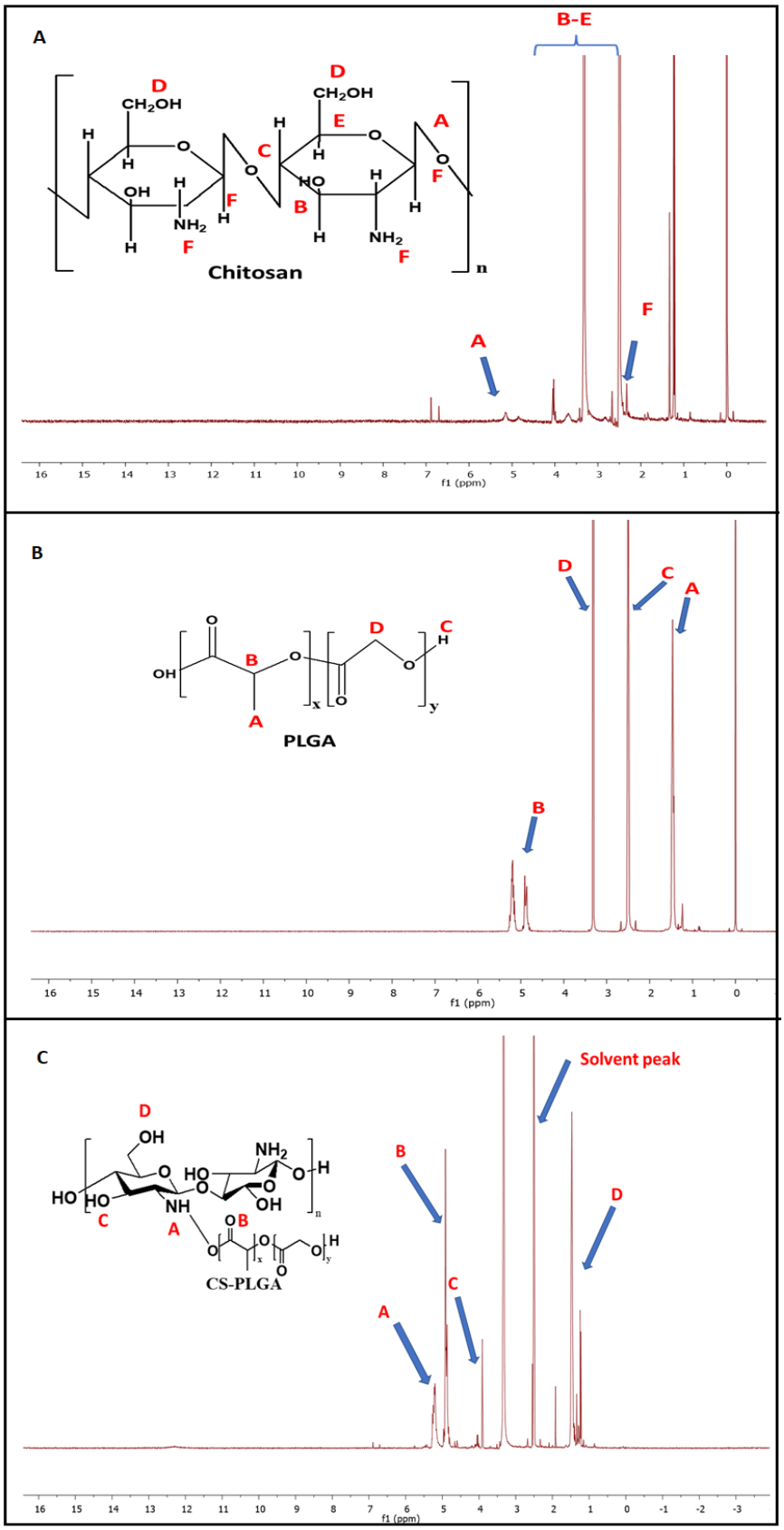

Fig. 3.2. The ^{1}H NMR spectra of Chitosan (A), PLGA (B), and CS-PLGA conjugate (C).

Table 3.1. The molecular weight of the synthesized polymers was determined by gel permeation chromatography.

	Mn	Mw	Mp	PDI	No of the mols attached
CS-PLGA	57209	59365	60133	1.756	0.977

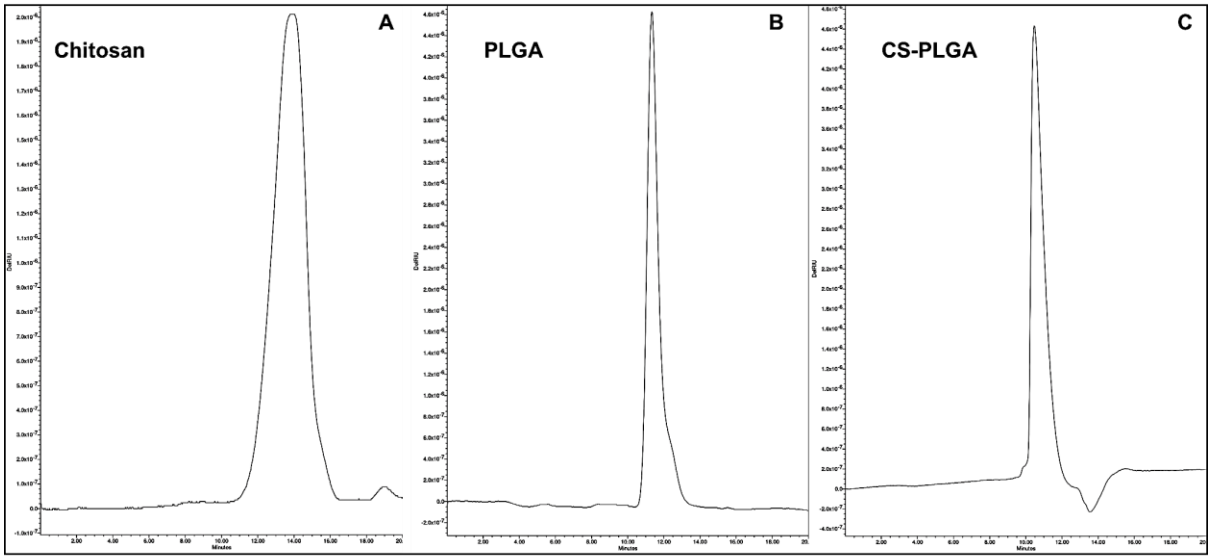

Figure 3.3. Gel Permeation chromatography. The chromatographic peaks of Chitosan (A), PLGA (B), and CS-PLGA conjugate (C).

Polymers CS-PLGA and poloxamers of various ratios exhibited micelles formation at a concentration of 1.698 µM for both CF68127(5), CF127(5), and 1.397 µM for CF68(10) and CF127(10), as determined from both pyrene incorporation and surface tension techniques (**Fig. 3.4B&C**). The presence of hydrophilic and hydrophobic polymers resulted in the self-assembly of the polymers to form Ms, which were used as a carrier to load Mox. CF68/127(10) formed micelles at a lower concentration than the CF68/127(5) as the higher pluronic content in CS-PLGA: pluronic, 1: 10 ratio over 1: 5 favored the self-assembly process of the mixed micelles. The micellization is due to the differences in the solubility of PEO and PPO blocks, and the PPO/PEO ratio concentrations determine the micellar formation. The higher concentrations of poloxamers in the CF68/127(10) have more PEO/PPO blocks which offer more HLB (Hydrophilic-Lipophilic Balance), resulting in more solubility of polymers and micellar formation at low concentrations (Bodratti & Alexandridis, 2018). The higher pluronic content in the Ms imparted higher drug

loading and entrapment efficiency. The Mox-loaded formulations showed small particle sizes with low PDI (0.1-0.3), indicating monophasic size distribution (Ghezzi et al., 2021). The hydrophobic core of Ms acts as a drug loading site, and the drugs get encapsulated through physical/chemical interactions (Simões et al., 2015). The Mox-Ms had shown positive surface charge with high zeta potential values (**Table 3.2, Fig. 3.4E**). The high zeta potential indicates the higher stability of the Mox-Ms in which the particles repel each other and prevent aggregation of the formulations. The ionized amino groups of CS attributed the positive charge to the formulations, and the results were similar in accordance with the findings of Liang Li et al. (L. Li et al., 2018). The morphology of the Ms was spherical, as determined by SEM studies (**Fig. 3.4D**). XRD analysis represented Mox peaks at 10, 15, 20, 25, 30, and 40 2θ. In contrast, the peaks were absent in all the formulations (**Fig. 3.4F**). The disappearance of Mox peaks in the mixed micelles XRD spectra proved that the Mox was encapsulated in the polymer. DSC analysis displayed no characteristic endothermic peak at 270 °C and 325 °C, present in free Mox (**Fig. 3.4G**). The absence of an endothermic peak of Mox in the Ms further proved that the drug was encapsulated in the micelles. Mox-Ms showed sustained drug release. Formulations have shown a similar release pattern with a gradual release of 86.88 ± 5.23 %, 90.33 ± 7.22 % of Mox from M@CF68(5)Ms, M@CF68(10)Ms and 83.34 ± 6.98 % and 91.48 ± 5.22 % from M@CF127(5,10)Ms, respectively in 24 h. Free Mox was released from the dialysis bag at 94.00 ± 4.68 % in 6 h **(Fig. 3.4I)**. Higher pluronic content in the mixed micelles promoted favorable drug entrapment, leading to slower and more sustained drug release. Hydrophilic drugs tend to show low affinity towards the hydrophobic core of micelles; this might have resulted in poloxamers following diffusion-controlled release patterns (Abdeltawab et al., 2020). Chitosan, when used with poloxamers they retard the drug release rate due to the increased gel strength and viscosity of the composite. Karatas et al. found similar results wherein chitosan and poloxamers had shown controlled drug release (Karatas et al., 2014).

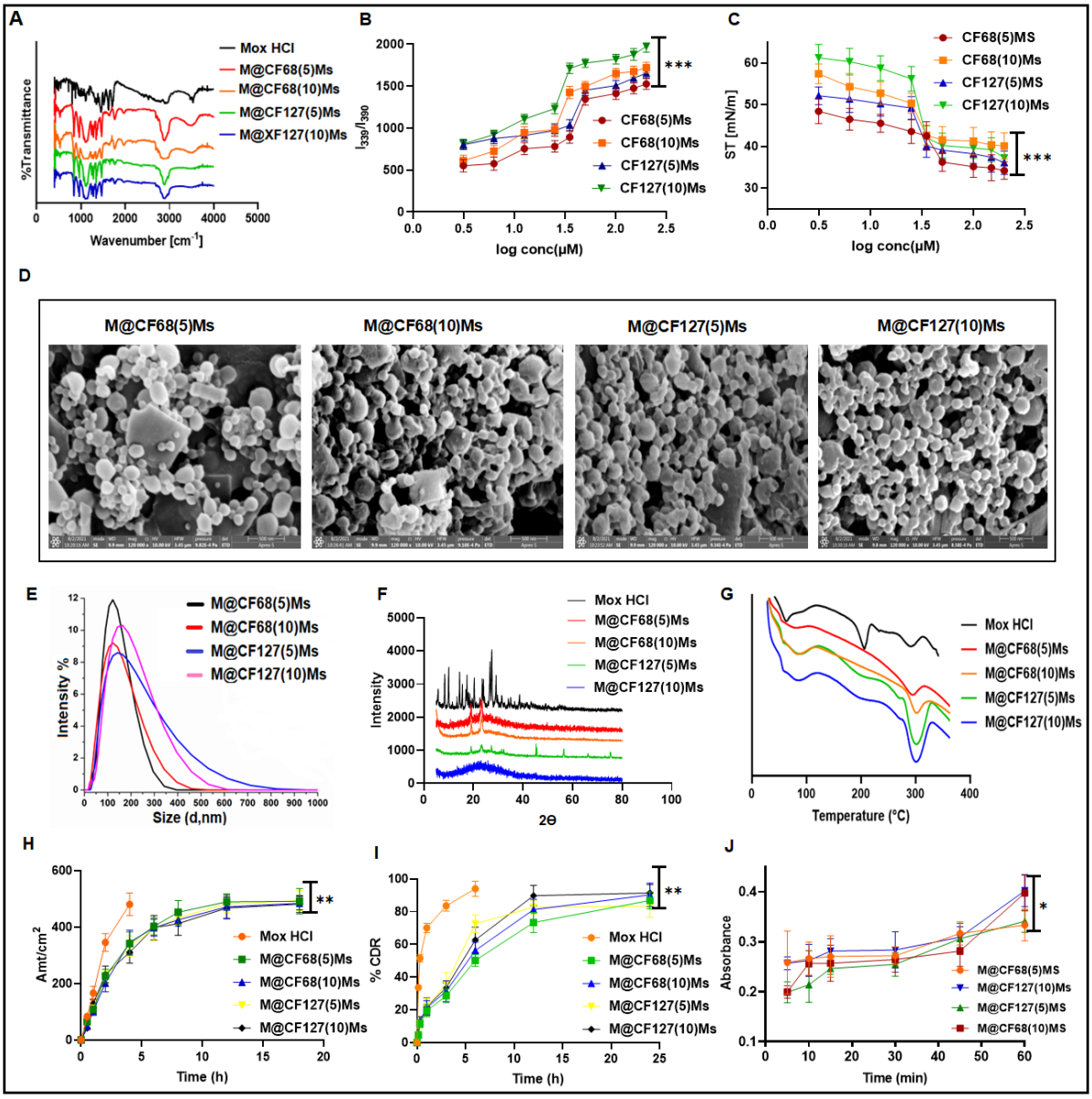

Figure 3.4. Physicochemical characterization of blank Ms and Mox-loaded Ms. FTIR spectra (A); Critical micelles concentrations by pyrene fluorescence technique (B) and by surface tension determination (C); Morphology of the Mox-Ms by scanning electron microscopy. Scale bar. 500 nm (D); Particle size distribution of Mox-Ms (E); X-ray diffraction analysis of Mox and Mox-Ms (F); DSC thermogram (G); Trans corneal permeation of Mox and Mox-Ms (H); *in vitro* drug release of Mox and Mox-Ms (I); Mucin turbidity assay of Mox-Ms (J). The data are represented as P<0.001 as ***, P<0.01 as ** and P<0.1 as *

Table 3.2. Particle size, PDI, Zeta potential (mV), %EE and DL of M@CF68/127(5/10)Ms

Formulation	CS-PLGA: Poloxamer	Size (nm)	PDI	Zeta Potential (Mv)	% EE	% DL
M@CF68(5)Ms	1:5	101.0 ± 2.0	0.2	31.0 ± 1.5	61.4	5.3
M@CF68(10)Ms	1:10	111.0 ± 2.0	0.3	32.0 ± 1.6	75.6	7.4
M@CF127(5)Ms	1:5	121.0 ± 1.0	0.3	33.0 ± 2.5	65.2	6.7
M@CF127(10)Ms	1:10	127.0 ± 1.0	0.3	35.0 ± 2.4	79.2	7.8

Next, the Franz diffusion cell apparatus determined the permeation of Mox-loaded micelles through the goat cornea. Free Mox showed release 480 ± 36 µg/cm^2 within 3 h, and formulations M@CF68(5)Ms, M@CF68(10)Ms had exhibited 491 ± 45, 484 ± 24 µg/cm^2 of permeation whereas, M@CF127(5)Ms, M@CF127(10)Ms permeated 493 ± 36, 481 ± 30 µg/cm^2 respectively (**Fig. 3.4H**). The permeation was maximum with M@CF68(10)Ms and M@CF127(10)Ms compared to other formulations. The concentration and composition of the poloxamers define the rate of drug release. Due to the presence of compact micellar arrangements of the Ms, the formulations have shown slow diffusion (Abdeltawab et al., 2020). The study showed the potential of the developed polymeric carrier to permeate through the corneal surface more potentially and deliver the drug, which is beneficial for exerting an antibacterial effect in deep corneal infections.

There was a slight increase in the viscosity with all the formulations at a concentration of 3.0 %w/v. Apart from the effect of concentration, the constant dynamic viscosity was observed with the increase in temperature, indicating the solutions had shown Newtonian behavior, and a similar effect was observed by Henda et al. (Ben Henda et al., 2013). Upon increasing the concentration, a noticeable phase transformation was observed after 32 °C in all the formulations (**Fig. 3.5**). The viscosity was higher for F127-incorporated Ms with a sharper phase change compared to F68, and in a higher ratio of incorporation, 1: 10 over 1: 5, this may be due to the presence of more PPO

groups in F127, and with an increase in the concentration of F127, and the temperature the hydrodynamic volume of micelles decreases due to the enhancement of hydrophobic interactions and change to the PEO properties resulting in increased viscosity (Mortensen & Pedersen, 1993).

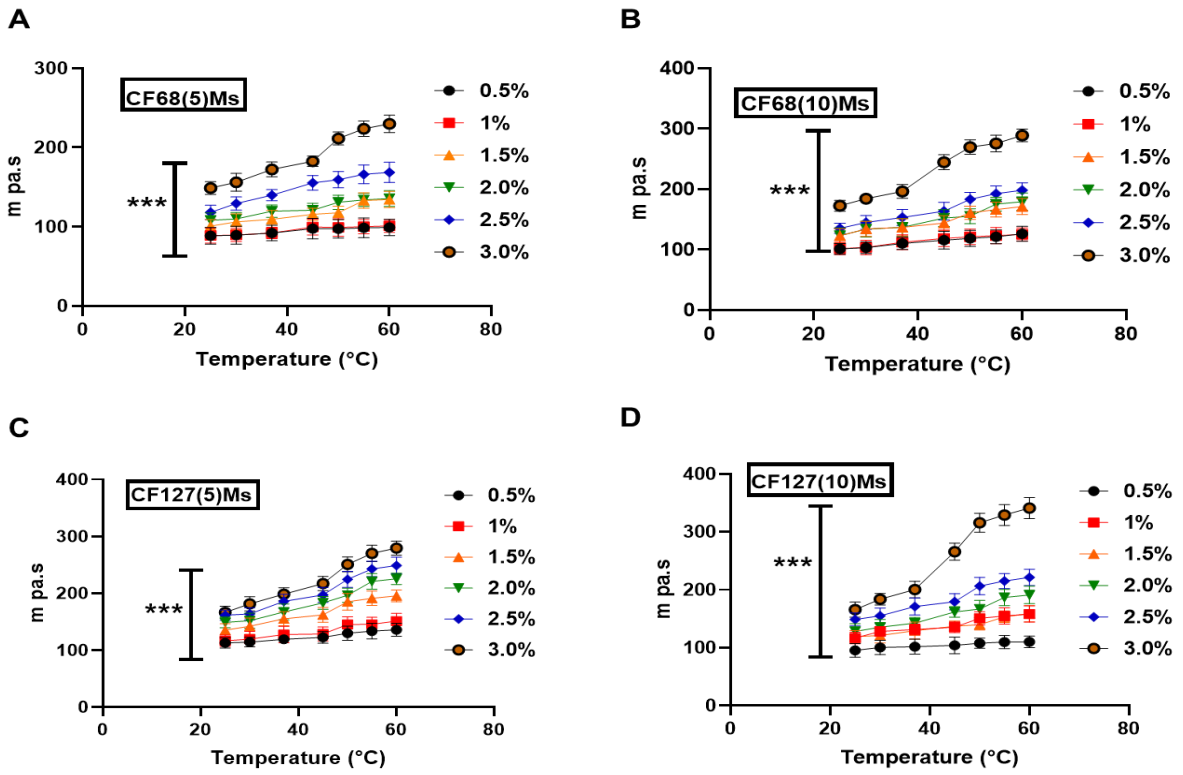

Figure 3.5. Temperature-dependent viscosity of CF68(5)Ms (A), CF68(10)Ms (B), CF127(5)Ms (C), CF127(10)Ms (D) at various concentrations. The data are represented as P<0.001 as ***.

The mucoadhesive forces analyzed by texture analyzer were 9, 17 gm/cm^2 for CF68(5)Ms, CF68(10)Ms and 8, 24 gm/cm^2 for CF127(5)Ms, CF127(10)Ms, respectively (**Fig. 3.6A**). From the mucoadhesion test by falling liquid method, the Ms adhered to the goat cornea after rinsing with STF was found to be 15, 35 % for CF68(5)Ms, CF68(10)Ms and 18, 37 % for CF127(5)Ms, CF127(10)Ms, respectively (**Fig. 3.13C&D**), indicating that the CF68(10)Ms and CF127(10)Ms retained for a longer time when compared to the other formulations after continuous washing of the corneal surface with STF. The mucin turbidity study showed the interaction of micelles, CF68(5)Ms, CF68(10)Ms at an absorbance of 0.33 ± 0.03, 0.39 ± 0.03 and CF127(5)Ms,

CF127(10)Ms at an absorbance of 0.34 ± 0.02, 0.40 ± 0.03, respectively after 60 min (**Fig. 3.4**). The result indicated that the mucoadhesivity was higher with higher pluronic proportions, 1: 10 over 1: 5 in Ms (in CF68(10)Ms and CF127(10)Ms) than with the other two formulations. Cationic amine groups of chitosan and negatively charged sialic acids in the mucin could have electrostatic interaction for binding the Ms to mucin. Further, higher pluronic concentration helped in internalization by the tissues. A similar result was observed by Gratieri et al. (Gratieri et al., 2010). The muco-adhesivity and corneal tissue penetrability of the Ms increased the Mox's bioavailability in the deep corneal tissues, resulting in a superior antibacterial effect (M. M. Silva et al., 2017).

The contact angle for the CF68(5)Ms, CF68(10)Ms was found to be 22.12 ± 2.22, 41.85 ± 1.72, respectively, and CF127(5)Ms, CF127(10)Ms were found to be 22.63 ± 2.01, 43.41 ± 1.74, respectively at a concentration of 3 %w/v (**Fig. 3.6B**). The contact angle of the formulations suggests that the formulations have even spread on the corneal surface. The F127 formulation demonstrated high contact angle compared to F68 due to high PPO groups in F127 poloxamer impeding high hydrophobicity. The formulations CF68/127(10)Ms have a high concentration of poloxamers with a high amount of PPO groups compared to the CF68/127(5)Ms, therefore, resulting in an increased contact angle (Burnett et al., 2012).

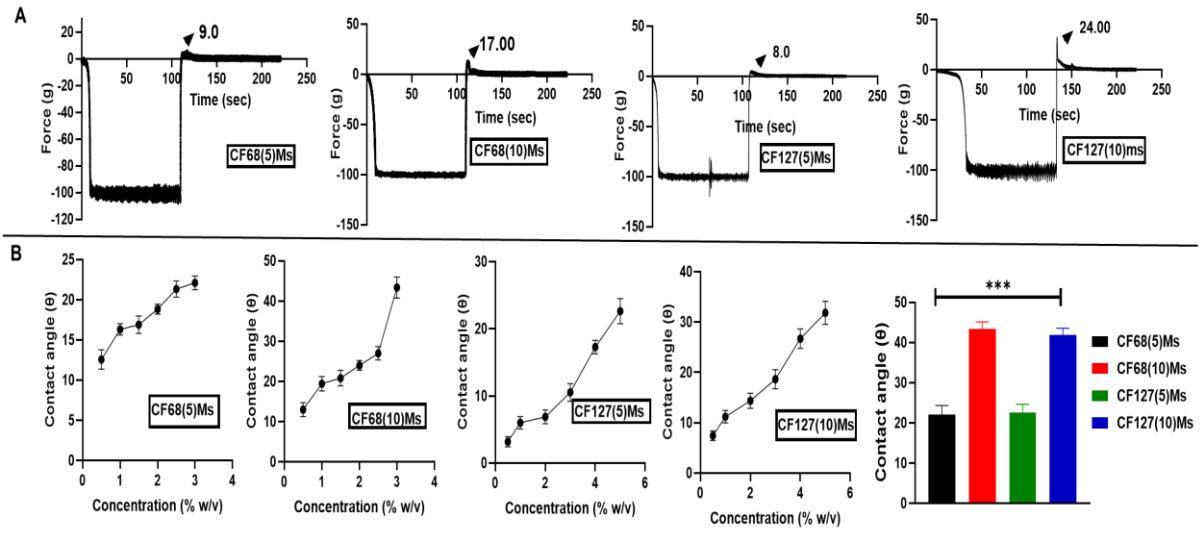

Figure 3.6. Mucoadhesive study of CF68/127(5/10)Ms by texture analyzer (A); Determination of contact angle for CF68/127(5/10)Ms at various concentrations (B). The data are represented as P<0.001 as ***.

The stability of the formulations was assessed at room temperature and 4 °C for 7 days. The particle size of the Ms has increased up to ~500 nm at room temperature. On the contrary, a slight increase in the particle size up to ~50 nm in all four formulations was observed at 4 °C, as shown in **Fig. 3.7**, indicating the need for refrigeration during storage.

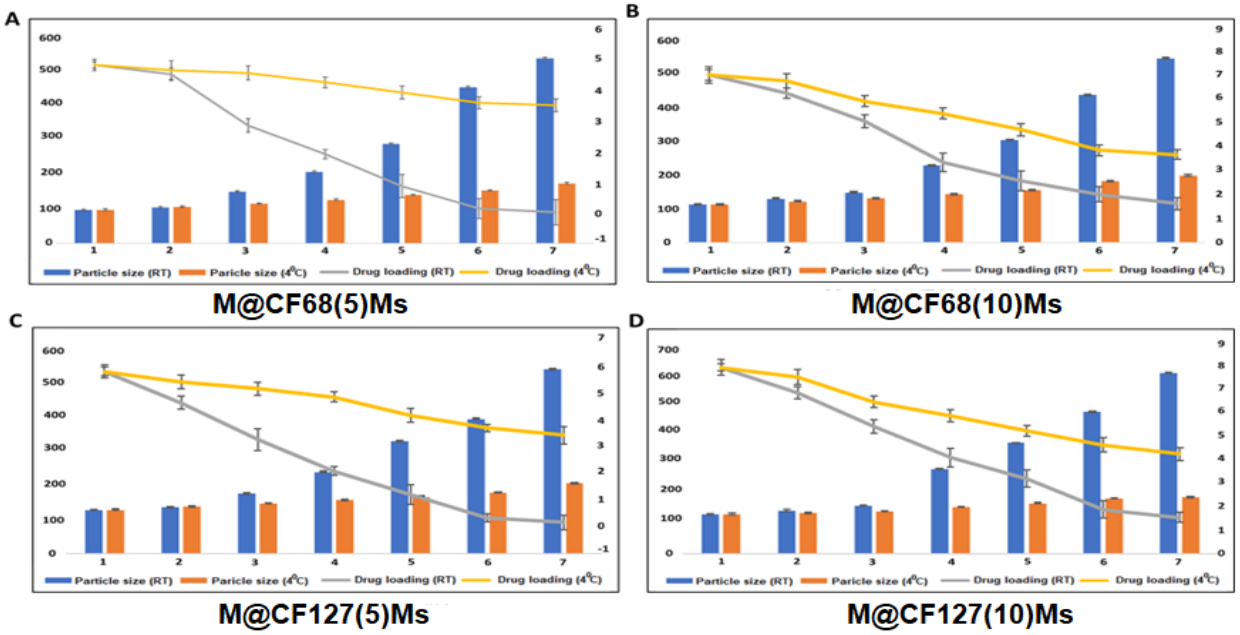

Figure 3.7. Stability assessment of M@CF68/127(5/10)Ms studied for 7 days at room temperature (RT) and 4 °C. The histogram determines the change in particle size and drug loading on various days.

3.3.2. Cell studies

The blank Ms were non-toxic to the human corneal epithelial cells, as judged by the cell viability study (**Fig. 3.8**). The reversal of corneal epithelial membrane integrity following treatment was analyzed by trans-epithelial electrical resistance measurement. The highest deviation of 110.00 ± 2.73, 104.57 ± 4.84 Ohm.cm^2 at 240 min was realized by M@CF68(10)Ms, M@CF127(10)Ms,

respectively. Comparatively, M@CF68(5)Ms, M@CF127(5)Ms showed lower deviation, upto 130.25 ± 2.12, 141.57 ± 4.96 Ohm.cm^2, respectively from the starting ohmic resistance of 170 Ω cm^2 (**Fig. 3.9F, G**). The Mox-Ms disturbed the membrane integrity, showing a maximum amount of perturbation by M@CF68(10)Ms and M@CF127(10)Ms, which could be due to the ability of chitosan and increased surfactants proportions to penetrate the tissue. The positive charge of chitosan in systems with pH values below the PKa of chitosan (< 6.5) interacts with the interior tight junctions or the cell surface containing negatively charged glycoproteins (J. Smith et al., 2004a). However, the integrity of the cell layer reached normalcy after some time without damaging the membrane. TEER analysis is a non-invasive toxicity model to quantify barrier tissue integrity following treatment. The results indicated the safety of the topically administered formulations. Further, an MTT assay was performed on HCE cells to analyze cytotoxicity. The viability of the cells after the treatment with the micelles, CF68(5)Ms, CF68(10)Ms was found to be ~85, and 82 %, respectively (**Fig. 3.8 A&B**) after 48 h and CF127(5)Ms, CF127(10)Ms was found to be ~85, 81 % viable after 48 h treatment respectively (**Fig. 3.8 C&D**). The formulations were not toxic throughout the incubation and at the tested concentration, and similar results were observed in a previous study (Cosco et al., 2014).

The cellular uptake of the Ms was determined in HCE cells grown in monolayers or spheroids. The CF68/127(10)Ms penetrated upto 60 µm, observed by Z-stack analysis, compared with the lower ratio of CF68/127(5)Ms, which showed penetration up to 20 µm after 4 h treatment as shown in (**Fig. 3.9A, B, C&D**).

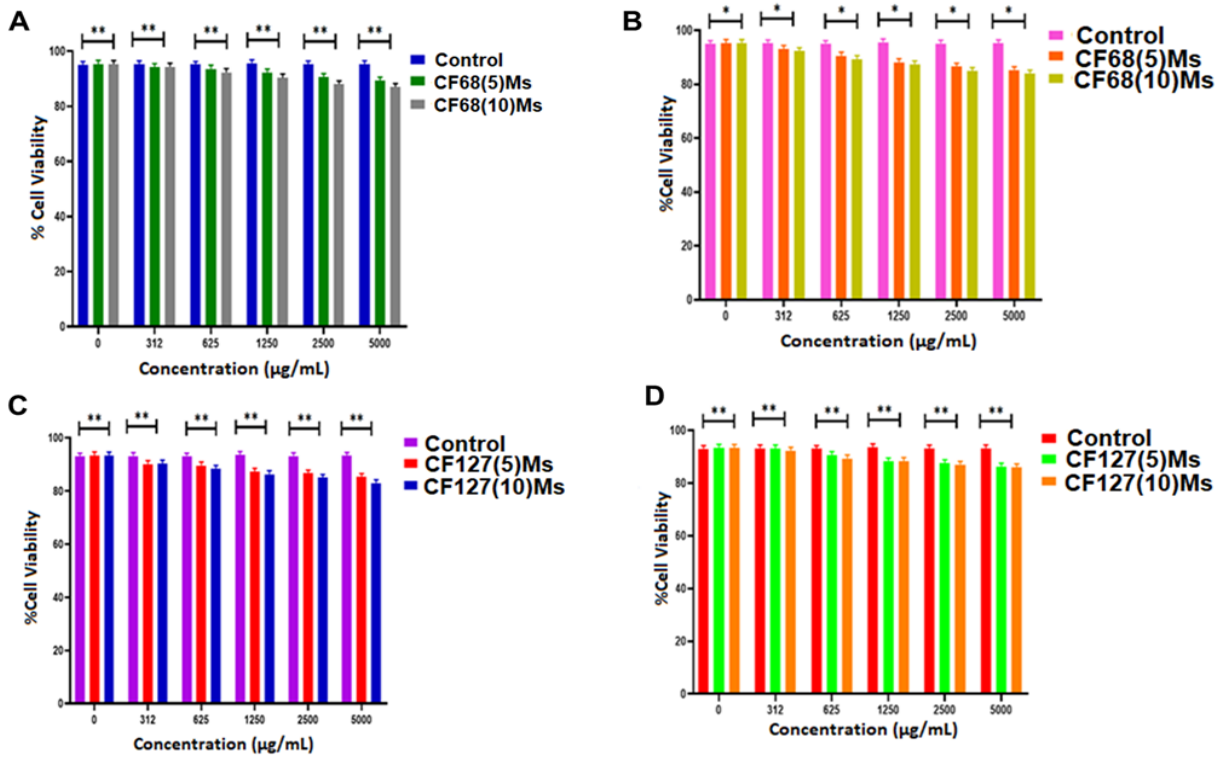

Figure 3.8. % Cell viability of HCE cells treated with CF68(5/10)Ms for 24 (A) and 48h (B) and CF127(5/10)Ms for 24 (C) and 48h (D). The data are represented as P<0.01 as ** and P<0.1 as *.

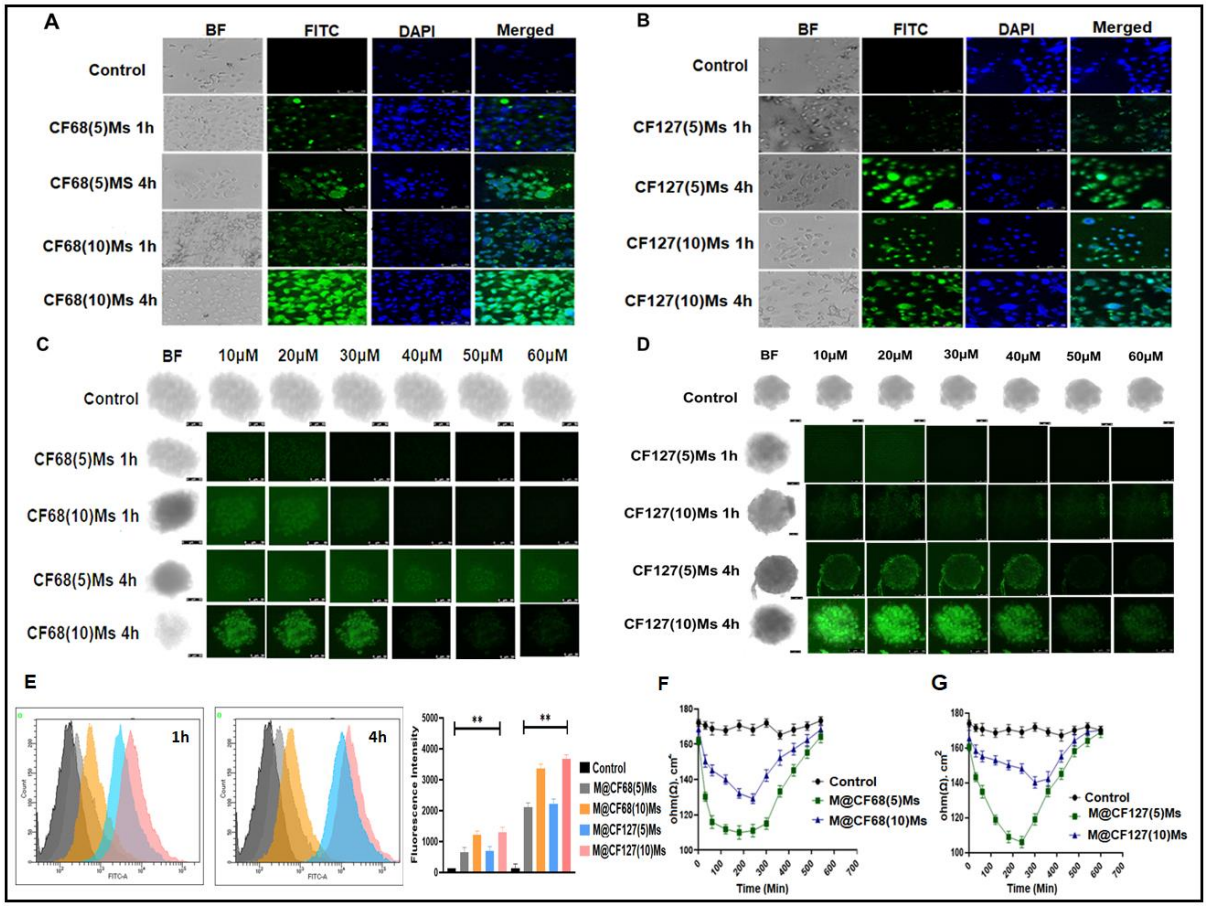

Figure 3.9. Cellular uptake of CF68(5/10)Ms (A), CF127(5/10)Ms (B) by HCE cells in monolayers for 1 and 4 h. Spheroidal uptake study of HCE cells treated with CF68(5/10)Ms (C) and CF127(5/10)Ms (D) for 1 and 4 h, respectively. The histogram plot represents the cellular uptake of M@CF68/127(5/10)Ms by flow cytometry for 1 and 4 h and the bar graph plot (E). TEER study using HCE cells grown in multilayer and treated with M@CF68/127(5/10)Ms (F & G). The data are represented as $P<0.01$ as **.

Micellar uptake study on HCE cells using flow cytometry demonstrated the geometric mean fluorescence of 665 ± 148, 1214 ± 126, for CF68(5)Ms, CF68(10)Ms, and 701 ± 138, 1312 ± 152 for CF127(5)Ms, CF127(10)Ms, respectively after 1 h, and the fluorescence was increased to 2114 ± 137, 3361 ± 144 for CF68(5)Ms, CF68(10)Ms; 2224 ± 152 and 3685 ± 127 for CF127(5)Ms, CF127(10)Ms, respectively, after 4 h incubation time (**Fig. 3.9**). The time dependant uptake improvement in cellular uptake was observed for all formulations, with M@CF127(10)Ms

displaying the highest cellular association in both monolayers and spheroids having a statistical difference of **P<0.01, **** compared to the other formulations. The reason could be incorporating the penetration enhancer, F127, in the micelles (Fischer et al., 2011). The small particle size of all the formulations could easily permeate through the cell membrane. No sign of irritancy or hemorrhage was observed with the Mox-Ms (**Fig. 3.10**), as tested in the HET-CAM study.

3.3.3. Bacterial Studies

The MIC and MBC of *P aeruginosa* and *S aureus* were determined by measuring OD, and MTT assay, respectively. MICs were found to be 0.25 and 2.0 µg/mL for M@CF68(5)Ms, M@CF127(5)Ms, respectively, as shown in **Fig. 3.10B, C, D & E**. M@CF68(10)Ms, M@CF127(10)Ms have shown the highest inhibition zone with 20.0 ± 0.1, 24.3 ± 0.2 mm for *P aeruginosa* and 24.0 ± 0.1, 27.3 ± 0.3 mm for *S aureus* respectively as shown in the (**Fig. 3.10F**, **Table 3.3**). The zone of inhibition was observed twice more than in the free Mox solution. The highest inhibitory zone was observed with the M@CF127(10)Ms against the pathogenic bacteria, *P aeruginosa*, and *S aureus*.

Table 3.3. The diameter (mm) of the zone of inhibition for bacteria after treatment with moxifloxacin and M@CF68/127(5/10)Ms.

Formulation	Zone of Inhibition (mm)	
	P aeruginosa	***S aureus***
Mox	13.0 ± 0.1	17.3 ± 0.2
M@CF68(5)Ms	19.3 ± 0.2	22.6 ± 0.2
M@CF68(10)Ms	20.0 ± 0.1	24.0 ± 0.1
M@CF127(5)Ms	22.3 ± 0.3	24.3 ± 0.1
M@CF127(10)Ms	24.3 ± 0.2	27.3 ± 0.3

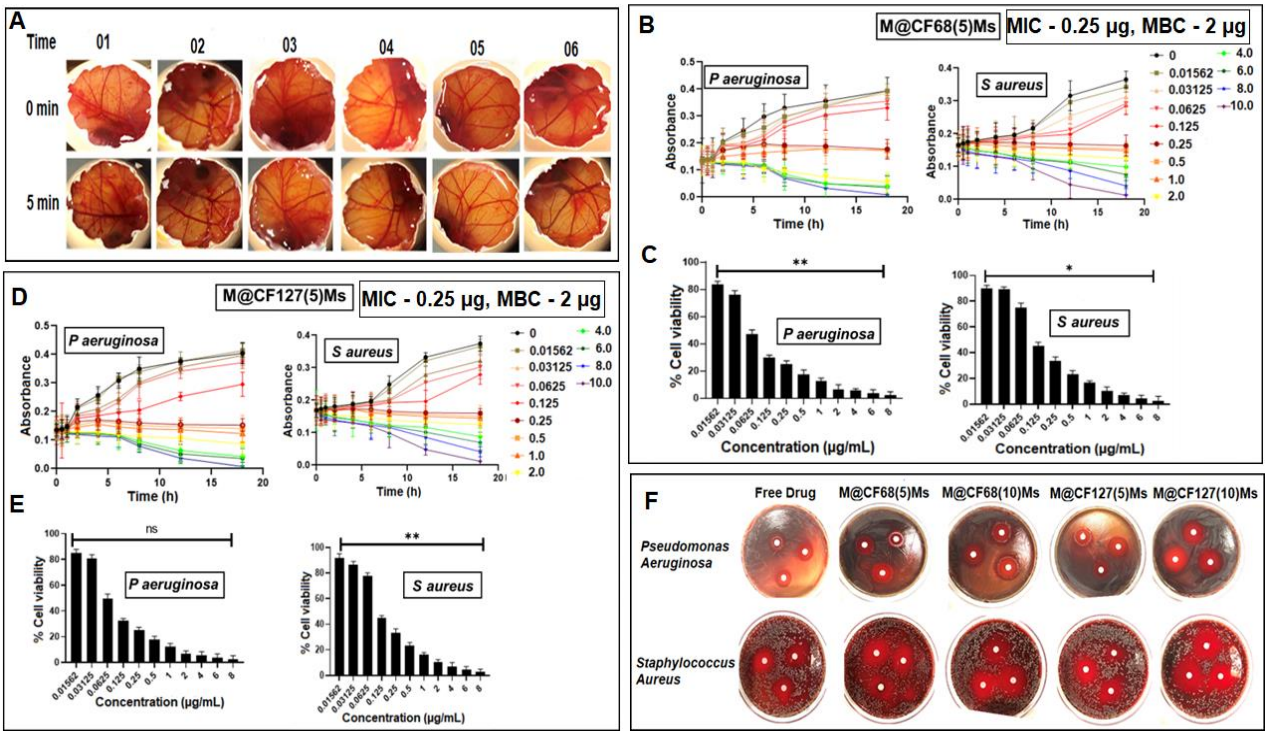

Figure 3.10. HET-CAM test (A). Display of the photograph of CAM membrane exposed to control (01), Mox (02), M@CF68(5)Ms (03), M@CF68(10)Ms (04), M@CF127(5)Ms (05), and M@CF127(10)Ms (06), respectively after 5 min treatment (A). Determination of minimum inhibitory concentration (MIC) of M@CF68(5)Ms (B), M@CF127(5)Ms (D) by optical density measurement (OD_{600}) against *P aeruginosa* and *S aureus* respectively; determination of minimum bactericidal concentration (MBC) by MTT assay against *P aeruginosa* and *S aureus* (C & E) respectively. Zone of inhibition (F). Photographs of the sheep blood agar plates cultured with *P aeruginosa* and *S aureus* and treated with formulations. The data are represented as $P<0.01$ as **, $P<0.1$ as *, and ns- no significance.

The penetration of mixed micelles into the *P aeruginosa and S aureus* biofilms after the treatment was analyzed by confocal microscopy. The results indicated that CF68(10)Ms, CF127(10)Ms showed the highest penetration of ~10 µM at 1 h and ~17 µM at 4 h and comparatively, to other mixed micelles CF68(5)Ms, CF127(5)Ms (**Fig. 3.12A&B**) showing time-dependent penetration

efficiency of the micelles. Live/dead assay for the bacteria treated with M@CF68/127(10)Ms have shown more dead cells indicated with red fluorescence (PI labeled) at 4 h from the microscopic images captured using a fluorescence microscope (**Fig. 3.11A&B**). The study mentioned above was also quantitively determined by FACS, M@CF68(10)Ms, M@CF127(10)Ms had shown more number dead cell population in Q3 and Q4 quadrants having the total population of 83, 85% dead cells in *P aeruginosa* and 76, 81% in *S aureus*. In comparison, M@CF68(5)Ms and M@CF127(5)Ms had shown the Q3 and Q4 populations of 61, 65% for *P aeruginosa* and 59, 63% for *S aureus*, respectively (**Fig. 3.11C&D**). The largest population of dead cells was found with the treatment of M@CF68(10)Ms and M@CF127(10)Ms ratio after 60 min incubation. The live/dead assay for *P aeruginosa* and *S aureus* biofilms treated with M@CF68(10)Ms, M@CF127(10)Ms had killed the bacteria more after 4h treatment than M@CF68(5)Ms, M@CF127(5)Ms (**Fig. 3.12C&D**). The study showed that the developed micelles could effectively penetrate the bacteria's cell wall and biofilm layer and exhibit a significant bactericidal effect. The increased bactericidal effect of the formulations is also due to the presence of positive groups on the chitosan, which hydrolyses the peptidoglycans present in the bacterial cell wall by ionic interactions, thereby provoking the lesion of intracellular electrolytes, causing the bacteria to death. The advantage of the antimicrobial effect of chitosan is that it gives more capability to the Mox and provides combined efficacy in treating biofilms (Goy et al., 2016).

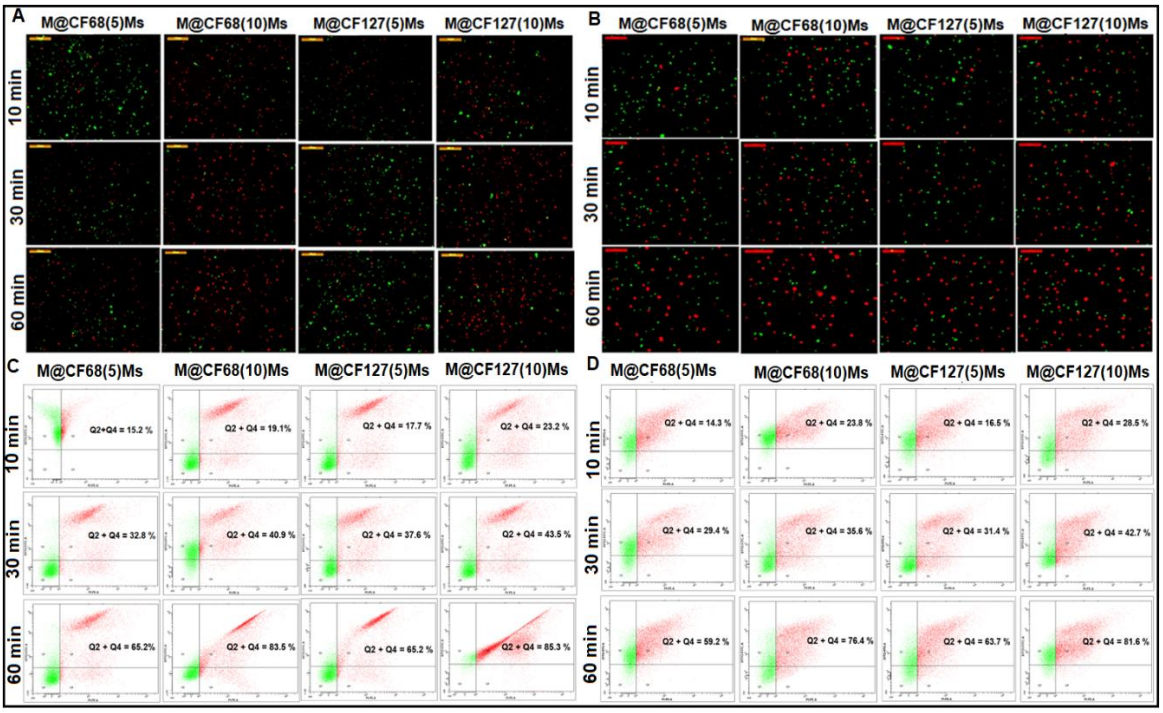

Figure 3.11. Live/dead assay of *P aeruginosa* and *S aureus* treated with M@CF68/127(5/10)Ms. The fluorescence images of bacteria treated with M@CF68/127(5/10)Ms for 10, 30, and 60 min, *P aeruginosa* (A) and *S aureus* (B), scale bar 100 μm; the flow cytometric quadratic dot plot diagram displaying the SYTO-9 and PI-stained cells populations (C&D). The cells in the Q1, Q2, Q3, and Q4 quadrants represent live and dead cell populations, respectively.

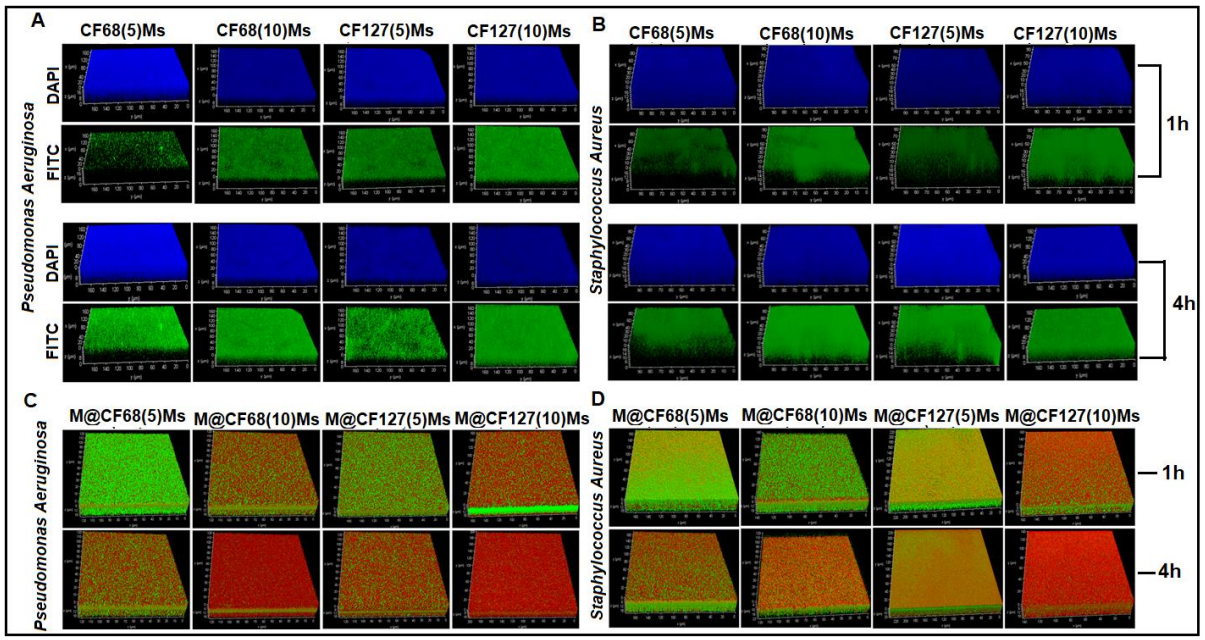

Figure 3.12. Confocal microscopic images of biofilms. Uptake of M@CF68/127(5/10)Ms following treatment for 1-4 h in *P aeruginosa* (A) and *S aureus* (B) biofilms. Live-dead cells assay following treatment in *P aeruginosa* (C) and *S aureus* (D) biofilms. Biofilms were stained with DAPI and FITC-labeled formulations for uptake study (A and B) and SYTO-9 and PI to visualize live and dead cell populations (C and D).

3.3.4. *In vivo* animal studies:

3.3.4.1. Corneal retention

The ocular retention time of the mixed micelles in the eyes of Balb/c mice was visualized using an *in vivo* imaging system. The C6@CF68(5)Ms, C6@CF68(10)Ms, C6@CF127(5)Ms, and C6@CF127(10)Ms displayed fluorescence of $5.32e^{+009}$, $6.78e^{+010}$, $7.82e^{+009}$, and $9.08e^{+010}$ AU, 5 min post-administration at the region of interest (ROI), respectively. It was further reduced to $4.91e^{+009}$, $3.025e^{+010}$, $6.12e^{+009}$, and $5.63e^{+010}$ for C6@CF68(5)Ms, C6@CF68(10)Ms, C6@CF127(5)Ms, and C6@CF127(10)Ms, respectively after 30 min. The intensity lasted till 180 min for C6@CF68(5)Ms and C6@CF127(5)Ms with ROI values of $8.69e^{+008}$ and $2.34e^{+009,}$ respectively, whereas C6@CF68(10)Ms and C6@CF127(10)Ms retained on the ocular surface till

240 min with ROI value of $1.14e^{+009}$ and $2.78e^{+009}$, respectively (**Fig. 3.13A&B**). The results indicated a higher amount and longer corneal retention of C6@CF68(10)Ms and C6@CF127(10)Ms, the latter being the highest and longest. It has been observed that the formulation could withstand the shearing forces in the eye due to reduced lacrimal drainage, and the findings were similar to Gratieri et al. (Gratieri et al., 2010). The electrostatic interactions between the chitosan and mucus layer of the eye lead to a longer retention time of the formulation. Similarly, when studied using the goat cornea, the highest retention was observed with C6@CF68(10)Ms and C6@CF127(10)Ms (**Fig. 3.13C&D**). These formulations can greatly reduce the dose administration frequency of topically administered ophthalmic formulations.

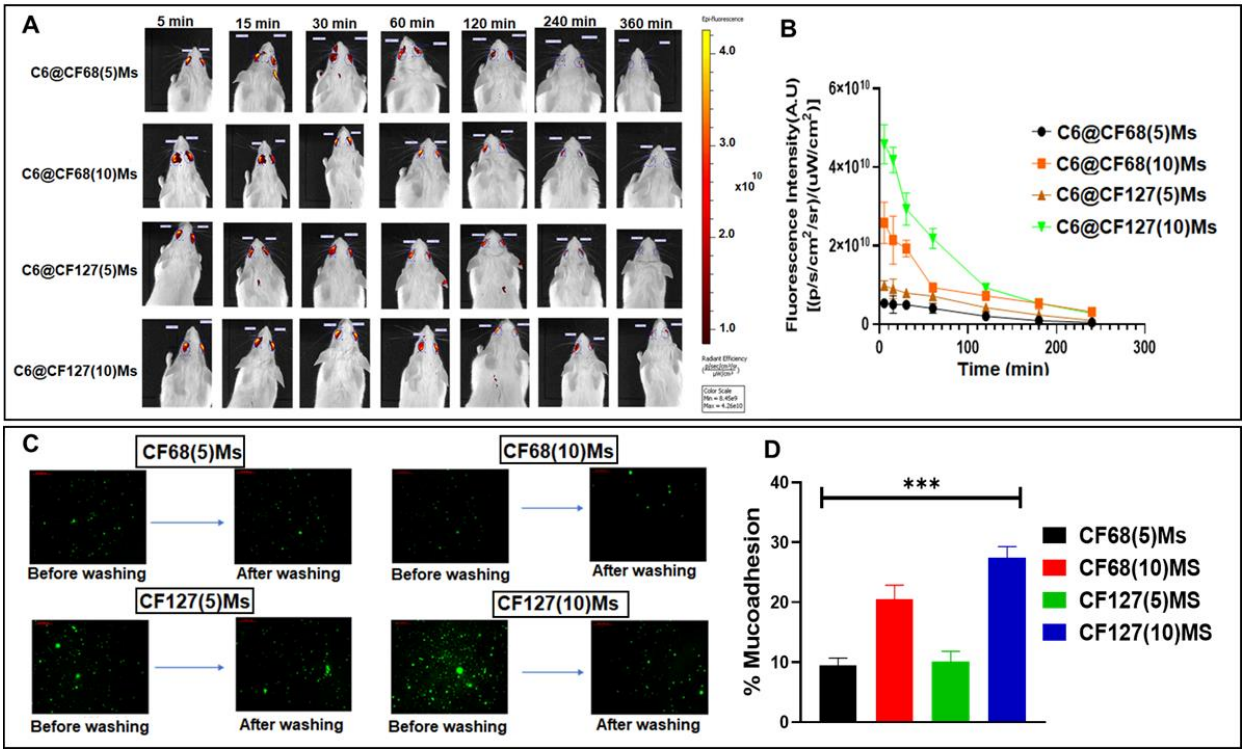

Figure 3.13. Real-time *in vivo* fluorescence imaging of mice administered C6@CF68/127(5/10)Ms topically on eyes (A); graphical representation of mean ocular fluorescence intensity following treatment with formulations (B); Mucoadhesive retention study determined by falling liquid method, fluorescent images of CF68/127(5/10)Ms (fluorescently labeled) retained after washing on goat cornea (C), graphical representation of % Mucoadhesion

of mixed micelles retained after washing with STF(D). The data are represented as $P<0.001$ as ***.

3.3.4.2. Therapeutic efficacy

Keratitis-induced Balb/c mice by *S aureus* and C57BL/6 by *P aeruginosa* were treated with free Mox and four formulations. The images of the cornea taken with a macro lens showed that all the mice developed bacterial keratitis (**Fig. 3.14A** and **B**). The mean CFU counts of the BK-infected mice (*P aeruginosa*) treated with CF68-based Ms, M@CF68(5)Ms, M@CF68(10)Ms were 3520 ± 127, 2600 ± 156, respectively, with mean clinical scores of +2.8 ± 0.2, +1.8 ± 0.2. The CFUs for M@CF127(5)Ms and M@CF127(10)Ms were 3500 ± 201 and 1390 ± 114, respectively, with mean clinical scores of +3.6 ± 0.2 and +1.3 ± 0.2. Free Mox administered cornea showed an average CFU count of 5070 ± 124 with a clinical score of +4.3 ± 0.4. Similarly, the mean CFU counts for the treatment groups of M@CF68(5)Ms, M@CF68(10)Ms, M@CF127(5)Ms, and M@CF127(10)Ms in *S aureus*-induced BK were 1580 ± 217, 1000 ± 241, 1530 ± 145, and 770 ± 211, with mean clinical scores of +2.83 ± 0.23, +1.33 ± 0.23, +2.33 ± 0.62, and +0.83 ± 0.23, respectively. Free Mox administered cornea showed an average CFU count of 2160 ± 215 with a clinical score of +4.0 ± 0.23 (**Fig. 3.14C&D**). All four formulations, M@CF68/127(5/10)Ms and M@CF127(5/10)Ms, inhibited infection progression effectively compared to the free drug. The treatment with M@CF68(10)Ms and M@CF127(10)Ms minimized the CFU count significantly compared to the other Ms with the ratio of 1: 5. The cross sections of the mice cornea treated with hematoxylin-eosin (H & E staining) after the micellar treatment showed no damage to the tissue with the M@CF68(10)Ms and M@CF127(10)Ms compared to other formulations (**Fig. 3.14A&B)**. The study indicated that the developed M@CF127(10)Ms could inhibit the bacterial load most effectively by retaining on the corneal surface for a longer time, improving the penetration of loaded Mox, and showing the most robust bactericidal effect. The drawback of the conventional topical eyedrops involves lacrimal drainage and low drug availability at the site of

action, which was overcome by the newly developed M@CF127(10)Ms. The highest gelling ability of M@CF127(10)Ms prepared using pluronic F127 at a higher proportion would have impacted poor lachrymal drainage and corneal retention, leading to a superior antibacterial effect.

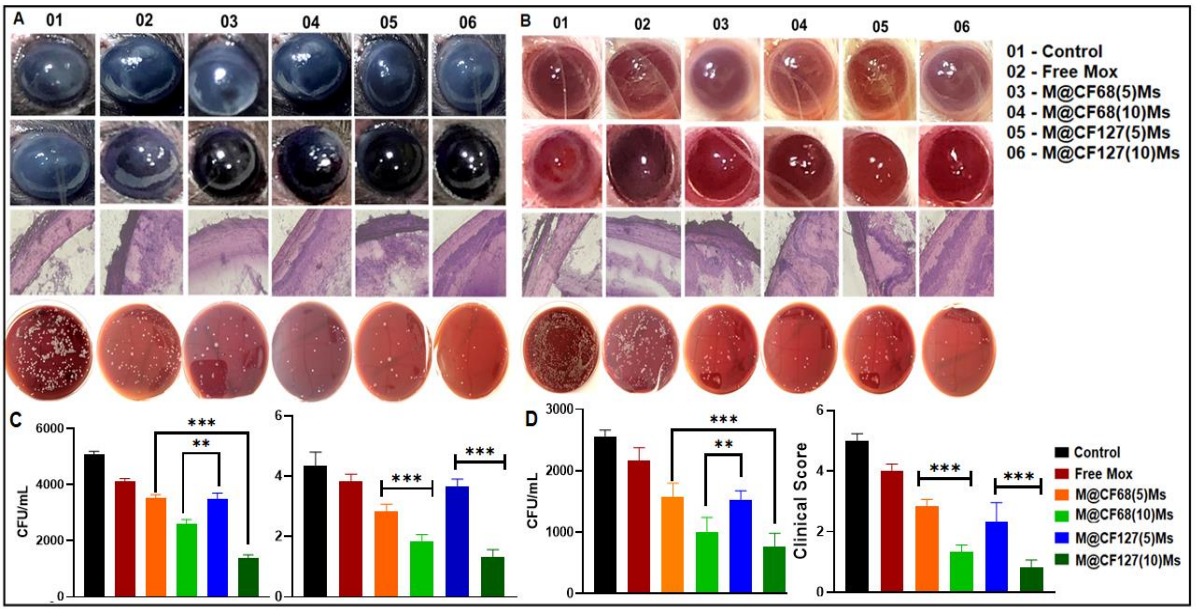

Figure 3.14. *In vivo* therapeutic efficacy of Mox and M@CF68/127(5/10)Ms in *P aeruginosa* (A) and *S aureus* (B) infected bacterial keratitis. The images of the cornea before and after the treatment regimen following H&E staining of the cross-sections of the cornea after the treatment and CFU count after the treatment; bacterial load following treatment (C), the clinical score (0 to 5) based on the two criteria (transparent and perforated) (D), the data are represented as $P<0.01$ as ** and $P<0.001$ as ***.

3.4. Conclusion

BK is a rapidly progressing sight-threatening corneal ulcer that requires a highly effective treatment regimen. However, conventional therapy fails to be effective due to its poor corneal retention, low penetration to the deeper corneal tissues, and need for frequent dosing. Here, we developed mixed micellar formulations of moxifloxacin using hybrid polymeric systems of chitosan-poly(lactide-co-glycolide) conjugate and pluronic F68 or F127 at a ratio of either 1: 5 or 1: 10. Thorough physicochemical characterization, *in vitro*, and *in vivo* studies were conducted to

confirm the fabrication, determine effective drug entrapment, stability, safety, corneal retention, penetration, gel formation, and therapeutic efficacy studies in *P. aeruginosa*, and *S. aureus* bacteria *in vitro*, and their BK-induced mice models *in vivo*. The results indicated that mixed micelles bearing higher pluronic proportions (1: 10) had better physicochemical properties, mucoadhesion, corneal penetration, and antibacterial performance in the *in vitro* and *in vivo* studies. The higher PPO units in F127 compared to F68 corrected the hydrophilic-lipophilic balance in M@CF127(10)Ms, resulting in higher self-assembling ability, drug loading, micellar stability, gelling property at ocular temperature, corneal tissue penetration, bacterial biofilm permeability compared to M@CF68(10)Ms, resulting in superior antibacterial effect *in vitro* and *in vivo*. Therefore, the newly developed nanoformulation, M@CF127(10)Ms, is multifunctional, easily scalable, non-irritant, non-toxic, and could be an effective treatment strategy for bacterial keratitis.

Chapter 4

Cationized Gelatin-Sodium Alginate Polyelectrolyte Nanoparticles Encapsulating Moxifloxacin as an Eye Drop to Treat Bacterial Keratitis

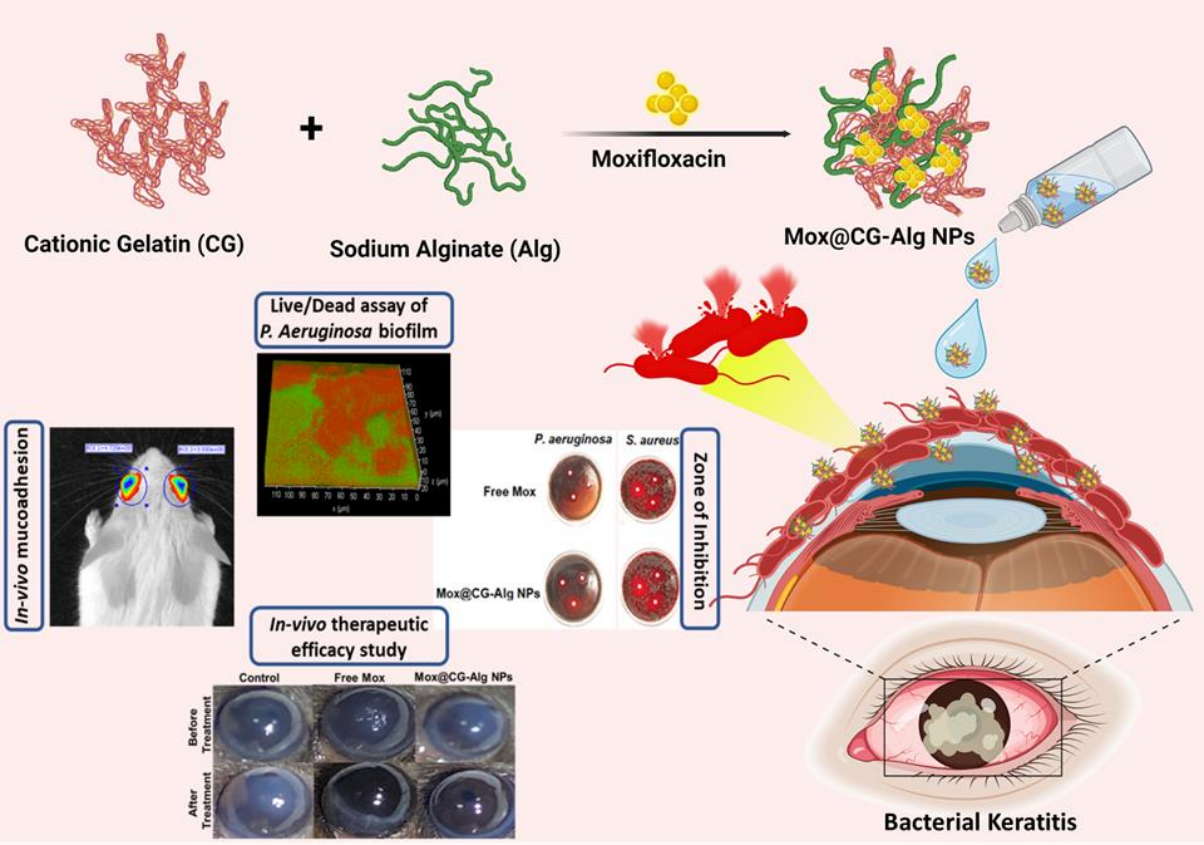

4.1. Introduction

Keratitis is an ocular infection that can potentially cause loss of vision if not treated early, and with delayed treatment, only 50% of eyes gain visual recovery (Jones, 1981). Bacterial Keratitis (BK) is mainly caused by gram-negative and gram-positive bacteria such as *Pseudomonas aeruginosa, Staphylococcus aureus, Streptococcus Pneumoniae,* and species of *Serratia*(Fleiszig & Evans, 2021; Limberg, 1991; Wong et al., 2012). The major factors responsible for BK include contact lens wear, ocular trauma, ocular surgery, antecedent ocular disease condition, deformation of lids, dry eyes, immunosuppression, and topical use of steroids (Ahn et al., 2011; *Analysis of the Risk Factors Predisposing to Fungal, Bacteri... : Indian Journal of Medical Research*, n.d.; Stapleton et al., 2012). The existing therapy for BK uses broad-spectrum fluoroquinolone antibiotics as eye drops. They achieve bactericidal efficacy by inhibiting DNA gyrase (topoisomerase II) and topoisomerase IV enzymes that are essential for bacterial replication and transcription, thereby causing cell death(Blondeau, 2004; Pestova et al., 2000). A newer generation of antibiotics is required as the incidence of resistance to earlier-generation fluoroquinolones has increased (Alexandrakis et al., 2000; Goldstein et al., 1999). Moxifloxacin and Gatifloxacin are fourth-generation antibiotics with advances in molecular structure resulting in antimicrobial potency against gram-negative and gram-positive bacteria(Blondeau, 2004; Fisher et al., 2003).

The major drawback of the existing therapy is the poor bioavailability of the drugs. Through conventional therapy, only 5% bioavailability is attained through eye drops; the remaining are wasted by blinking and tear flow. Apart from these, many ocular barriers hinder the therapeutic efficacy of eye drops, such as tear film, corneal epithelium, which allows only small and lipophilic drugs, conjunctiva, and blood-ocular barriers (Ahmed et al., 2022; Elsayed & Sayed, 2017). Eye drops constitute about 95% of the marketed ocular products intended to deliver medication to the anterior eye segment with a short residence time (Ahmed et al., 2022; Maulvi

et al., 2021). Recent advances in the ocular delivery systems are designed to deliver the drug in a sustained or extended manner aiming to improve the ocular bioavailability of drugs. Improving the ocular residence time of the drugs is the most challenging in developing nano-drug delivery systems(Desai et al., 2020; Grassiri et al., 2021; Souto et al., 2019). One promising way of improving ocular bioavailability and corneal residence time is by utilizing mucoadhesive polymers(Račić & Krajišnik, 2023). Polymers with mucoadhesive properties can form strong non-covalent interactions with the mucin. These interactions allow the polymers to remain at the application site and achieve prolonged action. The mucoadhesiveness of the polymers mainly depends upon the molecular weight, polymer chains, concentration, and functional groups (Dubashynskaya et al., 2019; Rodríguez et al., 2017; Yermak et al., 2022).

Polyelectrolyte Complexes (PEC) are emerging as a drug delivery cargo, mainly due to their low cost and ease of preparation. PEC preparation does not involve the use of organic solvents or cross-linkers. Polymers that contain ionizable groups in their structure are known as polyelectrolytes. These undergo complete or partial dissociation in an aqueous medium, leaving the polymers fully charged. Due to more repulsive force, polyelectrolytes are stretched out in an aqueous medium, increasing the viscosity of solutions as they restrict the solvent flow around and occupy more space. Polymers with oppositely charged ions have strong electrostatic interactions, resulting in a gain in entropy due to the dissociation of ions to the medium and forming PEC(Doi & Kokufuta, 2011; Sarika & James, 2016).

In the present work, moxifloxacin (Mox) loaded PEC nanoparticles (NPs) were prepared from gelatin (G), cationically modified gelatin, and anionic sodium alginate (Alg). The interaction between oppositely charged ions forms the PEC nanoparticles and can be used for encapsulating drugs, peptides, and vitamins. Denaturation of collagen prone to form gelatin, and its structural backbone contains free amino and carboxyl groups. Below the isoelectric

point, gelatin is cationized by amino group protonation. Gelatin dissolves in hot aqueous media and forms gel upon cooling. Gelling nature of gelatin results from strong hydrogen interaction between the carboxyl and amine groups. Gelatin carries a positive charge at pH below its isoelectric point in aqueous solution. Gelatin is biodegradable, biocompatible, and considered a nonimmunogenic agent (Li et al., 2011; Tseng et al., 2013). The study used the anionic polymer sodium alginate (Alg), a natural polysaccharide with β-D-mannuronate and α-L-glucuronate (G) residues extracted from marine algae.

Alg is a natural viscosity modifier with bioadhesive properties. It can form complexes with positively charged polymers because it has a rich natural source of high concentrations of carboxylic acid groups. These carboxylic groups are essential for forming amide bonds between the primary amino group of gelatin (Cafaggi et al., 2007; Friess, 1998; Sæther et al., 2008; Sarmento et al., 2007). The Mox-loaded NPs were thoroughly characterized for physicochemical parameters. The muco-adhesivity, retention, and penetration to the cornea were studied, followed by an assessment of the safety profile of the novel formulation. The anti-bacterial effect was judged using planktonic/biofilms of bacteria by detecting MIC, inhibitory zone diameter, and live-dead bacterial cell populations. Further, Mox@CG-Alg NPs bactericidal efficacy was investigated in the BK-induced mouse model.

4.2. Materials and methods

4.2.1 Materials

Type A Gelatin (porcine skin) high molecular weight (average molecular weight- 10,00,000 Da, gel strength: ~ 300g), sodium alginate (medium viscosity grade, viscosity in water less than 2000 cps, CAS number- 9005-38-3, average molecular weight: 2,50,000- 3,50,000 Da), and 3-4,5-Dimethylthiazole-2-yl)-2,5-diphenyltetrazolium bromide (MTT) were bought from Sigma-Aldrich, USA. Moxifloxacin was provided as a gift from Sentiss Pharma Pvt Ltd (Gurgaon,

India). Rhodamine B (Rh-B), SYTO 9, and propidium iodide (PI) were bought from Thermo Scientific, USA. The dialysis membrane of molecular weight cutoff (MCWO 3.5 KDa, and 12-14 KDa) was purchased from Spectrum Laboratories (USA). All the chemical reagents purchased were analytical grade from SRL Chemicals Pvt Ltd, India.

4.2.2 Methods

4.2.2.1 Synthesis of cationic gelatin

Cationized gelatin (CG) was prepared by dissolving 5g of gelatin in 100 mM phosphate buffer saline (PBS, pH 5) to the dissolved CG, ethylenediamine, and EDC (1-ethyl-3-3-dimethyl aminopropyl) carbodiimide. HCl salt was added at a molar ratio of 50 and kept under stirring, followed by adjusting the pH to 5 using 5 M HCl. The reaction was carried out at 37 °C for 18 h under continuous stirring. Further, the reaction mixture was dialyzed for 48 h against double distilled water at room temperature, followed by freeze-drying. The obtained CG was stored at 2-8 °C and utilized further. The reaction scheme is shown in **Figure 4.1A.**

4.2.2.2. Preparation of Gelatin/CG-Alg NPs

By simple amalgamation of Gelatin/CG and Alg solutions, Gelatin/CG-Alg polyelectrolyte complex can be obtained. Briefly, solutions of Alg, and Gelatin/CG, were prepared in PBS, pH 7.4. After vigorous stirring at room temperature for 5 min, an aqueous solution of Alg was added to the CG/Gelatin solution to obtain a polyelectrolyte complex. Different compositions of polyelectrolyte complexes were prepared by varying the amount of Gelatin/CG (2.5-10 mg) and Alg (2.5-10 mg) to optimize the formulation, as shown in **Table 4.1**. The PEC combination, the nanoparticles (NPs) showing the smallest particle size, was centrifuged and separated using the centrifuge at 13000 rpm for 15 min (**Figure 4.1D)**. The obtained nanoparticles were dried in a vacuum and used for further studies. Mox@CG-Alg NPs were prepared by adding 2 mg of Mox to the CG-Alg mixture, followed by vigorous stirring per the earlier procedure.

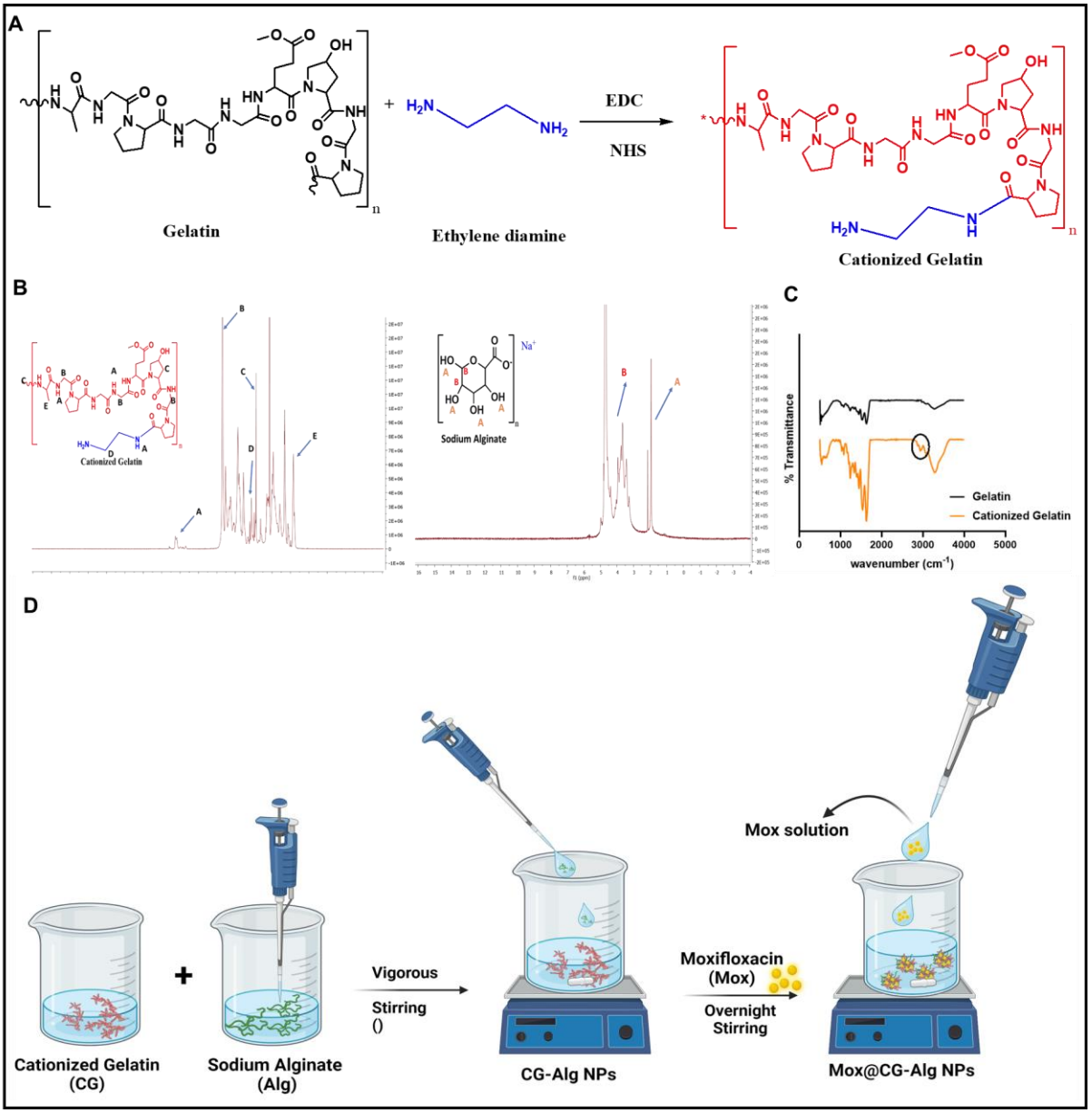

Figure 4.1. Synthetic scheme of cationized gelatin (**A**). Characterization of cationized gelatin. The ^{1}H NMR spectra of cationized gelatin, sodium alginate (**B**). FTIR spectra of gelatin and cationized gelatin (**C**). Graphical presentation of preparation of CG-Alg NPs (**D**).

4.2.3. Characterization of CG-Alg NPs

4.2.3.1. FTIR

As previously reported, Using the FTIR by applying the KBr pellet method, the functional groups of gelatin, cationized gelatin, blank NPs, and Mox@CG-Alg NPs were characterized,

and over the range of 400-4000 cm^{-1} the spectra were recorded using a JASCO 2000 - FTIR (Japan) (Ch et al., 2023).

4.2.3.2. Characterization of NPs

The particle size by dynamic light scattering (DLS) and surface charge of the NPs (100 dilutions, PBS pH 7.4) were evaluated using Malvern's zetasizer^{TM}ZEN 3600 instrument at 90º scattering angle at room temperature. The morphology of the NPs was assessed by scanning electron microscope (SEM) (Apreo Lo Vac, FEI, USA). The freezer-dried powders were spread on a carbon tape attached to the sample holder and then subjected to gold coating for 30 min. Then after placing the samples in the respective sample holders, the images were captured using SEM.

For determining the drug loading and the entrapment efficiency of NPs, the NPs were breached by methanol and analyzed as previously reported (Ch et al., 2021). The amount of Mox loaded in the nanoparticles was analyzed at 281 nm wavelength with the help of a UV-Visible spectrophotometer and determined using the equations given below:

$$\% \text{ Drug loading} = \frac{\text{Amount of drug entrapped in nanoparticles}}{\text{Total weight of NPs (polymer + drug)}} \times 100$$

$$\% \text{ Entrapment efficiency} = \frac{\text{The initial weight of the drug - the weight of the free drug}}{\text{The initial weight of the drug taken}} \times 100$$

4.2.3.4. Thermal analysis

Thermal analysis for the Mox, CG, sodium alginate, Mox@G-Alg NPs, and Mox@CG-Alg NPs was performed using a differential scanning calorimeter (DSC 60, Shimadzu, Japan), according to the reported method (Vysyaraju et al., 2022). Briefly, the free drug and NPs (3-5 mg) were weighted in pans made up of aluminum, followed by compression. The sample containing pans was analyzed over 40-300 ºC under atmospheric nitrogen at a 10 ºC/min increase in heat rate.

4.2.3.5. XRD

The crystallographic arrangement of Mox, Gelatin, CG, sodium alginate, Mox@G-Alg NPs, and Mox@CG-Alg NPs was studied using an X-ray diffractometer (ULTIMA-IV, Rigaku, Japan). The instrument was subjected to a voltage of 40 KV with the help of a CU anode, and the spectra were recorded at 2Ɵ from 5º to 70º at a 5º/min scanning rate.

4.2.3.6. Drug release study (*In vitro*)

The *in vitro* drug release study was carried out to determine the amount of Mox released from the Mox@CG-Alg NPs. Mox and Mox@CG-Alg NPs were added to a dialysis bag (MWCO 3.5 KDa) along with continual stirring at 300 RPM at 37 ºC in a 100 mL beaker of simulated tear fluid (STF), which has a pH of 7.4. At predefined intervals, 1 mL of the sample was removed and replaced with the new medium. The amount of drug released was analyzed using HPLC (Phenomenex C18 column) using a UV detector at a wavelength of 281 nm, and % cumulative drug release (CDR) was calculated.

4.2.3.7. Corneal Permeation by Franz diffusion

The permeability efficiency (*ex vivo*) of Mox and Mox@CG-Alg NPs (0.05% w/v of Mox) through goat corneal tissue was conducted utilizing a Franz cell diffusion apparatus. The corneal tissue was fixed over the receiving compartment containing STF (5 mL), pH 7.4, and the samples were taken in the donor compartment, which was later fixed with clamps. The experiment was conducted at 37 ± 1 °C under constant stirring (300 RPM). 300 µL of the sample was removed and replaced with fresh media from the receptor compartment at predetermined intervals. All the collected samples were passed through a 0.45 µM syringe filter, and the amount of Mox permeated through the cornea was analyzed using an HPLC at 281 nm.

4.2.3.8. Viscosity studies

The viscosity of the blank NPs of various concentrations (0.5-3 % w/v) was studied at different temperatures ranging from (25-60 °C) and shear rate from (0-1000 S^{-1}) with a rheometer (Anton-Paar, MCR 302, Austria). The viscosity of the samples was analyzed using the parallel plate method. Briefly, the samples were placed on the plate fixed at the bottom. To a mobile knob, a parallel plate was connected, and the sample's viscosity was analyzed at different temperatures and shear rates and plotted.

4.2.3.9. Determination of contact angle

The contact angle for the polymers and formulations was determined to analyze their hydrophilic and hydrophobic nature using a tensiometer (Biolin Scientific theta flex, Sweden). The pendant drop method was applied with an experimental condition of 600 µL of sample infill volume and adjusted 50 µL of drop volume. The goat cornea was placed at the bottom of the sample holder, and samples were pipetted using a vacuum. The angle at which the sample drop spread on the corneal tissue was determined.

4.2.4. Stability Studies

The stability experiments for the Mox@CG-Alg NPs were carried out at ambient room atmosphere (RT) and freezing condition (4 °C) for 30 days, and the results were displayed. They were also characterized for particle size and % DL.

4.2.5. Determination of mucoadhesivity

4.2.5.1. Mucoadhesive force by texture analyzer

The texture analyzer (Stable Micro Systems, UK) measured the detachment force of NPs from the goat as per the previously reported procedure (Ch et al., 2023a). Briefly, the goat intestine was obtained from the abattoir and washed with PBS of pH 7.4, and cut into desired size. Before experimenting, the intestinal tissue was soaked into the mucin (5% w/v) for about an hour. Then the tissue was fixed at the base and onto the moving arm of the instrument, and the

formulation was added (0.5 mL). The mucoadhesion force was assessed by adjusting the instrument's parameters, such as the speed of the moving arm to 0.5 mm/sec as pre-test speed. The contact force of 5 g and the 100 g applying force were used to measure the mucoadhesive force. The moving probe was kept in contact with the formulations for 120 sec, and the probe moved at a post-test speed of 0.1 mm/sec. The mucoadhesive strength was calculated as the force in grams necessary to detach the probe from the tissue.

4.2.5.2. Corneal retention time by falling liquid method

The falling liquid method determined the amount of nanoformulation retained on the goat corneal surface. Briefly, goat eyeballs were collected from the abattoir, and the eye was dissected for cornea and washed with PBS (pH 7.4). After washing, the cornea was incubated in mucin for 30 min. The Rhb-labelled formulation (200 µL, 0.5 mg/mL) was applied to the cornea and incubated for another 30 min. The cornea was attached to a falcon tube by applying a double-sided tape at an angle of 45º. A peristaltic pump was then used to help the STF of pH 7.4 pass over the cornea at a constant rate (1 mL/min). The NPs remaining after washing was assessed by fluorescence spectroscopy.

4.2.5.3. Determination of mucin interaction with NPs

To evaluate the mucoadhesive ability of CG-Alg NPs, a mucin turbidity study was performed in which 1 mg/mL of CG-Alg NPs was incubated with 2 mg/ mL mucin solution under constant temperature (37 ºC) and shaking (100 rpm). The reaction mixture's optical density (OD at 600nm) was analyzed using a UV-spectrophotometer.

4.2.6. Cell Culture

The Human Corneal Epithelial (HCE) Cells were procured as a gift from LV Prasad Eye Institute (LVPEI, Hyderabad). Dulbecco's modified Eagles medium F-12 (DMEM F-12), Fetal Bovine Serum (FBS), and penicillin/streptomycin solution (100 IU/mL) were purchased from

Himedia Laboratories (Mumbai, India). The cells were cultured and incubated in a complete media containing DMEM F12 supplied with FBS and antibiotics at 37 ºC with 5% CO_2.

4.2.6.1. HCE cell cytotoxicity assay

According to the previously reported protocol, the formulation's HCE cell cytotoxicity (*in vitro*) was determined using an MTT reagent(Kumbham et al., 2022). The 96-well plate was seeded with HCE cells in DMEM F12 complete media at 2 X 104 /well density and incubated at 37 ºC. The formulations of various concentrations were added to each well and incubated for 24 h. Control HCE cells were left untreated. After the incubation, the media in the wells were discarded, and MTT solution (5mg/mL, 100 µL) was added to each well and further incubated for 4h. Later, following incubation, the MTT solution was removed, replaced with DMSO (150 µL), and incubated for 30min. After the incubation, the samples' OD was recorded at 590 nm and 620 nm (reference wavelength) using a Spectramax microplate reader (Molecular Devices, USA). The viability of cells was determined using the equation given below:

$$\% \text{ Cell viability} = {}^{\text{OD of sample}}/_{\text{OD of control}} \text{ X } 100$$

OD of Sample = the OD of the cells after the treatment with drug-loaded NPs solution.

OD of control = the mean OD of the control cells. The data were represented as mean ± SD and carried out in triplicates.

4.2.6.2. Cellular Uptake Study

4.2.6.3. NPs cellular uptake analysis by confocal microscopy

According to previously reported protocol, the monolayer HCE cells and spheroids are incubated for 1 and 4 h with Rhb-CG-Alg NPs (Itoo et al., 2022b).

Uptake in monolayer cells

In HCE monolayer cellular uptake study, the HCE cells population with $5x10^4$ /well was seeded onto a coverslip and incubated overnight, followed by treatment with FITC labeled NPs (5 µg/mL in complete media without serum) for 1 and 4 h. After the incubation, PBS wash was given to the cells three times followed by staining the cells with DAPI (10 µg/mL, 100 µL) in PBS for 10 min. Further, the cells were washed again with PBS to remove the excess DAPI, and fixation of cells was performed using 4% paraformaldehyde for 20 min. Later, coverslips were fixed on the microscopic slides using fluoromount-G, and images were captured using a Leica Microsystem's confocal microscope (Germany). DAPI (350/460 nm) and FITC (485/510 nm) were used as the excitation and emission wavelengths for the images, which were then processed using Image J software.

Uptake in HCE spheroid cells

HCE spheroid cells were prepared using the liquid overlay method. The 12-well plate was filled with a sterile 1.5% w/v agar solution in 50 µL DMEM F 12, then HCE cells were seeded there at a population of 1 x 10^4/well (150 µL) and kept in continuous shaking. The spheroids were further treated with Rhb-labelled NPs after attaining the spheroidal diameter of approximately 800 µM and followed by incubation. Using a confocal microscope, Z-stacking pictures were acquired at various cell layers on the z-axis from the surface of the cells. Using Image J software, the acquired photos were further processed.

4.2.6.4. Cellular uptake by flow cytometer

HCE cells at a cell population of 0.2 x 10^6 cells/well were seeded in a 12-well plate and kept overnight incubated, then treated with the Rhb-NPs (Rhb- 5µg/mL) for 1 and 4h. After washing, the cells were trypsinized, followed by centrifugation at 1200 rpm for 5 min, and re-suspended in 0.5 mL of PBS, pH 7.4. The NPs uptake by HCE cells was assessed by determining the viable cells using flow cytometry (FACS ARIA III, BD Life Sciences). Using

the IDEAS application (version 6.0), the gating of the cells was performed using forward and side scatter plots. From the respective treatment groups, the fluorescence from the viable cells of HCE (10000) was recorded and represented graphically.

4.2.6.5. Determination of Trans-Epithelial Electrical Resistance (TEER)

Millicell®ERS-2, EVOM volt-ohm meter (Millipore, USA) determined the permeation of the NPs and the resistance of the transepithelial HCE cells after the treatment. The HCE cells (1 x 10^6) were seeded onto the 12-well membrane with permeable inserts coated with collagen (Corning™, USA). The cells were treated with formulations (100 µL, 2mg/mL of Mox) once the resistance value reached 170 Ω cm^2. The apical chamber of the insert was added with NPs and incubated for 5 min. The epithelial membrane voltage was analyzed at predetermined intervals by placing the electrode tips between the chambers.

4.2.7. HET-CAM test

The chorioallantoic membrane (CAM) evaluation after the treatment with formulations for redness/hemorrhage was observed as ocular irritancy per the previously published protocol (Ch et al., 2023a). Briefly, Fertilized hen's eggs incubated at 37 ± 0.5 ºC for 9-11 days were obtained from a hatchery farm. After confirming the development of CAM upon illuminating, with the help of a drilling tool and a spinning blade, a 2x2 cm^2 shell was broken out. To moisturize the inner membrane of the CAM, saline (0.5 mL) was added over the CAM, and after a few minutes, the solution was carefully removed without disturbing the CAM. The free drug and formulation were added to the CAM, and the toxicity was observed after 5 min. 1M NaOH and Saline were used as negative and positive controls, respectively.

4.2.8. *In vitro* anti-bacterial efficacy

4.2.8.1. C*ulturing of bacterial strains*

Bacteria, *Pseudomonas aeruginosa*, and *Staphylococcus aureus* were kindly gifted by LVPEI and BITS-Pilani, Hyderabad. The bacteria were grown aerobically at 37 ºC in Miller, Luria Bertani (LB) broth from HIMEDIA in India. Before conducting studies, bacterial strains were sub-cultured and diluted to achieve a bacterial concentration of 10^8 CFU/mL at an optical density (OD = 0.2@600 nm) followed by incubation at 37 ºC. For bacterial biofilms, both the bacteria were grown in LB broth at a density of 10^6 CFU/mL and incubated on coverslips in a 12-well plate for 48 h at 37 ºC followed by washing the coverslips with PBS, pH 7.4, and used for subsequent experiments.

4.2.8.2. Determination of MIC/MBC for Mox@CG-Alg NPs

The broth dilution technique (microtiter) was used to evaluate the minimum inhibitory concentration (MIC) according to the previously described protocol (Ch et al., 2023a). In a 96-well plate, 100 µL of bacteria at a population of 10^6 CFU/mL in LB broth was seeded 100 µL/well of formulation of concentrations over a range from 0 to 4 µg/mL followed by incubation at 37 ºC for 12 h. Using a microplate reader (Spectramax M4, Molecular Devices, USA) the visual turbidity was evaluated at OD@600nm at various intervals.

An MTT experiment was carried out to assess the MBC of bacterial strains to compare further the MIC value established by the microtiter dilution technique. Briefly, in a 96-well plate, the bacterial strains of population 10^6 CFU/mL (100 µL, in LB broth) were seeded in each well and incubated with formulation (0.1 mL) for 12 h at 37 ºC followed by the addition of MTT reagent (50 µL, 5 mg/mL) for 2 h. The MTT reagent was dissolved by adding DMSO to each well. The optical density of the well plate was then determined at 590 nm using a microplate reader, while reference absorption maxima were maintained at 620 nm. Using the formula, the proportion of viable cells was determined.

$$\% \text{ Cell viability} = {}^{\text{OD of sample}}/_{\text{OD of control}} \text{ X } 100$$

4.2.8.3. Zone of Inhibition (ZOI)

The bacteria were disseminated using a sterile spreader on nutrient agar plates at a 106 CFU/mL density. On the bacterial agar plates, sterile circular paper discs were prewetted in the formulation (1 mg/mL) for 30 min before being incubated for 24 h. After incubation, the diameter of the zone was measured, and pictures of the plates were captured.

4.2.8.4. Planktonic Bacterial viability assay

Planktonic bacteria at a 10^6 CFU/mL density were treated with Mox@CG-Alg NPs and incubated at 37 ºC at various intervals. After the incubation, the bacteria were centrifuged at 7000 rpm at room temperature for 10 min. The pellet was collected and washed three times with PBS, pH 7.4, followed by dispersion of the pellet in PBS (200 µL). The staining was done for the bacteria using SYTO 9 (33.4 µM) and propidium iodide (PI) (0.4 mM) at an equal ratio. After adding the staining mixture, the bacteria were incubated for 10 min in the dark. The images were taken using a fluorescence microspore (Leica, DMi8, Germany) at an excitation (485 nm)/emission (498 nm) wavelength.

For flow cytometric studies, fresh sub-cultured bacteria at a population of 10^6 CFU/mL were incubated at 37 ºC with the Mox@CG-Alg NPs (25 µg/mL) at various time points. After the incubation, the bacteria were centrifuged (6000 rpm) for 10 min. The supernatant was discarded and washed with PBS, pH 7.4, and redispersed in 500 µL of PBS. The staining procedure was performed as mentioned above for the treated bacteria. A gating procedure was performed to gate the live/dead cells using the FITC/PI lasers, and gated bacterial cells (10000) were evaluated using a FACS ARIA III flow cytometer (BD Life Sciences, USA). Using the FACSDiva application, the data was represented as quadrant plots.

4.2.8.5. bacterial biofilms viability assay

After the formation of bacterial biofilms, they were treated with Mox@CG-Alg NPs (25 µg/mL) and incubated for 4 h at 37 ºC. After the treatment, the biofilms are rinsed thrice with PBS pH 7.4 and stained, as mentioned in section 2.8.4. After staining, the 3D images of the biofilms were generated using a confocal microscope at an excitation/emission wavelength of 485/498 nm.

4.2.9. *In vivo* experiments

The Committee for the Purpose of Control and Supervision of Experiments on Animals (CPCSEA), BITS-Pilani Hyderabad, India, provided the guidelines for all animal treatments. C57BL/6 mice (18 g, 5 weeks old) were obtained from Vyas labs Pvt Ltd in Hyderabad, and the animals were given a week to become acclimated to the 19–25 ºC temperature range, 50–60% relative humidity, and nocturnal–diurnal cycles.

4.2.9.1. Determination of corneal retention time by *in vivo* fluorescence imaging

The coumarin 6 (C6) loaded CG-Alg NPs retention time over the cornea was analyzed using *in vivo* imaging to understand the mucoadhesive properties of the formulation. Briefly, Balb/C mice were anesthetized with isoflurane, and C6@CG-Alg NPs (10 µL) were given topically as an eye drop to each eye. At various time intervals, the fluorescence intensity was recorded with an exposure time of 30 sec, and images were captured until the signal disappeared using IVIS LUMINA (Perkin Elmer, USA). The region of interest (ROI) at all the time intervals was measured using Living Image software version 4.5.5.

4.2.9.2. Anti-bacterial efficacy studies in a bacterial keratitis-induced mice model

An intraperitoneal injection (150 µL) was given to the C57 mice for anesthetizing using ketamine/xylazine. Further, 1 mm deep abrasions were created over the corneal epithelium using a 25-gauge needle, followed by injection of bacteria (*P aeruginosa* (10^6 CFU/mL, 5 µL)) into both the eyes and allowed the mice to develop an infection. After the development of

infection, the mice were categorized and labeled as control, free drug, and Mox@CG-Alg NPs. The treatment was given for free Mox and Mox@CG-Alg NPs (5 µg/mL Mox, 15 µL) to the right cornea, and the treatment cycle was repeated every 12 h time interval. The control group was administered with PBS, pH 7.4. After the treatment, each mouse eye was photographed, and scoring was given based on the progress of the infection. Scoring from +0 to +5 was given based on the eye condition, where 0 being clear/slight opacity and 5 being full corneal perforation.

4.2.9.3. Determining the number of viable bacteria

The Quantification of viable bacteria was determined by plating the homogenized eye after the treatment on the nutrient agar plate. After the treatment, the animals were euthanized, and the cornea was dissected and homogenized with saline solution (0.9 % w/v). Then the solution was diluted and plated in the nutrient agar plate, followed by overnight incubation at 37 ºC. The number of viable bacterial was counted based on colonies obtained by using the following formula:

$$\text{Colony forming units} = \frac{\textbf{No.of colonies}}{\textbf{10 x dilution factor}} \text{ X } 1000$$

4.3. Results and Discussion

4.3.1. Cationic modification of gelatin

Ethylenediamine cationically modifies the positive charges on the gelatin, making them soluble in water at ambient temperature. Carboxyl groups of the gelatin are introduced with amino groups on the gelatin backbone by the reaction with ethylenediamine. The cationization of gelatin was confirmed with ^{1}H NMR spectroscopy, where peaks corresponding to protons of -CH_2 groups added by amino acids to the gelatin backbone were observed at 2.8 and 3.3 ppm, and the presence of OH groups was observed at 2.0 ppm for sodium alginate as shown in **Figure**

4.1B. The conjugation was further confirmed by the FTIR spectrum of gelatin and cationized gelatin (**Figure 4.1C**).

4.3.1.1. Optimization of G/CG-Alg NPs

The G-Alg NPs and CG-Alg NPS are prepared by experimenting with various concentrations of G/CG/Alg, and the polymer combination showing lower particle size was utilized for further studies. The experimental data representing various polymer concentrations, their mean particle size, and surface charge are displayed in **Table 1.**

Table 4.1. Experiments of G-Alg NPs (**a**) and CG-Alg NPs (**b**) with varied polymer concentrations and their effect on particle size and zeta potential.

a)

Exp	Amount of Cationized Gelatin (mg)	Amount of Sodium Alginate (mg)	Z avg (nm)	Zeta Potential (mV)
01	5	5	267.4 ± 3.7	-36 ± 3
02	10	5	529.6 ± 2.2	-28 ± 4
03	2.5	7.5	217.2 ± 4.0	-26 ± 3
04	5	10	411.3 ± 5.1	-32 ± 3
05	7.5	2.5	319.8 ± 4.9	-28 ± 2

b)

Exp	Amount of Gelatin (mg)	Amount of Sodium Alginate (mg)	Z avg (nm)	Zeta Potential (mV)
01	5	5	783.1 ± 5.2	-18 ± 2
02	10	5	1429.8 ± 7.7	-14 ± 3
03	2.5	7.5	417.2 ± 3.0	-23 ± 3
04	5	10	512.6 ± 5.8	-23 ± 4
05	7.5	2.5	1601.6 ± 8.1	-17 ± 2

4.3.2. Characterization, mucoadhesion, and drug release of CG-Alg NPs

The polyelectrolyte complex (PEC) nanoparticles were developed from G/CG and sodium alginate for Mox delivery. By increasing the volume of G/CG and keeping the volume of

alginate constant, the size of the PEC can be reduced **(Figure 4.2A)**. Alginate, a highly anionic polysaccharide, requires a very positively charged polyelectrolyte to neutralize alginate fully. Increased G/CG volume balances the negative charges on Alg more effectively, thereby reducing the PEC. The solution's concentration, ionic strength, and CG/Alg ratio all affect PEC formation. The entrapment of Mox in the G/CG-Alg NPs and the thermal stability of the formulation was further confirmed with DSC, where the Mox peak disappeared in the G/CG-Alg NPs thermograph, indicating that the Mox was completely entrapped inside the PEC **(Figure 4.2D)**. XRD analyzed the crystallinity of the Mox, Gelatin, CG, Alg, and Mox@G/CG-Alg NPs, and it was observed from the spectra that Mox has crystalline peaks. These crystalline peaks were absent in Mox@G/CG-Alg NPs, indicating the amorphous nature of the formulations **(Figure 4.2E)**. This could be because gelatin's helical structure changed due to cationization. The G-Alg NPs' particle size was more than the CG-Alg NPs; therefore, further studies were carried out using CG-Alg NPs **(Table 4.1b)**. The CG-Alg NPs after the drug loading was increased to 237.6 ± 3 nm and displayed a spherical shape from SEM analysis **(Figure 4.2B)**. The zeta potential of Mox@CG-Alg NPs was found to be -24.5 ± 3 mV. The drug-loaded complex developed a negative surface charge due to the reduction of protons of the acid groups on the sodium alginate. The EE and DL were 75.1 ± 2.5 and 9.5 ± 0.5 %, indicating the drug was well encapsulated and loaded in the CG-Alg NPs **(Table 4.2)**. The contact angle for the polymers G, CG, sodium alginate, and formulations G-Alg NPs, and CG-Alg NPs was decreased with an increase in concentration, indicating the hydrophilicity of the formulations that led to even spreading over the goat cornea **(Figure 4.3E, F, and G).**

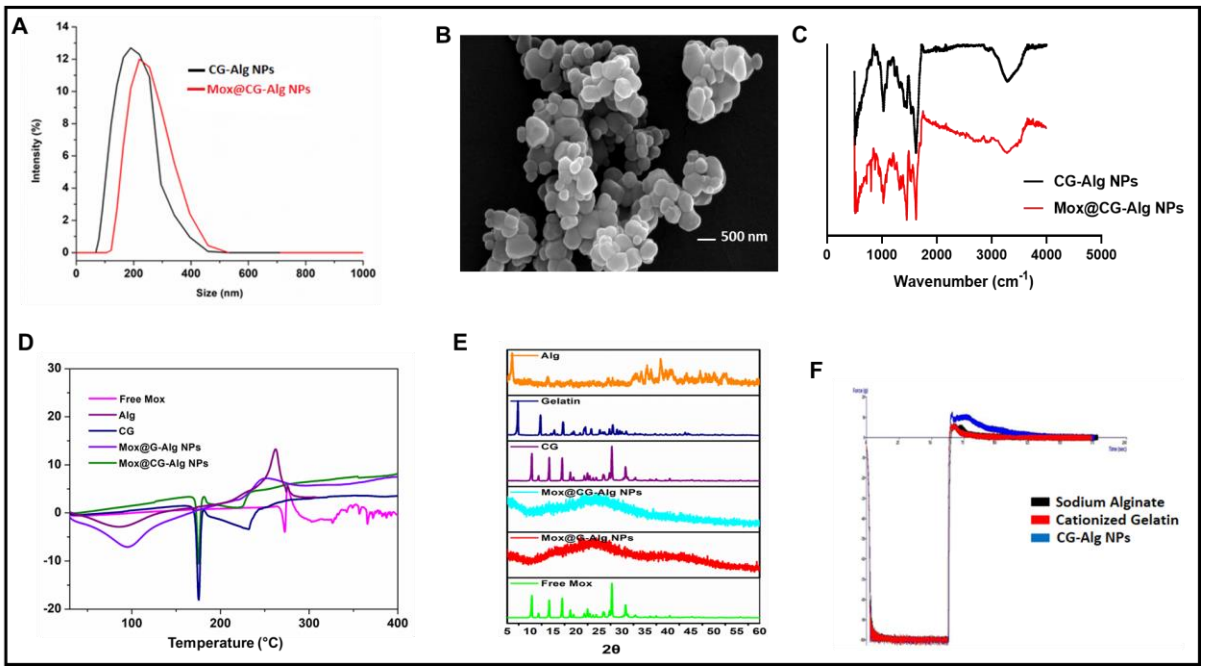

Figure 4.2. Physicochemical characterization of blank NPs and Mox@CG-Alg NPs. Particle size distribution and morphology of Mox@CG-Alg NPs by DLS method (**A**) and scanning electron microscopy (**B**); FTIR spectroscopy of blank NPs and Mox@CG-Alg NPs (**C**); dynamic Scanning calorimetry thermogram (**D**); X-ray diffraction (**E**); mucoadhesive study by texture analyzer (**F**).

Table 4.2. Mean particle diameter, PDI, surface charge, and drug loading efficiencies of optimized formulations.

Formulation	Size (nm)	PDI	Zeta Potential (mV)	EE%	%DL
CG-Alg NPs	217.2 ± 4	0.22 ± 0.05	-26.3 ± 3	—	—
Mox@CG-Alg NPs	237.6 ± 3	0.28 ± 0.03	-24.5 ± 3	75.1 ± 2.5	9.5 ± 0.5

Human eye tear fluid has a physiological pH of 7.2, and the release study was performed in the STF, pH 7.2, resembling the human eye tear fluid. Mox's burst release can be observed from the release pattern, as shown in **Figure 3H**. Whereas the Mox@CG-Alg NPs had shown controlled drug release over the course of 18 h. Almost 96% of the Mox was released in 18 h.

From the diffusion studies through the cornea, about 75% of the drug got permeated through the goat cornea resulting in controlled release of Mox from CG-Alg NPs **Figure 3I**. The small size of the NPs resulted in better permeation through the corneal tissue. The negatively charged Alg has a stable surface charge at pH 7.2, which led to less electrostatic interaction of Mox and exhibited controlled release.

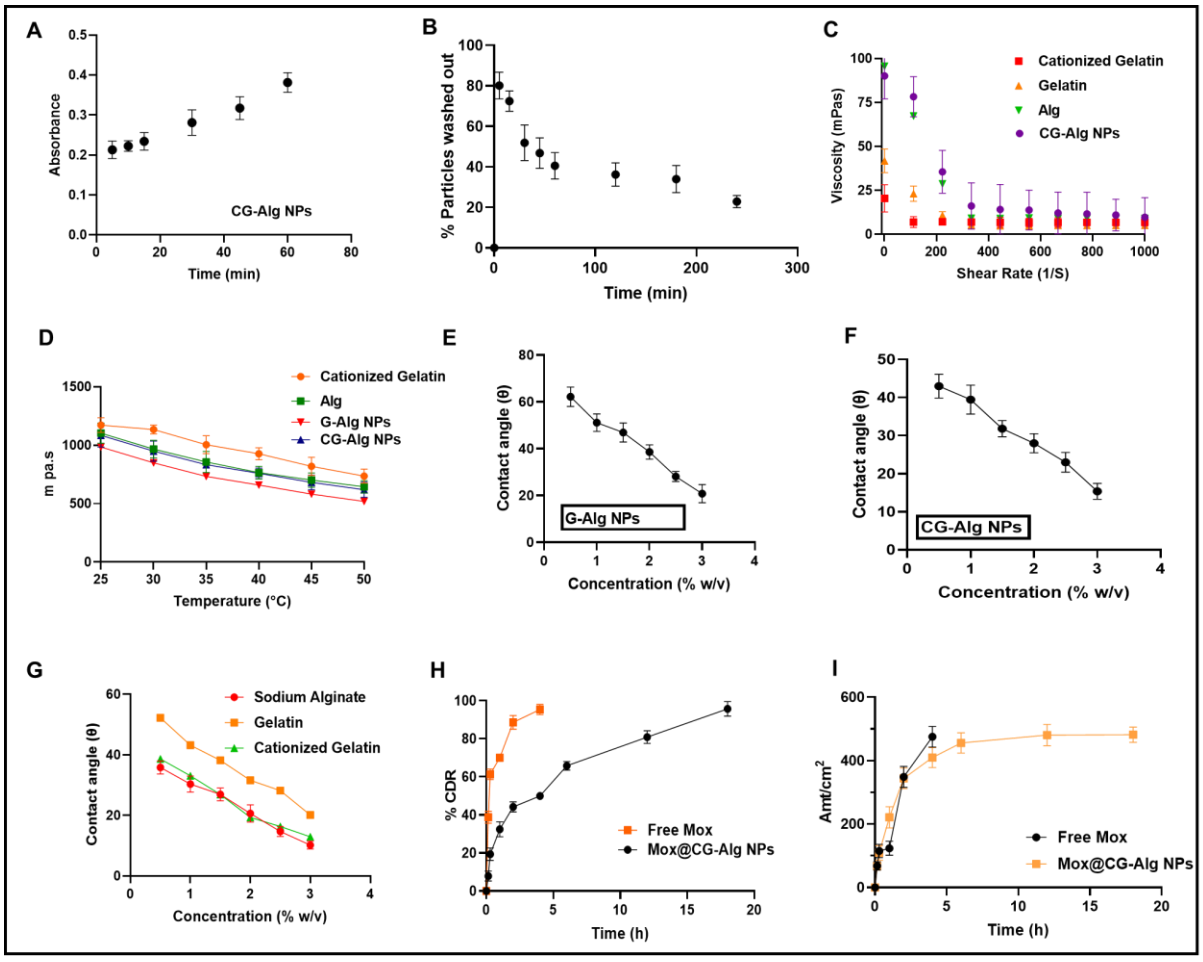

Figure 4.3. Mucoadhesive studies. Mucin turbidity study of CG-Alg NPs (**A**); mucoadhesivity of Rhb-CG-Alg NPs by falling liquid method (**B**). Rheology studies. Viscosity vs shear rate (**C**); temperature-dependant viscosity (**D**); Contact angle of formulations G-Alg NPs (**E**), CG-Alg NPs (**F**); contact angle of free polymers at various concentrations (**G**); The drug release

(*in vitro*) of Mox and Mox@CG-Alg NPs (**H**); trans-corneal permeation of Mox@CG-Alg NPs (**I**).

There was a significant difference in the viscosity of CG compared to the Alg and CG-Alg NPs. After cationization, the triple helical structure of the gelatin ruptures, leading to reduced hydrogen bonding interactions. The protonation of amino groups makes the gelatin molecules less available for hydrogen bonding. The viscosity was further reduced by increasing the temperature and shear rate(Jalaja et al., 2015). Compared to the G, CG, the sodium alginate and CG-Alg NPs had higher viscosity at 25 ºC; this may be due to the good ionic interaction between the negative and positive groups of the sodium alginate groups of the CG that led to the rise in viscosity **(Figure 4.3C&D)**. Also, sodium alginate's negatively charged carboxyl groups produce repulsive effects and increase its water-binding capacity (Shinde & Nagarsenker, 2009). For 30 days, the formulation's stability was tested at room temperature and 4 ºC. The particle size increased to ~580 nm at room temperature and ~50 nm at 4 ºC. The drug loading was also decreased relatively at room temperature compared to 4 ºC. This indicates that refrigeration is required for the formulation **(Figure 4.4)**. The mucoadhesive properties of PEC were thoroughly assessed, and texture analyzer analysis revealed that CG-Alg NPs had shown a higher mucoadhesive force of 15 g/cm^2 (**Figure 4.2F**).

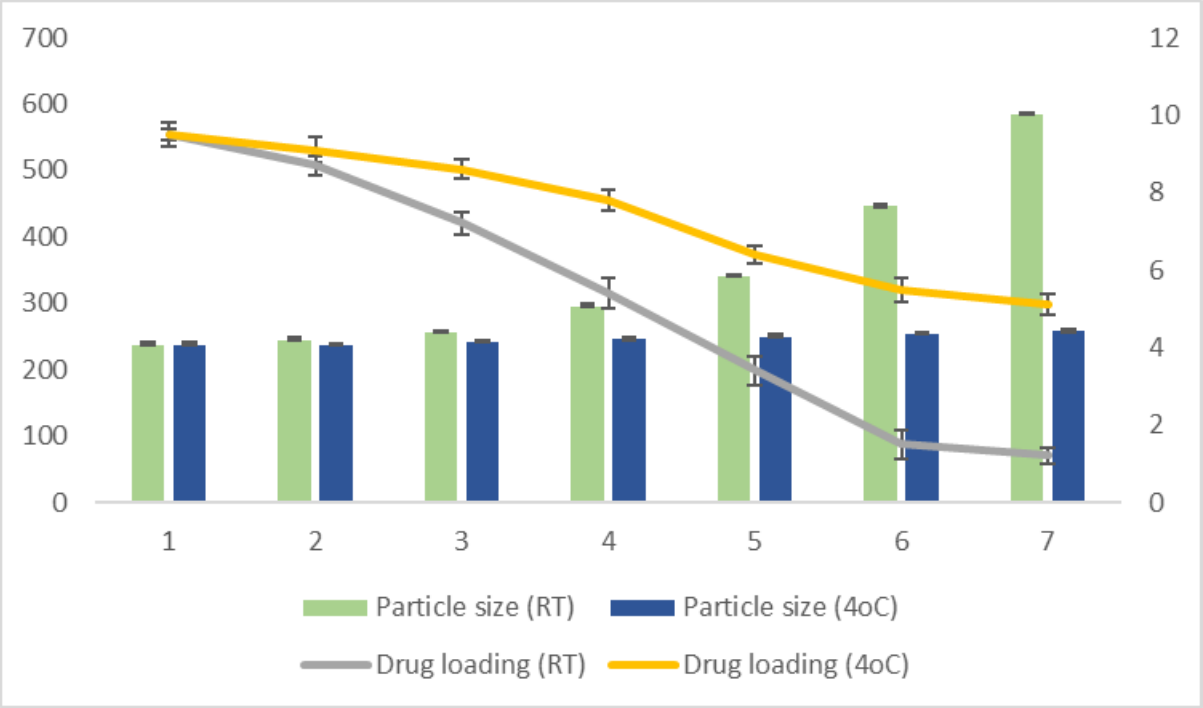

Figure 4.4. The stability of Mox@CG-Alg NPs studied for 30 days at room temperature (RT) and 4ºC.

In contrast, cationic gelatin and sodium alginate showed a force of 9 and 7 g/cm^{2,} respectively **(Figure 4.2F)**. From the mucoadhesive falling liquid method, it was found that 22.8 ± 3.2 % of CG-Alg NPs adhered after 240 min. From the mucin turbidity study, a gradual increase in the interaction of mucin and NPs was observed with respect to time, as Alg is known to be an anionic mucoadhesive polymer with carboxyl groups that may form hydrogen interactions with the hydroxyl groups of mucin glycoproteins. Gelatin has a high level of amine and carboxyl groups which are important for the flexibility of the polymer backbones and are thought to be essential for the mucoadhesive process (Szekalska et al., 2023).

4.3.4. Cell Studies

The NPs have shown no toxicity to the HCE Cells after the formulation treatment for 24 h, determined by MTT assay. Results showed that ~86 % of the cells were viable at higher concentrations after the 24 h incubation **(Figure 4.5A)**. TEER is a sensitive method to confirm the cellular integrity and permeability of the cellular monolayer. This study observed that the

CG-Alg NPs had disturbed the membrane integrity, and the maximum perturbation was 110.57 ± 3.61 Ohm.cm^2 Nevertheless, after 600 minutes, the cell layer's integrity returned to normal without damage. **(Figure 4.5C)**. The confocal cellular uptake study of the Rhb-CG-Alg NPs from the HCE monolayer cells was more internalized after 4 h of incubation at a concentration of 100 µg compared to 50 µg **(Figure 4.5D)**. A similar result was observed with the 3D spheroid model of HCE cells displaying spheroidal penetration upto 100 µM with the Rhb-CG-Alg NPs (250/500 µg/mL) after 4 h compared to the 1 h incubation that showed penetration upto 80 µM **(Figure 4.5E)**. The cellular uptake was further quantified using flow cytometry. The results showed that CG-Alg NPs (50/100 µg) had shown mean fluorescence of 1926 ± 40 and 2634 ± 37, respectively, after 4 h of incubation **(Figure 4.5B)** and formulation with CG-AlG NPs (100 µg) had shown stastical significance of ***, $p<0.001$ when compared to the other formulation . No sign of hemorrhage and irritancy was observed with CG-Alg NPs treated on CAM, and the images were as shown in **Figure 4.6E.**

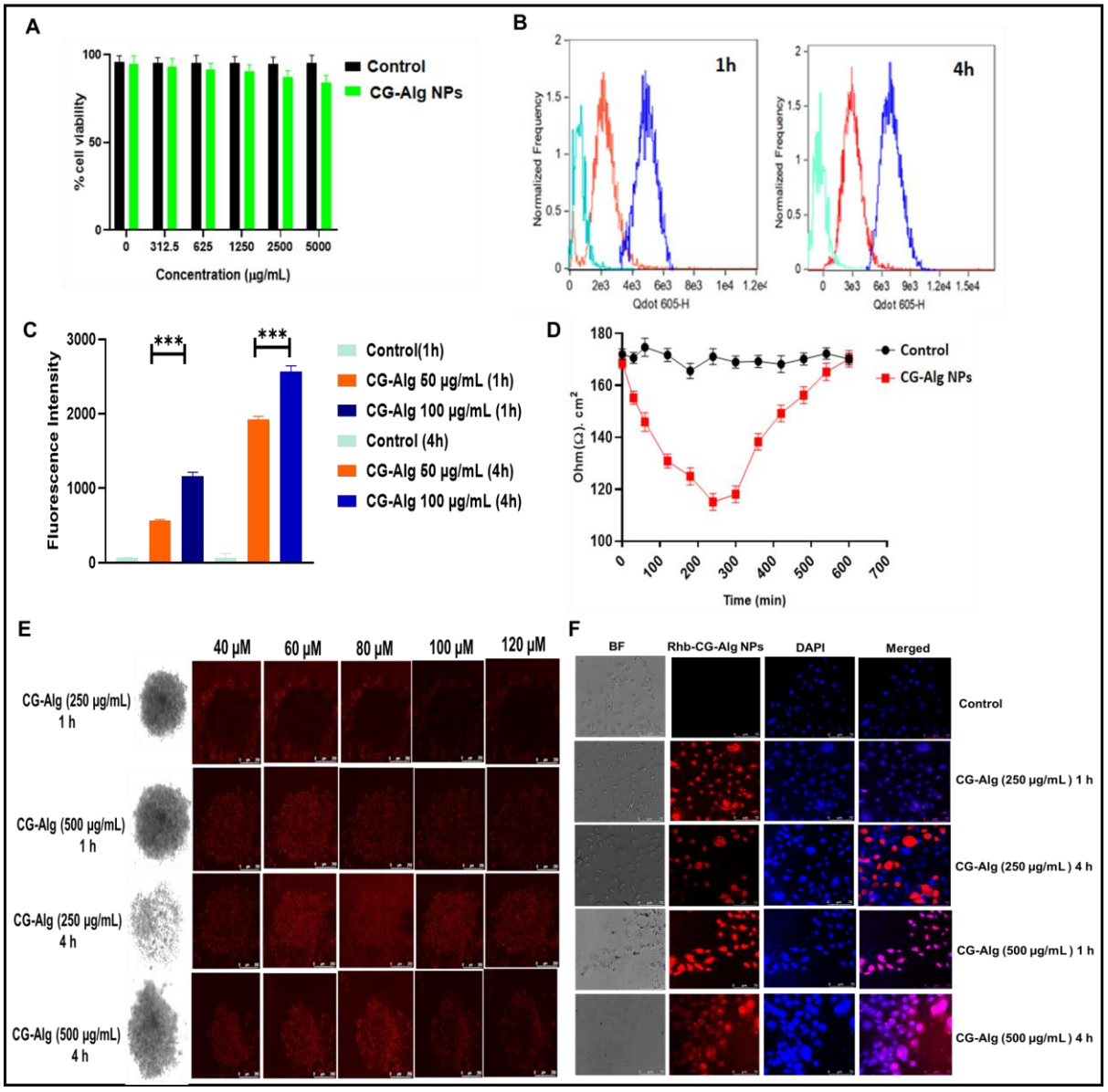

Figure 4.5. Cytotoxicity of HCE cells treated with CG-Alg NPs determined by MTT assay (**A**); the graphical representation of HCE cellular uptake of CG-Alg NPs determined by flowcytometry (**B**); TEER study of HCE multilayer cells incubated with CG-Alg NPs (**C**); HCE cells spheroidal uptake of Rhb-CG-Alg NPs treated for 1 and 4 h (**D**); and monolayer HCE cellular uptake of Rhb-CG-Alg NPs for 1 and 4 h respectively (**E**). *** represents $p<0.001$

4.3.5. Antibacterial Studies

By evaluating OD (MIC) and MTT test (MBC), the inhibitory and bactericidal concentrations of Mox@CG-Alg NPs on *P. aeruginosa* and *S. aureus* were determined. The MIC and MBC

for *P. aeruginosa* were 0.25 µg/mL and 2 µg/mL, respectively. The MIC and MBC for *S. aureus* were 0.5 µg/mL and 4 µg/mL, respectively. The formulation was found to be more effective on *P. aeruginosa* than *S. aureus;* this could be because the gelatin backbone contains positive groups, which allows it to bind to the negatively charged cell wall of *P. aeruginosa,* resulting in cell wall damage leading to a bactericidal effect (Wen et al., 2020) The zone of Inhibition (ZOI) was 20.1 ± 2.2 and 23.3 ± 1.4 mm for *P. aeruginosa* and *S. aureus,* respectively **(Figure 4.6, 4.7)**.

Bacterial viability on planktonic bacteria/ biofilms was assessed by live/dead assay. The bacteria treated with Mox@CG-Alg NPs showed more dead cells after 1h in both *P. aeruginosa* and *S. aureus* bacteria. The fluorescence images captured from a microscope displayed red fluorescence (PI) **(Figure 4.8A).** The live/Dead assay study was further confirmed quantitatively by flow cytometry. After 60 minutes, Mox@CG-Alg NPs showed a dead population in the Q3 + Q4 quadrants, with a total dead population of 73% for *P. aeruginosa* and 68% for *S. aureus* **(Figure 4.8B)**. In the Live/dead assay, the 3D images of both P. aeruginosa and S. aureus biofilms treated with Mox@CG-Alg NPs showed more dead cells after 4h compared to 1 h, as shown in **(Figure 4.8C&D)**. The increased bactericidal effect with respect to time indicates the ability of the formulation to penetrate the bacterial cell wall efficiently. This could be possible by the ionic contact between the gelatin's positive groups and the peptidoglycans' negative groups, which encourages the lesion of the bacterial cell's internal electrolytes. wall ultimately leading to bacterial cell death and a similar outcome was seen by Mahor et al. (Mahor et al., 2016).

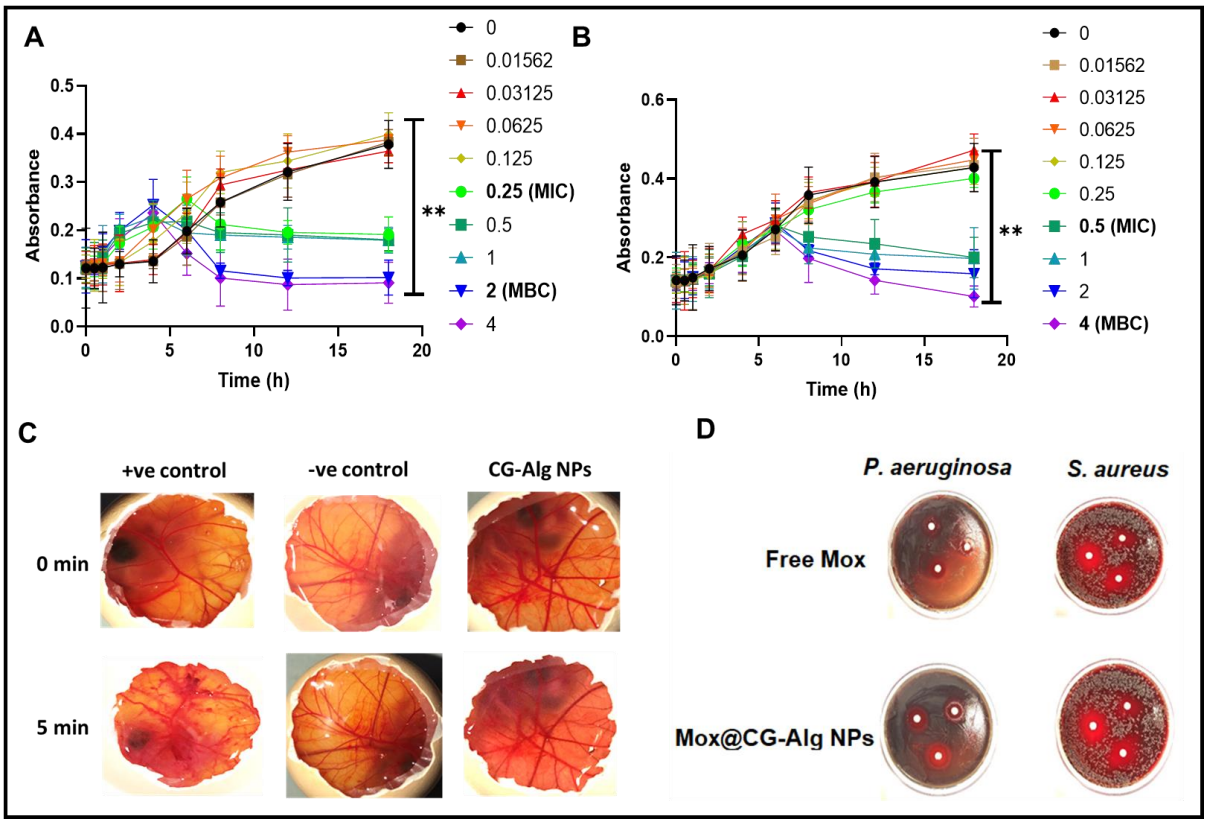

Figure 4.6. Graph representing the minimum inhibitory concentration (MIC) of Mox@CG-Alg NPs treated *P. aeruginosa* (**A**) and *S. aureus* (**B**) analyzed at optical density ($OD@_{600}$); HET-CAM test, photographs of CAM membrane exposed to positive/negative control and CG-Alg NPs (**C**). Images of blood agar plates grown with *P. aeruginosa* and *S. aureus* and treated with free Mox and Mox@CG-Alg NPs show the zone of inhibition (ZOI). (**D**). Data are represented as mean ±SD (n=3, $p<0.01$ as **).

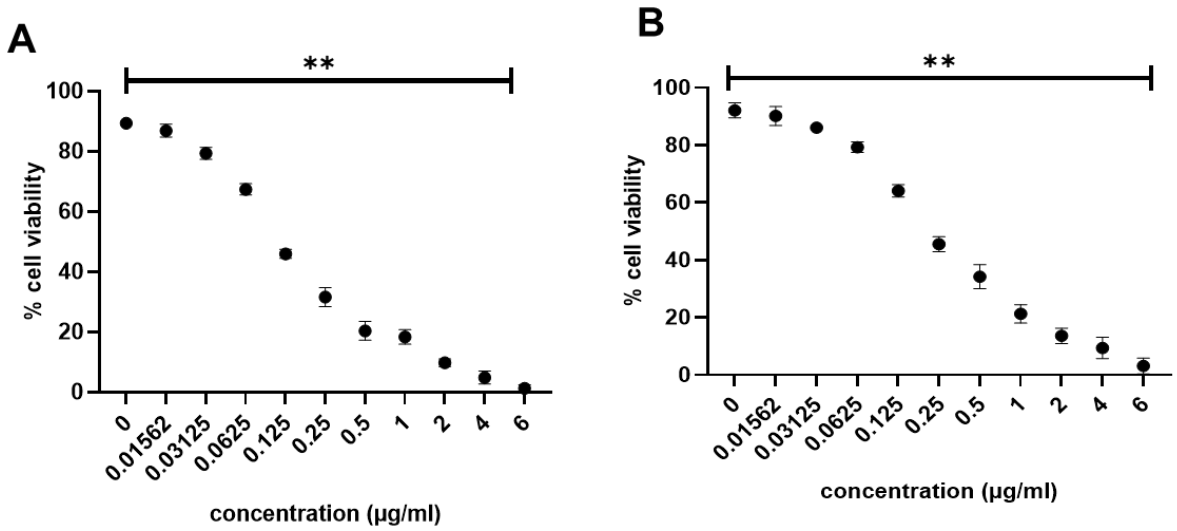

Figure 4.7. Determination of minimum bactericidal concentration (MBC) analyzed by MTT assay against *P. aeruginosa* (**A**) and *S. aureus* (**B**).

Table 4.3. The zone of inhibition for bacteria in diameter (mm) treated with Mox@CG-Alg NPs

Formulation	Zone of Inhibition (mm)	
	P. aeruginosa	*S. aureus*
Mox@CG-Alg NPs	20.1 ± 2.2	23.3 ± 1.4

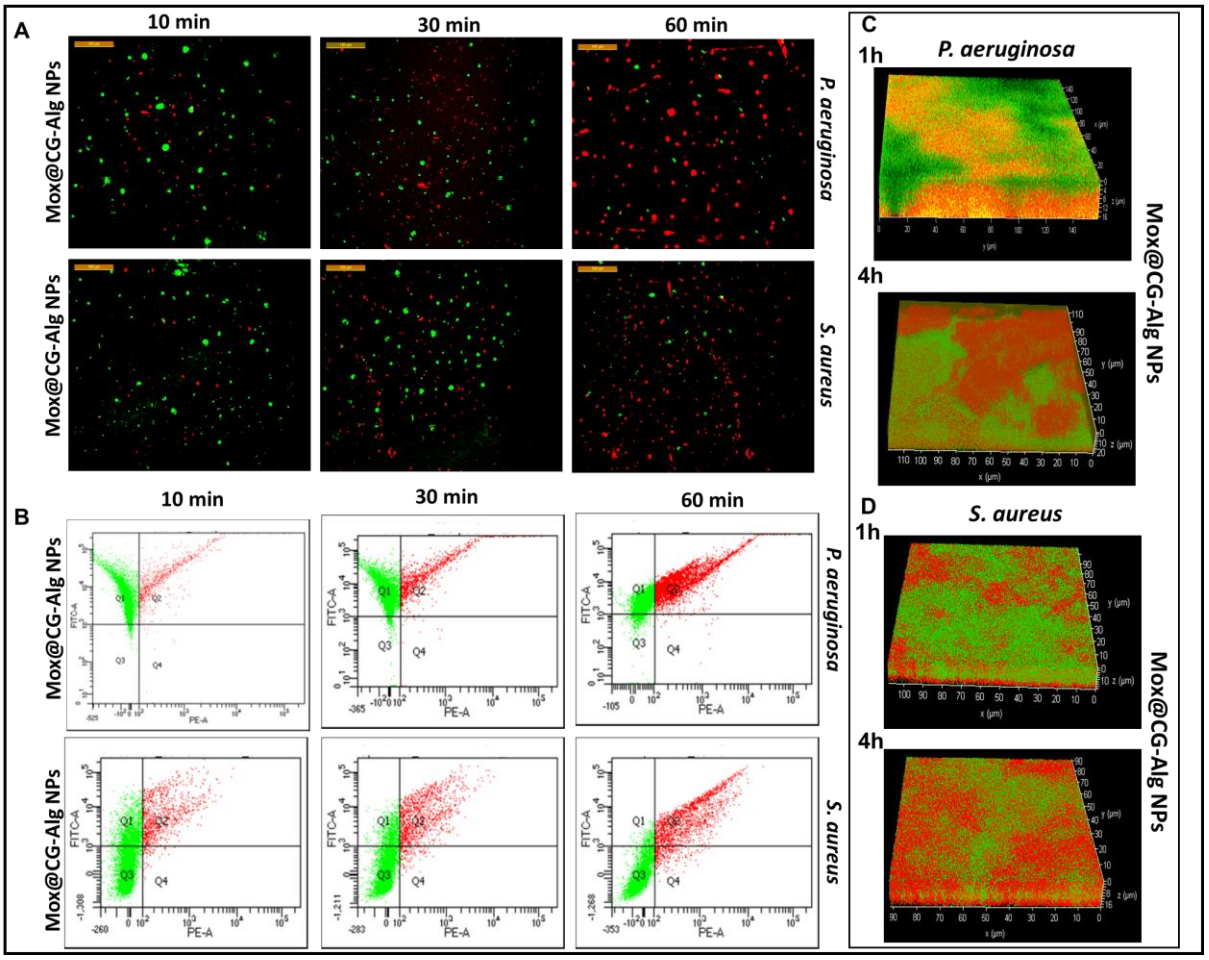

Figure 4.8. Planktonic bacteria viability assay with *P. aeruginosa* and *S. aureus* treated with Mox@CG-Alg NPs followed by staining with SYTO-9 and PI. The fluorescence images of bacteria after the treatment for 10-60 min. Scale bar 100 µm (**A**); the flowcytometric quadrants plot displaying live and dead populations of bacteria incubated with Mox@CG-Alg NPs and stained with SYTO-9 and PI (**B**). Confocal 3D images of biofilms *P. aeruginosa* (**C**) and *S. aureus* (**D**) treated with Mox@CG-Alg NPs for 1 and 4h.

4.3.6. *In vivo* animal experiments

4.3.6.1. *In vivo* imaging for Corneal retention time determination

The retention time of C6@CG-Alg NPs over the Balb/c mice cornea was analyzed, and the fluorescence was determined by *in vivo* imaging system. The ROI was found to be 3.81e+009 ± 2.61e+009 after 5 min, and the fluorescence intensity lasted till 240 min with an ROI of

4.23e+008 ± 1.241e+008. The results indicated that the formulation retained over the cornea for longer and penetrated the cornea. The longer retention time of formulation is due to the ability of CG to form electrostatic interaction with mucin **(Figure 4.9A, B)**.

4.3.6.2. Bactericidal efficacy study

Bk-induced C57 mice by *P. aeruginosa* were treated with the Mox and the Mox@CG-Alg NPs. The images before and after the treatment were captured with a macro lens attached to a digital camera. All the images indicated that all the mice developed an infection **(Figure 4.9C)**. After the treatment, the mean CFU/mL of the free drug group and the Mox@CG-Alg NPs was found to be 811 ± 118 and 321 ± 105, respectively, with a clinical score of 3.5 ± 0.33, 1.7 ± 0.2 for free drug and formulation. The control group had shown 3891 ± 227 CFU/mL with a clinical score of 4.6 ± 0.4 **(Figure 4.9D, E)**. The results indicated that the formulation was more effective than the free drug, where the bacterial load was drastically reduced, demonstrating the penetration efficacy of the NPs into the mice's cornea. The newly developed formulation has overcome the drawbacks associated with conventional topical dosage forms.

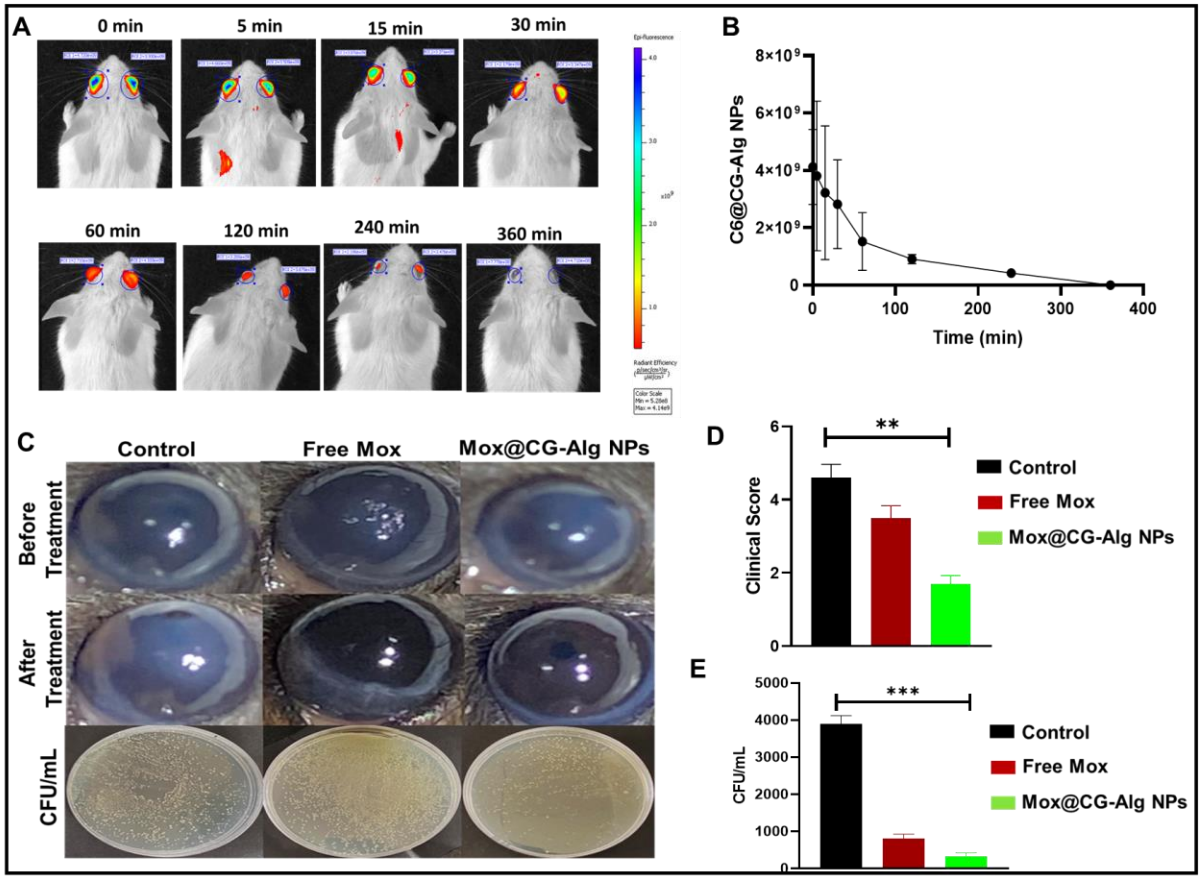

Figure 4.9. *In vivo* corneal retention studies and therapeutic efficacy studies of NPs. Mice cornea *in vivo* real-time fluorescence imaging after administering C6@CG-Alg NPs (**A**). The mean fluorescence retained was represented graphically (**B**); *in vivo* therapeutic efficacy of Mox and Mox@CG-Alg NPs in *P. aeruginosa* infected bacterial keratitis, and photographs of CFU plated after the treatment (**C**); the clinical score given based on the criteria of transparency and perforation of mice cornea after the treatment (**D**); and the colony forming units count after the treatment (**E**).

4.4. Conclusion

A mucoadhesive PEC NPs system was developed using G/CG and Alg loaded with Mox. Thorough physicochemical characterization was performed to analyze the size, uniformity, morphology, % EE and % DL of the NPs. Further, mucoadhesive, toxicity, and NPs uptake studies were performed on the HCE cell line. The antibacterial efficacy of the formulation was

determined against *P. aeruginosa* and *S. aureus* (*in vitro*) and Bk-induced mice models (*in vivo*). The strong electrostatic interaction between the cationic amine groups of CG and anionic carboxyl groups of Alg resulted in the formation of PEC NPs. The optimized Mox@CG-Alg NPs were nanosized particles with low polydispersity. The cationic groups interacted with mucin over the cornea, increasing the corneal residence time and increasing penetration of the NPs into the cornea. The NPs were safe for ocular application and exhibited a strong antibacterial effect compared to free Mox, indicating the effectiveness of the nanoformulations. The *in vivo* study demonstrated that the NPs could significantly reduce the bacterial load in the infected cornea and clear the corneal opacity caused by bacterial biofilm compared to conventional Mox eye drop formulation. Overall, Mox's developed novel polyelectrolyte complex formulation shows the potential for clinical translation owing to its scalability, safety, and effectiveness in treating bacterial keratitis.

Chapter 5

3D-Printed Inherently Antibacterial Contact Lens-like Patches Carrying Antimicrobial Peptide Payload for Treating Bacterial Keratitis

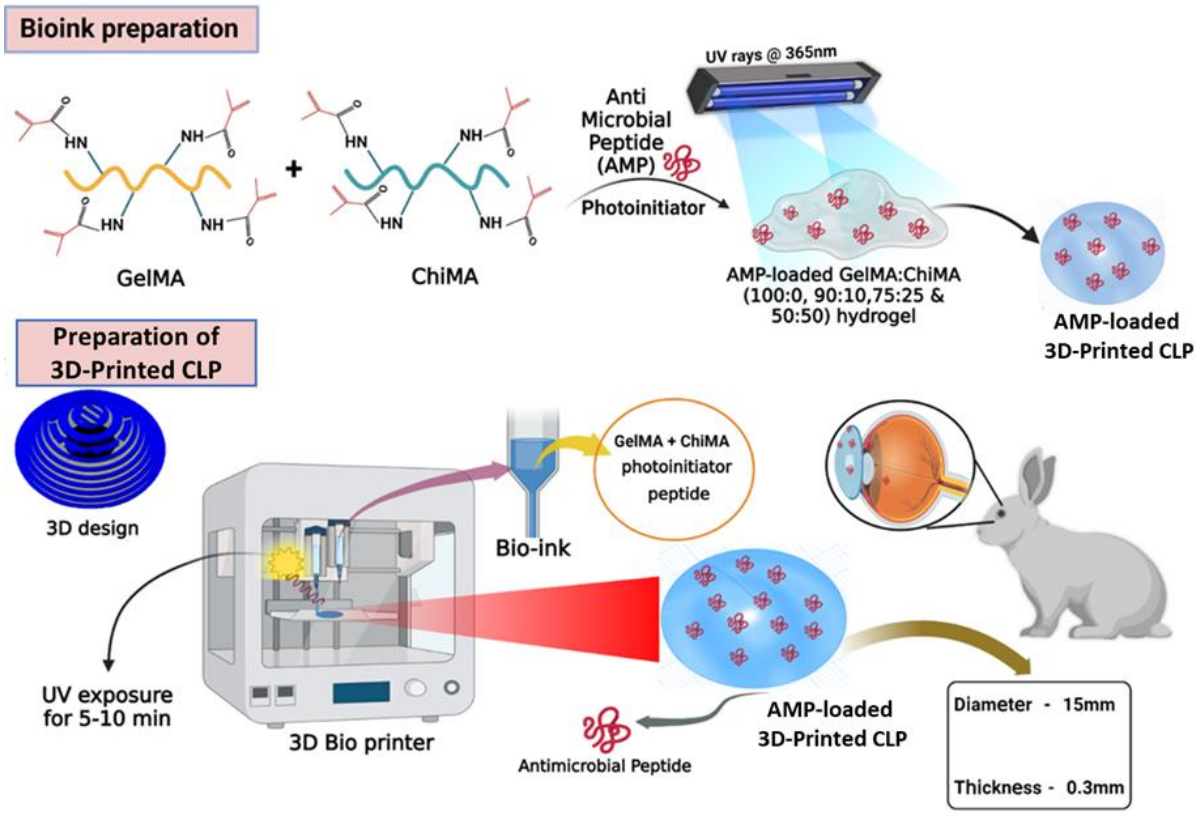

5.1 Introduction

Bacterial Keratitis (BK) is one of the ocular infections, constituting most cases of infectious keratitis types in developed and developing countries, and has estimated cases of around 2.5-799 cases per 0.1 million population/ year (O'Brien, 2003; Ting, Cairns, et al., 2021; Ubani-Ukoma et al., 2019). Serious problems arise if not treated properly, which could lead to severe sight-threatening complications such as ocular morbidity, corneal scarring, perforation, and blindness. The cornea's underlying condition and the bacteria's pathogenicity decide the progression and severity of the infection; corneal destruction may occur within 24 - 48 h of infection. The timely institution of therapy in appropriate dosages is the only way to control corneal infection (Al-Mujaini et al., 2009c; Bourcier et al., 2003; Miedziak et al., 1999; Vajpayee et al., 2000). Various factors such as contact lens use, LASIK surgery, post-ocular surgery, damaged cornea, chronic use of immunosuppressive drugs, ocular trauma, and other ocular conditions are some significant risk factors responsible for the etiology and pathogenesis of BK (Bialasiewicz et al., 2006; Jian et al., 2017; Lim et al., 2016; Poggio et al., 1989). The BK is mainly caused by Gram-negative and Gram-positive bacteria, including p*seudomonas aeruginosa*, *Staphylococcus aureus,* and *Streptococcus pneumoniae,* which are the most common pathogens accounted for most of the corneal infections (Daniell et al., 2003; Paradiso et al., 2016; Robertson et al., 2017). The current therapy for BK involves installing fluoroquinolone eye drops hourly for at least 2 days (Austin et al., 2017b; Daniell et al., 2003; Gangopadhyay et al., 2000). Despite having low drug bioavailability of 1-5%, around 90% of the ocular medications on the market are eyedrops (Carvalho et al., 2015a; Gulsen & Chauhan, 2005). The drugs are instilled as eyedrops undergo rapid lacrimal drainage. Approximately 5% of drugs permeate the corneal membrane due to the eye drop's less contact time of only 5min with the corneal epithelia (H. J. Jung et al., 2013a). Frequent administration of eyedrops overcomes the challenges with low bioavailability, but frequent installation of eyedrops raises difficulties in patient compliance that would result in poor prognostication (Winfield et al.,

1990). The current therapy of fluoroquinolone eyedrops, on frequent administration, poses a greater risk of developing multidrug resistance (MDR). Among many bacterial strains, it is reported that 30% of *S. aureus* bacteria have developed resistance against fluoroquinolones and gram-negative bacteria; *P. aeruginosa* also has similar MDR rates (Egrilmez & Yildirim-Theveny, 2020d).

The researchers have tried to overcome the challenges with the topical administration of eye drops and tackle MDR, including ocular implants, ocular inserts, developing mucoadhesive polymers, nanoparticles, intraocular injections, *in situ* gels, microneedle devices and contact lenses (CLS). However, improving the bioavailability of drugs in the anterior eye segment and developing an effective delivery system is a work in progress (Baranowski et al., 2014c; Gade et al., 2020; A. Patel, 2013). Contact lens-like patches (CLP) can be a promising strategy to improve ocular bioavailability. CLP is widely used for correcting vision and can be explored as a drug delivery system. Therapeutic agents released from the CLP towards the cornea can adhere to the corneal epithelia for 30 min compared to the 5min adherence of eyedrops. The increased contact time of CLP significantly increases the bioavailability of ocular medications to about 50% compared to 1-5% for eye drops (Carvalho et al., 2015b; H. J. Jung et al., 2013b; Maulvi et al., 2018). Patient compliance can be improved with the CLP, as frequent administration of eyedrops in the treating BK can be replaced with the CLP. Besides these advantages, CLP also offers the prolonged release of medicament, facilitating eye protection and sealing wound leakage, aiding healing (Grinninger et al., 2015; Kakisu et al., 2013).

Antimicrobial peptides (AMPs) have emerged as a potential strategy to overcome the challenges of MDR. AMPs have major advantages and are effective over a broad spectrum of bacteria. Some include rapid killing, anti-biofilm activity, low cytotoxicity, and minimal chance of developing resistance in bacteria (Cometta et al., 2022). AMPs are a collective group of diverse proteins that acts as the front line of defense and helps mount attacks from invading pathogens (W & S, 1999).

S100A12, also known as calgranulin C, belongs to the family of S100 proteins. S100A12 has exhibited antibacterial activity against several pathogens, such as *C. jejuni*, *H. pylori*, and *M. leprae*.

Along with their antibacterial activity, S100A12 is associated with human pathologies and inflammatory responses. These peptides bind to different transition metal ions, including, Zn^{2+} and $Ca^{2+,}$ and interact with several immune signaling pathways, such as TLR4 and RAGE. P. Mishra et al. have reported the elevated expression of S100A12 in corneal tissues of patients with *P aeruginosa*-infected BK. In this study, S100A12 was found to have downregulated the expression of biofilm formation genes, redox pathways, and pyoverdine synthesis of the bacteria (Mishra et al., 2022). Here, we have developed 3D-printed contact lens-like patches using hydrogels loaded with AMP (S100A12) for treating BK infected rabbit model.

Gelatin Methacryloyl (GelMA) and Chitosan Methacryloyl (ChiMA) hydrogels are used in this study for 3D printing the CLP. Hydrogels are 3D networks obtained from crosslinked polymer chains and can absorb and hold large volumes of water or aqueous solutions. These possess excellent mechanical strength and biodegradable, biocompatible properties with high oxygen permeability and porosity, making them suitable for delivery systems to treat diseases (Baniasadi, Polez, et al., 2021). GelMA and ChiMA, both polymers, impart mucoadhesivity to the cornea along with excellent mechanical strength and chitosan used in the ChiMA synthesis known to exhibit antibacterial activity, making them perfect candidates for 3D printing.

In recent years, 3D printing technology opened avenues for developing 3D hydrogel scaffolds with precise structure control, and extensive research has been going in many biomedical applications. This study used extrusion-based printing to print the materials. In extrusion-based printing, the materials are printed layer-by-layer by deposition of bioink through computer-controlled microneedles/tips. The 3D printing technique is low cost, simple to construct, and facilitates the

ability to work with different bioinks simultaneously. By maintaining the viscoelastic properties of the polymers at applied pressures, 3D scaffolds can be fabricated with the help of a 3D printer (Ajdary et al., 2021; Baniasadi, Polez, et al., 2021; M'Barki et al., 2017; P. T. Smith et al., 2018). In this study, the GelMA/ChiMA CLP were printed along with S100A12. The AMP-loaded CLP exhibited significant mucoadhesivity and could destroy the biofilm and significantly reduce the bacterial load in the BK-infected rabbit models.

5.2 Materials and methods

5.2.1 Materials

Gelatin from porcine skin (~Mw- 100 KDa, gel strength ~300 g Bloom, Type A), medium molecular weight Chitosan (Mw = 190-310 KDa, <85% degree of *N*-deacetylation) and 2-Hydroxy-4′-(2-hydroxyethoxy)-2-methylpropiophenone (Irgacure 2959) were purchased from the Sigma-Aldrich, USA. Methacryloyl chloride (stabilized with MEHQ) was purchased from Baoji Guokang Bio-Technology Co., Ltd, China. Dialysis membrane (MWCO 6-8 KDa) was obtained from Spectrum Laboratories, Inc. (USA). The peptide (S100A12) was synthesized at Dr. Sanhita Roy's lab, LV Prasad Eye Institute, Hyderabad, India.

5.2.2. Synthesis and Characterization

5.2.2.1. *Gelatin Methacryloyl (GelMA)*

The synthesis of GelMA was prepared by reacting gelatin with methacryloyl chloride (MC) at a mol ratio of 1:50. GelMA was prepared by dissolving gelatin (10 % w/v) in 0.25 M carbonate bicarbonate buffer (CB buffer) pH 9.0 at 55 ºC and kept for stirring for 2 h until completely dissolved. MC was added dropwise under vigorous stirring. The reaction was continued for another 2 h under a nitrogen atmosphere, and the reaction was stopped by diluting the reaction mixture with CB buffer. The reaction mixture was later dialyzed using a dialysis bag (MWCO 6-

8 KDa) at 50 ºC against ultrapure water to remove unreacted MC. The obtained solution was freeze-dried and stored for further use (P. Joshi et al., 2021).

5.2.2.2. *Chitosan Methacryloyl (ChiMA)*

The synthesis of ChiMA was prepared by reacting chitosan with methacryloyl chloride at a mol ratio of 1:50. ChiMA was prepared by dissolving chitosan (10 % w/v) in 2% glacial acetic acid (15-20 mL) at 25 ºC under stirring until completely dissolved. MC was added to the chitosan solution dropwise under vigorous stirring, and the reaction was kept in a nitrogen atmosphere for 4 h at room temperature. The reaction mixture was dialyzed (MWCO 6-8 KDa) against ultrapure water at 25 ºC, freeze-dried, and stored for further use (P. Joshi et al., 2021).

5.2.3. Characterization of GelMA/ChiMA

Infrared spectra for dry gelatin, chitosan, and GelMA/ChiMA were obtained using the KBr pellet method using a Fourier Transform Infrared Spectrometer (JASCO-4200, Japan). The spectra were recorded between 400-4000 $cm^{-1,}$ and the functional groups were identified. The ^{1}H NMR spectra were obtained using a 300 MHz NMR spectrometer at 25 ºC. 1.5 mL of Deuterated water (D_2O) and Deuterated DMSO were used as the solvent for 4-5 mg of GelMA and ChiMA, respectively. Spectra were recorded using a Bruker spectrometer (Bruker, USA). Obtained spectrum was integrated and phase-corrected by using Mest Re Nova software.

5.2.4. Degree of Methacrylation (DoM)

The number of methacrylate groups conjugated to Gelatin and Chitosan was determined by ninhydrin assay with slight modifications(Modaresifar et al., 2018). 2% w/v ninhydrin in ethanol was prepared and sonicated to dissolve completely, and modified Gelatin/Chitosan solutions (0.05-0.5% w/v) were prepared by dissolving Gelatin solutions in deionized water and chitosan solutions in 0.1% (w/v) acetic acid. GelMA/ChiMA polymeric solutions (0.5 mL) were added to 5 mL ninhydrin solution, 1.25 mL of 4M phosphate buffer (pH 5.5), and stirred for 12h in the dark at

25º C. The samples were analyzed using a UV-Visible spectrophotometer (Jasco, Japan) at 570nm. A standard curve determined the slope plotted for the modified and unmodified polymer solutions. % of the degree of methacrylation was calculated using the following equation.

$$DOM = \left(1-\frac{m_{GelMA/ChiMA}}{m_{Gelatin/Chitosan}}\right) \times 100\%$$

$\mathbf{m_{Gelma/ChiMA}}$- slope of GelMA/ChiMA and $\mathbf{m_{Gelatin/Chitosan}}$- slope of Gelatin/chitosan

5.2.5. Preparation of hydrogel using GelMA/ChiMA

The hydrogels were prepared by mixing the various proportions of GelMA/ChiMA into the Phosphate Buffer Saline (PBS), pH 7.4., The final concentration of hydrogel was fixed at 10% w/v containing various proportions of GelMA/ChiMA as follows: 100% GelMA (GelMA100), 90% GelMA: 10% ChiMA (GC90), 75% GelMA: 25% ChiMA (GC75), 50% GelMA: 50% ChiMA (GC50). The hydrogels were prepared by dissolving different proportions of the synthesized polymers into the PBS/ PBS containing photoinitiator (2% w/v, Irgacure 2959) and stirred until completely dissolved.

5.2.6. Synthesis of Rhodamine b (Rhb) conjugated Gelatin

Gelatin (100mg, 0.001 µmol) and Rhodamine b (Rhb) (0.536 mg, 0.001 µmol) were taken in equal mol ratios and dissolved in water (20 mL). First, EDC (0.5751 mg) and NHS (0.3471 mg) were dissolved in DMSO (3 mL), Rhb was added to the reaction mixture, and the reaction was kept for 2 h under continuous stirring. Triethylamine (100 µL) was added to the reaction mixture, which continued for 24 h under an N_2 atmosphere. The reaction mixture was dialyzed using 6-8 KDa (Spectrum laboratories, USA) for 24 h, lyophilized, and stored for further use.

5.2.7. Rheological Characterization of GelMA/ChiMA hydrogels

The rheological of GelMA/ChiMA hydrogels with or without a PI was characterized via the parallel plate method using an Anton-Paar rheometer (MCR 302, Austria) with a 37 mm diameter

plate 0.3 mm gap between the plates. The storage modulus of the hydrogels was determined at a constant strain rate of 5% with an amplitude sweep from 0.1 – 10 Hz frequency. Viscosity studies were carried out for each sample as a function of shear rate ramping from 0.1-1000 S^{-1} . 10 % w/v was used to carry out all the rheology studies for GelMA: ChiMA (100:0, 90:10, 75:25, 50:50) hydrogels**.**

5.2.8. Effect of sterilization on hydrogels

The GelMa/ChiMA hydrogels were sterilized using autoclaving per previously reported protocol (Rizwan et al., 2020). The lyophilized GelMA/ChiMA powders were dissolved in ultra-purified water containing a photoinitiator and autoclaved at 121 ºC for 20 min, followed by an analysis of their rheological characteristics such as storage modulus was determined as mentioned in the above section 2.7.

5.2.9. Isolation and Analytical Method Development for S100A12

S100A12, a host defense peptide, was purified by using the plasmid pET-hS100A12 as described in (Mishra et al., 2022) with the help of a nickel affinity chromatography kit (HOOK™ 6X His Protein Purification Kit, GBiosciences, Cat. # 786-630) using manufacturer's protocol. It is a 92 amino acid peptide (Yamamura et al., n.d.) and consists of four α-helices, two Ca^{+2} binding EF-hand loops, and two hinge motifs (Q. Wang et al., 2019).

The S100A12 Protein sequence is as follows-

MTKLEEHLEGIVNIFHQYSVRKGHFDTLSKGELKQLLTKELANTIKNIKDKAVIDEIF
QGLDANQDEQVDFQEFISLVAIALKAAHYHTHKE

The Analytical method for AMP was developed using High-Performance Liquid Chromatography (HPLC), Shimadzu. The mobile phase consisted of 70% Acetonitrile + 0.1% Trifluoro Acetic Acid (TFA) as an organic phase and water + 0.9% (TFA) as the aqueous phase.

Organic: Aqueous phase was 0.9: 0.1 with a flow rate of 1mL/min. The peptide was detected using a PDA detector at a UV-Visible wavelength of 280 nm.

5.2.10. 3D printing of GelMA/ChiMA hydrogels and AMP-loaded CLP

All 3D printing procedures in this study were carried out using the Bio X 3D printer (Cellink, Sweden). The scaffold CLP was designed using the software Autodesk Fusion 360, 2022. The g-code file was generated from the geometry using the Slicer of the software Cellink Heartware 2.4.1. Fundamental modeling values for the CLP were diameter, 15 mm; and thickness, 0.3 mm. The printer head and the bed temperature were controlled at 26º and 9 ºC, respectively. Extrusion type 27G printer tip and other parameters such as printing speed 10mm/s, pressure, 40-60 KPa, and 80% infill density were used. Bioink was prepared by dissolving different proportions of synthesized polymers GelMA100, GC90, GC75, and GC50 into the PBS at a bioink concentration of 10% w/v, and methanol containing 2% w/v Irgacure 2959 was stirred until completely dissolved (Zhu et al., 2019). Printing was carried out according to the set parameters. After the printing, CLS was exposed to UV radiation at 365 nm to photo-polymerize for 2 min. AMP-loaded CLS (100/500 µg) were prepared by mixing AMP (500 µg/CLP) into the bioink and stirring vigorously for 1h. The AMP-loaded bioink was used for 3D printing per the abovementioned parameters. The printed scaffolds were stored in sealed boxes at 4ºC, away from moisture. As mentioned above, the Rhb-GelMA/ChiMA hydrogels (containing 1% w/v, Rhb-Gelatin) of various proportions are prepared.

5.2.11. Printability assessment of printed scaffolds

After printing, the printability assessment of the 3D-printed CLP was performed by measuring the diameter, thickness, porosity, and mean pore size of all the printed scaffolds were determined from the SEM images and analyzed using the Image J software.

5.2.12. Scanning Electron Microscopy

GelMA100, GC 90/75/50 CLP were placed on a holder attached to carbon tape. Printed scaffolds were evenly distributed on a tape and gold-coated for 30 min. The samples were placed on a sample holder, and images were taken using a Field Emission Scanning Electron Microscope (Apreo Lo Vac, FEI, USA).

5.2.13. Mucoadhesive study of GelMA, ChiMA hydrogels/ CLP

The mucoadhesive strength of the hydrogels (10 % w/v), GelMA100, GC90, GC75, GC50, and 3D-printed CLP, were determined by a Texture analyzer (Stable Micro Systems, Surrey, UK) using goat cornea. The goat cornea obtained from the slaughterhouse was cleaned and rinsed thoroughly with normal saline. The cornea was incubated in the 10 % w/v mucin solution for 30 min before the study. The goat cornea was fixed between the basement probe and the moving probe of the texture analyzer. The moving arm traveled at a speed of 0.5 mm/s and contacted the hydrogels (200 µL) placed on the cornea at 5 g of contact force; a contact force of up to 100g was applied to the mucus membrane and held for 300 s; then, the probe moved up at a speed of 0.1 mm/s. The force (g) required to detach the probe from the corneal membrane was noted as mucoadhesive strength.

5.2.14. Mucoadhesive Study: Falling Liquid method

The falling liquid method was used to determine the mucoadhesive property of the 3D-printed CLS as per the previously published work (Ch et al., 2023b), the goat eyeballs were procured from the slaughterhouse, and the corneal tissue was dissected and stored in STF pH 7.4. Rhb conjugated 3D printed CLP were placed over the cornea on a falcon tube wall using double-sided tape at an angle of 45º. STF, pH 7.4, was allowed to flow over the cornea using a peristaltic pump at a controlled flow rate of 1 mL/min. The washing of the film and % remaining was determined by measuring the fluorescence after 6 h.

5.2.15. Swelling ratio

The swelling (%) of printed scaffolds was determined by weighting the immersed CLP in PBS solution. The CLP's initial weight (Wi) was noted down, followed by immersion. Pre-determined time points, the CLP were removed, and the excessive medium was discarded by wiping with the tissue paper and weighed immediately (W_t). The following equation determined swelling ratio (%) equation.

Swelling ratio (%) = $\frac{Wi-Wt}{Wt}$ X 100

5.2.16. Transmittance Study

The transmittance spectra for the printed scaffolds were determined using a UV-Visible spectrophotometer (Jasco, Japan). Each lens was inserted into the sample holder and placed within the spectrophotometer. The baseline transmittance was measured and recorded before starting the experiment. The spectral scan was performed at a scan speed of 5nm/s for the wavelength band 350-750 nm and recorded (Rahmani et al., 2014).

5.2.17. Corneal permeation study: Franz cell diffusion

Ex vivo permeability study of AMP loaded printed scaffolds (500 µg/CLP) were carried out by using Franz diffusion cell using a goat corneal tissue. Corneal tissue was placed over the receptor compartment containing STF (5 mL), pH 7.4, and the CLP were placed on the donor compartment, later fixed with clamps. The assembly was maintained at 37±1 °C under constant stirring (300 RPM). 300 µL of the sample was withdrawn and replaced with fresh media from the receptor compartment at pre-determined intervals. Withdrawn samples were filtered using a 0.45 µM syringe filter, diluted if necessary, and quantified for AMP content by HPLC at 280 nm. The percentage of peptide permeated through the corneal tissue was calculated.

5.2.18. Cell culture

The human corneal epithelium (HCE) cell line was obtained from Dr. Sanhita Roy's lab at the L.V. Prasad Eye Institute, Hyderabad, India. Bovine Serum (FBS), Dulbecco's modified Eagle's

medium F-12 (DMEM F-12), and penicillin/streptomycin solution were purchased from Himedia Laboratories (Mumbai, India). f-12 media containing fetal bovine serum (10%) and penicillin/streptomycin (100 IU/mL) was used to sub-culture HCE cells and incubated at 37°C with 5% CO_2 at humidified sterile atmosphere.

5.2.18.1. Cytotoxic study: MTT Assay

MTT assay was performed to determine the *in vitro* cytotoxicity of the HCE cells as per the previously published protocol (Kumari, Paul, Bobde, et al., 2020). A 96-well plate containing HCE cells of 2 x 10^4 density/well were seeded in DMEM-F12 complete growth media and incubated at 37 °C for 24 h. Hydrogels of 10% w/v GelMA100, GC90, GC75, and GC50 were added to wells and incubated for 24 h. No treatment was given to the control HCE cells. After 24 h, supernatant media was discarded and added with 100µL of MTT solution (5 mg/mL), incubated for 4 h, then replacement of MTT solution with 150 µL of DMSO and incubated for 2 h. The absorbance of the well plate was analyzed using a microplate reader (Spectramax™, Molecular Devices, USA) at 590 nm (reference wavelength 620 nm). The following equation was used to calculate the percent cell viability:

% Cell viability= Abs (sample) /Abs (blank) X 100, where Abs (sample) = the absorbance of the cells treated with hydrogels. Abs (blank) = the average absorbance of the control cells. The study was carried out in triplicates and expressed as mean ± SD.

5.2.18.2. Trans-epithelial Electrical resistance (TEER) measurement

The permeation of the hydrogels and the TEER of the HCE cells after the treatment was determined by the EVOM volt-ohm meter (Millicell®ERS-2, Millipore). HCE cells (1 x 10^6) were seeded onto the 12-well membrane with permeable inserts coated with collagen (Corning™, USA). Cells were treated with AMP (500 µg) loaded GelMA100, GC90, GC75, and GC50 hydrogels (105 w/v) only after the TEER value reached 170 Ω cm^2. Formulations were added to

the apical chamber of the insert and incubated for 5 min. At pre-determined time intervals, the voltage was measured by placing the electrode tips between the chambers.

5.2.19. Bacterial strains

Pseudomonas aeruginosa (PA01), *Staphylococcus aureus* (MTCC 95), and *Streptococcus Pneumoniae* (ATCC 49619) were obtained from LV Prasad Eye Institute and BITS-Pilani Hyderabad, India. Strains (*P. aeruginosa* and *S. aureus*) were cultured in Luria Bertani (LB) Broth, Miller (HIMEDIA, INDIA), and *S. pneumoniae* were cultured in Todd-Hewitt broth at 37 °C, and 85 % relative humidity aerobically. Bacteria were incubated, and subculturing was given to attain a bacterial concentration at an OD@600nm of 0.2 for *P. aeruginosa* (10^8 CFU/mL), 0.6 for *S. aureus* (10^9 CFU/mL) and 0.2 for *S. pneumoniae* (10^6 CFU/mL) incubated at 37 °C (200 µL of overnight culture in 5 mL of LB broth). Diluted bacteria (PBS/LB broth) were used for further studies.

5.2.19.1. Biofilm Culture

P aeruginosa (10^6 CFU/mL) in LB Broth was incubated on a coverslip in a 12-well plate at 37 °C and 85 % relative humidity for 2 days. The next day, the coverslips were removed and washed with PBS, pH 7.4, and utilized for further studies.

5.2.19.2. Determination of MIC and MBC

The Minimum Inhibitory Concentration (MIC) and Minimum Bactericidal Concentration (MBC) were determined for AMP as per the previously published protocol (Ch et al., 2021c). In broth media, *P. aeruginosa, S. aureus,* and *S. pneumoniae* concentrations were adjusted to a 10^6 CFU/mL *density*. 100 µL of the bacteria were added to each well of 96 well plates and treated with 100 µL of various concentrations (0-250 µg/ mL) of S100A12, followed by incubation at 37 °C for 12h. Each well's visual turbidity and optical density were observed at different time points by measuring the absorbance at 600 nm. MTT assay was used to determine the MBC to compare with

the microtiter broth dilution method. 100 µL of S100A12 of varying concentrations (0-100 µg/mL) were added to *P. aeruginosa*, *S. aureus,* and *S. pneumoniae* (10^6 CFU/ mL in respective broth media) in a 96 well plate and incubated at 37 °C for 12 h, followed by adding 50 µL of the MTT solution (5 mg/mL) and further incubated for 2h. After the incubation, the MTT solution was removed, and dimethyl sulfoxide was added to each well to dissolve the MTT reagent. Optical density was measured at 590 nm using a microplate reader instrument (Spectramax M4, Molecular Devices, San Jose, USA), keeping reference absorption maxima at 620 nm. The below-mentioned equation was used for calculating the percentage of cell viability.

% Cell viability = (Abs of sample)/(Abs of control) x 100

5.2.19.3. Zone of inhibition study (ZOI)

The ZOI of the GC50 CLP, and GC50 CLP (100/500 µg of AMP/CLP) was determined by the agar plate method. The *P. aeruginosa* bacteria were adjusted to 10^6 CFU/mL density and spread over the solidified nutrient agar plates with sterile spreaders. CP were placed on the bacteria-inoculated agar plates and kept for overnight incubation. The diameter of the zones of inhibition was measured after the incubation, and pictures were captured using the digital camera.

5.2.19.4. Live/Dead Assay of Planktonic bacteria treated with 3D printed scaffolds

5.2.19.4.1. *Confocal Microscopy*

P. aeruginosa bacteria of 10^6 CFU/mL density were treated with GelMA100 CLP, and GC90/75/50 CLP loaded with 500 µg of AMP/CLP were kept at incubation for 1 and 4 h at 37 °C followed by centrifugation of the bacteria at 6000 rpm for 10 min at 25 °C. The bacterial pellet was washed twice with sterile physiological saline solution (0.9 % w/v NaCl) and dispersed in 200 µL of pH 7.4 sterile PBS. 3 mL of the staining mixture of SYTO 9 and Propidium iodide (PI) (1:1) in concentrations of 33.4 µM and 0.4 mM, respectively, kept in the dark for 10min. After 10 mins,

the bacteria's images were captured using a fluorescence microscope (ex/em. 485/498 nm) (Leica, DMi8, Germany).

5.2.19.4.2. *Flow cytometry*

Freshly sub-cultured *P. aeruginosa* in LB broth media was used for flow cytometry studies. Adjusting the bacterial density, bacteria were centrifuged at 6000 rpm for 10 min, followed by washing with PBS (1X, pH 7.4) and resuspended in 500 µL of PBS. GelMA100 CLP, and GC90/75/50 CLP loaded with 500 µg of AMP/CLP were added to the bacterial suspension and incubated for 1 and 4 h at 37 °C (under shaking). Staining with SYTO 9 and PI was done as mentioned above, untreated bacterial suspensions were used as a control, and 10,000 gated cells were analyzed using a flow cytometer (FACS ARIA III, BD Life Sciences, CA, USA) using FITC and PI lasers. Data was graphically represented in quadrant plots using BD FACSDiva Software.

5.2.19.5. Bacterial Biofilm inhibition study

5.2.19.5.1. *Confocal Microscopy*

Biofilms of *P. aeruginosa* were incubated with GelMA100 CLP, and GC90/75/50 CLP loaded with 500 µg of AMP/CLP for 1 and 4 h at 37°C. Biofilms were washed twice with sterile physiological saline solution (0.9 % w/v NaCl) and stained using SYTO 9 and PI. The staining solution was prepared by mixing SYTO 9 and PI at 33.4 µM and 0.4 mM concentrations, respectively. Bacterial staining was performed by adding 3 µL and 5 µL of SYTO 9: PI (1:1) kept in the dark for 10 min. The bacteria's biofilm 3D images were generated and captured using a confocal microscope (ex/em. 485/498 nm) (Leica, DMi8, Germany).

5.2.19.5.2. *Scanning Electron Microscopy*

After the treatment with the GelMA100 CLP, and GC90/75/50 CLP loaded with 500 µg of AMP/CLP, the biofilms were washed twice with sterile 0.9% w/v NaCl solution. Fixation of the biofilms was made using 2.5% w/v formaldehyde overnight at 4ºC, followed by washing with

sterile PBS. Biofilms were dehydrated with gradient alcohol concentration (30,50,70 and 90%) and mounted to an aluminum sub, followed by gold-coated sputtering. The samples were analyzed, and images were captured using Field Emission Scanning Electron Microscope (Apreo Lo Vac, FEI, USA).

5.2.19.6. *In vitro* antibacterial study

The bactericidal efficacy of the GelMA100 CLP, and GC90/75/50 CLP loaded with 500 µg of AMP/CLP was determined by incubating the printed scaffolds in the planktonic *P aeruginosa* (10^6 CFU/mL) for 24 h. After 24 h, the bacteria were diluted and plated on the solid agar plate to determine the CFU.

5.2.20. *In vivo* antibacterial study

New Zealand male rabbits (5 months old), between 1.5-2.5 kg, were used for the animal studies. All the animal experiments complied with the National Research Council's Guide for the Care and Use of Laboratory Animals (eighth edition). The study was conducted with approval from the Institutional Animal Ethics Committee of BITS-Pilani, Hyderabad, and the experiments were carried out under veterinary supervision. Animals were accustomed to the following conditions: 25 ºC at 50−60% humidity with free access to food and water.

P. aeruginosa was diluted to 10^3 CFU/mL in sterile PBS; pH 7.4 was used to constitute corneal infection. Rabbits were divided into groups such as control, free peptide, and formulations GelMA100 CLP (100 µg of AMP), GC50 CLP (100 µg of AMP), and GC50 CLP (100 µg of AMP). Both eyes were infected with BK (n=3) in each group, and the control group was left untreated. The local anaesthesia Lidocaine HCl was applied on the corneal surface before injecting *P. aeruginosa* (20 µL, 10^3 CFU/mL) intrastromal into both rabbit corneas using a 30-gauge needle. After the confirmation of BK in the rabbit cornea, treatment was started. The free peptide group was treated with 100 µg of AMP every 6 h, whereas the formulation groups were treated with

AMP-loaded 3D printed CLP by placing them on each cornea. The treatment cycle was repeated every 12 h until a significant therapeutic effect was observed. Before each therapy, the eyes of the rabbit from each group were analyzed, a clinical score (0-5) was given, and the score was graded for each eye. All animals were euthanized with intravenous injection (IV) of Thiopentone Sodium (150 mg/Kg). The corneas were dissected, aseptically removed, and stored in eppendorf tubes containing PBS, pH 7.4. The corneas were homogenized at 25000 rpm for 2 min using a high-speed homogenizer. Samples were diluted, plated on agar plates, and incubated at 34 ºC for 12-18 h. The number of viable bacteria was determined by counting the colonies formed on plates.

5.3. Results and Discussion

5.3.1. Characterization of GelMA/ChiMA

Gelatin/Chitosan to Methacryloyl chloride at a mol ratio of (1:50) was utilized to produce GelMA/ChiMA by a covalent reaction in which methacrylate groups on the methacryloyl chloride bind to the amine groups of Gelatin/Chitosan. The presence of a polypeptide backbone with several functional groups, such as amino acids and carboxyl groups on the Gelatin/Chitosan, can be used for grafting the molecules such as Methacryloyl (MA), and the grafting of MA was confirmed by ^{1}H NMR by observing acrylamide double bond formed in GelMA/ChiMA (**Figure. 5.1C&D**). Peaks of acrylate protons from the methacrylate are observed between 5-6 ppm, and the methyl functional group from methacrylate peaks were observed between 1.5-2 ppm. Double bond was confirmed at 5.3 and 5.6 ppm in both GelMA and ChiMA. This reveals the successful modification of MA into Gelatin/Chitosan molecules. The conjugation of MA groups was also confirmed from the FTIR spectrum of GelMA/ChiMA; absorption bands of N-H and C-H are observed at 3296 and 2938 cm^{-1}. Amide I, II, and III at 1625, 1562, and 1238 cm^{-1} reflect the CH_2 wagging vibrations, amide N−H in-plane bending, and C−H stretching vibrations, respectively, were observed in the GelMA spectrum. In the ChiMA spectrum, the characteristic peaks of chitosan are at 3355 cm^{-1} (O-H stretching), 2867 (C-H stretching), and 1151 cm^{-1} (C-O-C bridge asymmetric

stretching). Absorption bands at 1062, 1321, 1535, and 1654 cm^{-1} represent the C-O stretching, N-H cm^{-1} stretching of amide II, and C-H stretching (**Fig. 5.1E&F**). The degree of methacrylation (DoM) of GelMA/ChiMA determined by ninhydrin assay showed that both polymers had undergone significant substitution with 68.1% and 66.1% GelMA and ChiMA, respectively, indicating good modification.

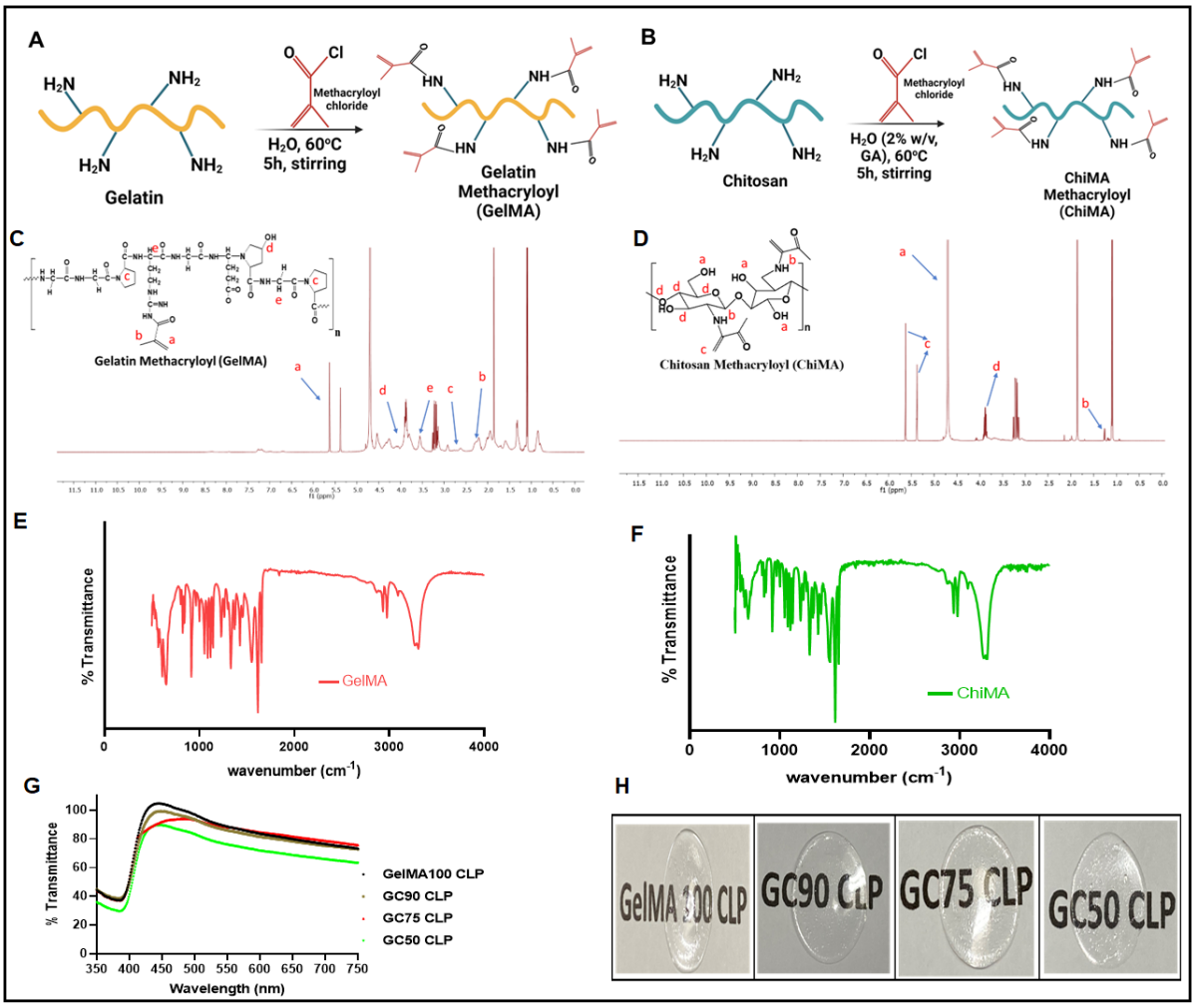

Figure 5.1. The synthesis scheme of GelMA conjugate (A); and ChiMA (B). The ^{1}H NMR spectrogram of GelMA (C); and ChiMA (D); FTIR spectra of GelMA (E) and ChiMA (F); spectral transmittance curves of GC(100/90/75/50) CLP (G); transparency of 3D-printed scaffolds (H).

5.3.2. Rheological and physicochemical characterization of hydrogels/printed scaffolds

DoM correlates with the hydrogels' porosity, pore size, storage modulus, and swelling behaviors. Storage modulus determines the ability of the hydrogel to store energy. The storage modulus of

the GelMA100, GC90, GC75, and GC50 hydrogels without PI at 1Hz was found to be 91.88 ± 0.66, 120.06 ± 0.36, 166.06 ± 0.54, and 170.98 ± 0.76 Pa respectively whereas hydrogels GelMA100, GC90, GC75, and GC50 with PI, had shown storage modulus of 169.11 ± 0.56, 277.49 ± 0.65, 471.23 ± 0.65, and 580.8 ± 0.51 Pa at 1Hz. At low frequencies, the capacity to retain the strength of the hydrogel remains high due to the lower shear rate. A similar observation was obtained with the GelMA100, GC90, GC75, and GC50 without PI at 1 Hz. But upon reacting the polymer with PI, the hydrogels' storage modulus increased at 1Hz. This is due to the ability of the photoinitiator to crosslink with the hydrogels, thereby increasing their mechanical stability. Increasing the frequency, the shear rate also increases, and it inputs more energy onto the polymer; thereby, polymers start to lose their energy. The high storage modulus of GelMA100, GC90, GC75, and GC50 indicated that the hydrogels possess good mechanical strength and are good candidates for 3D printing (Baniasadi, Madani, et al., 2021). The viscosity of the hydrogels was also analyzed with an increasing shear rate. The viscosity of the hydrogels GelMA100, GC90, GC75, and GC50 at 125 S^{-1} was found to be 175.31±13.20, 200.28±8.39, 255.46±16.83, and 301.84±19.27 Pa, respectively, for hydrogel without PI and 200.18±11.52, 231.48±9.11, 316.39±12.44, and 440.08±18.63 Pa with PI (**Figure. 5.2A&B**). The pseudoplastic behavior of the hydrogels was exhibited by GelMA/ChiMA, where the viscosity of the hydrogels was decreased upon increasing the shear rate. CLP with high transparency with good visibility is crucial for vision; the % transmittance and transparency for the printed scaffolds were determined (**Figure. 5.1G&H**). The results indicated that optimizing the GelMA: ChiMA ratios had not affected the transmittance and transparency of the CLP (**Table 5.1**).

Table 5.1. % Transmittance of 3D-printed scaffolds

Formulation	**% Transmittance @ 420nm**

GelMA100 CLP	93.66
GC90 CLP	86.18
GC75 CLP	84.27
GC50 CLP	79.24

The rheological characteristics of GelMA/ChiMA hydrogels after sterilization were analyzed, and observed that the mechanical properties of the hydrogels were slightly lowered compared to the unsterilized hydrogels (**Figure 5.3**). This is due to the thermal degradation of the polymers, but it does not affect the printability, and these findings were similar to the Rizwan et al. (Rizwan et al., 2020).

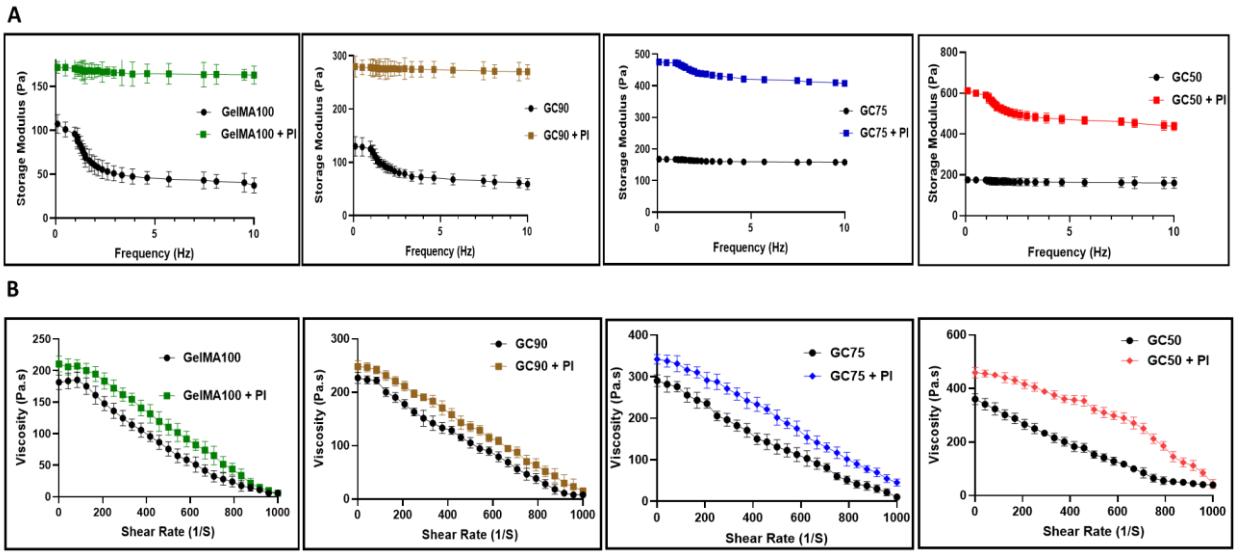

Figure 5.2. Rheological properties of GelMA and ChiMA hydrogels. Storage modulus determination of GelMA/ChiMA hydrogels by frequency sweep test (A); Viscosity shear rate of GelMA/ChiMA hydrogels highlights the shear thinning properties of hydrogels (B). PI-Photoinitiator.

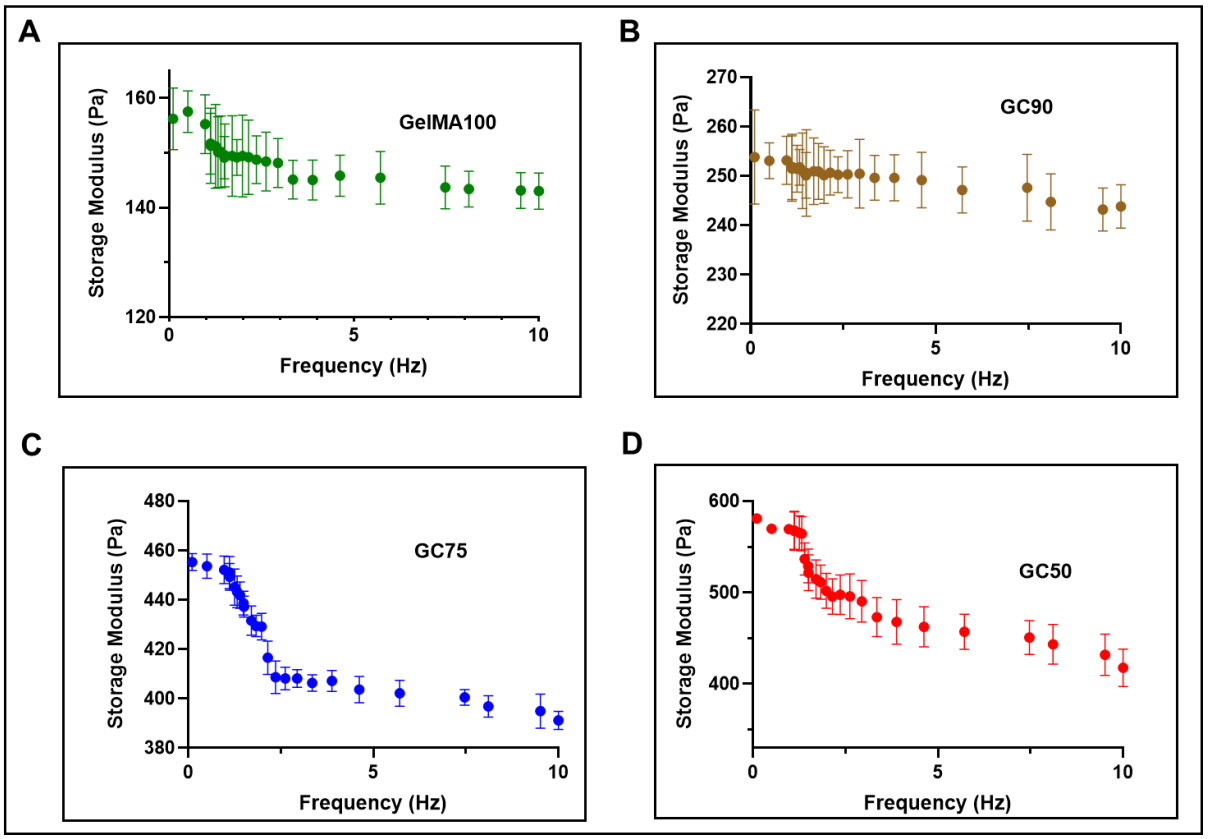

Figure 5.3. Rheological properties of GelMA and ChiMA hydrogels with photoinitiator (PI). Storage modulus determination of GelMA/ChiMA hydrogels by frequency sweep test after sterilization (A).

The mucoadhesive strength of the hydrogels and printed scaffolds was analyzed by texture analyzer and falling liquid method. The force (g) required to detach the probe from the corneal membrane was noted as mucoadhesive strength. Hydrogels with GelMA100, GC90, GC75, and GC50 without PI had shown mucoadhesive strength of 185, 330, 346, and 390g, respectively, whereas the hydrogels with PI had 285, 350, 385, and 435g. Mucoadhesive strength of printed scaffolds GelMA100, GC90, GC75, and GC50 CLP was found to be 10.52, 10.86, 20.55, and 24g, respectively (**Fig. 5.4)**. The results showed that the hydrogel GC50 with or without PI and the GC50 CLP had high mucoadhesive strength when compared to the other formulations this is due to the presence of cationic charge on the surface of chitosan and its ability to form hydrogen and ionic bonds between the positive amine groups and negatively charged sialic acid residues of mucin glycoproteins. It also has amine groups that would create strong interactions with mucin,

like chitosan (Sogias et al., 2008b). Adding PI to the hydrogels significantly increased mucoadhesivity due to PI's ability to make complexes upon exposure to UV light. The amount of hydrogel retained on the cornea after the washing is quantified, and results have shown that the GelMA100, GC90, GC75, and GC50 CLP have retention of about 59.67, 62.84, 70.95 and 75.97% after 120 min in (**Fig. 5.5F)**.

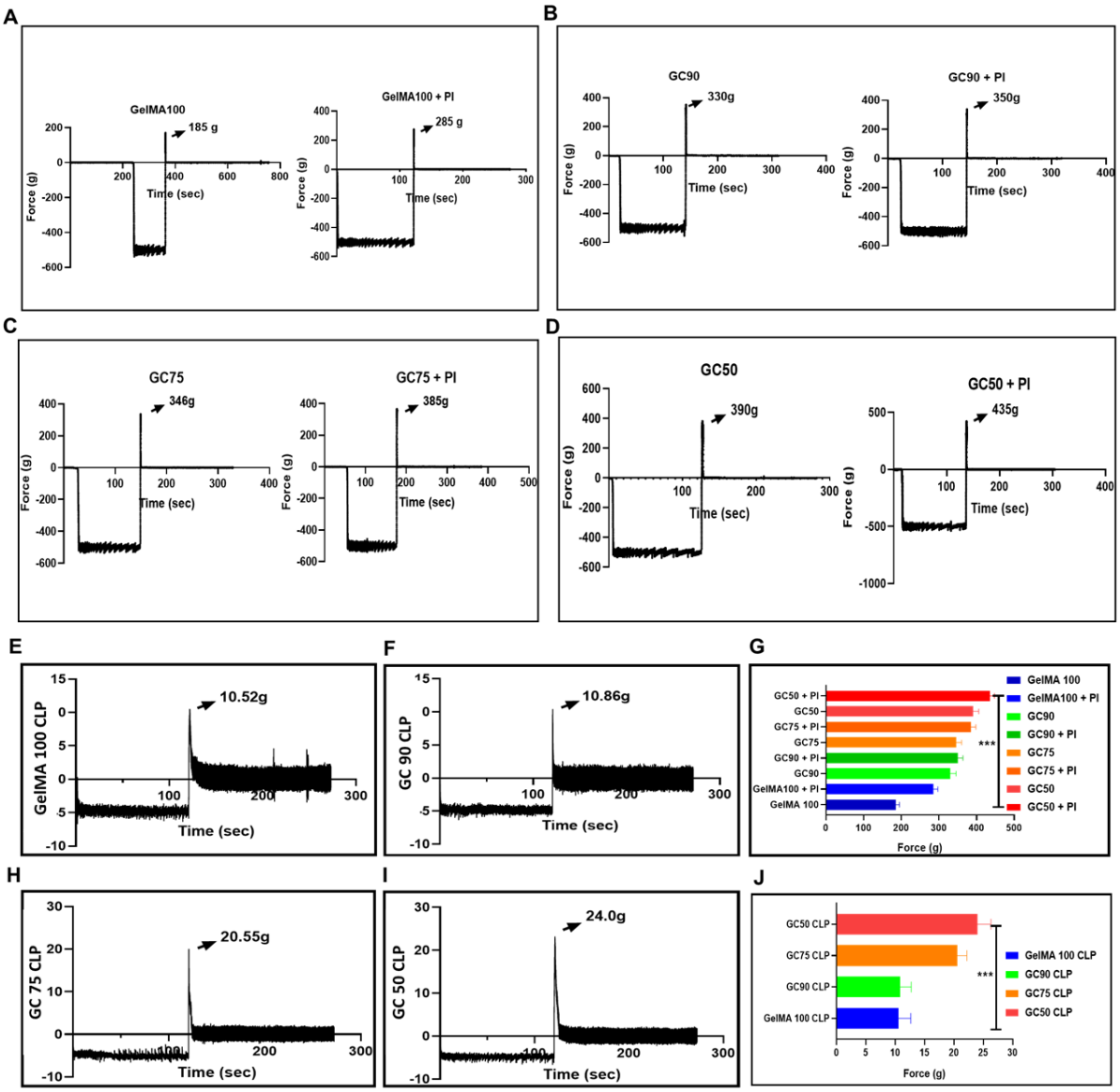

Figure 5.4. Mucoadhesive study of GelMA/ChiMA hydrogels and 3D-printed contact lenses determined by Texture Analyzer. Graphs representing the mucoadhesive force (g) of GC(100/90/75/50) hydrogels with and without PI (A,B,C&D); graphs representing force (g) of

GelMA100, GC(90/75/50)CLP. Bar graph of GelMA/ChiMA hydrogels and CLP. Data are represented as mean ±SD (n=3, $p<0.01$ as ***).

The SEM images showed a uniform distribution, the hydrogels GelMA/ChiMA have excellent compatibility, and no disorganized scaffolds were observed for contact lenses after printing (**Figure. 5.6**). Polymer concentration affects the porosity; since, in this study, the polymer concentrations are varied, there was a difference in the porosity and pore size was observed. Open pores of CLP play a significant role as they favor the migration of the therapeutic agent and help in subsequent attachment to the cell membrane. The porous nature of hydrogels also provides a high surface area which is helpful in wound healing and other inflammatory conditions to offer an easy exchange of essential nutrients and oxygen at the site of action. A concentration-dependent increase of pore size and porosity was observed for all the hydrogels, and GC50 showed high porosity and pore size due to the high-water uptake capacity of the polymers GelMA and ChiMA (**Table. 5.2**). The pore size of the hydrogel increases with the amount of absorbed water. Printability assessment of the 3D-printed scaffolds was determined. The diameter of the GelMA100, GC90, GC75, and GC50 CLS after the printing was found to be 15.04±0.24, 14.84±0.07, 14.84±0.27 and 14.40±0.32 mm, respectively. The thickness of the GelMA100, GC90, GC75, and GC50 CLP was found to be 0.33±0.01, 0.31±0.02, 0.31±0.02 and 0.31±0.03 mm, respectively. The CLP printed was robust and had a negligible difference in diameter and thickness.

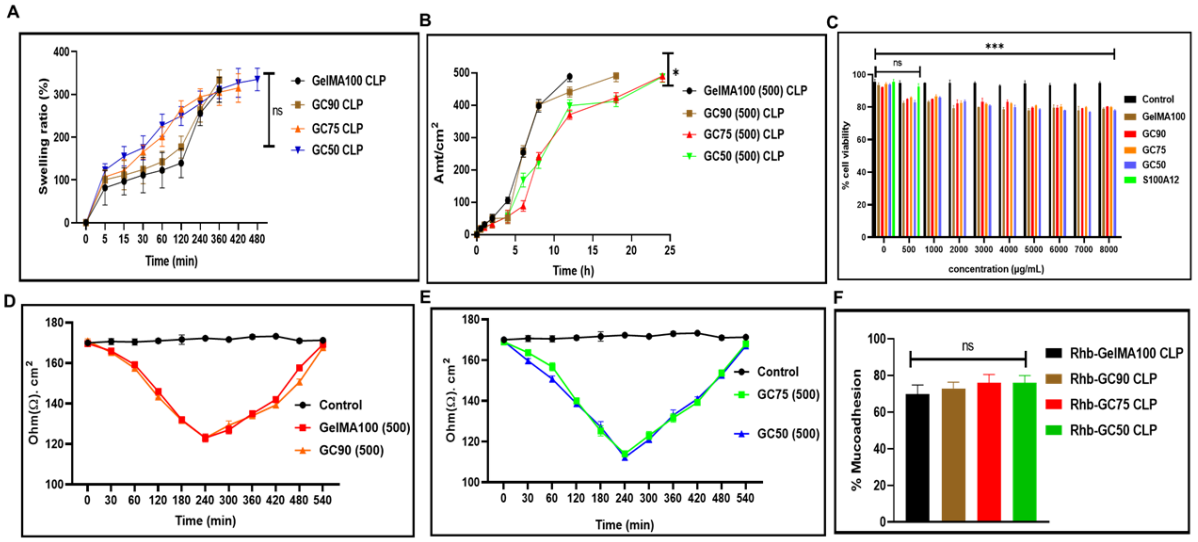

Figure 5.5. Swelling ratio, trans corneal permeation, and cell studies of hydrogels/CLP. Swelling ratio of CLP (A); trans corneal permeation of AMP (500 µg) loaded GC(100/90/75/50)500 CLP (B); % cell viability of HCE cells treated with GC(100/90/75/50)500 hydrogels and S100A12 (C); TEER study of HCE cells treated with S100A12 loaded GelMA 100, GC90 hydrogels (D) and GC(75/50) hydrogels (E); Data are represented as mean ±SD (n=3, $p<0.01$ as ***) ns- no significance.

Table 5.2. Printing assessment of the 3D-printed scaffolds

Formulation	Diameter (mm)	Thickness (mm)	Pore size (µm)	Porosity (%)
GelMA100 CLP	15.04±0.24	0.33±0.015	36.79±1.691	61±2
GC90 CLP	14.84±0.07	0.31±0.02	46.82±1.882	62.66±1.52
GC75 CLP	14.84±0.27	0.31±0.025	50.62±3.941	72.66±1.5
GC50 CLP	14.40±0.32	0.31±0.03	52.04±0.833	76±1

The swelling ratio determines the increase in the weight of the hydrogel due to water absorption. GelMA100 GC90 CLP has shown a swelling index of 310.70±29.13 and 333.81±23.67 % after 360 min, and GC75 and GC50 CLP have 315.18±33.21 and 335.14±26.44 % after 420 and 480 min, respectively (**Figure. 5.5A**). A high swelling ratio favors the migration of active ingredients to the target site, keeps the cornea's moisture, and prevents dry eye formation. The swelling ratio

of the formulations has shown a time-dependent increase, and a significant effect was observed with the formulations GC90 and GC50 CLP. The high-water absorption capacity of the CLP could be due to the availability of free hydroxyl groups of MA and the ability of GelMA/ChiMA polymers to form hydrogen bonding upon interaction with water(Shie et al., 2020)**.** The percentage of AMP permeated through the corneal tissue was analyzed by Franz diffusion cell. The amount of AMP permeated through the corneal tissue was found to be similar with all the AMP-loaded CLP after 18 h. The CLP demonstrated the sustained release of the peptide from the hydrogel matrix (**Figure. 5.5B**).

5.3.3. *In vitro* cell studies

The cytotoxicity of the formulations and the peptide was determined by MTT assay. The hydrogels and the AMP were found to be non-toxic to the HCE cells at the tested dose over incubation time with having cell viability of 79.05 ± 0.56, 80.07 ± 0.39, 79.89 ± 0.49, 78 ± 0.41 and 92.51 ± 1.84 % for the GelMA100, GC90, GC75, GC50 hydrogels, and AMP respectively (**Figure. 5.5C**). The cornea is especially prone to infection because it has a moist mucosal surface and is continuously exposed to the external environment, making it vulnerable to various microbes. The integrity of the cornea's tight junctions determines the effectiveness of the barrier in preventing microbial invasion. Tight connections between epithelial cells restrict fluid, molecules, and ions from moving between them. The epithelial membrane significantly impedes the free diffusion of substances from the eye to the anterior chamber. This can be used to measure the barrier integrity and permeability of HCE monolayers by studying TEER (Mannermaa et al., 2006b). The results showed that the hydrogels with GelMA100, GC90, GC75, and GC50 (500) had a permeability of 123.33 ± 2, 123.13 ± 1, 114 ± 1, and 112 ± 1.52 Ω $cm^{2,}$ respectively. GC50 (500) formulation has shown the highest membrane permeability compared to other formulations. Hydrogels were able to disrupt the monolayer of the cells, and GC50 (500) penetrated deeper into the multilayer epithelial cell layer and returned to a normal state without damaging any cells. The study suggests that the prepared formulations could

permeate through the cell layer and maintain cellular integrity, and this is due to the presence of chitosan in the printed scaffolds. Chitosan facilitates the permeation of active ingredients by disrupting the tight intercellular junctions through the loss of membrane-associated ZO-1 and increases the permeation in the cornea via intracellular uptake and intercellular pathways (J. Smith et al., 2004b) (**Figure. 5.5D &E**).

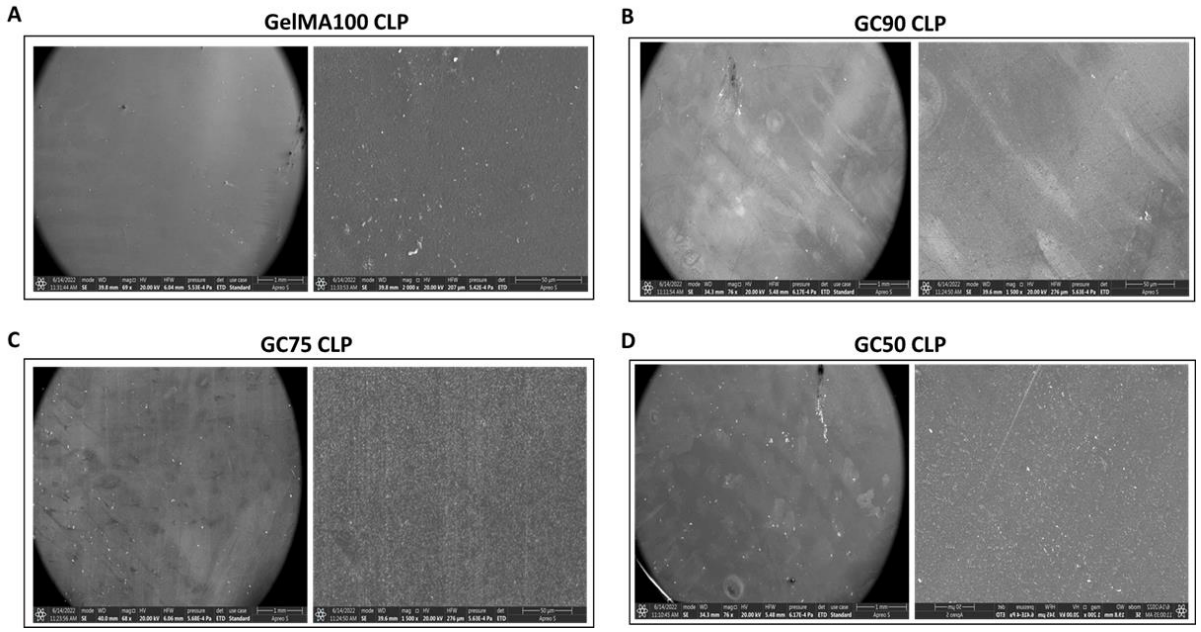

Figure 5.6. Morphology of CLP determined by Scanning Electron Microscopy of GelMA100 CLP (A); GC90 CLP (B); GC75 CLP (C); and GC50 CLP (D).

5.3.4. *In vitro* bacterial studies

The MIC and MBC of the AMP against *P. aeruginosa, S. aureus, and S. pneumoniae* were determined by measuring optical density and MTT assay, respectively. Results showed that the MIC value of AMP for *P. aeruginosa*, *S. aureus,* and *S. pneumoniae* was 20, 20, and 17.5 µg, respectively (**Figure. 5.7A**). Less than 50% viability was achieved for *P. aeruginosa*, *S aureus,* and *S. pneumoniae* at a concentration of 80, 80, and 90 µg, respectively (**Figure. 5.7B**). IC50 values were also calculated, which were 77.50, 66.92, and 65.02 µg for *P. aeruginosa*, *S. aureus,* and *S. pneumoniae,* respectively (**Figure. 5.7C**). AMP inhibited all the bacterial strains at minimum concentrations. The bactericidal effect was observed at maximum with *S. pneumoniae.*

IC50 values of AMP against the bacterial strains were derived, and the lowest IC50 values were found with *S. pneumoniae*, followed by *P. aeruginosa* and *S. aureus.* on the MIC, MBC, and IC50 values of AMP.

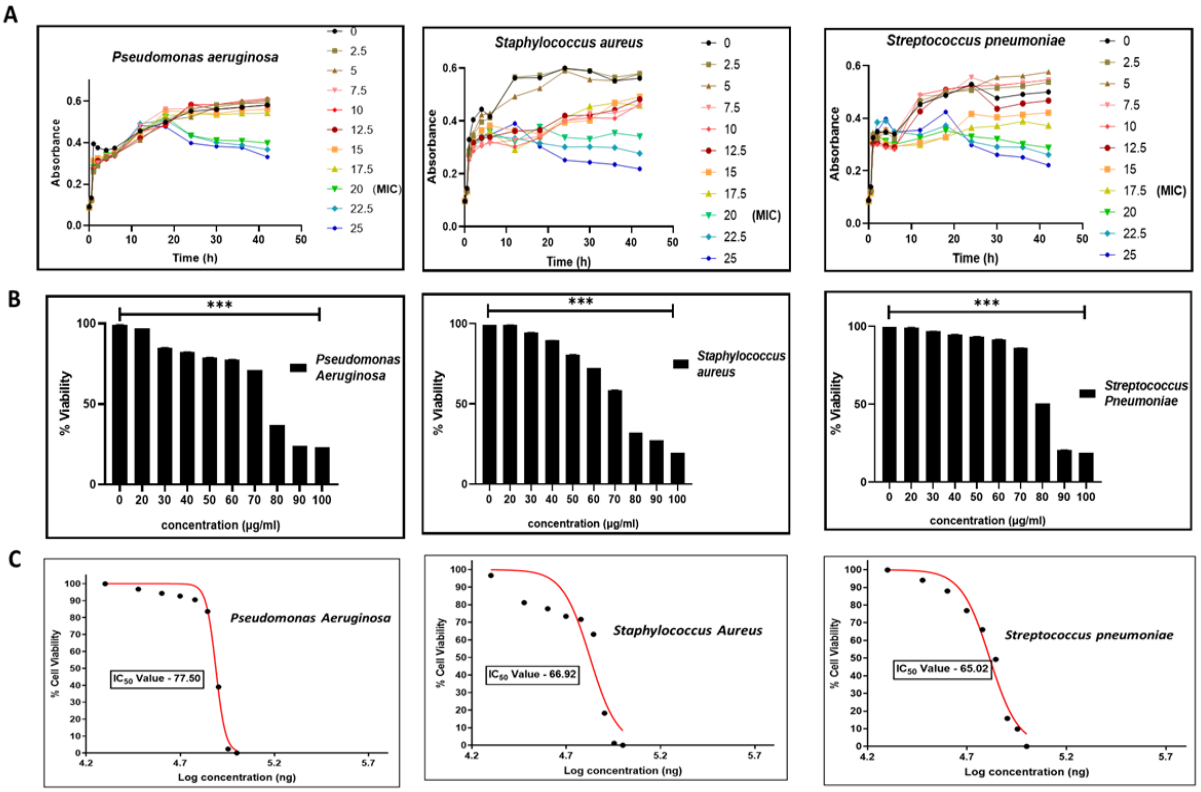

Figure 5.7. Determination of minimum inhibitory concentration (MIC) of S100A12 peptide by measuring optical density (OD_{600}) against *P. aeruginosa*, *S. aureus*, and *S. pneumoniae*, respectively (A); minimum bactericidal concentration (MBC) determination of S100A12 by MTT assay against *P. aeruginosa*, *S. aureus*, and *S. pneumoniae* respectively (B); and determination of IC_{50} value for S100A12 against *P. aeruginosa*, *S. aureus*, and *S. pneumoniae* respectively (C). Data are represented as mean ±SD (n=3, $p<0.01$ as ***).

This suggests that S100A12 was found to be more effective with *P. aeruginosa* compared to other strains. ZOI of the GC50 CLP loaded with AMP of 100 and 500 µg/CLP was determined by the agar-plate method, and results showed that GC50 CLP (500 µg, AMP) had shown a diameter of 45 ± 0.14 mm compared to GC50 CLP (100 µg, AMP) with a diameter of 38 ± 0.41 mm. GC50 CLP without AMP has shown a ZOI of 18 ± 0.3 mm, indicating that the

chitosan present in the formulation also can inhibit the bacteria. The maximum zone diameter was observed with GC50 (500) CLP compared to the other formulations. Evaluating the antibacterial efficacy of chitosan present in GC50, the ZOI for the GC50 CLP without AMP loading showed minimum zone diameter, suggesting that both AMP and chitosan in GC50 CLP have a synergetic effect against the bacteria and the antibacterial efficacy of chitosan was well reported (J. Li & Zhuang, 2020). The zone diameter and the images of ZOI are represented in **Table 5.3** and **Figure. 5.8C.**

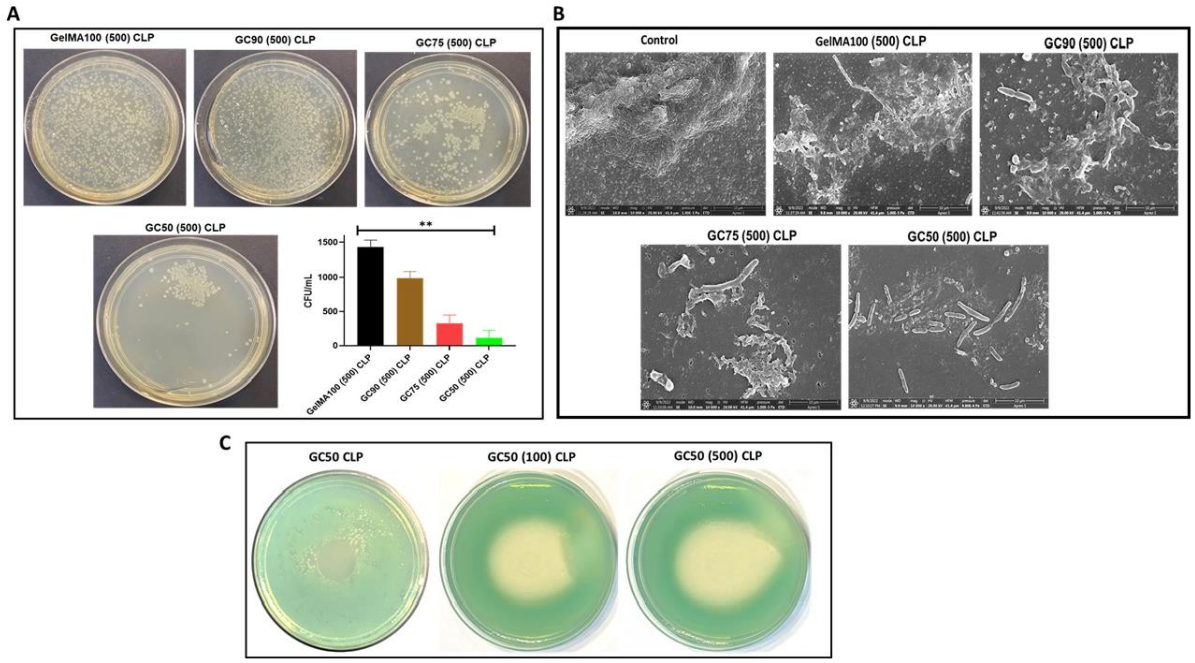

Figure 5.8. *In vitro* antibacterial study and CFU plated on agar plates treated with GC(100/90/75/50)500 CLP (**A**); the biofilm inhibition study of *P. aeruginosa* treated with GC(100/90/75/50)500 CLP determined by scanning electron microscopy after 4 h treatment (**B**); zone of inhibition of bacterial growth, *P. aeruginosa* treated with GC50 CLP, GC50(100) CLP and GC50(500) CLP respectively (**C**). Data are represented as mean ±SD (n=3, $p<0.01$ as **).

Table 5.3. The diameter (mm) of the zone of inhibition for bacteria after treatment with GC50 CLP,GC50 (100/500)CLP

Formulation	ZOI (mm)
GC50 CLP	18 ± 0.3
GC50(100) CLP	38 ± 0.41
GC50(500) CLP	45 ± 0.14

The *in vitro* bacterial biofilm inhibition of *P. aeruginosa* after treatment with GelMA100, GC90/75/50 CLP (500 µg, AMP) was then visualized under SEM. There was significant inhibition of biofilm was observed with the formulation GC50 CP (500), as shown in **Figure. 5.8B.** In *in vitro* antibacterial efficacy study, the colony-forming units (CFU/ mL) after the treatment with the GelMA100, GC90, GC75, and GC50 CLP (500 µg, AMP) were found to be 1432 ± 101, 989 ± 97, 328 ± 121 and 112 ± 111 CFU/ mL respectively (**Figure. 5.8A**). Further, to validate the bacterial efficacy, a live/dead assay was performed for both planktonic bacteria and biofilms of *P. aeruginosa.* After the treatment with printed scaffolds loaded with 500 µg, AMP, the volume of live/dead cells was visualized under the fluorescence microscope. Formulation GC50 CLP has shown high therapeutic efficacy compared to the other formulations. Fluorescence microscope images of bacterial cells treated with printed scaffolds loaded with 500 µg, AMP indicated a live/dead population of bacteria. GelMA100 CLP displayed a higher population of SYTO-9 labeled cells compared to PI labeled populations, and GC50 CLP displayed more red cells compared to other formulations (**Figure. 5.9A**). A similar result was observed in live/dead assay of *P. aeruginosa* biofilms treated with printed scaffolds in which, GC50 CLP (500 µg, AMP) indicated more dead population in 3D images of biofilms captured by confocal microscopy (**Figure. 5.9C**). Quantitative assessment of live-and-dead cell populations was performed by flow cytometry, where Q1 and Q3 quadrants represent live cells, and the shifted cells in Q2 and Q4 quadrants represent the dying/dead cells population (**Figure. 5.9B**). Q2 and Q4 populations were estimated to be 45.1, 57.2, 63.2, and 72.4% for printed scaffolds loaded with 500 µg, AMP, in *P.*

aeruginosa. Formulation with GC50 CLP has the maximum dead population compared to the other formulations; this may be due to the high polymer concentration of chitosan in the GC50 CLP, which might have shown the synergetic effect along with the AMP. The prolonged and significant antibacterial activity of the CLP after 4 h is due to the release profile of AMP because the matrix degradation is slow. Once CLP starts to solubilize in the ocular environment, the entrapped AMP in the matrix diffusion occurs from the pore structures, and porous structures have an important role in the release profile of AMP. Having the advantage of releasing the AMP sustainably, the presence of chitosan in the CLP has an additional impact on the antibacterial activity, which displayed a synergistic effect. Chitosan's inhibitory mechanism on bacteria mainly involves the disruption of the cytoplasmic membrane of bacteria. This is possible because of cationic groups on chitosan's backbone, whereas bacterial cell walls contain negatively charged surfaces. This binding mechanism disrupts the bacteria's cytoplasm (An et al., 2010; Shao et al., 2019).

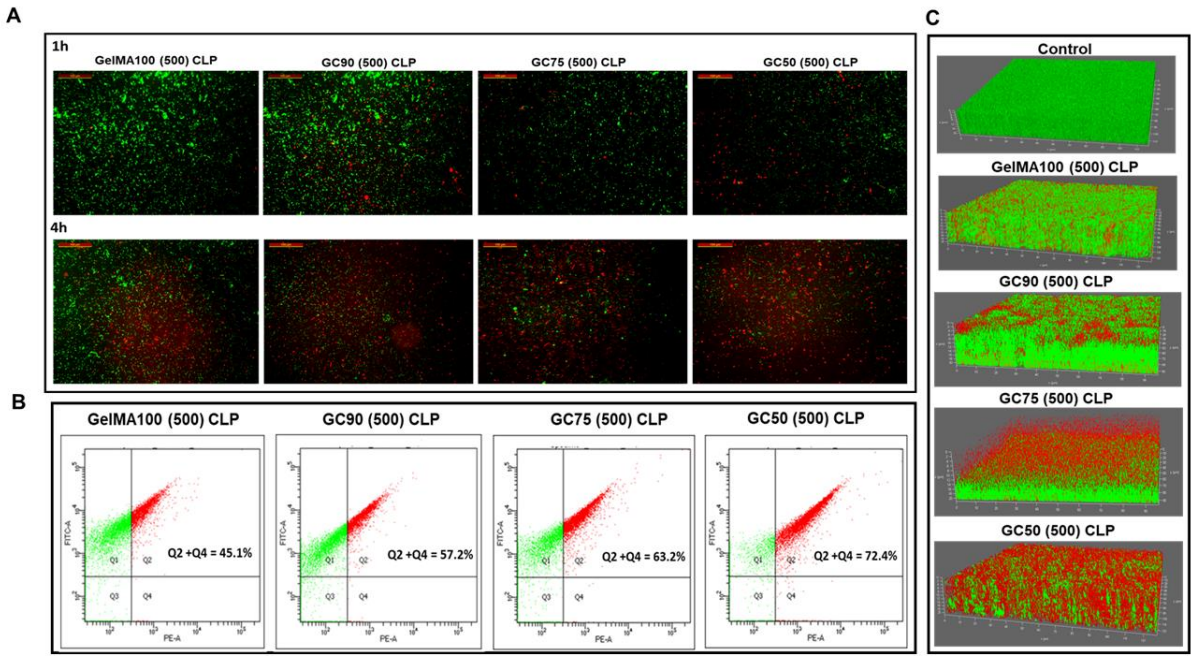

Figure 5.9. Live/dead assay of *P. aeruginosa* treated with AMP-loaded printed scaffolds (500 µg). The fluorescence images of bacteria treated with GC(100/90/75/50)500 CLP for 1 and 4 h, *P. aeruginosa* (A) scale bar 100 µm; the flow cytometric quadratic dot plot diagram displaying the SYTO-9 and PI-stained cells populations (B); the cells in the Q1, Q2, Q3, and

Q4 quadrants represent live and dead cell populations, after 4 h respectively. Live/Dead assay of *P. aeruginosa* biofilms treated with GC(100/90/75/50)500 CLP for 4 h and 3D images of biofilm stained with PI and SYTO 9 (C).

5.3.5. *In vivo* antibacterial study

Further, the antibacterial efficacy of S100A12 (100), GelMA100 (100), and GC50 CLP (100/500 µg, AMP) was analyzed in a bacterial keratitis-induced rabbit model. In an *in vivo* antibacterial study, the corneal images of the rabbits taken by the camera indicated that all the animals had developed BK. The mean CFU load of the groups treated with S100A12 (100), GelMA100 (100), and GC50 CLP (100/500 µg, AMP) were 13433 ± 529, 6783 ± 301, 5200 ± 361 and 916 ± 125/ mL, respectively and with the mean clinical scores of 3.5 ± 0.5, 1.8 ± 0.2, 1.4 ± 0.2 and 0.8 ± 0.2 respectively and control group has mean CFU of 18916 ± 629 with a mean clinical score of 4.6 ± 0.5. GC50 CLP (500) has the maximum effect with a CFU of 916 ± 125/ mL and a clinical score of 0.8 ± 0.2 (**Figure. 5.10**). Results indicated that GC50 (500) CLP significantly reduced the cornea's bacterial load. The treatment was assessed by counting the live bacteria colonies on the agar plate. GelMA100(100) and GC50 (100) CLP reduced the bacterial load two folds compared to the S100A12 peptide. The clinical score of the GC50 (500) CLP was significantly low compared to the other treatment groups, and the cornea images of the animals after the treatment justify the score and CFU. Results indicated that GelMA100 (100) and GC50 CLP (100/500 µg, AMP) treated rabbits significantly reduced the live bacterial count compared to the free peptide and control group. Free S100A12 was used as a topical eye drop. It resulted in a high colony count (CFU/ mL) of *P. aeruginosa*, indicating that the treatment regimen was ineffective and could not penetrate the ocular and bacterial cell membranes. The contact lens is a novel drug delivery approach; the formulations could adhere to the corneal membrane for an extended time and avoid repetitive dosing resulting in significantly reduced bacterial load.

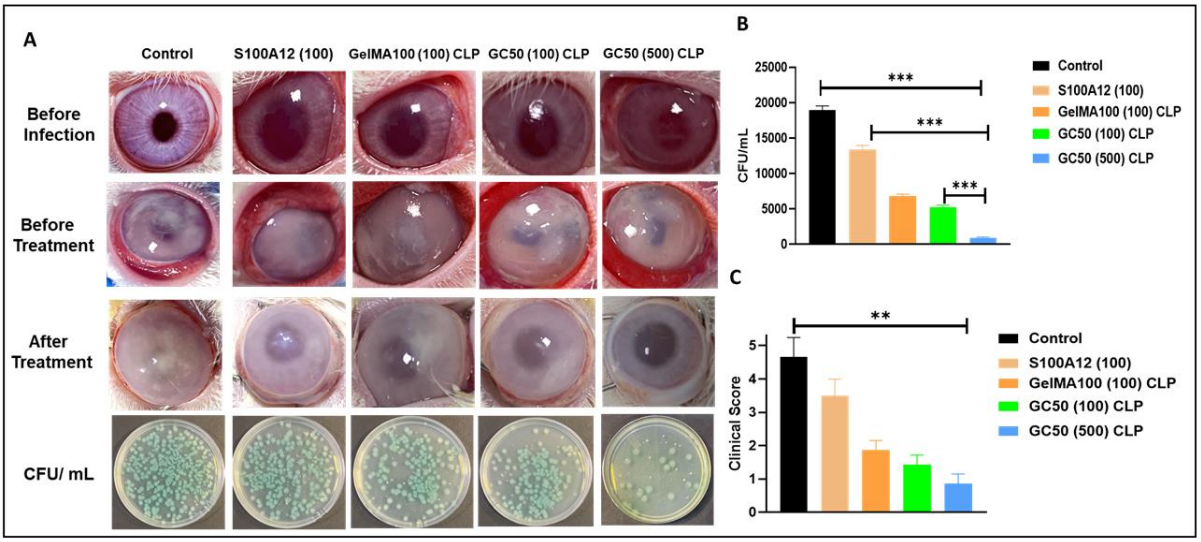

Figure 5.10. *In vivo* therapeutic efficacy of free S100A12 and GelMA100 (100) CLP, GC50(100/500) CLP in *P. aeruginosa* infected bacterial keratitis. The images of the cornea before and after the treatment regimen; (**A**); the clinical score (0 to 5) based on the two criteria (transparent and perforated) (**B**) bacterial load following treatment (**C**) the data are represented as n=3, P<0.01 as **, and P<0.001 as ***.

Corneal patches have better retention time on the corneal surface than conventional eye drops[55] and greatly reduce the lacrimal drainage of the therapeutic agent, thereby increasing the accumulation of high concentrations of antimicrobial agents at the corneal tissue and allowing free passage of antimicrobial agents through the open pores of the lens resulting in increased corneal penetration. The availability of a large amount of therapeutic agents at the site of action increases the therapeutic efficacy of the contact like-patches compared to the conventional eye dosage forms. The developed delivery system could be a potential candidate for treating bacterial keratitis.

5.4. Conclusions

In this study, we developed 3D-printed contact lenses- like patches comprising GelMA/ChiMA hydrogels as printable bioink, which was optimally irradiated to obtain the crosslinking and formation of CLP structure with suitable mechanical characteristics. The hydrogels and CLP have good mucoadhesive strength, increasing the loaded AMP's trans-corneal permeation. The 3D printed CLP have demonstrated significant water absorption capability with sustained release of

AMP while at the same time, the AMP loaded CLP have shown good antibacterial effect and were able to penetrate the bacterial biofilm and realize their eradication. Along with the AMP, chitosan in the bioink has shown a bactericidal effect against *P. aeruginosa*. Further animal experiments with the *P.aeruginosa*-induced BK rabbit model were performed, demonstrating that the AMP-loaded CLP reduced the bacterial load significantly compared to the free AMP. The dosing of AMP could be controlled in the lenses depending upon the severity of infection in patients, indicating their use as a personalized medicine. Therefore, the newly developed AMP-loaded CLP could be a powerful treatment option for severe BK infections, which could be clinically translatable as a personalized therapy for bacterial keratitis.

Chapter 6

Comparison of Polymeric nanoparticles/micelles

6.1 Introduction

A promising approach for efficient antibacterial efficacy in BK is the delivery of Moxifloxacin (M/Mox) entrapped in mucoadhesive/thermoresponsive polymeric micelles/nanoparticles. In this investigation, copolymer nanoparticles (NPs), mixed micelles (Ms), and polyelectrolyte complex (PEC) were prepared based on the polymer of methoxy polyethylene glycol-Hydroxy Propyl Methacrylamide (mPEG-HPMA), Chitosan-poly(lactide-*co*-glycolide)/Poloxamer mixed micelles, and Cationized Gelatin (CG) – Sodium Alginate (Alg) loaded with Moxifloxacin (Mox). Various physicochemical characterization studies on polymer and Mox-loaded polymeric NPs were performed, which included characterizations via UV, IR, ^{1}H NMR, and gel permeation chromatography for polymers, and dynamic light scattering, DSC, XRD techniques, determination of critical micellar/aggregation concentration, percent drug loading, encapsulation efficiency, drug release, mucoadhesive studies, and temperature dependant viscosity studies for micelles/NPs. The drug-loaded micelles/NPs formed with a smaller particle size and narrow size distribution. Studies on the *in vitro* drug release and cellular uptake of the dual-drug delivery system revealed that the micelles/NPs were efficiently taken up by the cells and simultaneously released drugs.

Moreover, the polymeric micelles/NPs showed no cytotoxicity in Human Corneal Epithelial (HCE) cells, and this was further confirmed with the HET-CAM test, in which no hemorrhage was observed with all the formulations. Significant bacterial efficacy was observed with all the formulations against Gram-negative and Gram-positive bacteria compared to the free drug. Higher penetration of polymeric micelles/ NPs was observed in 3D spheroids, and formulations could disrupt the epithelial membrane after treatment. In the *in vivo* antibacterial efficacy study, Mox-loaded polymeric micelles/NPs significantly reduced the bacterial load in the BK-induced mice after the treatment compared to free Mox.

6.2 Comparison of physicochemical characteristics

The particle size, zeta potential, EE% and DL% of the optimized formulations of Mox-mPEG-HPMA (1:70, 1:100, and 1:150), M@CF68/127(5/10)Ms, Mox@CG-Alg NPs are given Table 6.1. The micelles/ nanoparticles were spherical, and the particle dispersion indexes (PDI, 0.28–0.42) revealed that the micelles/nanoparticles had an acceptable size distribution and negative zeta potential that may stabilize micelles. The increase in %DL in the case of Mox@CG-Alg NPs could be due to the strong ionic interaction due to the complex formation of CG and Alg, which could encapsulate Mox in the nanoparticles.

Table 6.1: Physicochemical characteristics of Polymeric Nanoparticles/micelles.

Compound name	**Particle size (nm)**	**PDI**	**Zeta Potential**	**Encapsulation efficiency (%)**	**Drug loading (%)**
Mox-mPH NPs (1:70)	228 ± 2.15	0.42 ± 0.11	-19.79 ± 1.32	47.5 ± 1.74	4.31 ± 1.21
Mox-mPH NPs (1:100)	251.8 ± 1.96	0.41 ± 0.25	-19.93 ± 2.34	62.9 ± 1.55	5.71 ± 1.08
Mox-mPH NPs(1:150)	116.2 ± 2.24	0.39 ± 0.18	-20.41 ± 1.62	83.2 ±1.29	8.32 ± 1.47
M@CF68(5)Ms	101.0 ± 2.0	0.3	31.0 ± 1.5	61.4	5.3
M@CF68(10)Ms	111.0 ± 2.0	0.3	32.0 ± 1.6	75.6	7.4
M@CF127(5)Ms	121.0 ± 2.0	0.3	33.0 ± 2.5	65.2	6.7
M@CF127(10)Ms	127.0 ± 2.0	0.4	36.0 ± 2.4	79.2	7.8
Mox@CG-Alg NPs	237.6 ± 3	0.28	-24.5 ± 3	75.1 ± 2.5	9.5 ± 0.5

The CAC/CMC concentration of mPH NPs, and CF68/127(5/10)Ms was found to be 1.544, 1.397, 1.096 µM for mPH NPs (1:70, 100. And 150), and 1.698 µM for both CF68127(5), CF127(5), and 1.397 µM for CF68(10) and CF127(10) respectively. These copolymers exhibited thermodynamic stability due to the low CMC/CAC of the micelles, and they were able to maintain micellar form after dilution. Given that, conjugation of HPMA and PLGA could add to the hydrophobic interactions between the polymer chains in the micelle core and stabilize the structure. Low CAC/CMCs of mPH NPs, and CF68/127(5/10)Ms might have some advantages, such as stability against dissociation. An *in-vitro* drug release study revealed that free Mox was released faster (about 90%) within 4 h from Mox solution than formulations. In contrast, Mox-mPH NPs (1:70, 100, and 150), M@CF68/127(5/10)Ms, and Mox@CG-Alg NPs showed controlled release ~95 % release of Mox over 18 h at STF, pH 7.2. The HLB between the conjugated polymers made the release path longer for the Mox, as well the hydrophobic conjugation decreased the diffusion of Mox molecules from the micelles/NPs.

6.3 Conclusion

The physicochemical characteristics of all the polymer-based micelles/NPs revealed that M@CF68/127(5/10)Ms is relatively better regarding particle size, PDI, drug loading (%), and *in vitro* release study. However, all the nanocarriers have performed better than conventional formulations of the drug.

Chapter 7

Conclusion

Conclusion

Nanoparticulate drug delivery systems have overcome the drawbacks of conventional drug delivery. Mucoadhesive drug delivery systems have been an emerging strategy to deliver drugs to the anterior and posterior segments of the eye. The mucoadhesive nanoparticulate systems overcome the drawbacks such as lacrimal drainage, poor penetration, poor corneal residence time, and low bioavailability of the drugs at the site of action. Selecting the polymers plays a crucial role in the design of mucoadhesive systems. A wide variety of mucoadhesive polymers have been explored as nano-drug delivery systems for ocular drug delivery.

Polyethylene glycol (PEG) and Hydroxypropyl Methylacrylamide (HPMA) are the prominent hydrophilic polymers. The unique capability of altering Hydrophilic-Lipophilic Balance (HLB) by altering its monomer units of HPMA can be utilized to design nanoparticles. PEG is the most popular hydrophilic polymer approved by the United Stated Food and Drug Administration (US FDA) for clinical use. PEG offers many advantages, including lack of charge, immunogenicity, biodegradability, low poly dispersity, and easy conjugation whereas, HPMA has temperature-sensitive properties and the viscosity of the polymer changes at eye temperature. This unique property can be utilized to improve the corneal residence time of the polymers.

Nanoparticles prepared using mucoadhesive polymers such as chitosan have recently emerged as potential nanocarriers for increasing the corneal residence time of the formulations. Chitosan is a promising candidate for the mucoadhesive approach as it offers positive amine groups on the backbone of the molecular structure. These amine groups interact with the negative sialic acid groups in the mucus over the cornea forming strong interaction between them, thereby increasing the corneal residence time. Chitosan is also a biodegradable polymer and can be conjugated with polymers such as Poly lactide glycolic acid (PLGA) and poloxamers for

making nanoparticulate systems such as micelles. Poloxamers are non-ionic amphiphilic thermoresponsive polymers that can increase the formulation's viscosity at the eye temperature. So, we can conclude that chitosan, PLGA, and poloxamers can be utilized to make nanoparticulate systems. Besides designing nanoparticulate systems using chitosan, its structure can be methacrylated as a photocurable hydrogel chitosan methacryloyl (ChiMA).

Drug delivery systems such as nanoparticles/hydrogels/contact lenses using Gelatin are an emerging science in treating ocular infections. Gelatin offers unique advantages such as it can be modified structurally to design cationized gelatin, which can be used along with anionic sodium alginate to design polyelectrolyte complexes, and Gelatin can be methacrylated to use as a photocurable hydrogel Gelatin Methacryloyl (GelMA). GelMA can be used with ChiMA to synthesize a hydrogel that can be used for 3D bioprinting. Drug delivery through contact lenses is a promising approach where drug wastage through lacrimal drainage can be significantly avoided. The penetration ability of active ingredients through the cornea can be enhanced. Recently, 3D bioprinting has been in the limelight for its robust printing capabilities of scaffolds within less time, making them suitable for personalized medicine having the suitability of loading required dose.

The current study was focused on delivering Mox for treating BK, which requires frequent administration and has poor bioavailability in the cornea. Mox has been loaded into the various polymeric mucoadhesive and thermoresponsive nanoparticulate systems such as mPEG-HPMA NPs, CF68/127(5/10)Ms, CG-Alg NPs to enhance its corneal penetration, bioavailability, and therapeutic efficacy. These polymer conjugates/ nanoparticulate systems were initially characterized with ^{1}H NMR, GPC, FTIR, DSC, XRD, Particle size, and drug loading. The nanoformulations were optimized using the Design of Experiments. The *in vitro*/*in vivo* mucoadhesive properties of the formulations were analyzed. The Mox-loaded formulations were evaluated for *in vitro* cellular uptake, cytotoxicity, and TEER in HCE cells.

Further *in vitro* bacterial efficacy studies were performed in Gram-positive and Gram-negative planktonic and bacterial biofilms. All the Mox-loaded formulations were further evaluated for *in vivo* therapeutic efficacy in bacterial keratitis-induced mice models.

Contact lens-like patches are 3D-Printed using GelMA and ChiMA hydrogels and designed as a novel therapeutic delivery system. An antimicrobial peptide (S100A12) was used as a therapeutic agent and loaded into the bioink with a photoinitiator. The polymer conjugates/hydrogels were thoroughly characterized using ^{1}H NMR, FTIR. The rheological properties were evaluated, such as storage modulus, viscosity, and printability assessment. The *in vitro* mucoadhesive properties, cytotoxicity, and TEER studies were performed. The *in vitro* bacterial efficacy studies were performed in Gram-negative planktonic and bacterial biofilms. Further, the therapeutic efficacy of the peptide-loaded CLP were evaluated in BK induced rabbit model.

In the first objective of the work, we improved therapeutic efficacy by preparing a nanoparticle form of moxifloxacin using a block copolymer combining two hydrophilic segments, mPEG, and poly(HPMA), at different molar ratios (1:70,100 and 150). The polymer and the Mox-loaded polymeric NPs were physicochemically characterized, and formulation parameters were optimized. The Mox-mPH NPs demonstrated optimum drug loading, sustained drug release, mucoadhesion, corneal retention, and penetration. The *in vitro* studies using the bacterial strain *Pseudomonas aeruginosa*, *Staphylococcus aureus*, and *Streptococci pneumoniae* demonstrated superior antibacterial efficacy of Mox-mPH NPs than the free Mox. The mPH NPs (1:150) demonstrated the highest therapeutic benefit in the *in vitro* and *in vivo* studies than other nanoparticles and the conventional free Mox solution. Therefore, the newly developed eye-compatible nanomedicine of moxifloxacin could be a promising treatment option that qualifies for further exploration in bacterial keratitis.

In the second objective, Here, we developed mixed micellar formulations of moxifloxacin using hybrid polymeric systems of chitosan-poly(lactide-co-glycolide) conjugate and pluronic F68 or F127 at a ratio of either 1: 5 or 1: 10. Thorough physicochemical characterization, *in vitro*, and *in vivo* studies were conducted to confirm the fabrication, determine effective drug entrapment, stability, safety, corneal retention, penetration, gel formation, and therapeutic efficacy studies in *P. aeruginosa*, and *S. aureus* bacteria *in vitro*, and their BK-induced mice models *in vivo*. The results indicated that mixed micelles bearing higher pluronic proportions (1: 10) had better physicochemical properties, mucoadhesion, corneal penetration, and antibacterial performance in the *in vitro* and *in vivo* studies. The higher PPO units in F127 compared to F68 corrected the hydrophilic-lipophilic balance in M@CF127(10)Ms, resulting in higher self-assembling ability, drug loading, micellar stability, gelling property at ocular temperature, corneal tissue penetration, bacterial biofilm permeability compared to M@CF68(10)Ms, resulting in superior antibacterial effect *in vitro* and *in vivo*. Therefore, the newly developed nanoformulation, M@CF127(10)Ms, is multifunctional, easily scalable, non-irritant, non-toxic, and could be an effective treatment strategy for bacterial keratitis.

In the third objective, we developed mucoadhesive PEC NPs using CG and Alg loaded with Mox. NPs were optimized using DoE. Thorough physicochemical characterization was performed to analyze the size, uniformity, morphology, % EE and % DL of the NPs. Mucoadhesive, toxicity, and NPs uptake studies were performed on the HCE cell line. The anti-bacterial efficacy of the formulation was determined against *P. aeruginosa* and *S. aureus* (*in vitro*) and the Bk-induced mice model (*in vivo*). The strong electrostatic interaction between the cationic amine groups of CG and anionic carboxyl groups of Alg resulted in the formation of PEC NPs. The NPs successfully encapsulated Mox and formed uniformed particles within nano size. The cationic groups were allowed to interact with mucin over the cornea, increasing the corneal residence time and increasing penetration of the NPs into the cornea, demonstrating

bacterial efficacy. Thus, the developed formulation is an effective treatment strategy for treating BK.

In the fourth objective, we developed 3D-printed contact lens-like patches comprising GelMA/ChiMA hydrogels as printable bioink, which was optimally irradiated to obtain the crosslinking and formation of CLP structure with suitable mechanical characteristics. The hydrogels and CLP have good mucoadhesive strength, increasing the loaded AMP's trans-corneal permeation. The 3D-printed CLP have demonstrated significant water absorption capability with sustained release of AMP. At the same time, the AMP-loaded CLP have shown good antibacterial effects and were able to penetrate the bacterial biofilm and realize their eradication. Along with the AMP, chitosan in the bioink has shown a bactericidal effect against *P. aeruginosa*. Further animal experiments with the *P. aeruginosa*-induced BK rabbit model were performed, demonstrating that the AMP-loaded CLP reduced the bacterial load significantly compared to the free AMP. The dosing of AMP could be controlled in the lenses depending upon the severity of infection in patients, indicating their use as a personalized medicine. Therefore, the newly developed AMP-loaded CLP could be a powerful treatment option for severe BK infections, which could be clinically translatable as a personalized therapy for bacterial keratitis.

Overall, developed nano-delivery systems/ contact lens-like patches could be a promising strategy for treating BK.

Chapter 8

Future scope of work

Future scope of work

In the rapidly advancing field of ocular drug delivery, the future perspective of mucoadhesive nanomedicine as eye drops holds immense promise. These NPs, have the potential to adhere to the ocular surface, have the ability to revolutionize the conventional treatment of various ocular disorders. Mucoadhesive nanoparticles as eye drops offeres numerous advantages including, sustained drug release, increased bioavailability, and reduced dosing frequency, which improves the patient compliance and overall therapeutic results. The ability of mucoadhesive nanoparticles to penetrate the substantial barriers offered by the ocular mucosa, providing effective drug penetration and sustained release at the target location, is one of their main advantages. Additionally, these nanoparticles' ability to adhere to the ocular surface for a longer period of time prolongs the drug's residence time while minimising systemic absorption and the likelihood of systemic adverse effects.

The therapeutic application of mucoadhesive nanoparticles as eye drops is anticipated to transform ocular medication delivery in the future, providing a viable substitute for current therapies. Their ability to distribute drugs with precision might result in more individualised and effective treatments, reducing adverse effects and enhancing patient compliance in treating BK. With ongoing research and technological advancements, the integration of smart nanotechnologies and personalized medicine will further optimize their clinical use, paving the way for a new era in ocular therapeutics that prioritizes efficacy, patient comfort, and overall ocular health. The potential applications of mucoadhesive nanoparticles as eye drops span across a wide range of ocular conditions not limited to bacterial keratitis, including glaucoma, macular degeneration, and various inflammatory disorders. Their versatility allows for the targeted delivery of different therapeutic agents, such as anti-glaucoma medications, anti-inflammatory drugs, and even gene therapies. As research and development in nanotechnology

continue to progress, the formulation of mucoadhesive nanoparticles can be tailored to cater to specific ocular pathologies, ensuring optimized treatment strategies for each condition.

Though challenges remain, such as ensuring long-term stability, biocompatibility, and cost-effectiveness of these nanoparticles, ongoing research efforts are continuously addressing these concerns. As interdisciplinary collaborations and technological advancements unfold, the translation of mucoadhesive nanoparticles from the lab to clinical practice appears ever more promising. The developed formulations have the potential to undergo preclinical and clinical trails thereby giving the better understanding of the effect of the formulation in real time so that the observed challenges can be addressed for future studies.

The future perspective of using contact lens-like patches as contact lenses in treating bacterial keratitis holds significant promise for revolutionizing the management of this sight-threatening condition. These innovative contact lens-like patches (CLP) offer a multifunctional approach, combining the benefits of both therapeutic agents and barrier protection. By incorporating antimicrobial agents directly into the patch material, these CLP can provide continuous and targeted drug delivery to the infected cornea, ensuring more efficient eradication of bacterial pathogens. Additionally, the CLP acts as a physical barrier, shielding the affected cornea from further external damage and microbial invasion. This integrated approach not only enhances treatment efficacy but also simplifies the administration process, improving patient compliance and reducing the need for frequent instillation of eye drops. As advancements in material science and nanotechnology continue, future ocular patches may further incorporate diagnostic components, enabling real-time monitoring of the infection and treatment response. Overall, ocular patches as contact lenses represent a promising avenue for bacterial keratitis treatment, offering a novel and patient-friendly solution that could potentially revolutionize the management of this serious ocular condition.

Chapter 9

References

Abdeltawab, H., Svirskis, D., & Sharma, M. (2020). Formulation strategies to modulate drug release from poloxamer based in situ gelling systems. *Expert Opinion on Drug Delivery*, *17*(4), 495–509. https://doi.org/10.1080/17425247.2020.1731469

Abud, T. B., Di Zazzo, A. Di, Kheirkhah, A., & Dana, R. (2017). Systemic immunomodulatory strategies in high-risk corneal transplantation. *Journal of Ophthalmic and Vision Research*, *12*(1), 81–92. https://doi.org/10.4103/2008-322X.200156

Afarid, M., Mahmoodi, S., & Baghban, R. (2022). Recent achievements in nano-based technologies for ocular disease diagnosis and treatment, review and update. *Journal of Nanobiotechnology*, *20*(1), 1–36. https://doi.org/10.1186/s12951-022-01567-7

Ahmed, I. (2003). The Noncorneal Route in Ocular Drug Delivery. *Ophthalmic Drug Delivery Systems, Second Edition*, 335–363. https://doi.org/10.1201/9780203912072.CH11

Ahmed, I., & Patton, T. F. (1985). Importance of the noncorneal absorption route in topical ophthalmic drug delivery. *Investigative Ophthalmology & Visual Science*, *26*(4), 584–587.

Ahmed, S., Amin, M. M., El-Korany, S. M., & Sayed, S. (2022). Corneal targeted fenticonazole nitrate-loaded novasomes for the management of ocular candidiasis: Preparation, in vitro characterization, ex vivo and in vivo assessments. *Https://Doi.Org/10.1080/10717544.2022.2103600*, *29*(1), 2428–2441. https://doi.org/10.1080/10717544.2022.2103600

Ahn, M., Yoon, K. C., Ryu, S. K., Cho, N. C., & You, I. C. (2011). Clinical aspects and prognosis of mixed microbial (bacterial and fungal) keratitis. *Cornea*, *30*(4), 409–413. https://doi.org/10.1097/ICO.0B013E3181F23704

Ahuja, A., Khar, R. K., & Ali, J. (2008). Mucoadhesive Drug Delivery Systems. *Http://Dx.Doi.Org/10.3109/03639049709148498*, *23*(5), 489–515. https://doi.org/10.3109/03639049709148498

Ajayi, B. O., Kio, F. E., & Otajevwo, F. D. (2011). Adhesive Capabilities of Staphylococcus Aureus and Pseudomonas Aeruginosa Isolated from Tears of HIV/AIDS Patients to Soft Contact Lenses. *Global Journal of Health Science*, *4*. https://www.academia.edu/30267084/Adhesive_Capabilities_of_Staphylococcus_Aureus_and_Pseudomonas_Aeruginosa_Isolated_from_Tears_of_HIV_AIDS_Patients_to_Soft_Contact_Lenses

Ajdary, R., Tardy, B. L., Mattos, B. D., Bai, L., & Rojas, O. J. (2021). Plant Nanomaterials and Inspiration from Nature: Water Interactions and Hierarchically Structured Hydrogels. *Advanced Materials*, *33*(28), 2001085. https://doi.org/https://doi.org/10.1002/adma.202001085

Alexandrakis, G., Alfonso, E. C., & Miller, D. (2000). Shifting trends in bacterial keratitis in South Florida and emerging resistance to fluoroquinolones. *Ophthalmology*, *107*(8), 1497–1502. https://doi.org/10.1016/S0161-6420(00)00179-2

Allen, C., Yu, Y., Eisenberg, A., & Maysinger, D. (1999). Cellular internalization of PCL20-b-PEO44 block copolymer micelles. *Biochimica et Biophysica Acta - Biomembranes*, *1421*(1), 32–38. https://doi.org/10.1016/S0005-2736(99)00108-X

Al-Mujaini, A., Al-Kharusi, N., Thakral, A., & Wali, U. K. (2009a). Bacterial Keratitis: Perspective on Epidemiology, Clinico-Pathogenesis, Diagnosis and Treatment. *Sultan Qaboos University Medical Journal*, *9*(2), 184. /pmc/articles/PMC3074777/

Al-Mujaini, A., Al-Kharusi, N., Thakral, A., & Wali, U. K. (2009b). Bacterial keratitis: Perspective on epidemiology, Clinico-Pathogenesis, diagnosis and treatment. *Sultan Qaboos University Medical Journal*, *9*(2), 184–195.

Al-Mujaini, A., Al-Kharusi, N., Thakral, A., & Wali, U. K. (2009c). *Bacterial Keratitis: Perspective on Epidemiology, Clinico-Pathogenesis, Diagnosis and Treatment* *ية، لتشخيصية ا / اخلروصي أركانا ،ثاكرال أوبينيدار والي وا لعالجية ا / لتهاب ا / لقر نية اجلرثومي: ألبعاد ا / لوبا ،ئية املرضية ا / لسر ير نادية ،اجمليني اهلل عبد* .(Vol. 9, Issue 2). Epub

Alqattan, B., Yetisen, A. K., & Butt, H. (2018). Direct Laser Writing of Nanophotonic Structures on Contact Lenses. *ACS Nano*, *12*(6), 5130–5140. https://doi.org/10.1021/ACSNANO.8B00222/ASSET/IMAGES/LARGE/NN-2018-002222_0007.JPEG

Al-Shehri, A., Jastaneiah, S., & Wagoner, M. D. (2009). Changing trends in the clinical course and outcome of bacterial keratitis at King Khaled Eye Specialist Hospital. *International Ophthalmology*, *29*(3), 143–152. https://doi.org/10.1007/s10792-008-9206-6

An, J., Yuan, X., Luo, Q., & Wang, D. (2010). Preparation of chitosan-graft-(methyl methacrylate)/Ag nanocomposite with antimicrobial activity. *Polymer International*, *59*(1), 62–70. https://doi.org/https://doi.org/10.1002/pi.2689

Analysis of the risk factors predisposing to fungal, bacteri... : Indian Journal of Medical Research. (n.d.). Retrieved April 17, 2023, from https://journals.lww.com/ijmr/Abstract/2009/30060/Analysis_of_the_risk_factors_predisposing_to.15.aspx

Anitha, A., Deepa, N., Chennazhi, K. P., Nair, S. V, Tamura, H., & Jayakumar, R. (2011). Development of mucoadhesive thiolated chitosan nanoparticles for biomedical applications. *Carbohydrate Polymers*, *83*(1), 66–73. https://doi.org/https://doi.org/10.1016/j.carbpol.2010.07.028

Ansari, Z., Miller, D., & Galor, A. (2013). Current thoughts in fungal keratitis: Diagnosis and treatment. *Current Fungal Infection Reports*, *7*(3), 209–218. https://doi.org/10.1007/S12281-013-0150-1

Argüeso, P., Guzman-Aranguez, A., Mantelli, F., Cao, Z., Ricciuto, J., & Panjwani, N. (2009a). Association of cell surface mucins with galectin-3 contributes to the ocular surface epithelial barrier. *The Journal of Biological Chemistry*, *284*(34), 23037–23045. https://doi.org/10.1074/JBC.M109.033332

Argüeso, P., Guzman-Aranguez, A., Mantelli, F., Cao, Z., Ricciuto, J., & Panjwani, N. (2009b). Association of Cell Surface Mucins with Galectin-3 Contributes to the Ocular

Surface Epithelial Barrier. *Journal of Biological Chemistry*, *284*(34), 23037–23045. https://doi.org/10.1074/JBC.M109.033332

Ashammakhi, N., Ahadian, S., Xu, C., Montazerian, H., Ko, H., Nasiri, R., Barros, N., & Khademhosseini, A. (2019). Bioinks and bioprinting technologies to make heterogeneous and biomimetic tissue constructs. *Materials Today Bio*, *1*, 100008. https://doi.org/10.1016/J.MTBIO.2019.100008

Aung, T. T., Yam, J. K. H., Lin, S., Salleh, S. M., Givskov, M., Liu, S., Lwin, N. C., Yang, L., & Beuerman, R. W. (2016). Biofilms of Pathogenic Nontuberculous Mycobacteria Targeted by New Therapeutic Approaches. *Antimicrobial Agents and Chemotherapy*, *60*(1), 24. https://doi.org/10.1128/AAC.01509-15

Austin, A., Lietman, T., & Rose-Nussbaumer, J. (2017a). Update on the management of infectious keratitis. *Ophthalmology*, *124*(11), 1678–1689.

Austin, A., Lietman, T., & Rose-Nussbaumer, J. (2017b). Update on the Management of Infectious Keratitis. *Ophthalmology*, *124*(11), 1678–1689. https://doi.org/https://doi.org/10.1016/j.ophtha.2017.05.012

Bacterial Keratitis Treatment & Management: Medical Care, Surgical Care, Consultations. (n.d.). Retrieved April 20, 2023, from https://emedicine.medscape.com/article/1194028-treatment

Ban, Y., Dota, A., Cooper, L. J., Fullwood, N. J., Nakamura, T., Tsuzuki, M., Mochida, C., & Kinoshita, S. (2003). Tight junction-related protein expression and distribution in human corneal epithelium. *Experimental Eye Research*, *76*(6), 663–669. https://doi.org/10.1016/S0014-4835(03)00054-X

Baniasadi, H., Madani, Z., Ajdary, R., Rojas, O. J., & Seppälä, J. (2021). Ascorbic acid-loaded polyvinyl alcohol/cellulose nanofibril hydrogels as precursors for 3D printed materials. *Materials Science and Engineering C*, *130*. https://doi.org/10.1016/j.msec.2021.112424

Baniasadi, H., Polez, R. T., Kimiaei, E., Madani, Z., Rojas, O. J., Österberg, M., & Seppälä, J. (2021). 3D printing and properties of cellulose nanofibrils-reinforced quince seed mucilage bio-inks. *International Journal of Biological Macromolecules*, *192*, 1098–1107. https://doi.org/https://doi.org/10.1016/j.ijbiomac.2021.10.078

Baranowski, P., Karolewicz, B., Gajda, M., & Pluta, J. (2014a). Ophthalmic drug dosage forms: Characterisation and research methods. *The Scientific World Journal*, *2014*. https://doi.org/10.1155/2014/861904

Baranowski, P., Karolewicz, B., Gajda, M., & Pluta, J. (2014b). Ophthalmic drug dosage forms: Characterisation and research methods. *The Scientific World Journal*, *2014*. https://doi.org/10.1155/2014/861904

Baranowski, P., Karolewicz, B., Gajda, M., & Pluta, J. (2014c). Ophthalmic Drug Dosage Forms: Characterisation and Research Methods. *The Scientific World Journal*, *2014*, 861904. https://doi.org/10.1155/2014/861904

Bartimote, C., Foster, J., & Watson, S. (2020). The Spectrum of Microbial Keratitis: An Updated Review. In *The Open Ophthalmology Journal* (Vol. 13, Issue 1). https://doi.org/10.2174/1874364101913010100

Ben Henda, M., Ghaouar, N., & Gharbi, A. (2013). Rheological Properties and Reverse Micelles Conditions of PEO-PPO-PEO Pluronic F68: Effects of Temperature and Solvent Mixtures. *Journal of Polymers*, *2013*, 768653. https://doi.org/10.1155/2013/768653

Bharathi, M. J., Ramakrishnan, R., Meenakshi, R., Padmavathy, S., Shivakumar, C., & Srinivasan, M. (2007). Microbial keratitis in South India: Influence of risk factors, climate, and geographical variation. *Ophthalmic Epidemiology*, *14*(2), 61–69. https://doi.org/10.1080/09286580601001347

Bharathi, M. J., Ramakrishnan, R., Vasu, S., Meenakshi, R., Shivkumar, C., & Palaniappan, R. (2003). Epidemiology of bacterial keratitis in a referral centre in south India. *Indian Journal of Medical Microbiology*, *21*(4), 239.

Bhatt, H., Kiran Rompicharla, S. V., Ghosh, B., & Biswas, S. (2019). α-Tocopherol Succinate-Anchored PEGylated Poly(amidoamine) Dendrimer for the Delivery of Paclitaxel: Assessment of in Vitro and in Vivo Therapeutic Efficacy [Research-article]. *Molecular Pharmaceutics*, *16*(4), 1541–1554. https://doi.org/10.1021/acs.molpharmaceut.8b01232

Bialasiewicz, A., Shenoy, R., Thakral, A., Al-Muniri, A. A., Shenoy, U., & Al-Mughairi, Z. (2006). Mikrobielle Keratitis. *Der Ophthalmologe*, *103*(8), 682–687. https://doi.org/10.1007/s00347-006-1363-2

Bíró, T., & Aigner, Z. (2019). Current approaches to use cyclodextrins and mucoadhesive polymers in ocular drug delivery-a mini-review. *Scientia Pharmaceutica*, *87*(3). https://doi.org/10.3390/scipharm87030015

Blondeau, J. M. (2004). Fluoroquinolones: mechanism of action, classification, and development of resistance. *Survey of Ophthalmology*, *49*(2), S73–S78. https://doi.org/10.1016/J.SURVOPHTHAL.2004.01.005

Bobde, Y., Biswas, S., & Ghosh, B. (2020a). Current trends in the development of HPMA-based block copolymeric nanoparticles for their application in drug delivery. *European Polymer Journal*, *139*(September), 110018. https://doi.org/10.1016/j.eurpolymj.2020.110018

Bobde, Y., Biswas, S., & Ghosh, B. (2020b). PEGylated N-(2 hydroxypropyl) methacrylamide-doxorubicin conjugate as pH-responsive polymeric nanoparticles for cancer therapy. *Reactive and Functional Polymers*, *151*(March), 104561. https://doi.org/10.1016/j.reactfunctpolym.2020.104561

Bodratti, A. M., & Alexandridis, P. (2018). Formulation of Poloxamers for Drug Delivery. In *Journal of Functional Biomaterials* (Vol. 9, Issue 1). https://doi.org/10.3390/jfb9010011

Bourcier, T., Thomas, F., Borderie, V., Chaumeil, C., & Laroche, L. (2003). Bacterial keratitis: predisposing factors, clinical and microbiological review of 300 cases. *British Journal of Ophthalmology*, *87*(7), 834. https://doi.org/10.1136/bjo.87.7.834

Bourges, X., Weiss, P., Daculsi, G., & Legeay, G. (2002). Synthesis and general properties of silated-hydroxypropyl methylcellulose in prospect of biomedical use. *Advances in Colloid and Interface Science*, *99*(3), 215–228. https://doi.org/10.1016/S0001-8686(02)00035-0

Burnett, D. J., Garcia, A. R., Lan, Y., & Ali, S. (2012). *Investigating the Surface Wettability of Poloxamers used for Solid Dispersions*. *1253*(2007), 18103.

Cafaggi, S., Russo, E., Stefani, R., Leardi, R., Caviglioli, G., Parodi, B., Bignardi, G., De Totero, D., Aiello, C., & Viale, M. (2007). Preparation and evaluation of nanoparticles made of chitosan or N-trimethyl chitosan and a cisplatin–alginate complex. *Journal of Controlled Release*, *121*(1–2), 110–123. https://doi.org/10.1016/J.JCONREL.2007.05.037

Calonge, M. (2001). The treatment of dry eye. *Survey of Ophthalmology*, *45 Suppl 2*(SUPPL. 2). https://doi.org/10.1016/S0039-6257(00)00205-8

Cameron, J. A. (1995). Shield Ulcers and Plaques of the Cornea in Vernal Keratoconjunctivitis. *Ophthalmology*, *102*(6), 985–993. https://doi.org/10.1016/S0161-6420(95)30925-6

Carvalho, I. M., Marques, C. S., Oliveira, R. S., Coelho, P. B., Costa, P. C., & Ferreira, D. C. (2015a). Sustained drug release by contact lenses for glaucoma treatment—A review. *Journal of Controlled Release*, *202*, 76–82. https://doi.org/https://doi.org/10.1016/j.jconrel.2015.01.023

Carvalho, I. M., Marques, C. S., Oliveira, R. S., Coelho, P. B., Costa, P. C., & Ferreira, D. C. (2015b). Sustained drug release by contact lenses for glaucoma treatment—A review. *Journal of Controlled Release*, *202*, 76–82. https://doi.org/https://doi.org/10.1016/j.jconrel.2015.01.023

Ch, S., Mishra, P., Bhatt, H., Ghosh, B., Roy, S., & Biswas, S. (2021a). Hydroxypropyl methacrylamide-based copolymeric nanoparticles loaded with moxifloxacin as a mucoadhesive, cornea-penetrating nanomedicine eye drop with enhanced therapeutic benefits in bacterial keratitis. *Colloids and Surfaces B: Biointerfaces*, *208*(August), 112113. https://doi.org/10.1016/j.colsurfb.2021.112113

Ch, S., Mishra, P., Bhatt, H., Ghosh, B., Roy, S., & Biswas, S. (2021b). Hydroxypropyl methacrylamide-based copolymeric nanoparticles loaded with moxifloxacin as a mucoadhesive, cornea-penetrating nanomedicine eye drop with enhanced therapeutic benefits in bacterial keratitis. *Colloids and Surfaces B: Biointerfaces*, *208*, 112113. https://doi.org/10.1016/J.COLSURFB.2021.112113

Ch, S., Mishra, P., Bhatt, H., Ghosh, B., Roy, S., & Biswas, S. (2021c). Hydroxypropyl methacrylamide-based copolymeric nanoparticles loaded with moxifloxacin as a mucoadhesive, cornea-penetrating nanomedicine eye drop with enhanced therapeutic benefits in bacterial keratitis. *Colloids and Surfaces B: Biointerfaces*, *208*, 112113. https://doi.org/https://doi.org/10.1016/j.colsurfb.2021.112113

Ch, S., Padaga, S. G., Ghosh, B., Roy, S., & Biswas, S. (2023a). Chitosan-poly(lactide-co-glycolide)/poloxamer mixed micelles as a mucoadhesive thermo-responsive moxifloxacin eye drop to improve treatment efficacy in bacterial keratitis. *Carbohydrate Polymers*, *312*, 120822. https://doi.org/10.1016/J.CARBPOL.2023.120822

Ch, S., Padaga, S. G., Ghosh, B., Roy, S., & Biswas, S. (2023b). Chitosan-poly(lactide-co-glycolide)/poloxamer mixed micelles as a mucoadhesive thermo-responsive moxifloxacin eye drop to improve treatment efficacy in bacterial keratitis. *Carbohydrate Polymers*, *312*, 120822. https://doi.org/10.1016/J.CARBPOL.2023.120822

Chang, C., Duan, B., Cai, J., & Zhang, L. (2010). Superabsorbent hydrogels based on cellulose for smart swelling and controllable delivery. *European Polymer Journal*, *46*(1), 92–100. https://doi.org/10.1016/J.EURPOLYMJ.2009.04.033

Chen, M., Li, L., Xia, L., Jiang, S., Kong, Y., Chen, X., & Wang, H. (2021). The kinetics and release behaviour of curcumin loaded pH-responsive PLGA/chitosan fibers with antitumor activity against HT-29 cells. *Carbohydrate Polymers*, *265*, 118077. https://doi.org/https://doi.org/10.1016/j.carbpol.2021.118077

Cheng, Y. H., Tsai, T. H., Jhan, Y. Y., Chiu, A. W. H., Tsai, K. L., Chien, C. S., Chiou, S. H., & Liu, C. J. L. (2016). Thermosensitive chitosan-based hydrogel as a topical ocular drug delivery system of latanoprost for glaucoma treatment. *Carbohydrate Polymers*, *144*, 390–399. https://doi.org/10.1016/j.carbpol.2016.02.080

Cholkar, K., Patel, A., Dutt Vadlapudi, A., & K Mitra, A. (2012). Novel nanomicellar formulation approaches for anterior and posterior segment ocular drug delivery. *Recent Patents on Nanomedicine*, *2*(2), 82–95.

Choy, Y. Bin, Park, J. H., & Prausnitz, M. R. (2008). Mucoadhesive microparticles engineered for ophthalmic drug delivery. *Journal of Physics and Chemistry of Solids*, *69*(5–6), 1533–1536. https://doi.org/10.1016/j.jpcs.2007.10.043

Chung, Y. C., Tsai, C. F., & Li, C. F. (2006). Preparation and characterization of water-soluble chitosan produced by Maillard reaction. *Fisheries Science 2006 72:5*, *72*(5), 1096–1103. https://doi.org/10.1111/J.1444-2906.2006.01261.X

Cometta, S., Jones, R. T., Juárez-Saldivar, A., Donose, B. C., Yasir, M., Bock, N., Dargaville, T. R., Bertling, K., Brünig, M., Rakić, A. D., Willcox, M., & Hutmacher, D. W. (2022). Melimine-Modified 3D-Printed Polycaprolactone Scaffolds for the Prevention of Biofilm-Related Biomaterial Infections. *ACS Nano*, *16*(10), 16497–16512. https://doi.org/10.1021/acsnano.2c05812

Cone, R. A. (2009). Barrier properties of mucus. *Advanced Drug Delivery Reviews*, *61*(2), 75–85. https://doi.org/10.1016/J.ADDR.2008.09.008

Cooper, R. C., & Yang, H. (2019). Hydrogel-based ocular drug delivery systems: Emerging fabrication strategies, applications, and bench-to-bedside manufacturing considerations. *Journal of Controlled Release*, *306*(May), 29–39. https://doi.org/10.1016/j.jconrel.2019.05.034

Cosco, D., Federico, C., Maiuolo, J., Bulotta, S., Molinaro, R., Paolino, D., Tassone, P., & Fresta, M. (2014). Physicochemical features and transfection properties of chitosan/poloxamer 188/poly(D,L-lactide-co-glycolide) nanoplexes. In *International journal of nanomedicine* (Vol. 9, pp. 2359–2372). https://doi.org/10.2147/ijn.s58362

da Silva, S. B., Ferreira, D., Pintado, M., & Sarmento, B. (2016). Chitosan-based nanoparticles for rosmarinic acid ocular delivery-In vitro tests. *International Journal of Biological Macromolecules*, *84*, 112–120. https://doi.org/10.1016/j.ijbiomac.2015.11.070

Daniell, M., Mills, R., & Morlet, N. (2003). Microbial keratitis: what's the preferred initial therapy? *British Journal of Ophthalmology*, *87*(9), 1167. https://doi.org/10.1136/bjo.87.9.1167

de Jonckheere, J. F. (1991). Ecology of Acanthamoeba. *Reviews of Infectious Diseases*, *13*(Supplement_5), S385–S387. https://doi.org/10.1093/CLIND/13.SUPPLEMENT_5.S385

de Lima, C. S. A., Varca, J. P. R. O., Alves, V. M., Nogueira, K. M., Cruz, C. P. C., Rial-Hermida, M. I., Kadłubowski, S. S., Varca, G. H. C., & Lugão, A. B. (2022). Mucoadhesive Polymers and Their Applications in Drug Delivery Systems for the Treatment of Bladder Cancer. *Gels 2022, Vol. 8, Page 587*, *8*(9), 587. https://doi.org/10.3390/GELS8090587

Desai, A., Shukla, M., Maulvi, F., & Ranch, K. (2020). Ophthalmic and otic drug administration: Novel approaches and challenges. *Novel Drug Delivery Technologies: Innovative Strategies for Drug Re-Positioning*, 335–381. https://doi.org/10.1007/978-981-13-3642-3_10/COVER

Determination of tear volume and tear flow - PubMed. (n.d.). Retrieved April 20, 2023, from https://pubmed.ncbi.nlm.nih.gov/5947945/

Dethorey, G., Daruich, A., Hay, A., Renard, G., & Bourges, J.-L. (2013). Kératites bactériennes sévères reçues aux urgences ophtalmologiques : analyse rétrospective de 268 cas. *Journal Français d'Ophtalmologie*, *36*(2), 129–137. https://doi.org/https://doi.org/10.1016/j.jfo.2011.12.013

Dey, S., Anand, B. S., Patel, J., & Mitra, A. K. (2005). Transporters/receptors in the anterior chamber: pathways to explore ocular drug delivery strategies. *Http://Dx.Doi.Org/10.1517/14712598.3.1.23*, *3*(1), 23–44. https://doi.org/10.1517/14712598.3.1.23

Di Tommaso, C., Bourges, J. L., Valamanesh, F., Trubitsyn, G., Torriglia, A., Jeanny, J. C., Behar-Cohen, F., Gurny, R., & Möller, M. (2012). Novel micelle carriers for cyclosporin A topical ocular delivery: In vivo cornea penetration, ocular distribution and efficacy studies. *European Journal of Pharmaceutics and Biopharmaceutics*, *81*(2), 257–264. https://doi.org/10.1016/J.EJPB.2012.02.014

Doi, R., & Kokufuta, E. (2011). Conductometric and light scattering studies on the complexation between cationic polyelectrolyte nanogel and anionic polyion. *Langmuir*, *27*(1), 392–398. https://doi.org/10.1021/LA1037519/ASSET/IMAGES/LARGE/LA-2010-037519_0007.JPEG

Drlica, K. (1999). Mechanism of fluoroquinolone action. *Current Opinion in Microbiology*, *2*(5), 504–508. https://doi.org/10.1016/S1369-5274(99)00008-9

Drlica, K., Malik, M., Kerns, R. J., & Zhao, X. (2008). Quinolone-mediated bacterial death. *Antimicrobial Agents and Chemotherapy*, *52*(2), 385–392. https://doi.org/10.1128/AAC.01617-06/ASSET/29A4C7CD-1B60-4DA8-AB19-85C98F706AD2/ASSETS/GRAPHIC/ZAC0020870530004.JPEG

Duane's ophthalmology | WorldCat.org. (n.d.). Retrieved April 20, 2023, from https://www.worldcat.org/title/duanes-ophthalmology/oclc/316126138

Dubashynskaya, N., Poshina, D., Raik, S., Urtti, A., & Skorik, Y. A. (2019). Polysaccharides in Ocular Drug Delivery. *Pharmaceutics 2020, Vol. 12, Page 22*, *12*(1), 22. https://doi.org/10.3390/PHARMACEUTICS12010022

Durand, M. L., Barshak, M. B., & Chodosh, J. (2021). Infectious Keratitis in 2021. *JAMA*, *326*(13), 1319–1320. https://doi.org/10.1001/JAMA.2021.0424

Egrilmez, S., & Yildirim-Theveny, Ş. (2020a). Treatment-Resistant Bacterial Keratitis: Challenges and Solutions . *Clinical Ophthalmology*, *14*, 287–297. https://doi.org/10.2147/OPTH.S181997

Egrilmez, S., & Yildirim-Theveny, Ş. (2020b). Treatment-Resistant Bacterial Keratitis: Challenges and Solutions. *Clinical Ophthalmology (Auckland, N.Z.)*, *14*, 287. https://doi.org/10.2147/OPTH.S181997

Egrilmez, S., & Yildirim-Theveny, Ş. (2020c). Treatment-Resistant Bacterial Keratitis: Challenges and Solutions. *Clinical Ophthalmology (Auckland, N.Z.)*, *14*, 287. https://doi.org/10.2147/OPTH.S181997

Egrilmez, S., & Yildirim-Theveny, Ş. (2020d). Treatment-resistant bacterial keratitis: Challenges and solutions. In *Clinical Ophthalmology* (Vol. 14, pp. 287–297). Dove Medical Press Ltd. https://doi.org/10.2147/OPTH.S181997

Elsayed, I., & Sayed, S. (2017). Tailored nanostructured platforms for boosting transcorneal permeation: Box–Behnken statistical optimization, comprehensive in vitro, ex vivo and in vivo characterization. *International Journal of Nanomedicine*, *12*, 7947–7962. https://doi.org/10.2147/IJN.S150366

Eltis, M. (2011). Contact-lens-related microbial keratitis: Case report and review. *Journal of Optometry*, *4*(4), 122–127. https://doi.org/10.1016/S1888-4296(11)70053-X

Ezisi, C. N., Ogbonnaya, C. E., Okoye, O., Ezeanosike, E., Ginger-Eke, H., & Arinze, O. C. (2018a). Microbial keratitis—A review of epidemiology, pathogenesis, ocular manifestations, and management. *Nigerian Journal of Ophthalmology*, *26*(1), 13. https://doi.org/10.4103/NJO.NJO_2_18

Ezisi, C. N., Ogbonnaya, C. E., Okoye, O., Ezeanosike, E., Ginger-Eke, H., & Arinze, O. C. (2018b). Microbial keratitis—A review of epidemiology, pathogenesis, ocular manifestations, and management. *Nigerian Journal of Ophthalmology*, *26*(1), 13. https://doi.org/10.4103/NJO.NJO_2_18

Ezisi, C., Ogbonnaya, C., Okoye, O., Ezeanosike, E., Ginger-Eke, H., & Arinze, O. (2018). Microbial keratitis—A review of epidemiology, pathogenesis, ocular manifestations, and management. *Nigerian Journal of Ophthalmology*, *26*(1), 13–23. https://doi.org/10.4103/njo.njo_2_18

Felt, O., Carrel, A., Baehni, P., Buri, P., & Gurny, R. (2000). Chitosan as tear substitute: a wetting agent endowed with antimicrobial efficacy. *Journal of Ocular Pharmacology and*

Therapeutics : The Official Journal of the Association for Ocular Pharmacology and Therapeutics, *16*(3), 261–270. https://doi.org/10.1089/JOP.2000.16.261

Felt, O., Furrer, P., Mayer, J. M., Plazonnet, B., Buri, P., & Gurny, R. (1999). Topical use of chitosan in ophthalmology: Tolerance assessment and evaluation of precorneal retention. *International Journal of Pharmaceutics*, *180*(2), 185–193. https://doi.org/10.1016/S0378-5173(99)00003-4

Fischer, S. M., Brandl, M., & Fricker, G. (2011). Effect of the non-ionic surfactant Poloxamer 188 on passive permeability of poorly soluble drugs across Caco-2 cell monolayers. *European Journal of Pharmaceutics and Biopharmaceutics*, *79*(2), 416–422. https://doi.org/https://doi.org/10.1016/j.ejpb.2011.04.010

Fisher, L. M., Heaton, V. J., Smith, H. J., Nichol, K. A., Hoban, D. J., & Zhanel, G. G. (2003). Dual activity of fluoroquinolones against Streptococcus pneumoniae. *Journal of Antimicrobial Chemotherapy*, *51*(2), 463–464. https://doi.org/10.1093/JAC/DKG059

Flaxman, S. R., Bourne, R. R. A., Resnikoff, S., Ackland, P., Braithwaite, T., Cicinelli, M. V., Das, A., Jonas, J. B., Keeffe, J., Kempen, J., Leasher, J., Limburg, H., Naidoo, K., Pesudovs, K., Silvester, A., Stevens, G. A., Tahhan, N., Wong, T., Taylor, H., … Zheng, Y. (2017). Global causes of blindness and distance vision impairment 1990-2020: a systematic review and meta-analysis. *The Lancet. Global Health*, *5*(12), e1221–e1234. https://doi.org/10.1016/S2214-109X(17)30393-5

Fleiszig, S. M. J. (2006). The Glenn A. Fry award lecture 2005. The pathogenesis of contact lens-related keratitis. *Optometry and Vision Science : Official Publication of the American Academy of Optometry*, *83*(12), 866–873.

Fleiszig, S. M. J., & Evans, D. J. (2021a). The pathogenesis of bacterial keratitis: studies with Pseudomonas aeruginosa. *Https://Doi.Org/10.1111/j.1444-0938.2002.Tb03082.x*, *85*(5), 271–278. https://doi.org/10.1111/J.1444-0938.2002.TB03082.X

Fleiszig, S. M. J., & Evans, D. J. (2021b). The pathogenesis of bacterial keratitis: studies with Pseudomonas aeruginosa. *Https://Doi.Org/10.1111/j.1444-0938.2002.Tb03082.x*, *85*(5), 271–278. https://doi.org/10.1111/J.1444-0938.2002.TB03082.X

Fleiszig, S. M. J., Kroken, A. R., Nieto, V., Grosser, M. R., Wan, S. J., Metruccio, M. M. E., & Evans, D. J. (2020a). Contact lens-related corneal infection: Intrinsic resistance and its compromise. *Progress in Retinal and Eye Research*, *76*. https://doi.org/10.1016/J.PRETEYERES.2019.100804

Fleiszig, S. M. J., Kroken, A. R., Nieto, V., Grosser, M. R., Wan, S. J., Metruccio, M. M. E., & Evans, D. J. (2020b). Contact lens-related corneal infection: Intrinsic resistance and its compromise. *Progress in Retinal and Eye Research*, *76*. https://doi.org/10.1016/J.PRETEYERES.2019.100804

Fleiszig, S. M. J., Kroken, A. R., Nieto, V., Grosser, M. R., Wan, S. J., Metruccio, M. M. E., & Evans, D. J. (2020c). Contact lens-related corneal infection: Intrinsic resistance and its compromise. *Progress in Retinal and Eye Research*, *76*, 100804. https://doi.org/https://doi.org/10.1016/j.preteyeres.2019.100804

Fleiszig, S. M. J., Zaidi, T. S., Ramphal, R., & Pier, G. B. (1994). Modulation of Pseudomonas aeruginosa adherence to the corneal surface by mucus. *Infection and Immunity*, *62*(5), 1799–1804. https://doi.org/10.1128/IAI.62.5.1799-1804.1994

Flemming, H. C., & Wingender, J. (2001). Relevance of microbial extracellular polymeric substances (EPSs) - Part I: Structural and ecological aspects. *Water Science and Technology*, *43*(6), 1–8. https://doi.org/10.2166/WST.2001.0326

Foster, T. J. (2019). Surface Proteins of Staphylococcus aureus . *Microbiology Spectrum*, *7*(4). https://doi.org/10.1128/MICROBIOLSPEC.GPP3-0046-2018/ASSET/82D9CB60-20B2-4F6D-A329-CFC343963396/ASSETS/GRAPHIC/GPP3-0046-2018-FIG9.GIF

Friess, W. (1998). Collagen – biomaterial for drug delivery. *European Journal of Pharmaceutics and Biopharmaceutics*, *45*(2), 113–136. https://doi.org/10.1016/S0939-6411(98)00017-4

Gade, S. K., Nirmal, J., Garg, P., & Venuganti, V. V. K. (2020). Corneal delivery of moxifloxacin and dexamethasone combination using drug-eluting mucoadhesive contact lens to treat ocular infections. *International Journal of Pharmaceutics*, *591*, 120023. https://doi.org/https://doi.org/10.1016/j.ijpharm.2020.120023

Gangopadhyay, N., Daniell, M., Weih, L., & Taylor, H. R. (2000). Fluoroquinolone and fortified antibiotics for treating bacterial corneal ulcers. *British Journal of Ophthalmology*, *84*(4), 378. https://doi.org/10.1136/bjo.84.4.378

Gaudana, R., Ananthula, H. K., Parenky, A., & Mitra, A. K. (2010). Ocular drug delivery. *The AAPS Journal*, *12*(3), 348–360. https://doi.org/10.1208/S12248-010-9183-3

Gaudana, R., Jwala, J., Boddu, S. H. S., & Mitra, A. K. (2009). Recent perspectives in ocular drug delivery. *Pharmaceutical Research*, *26*(5), 1197–1216. https://doi.org/10.1007/S11095-008-9694-0

Ghezzi, M., Pescina, S., Padula, C., Santi, P., Del Favero, E., Cantù, L., & Nicoli, S. (2021). Polymeric micelles in drug delivery: An insight of the techniques for their characterization and assessment in biorelevant conditions. *Journal of Controlled Release : Official Journal of the Controlled Release Society*, *332*, 312–336. https://doi.org/10.1016/J.JCONREL.2021.02.031

Ghilini, F., Pissinis, D. E., Miñán, A., Schilardi, P. L., & Diaz, C. (2019). How Functionalized Surfaces Can Inhibit Bacterial Adhesion and Viability. *ACS Biomaterials Science and Engineering*, *5*(10), 4920–4936. https://doi.org/10.1021/ACSBIOMATERIALS.9B00849/ASSET/IMAGES/LARGE/AB9B00849_0009.JPEG

Gipson, I. K., & Argüeso, P. (2003). Role of Mucins in the Function of the Corneal and Conjunctival Epithelia. *International Review of Cytology*, *231*, 1–49. https://doi.org/10.1016/S0074-7696(03)31001-0

Giuliano, E., Paolino, D., Fresta, M., & Cosco, D. (2018). Mucosal applications of poloxamer 407-based hydrogels: An overview. *Pharmaceutics*, *10*(3), 1–26. https://doi.org/10.3390/pharmaceutics10030159

Goldstein, M. H., Kowalski, R. P., & Gordon, Y. J. (1999a). Emerging fluoroquinolone resistance in bacterial keratitis: a 5-year review. *Ophthalmology*, *106*(7), 1213–1318.

Goldstein, M. H., Kowalski, R. P., & Gordon, Y. J. (1999b). Emerging fluoroquinolone resistance in bacterial keratitis: A 5-year review. *Ophthalmology*, *106*(7), 1213–1318. https://doi.org/10.1016/S0161-6420(99)00716-2

Goy, R. C., Morais, S. T. B., & Assis, O. B. G. (2016). Evaluation of the antimicrobial activity of chitosan and its quaternized derivative on E. Coli and S. aureus growth. *Revista Brasileira de Farmacognosia*, *26*(1), 122–127. https://doi.org/10.1016/j.bjp.2015.09.010

Grandi, G., Bianco, G., Boattini, M., Scalabrin, S., Iannaccone, M., Fea, A., Cavallo, R., & Costa, C. (2019). Bacterial etiology and antimicrobial resistance trends in ocular infections: A 30-year study, Turin area, Italy. *Https://Doi.Org/10.1177/1120672119896419*, *31*(2), 405–414. https://doi.org/10.1177/1120672119896419

Grassiri, B., Zambito, Y., & Bernkop-Schnürch, A. (2021). Strategies to prolong the residence time of drug delivery systems on ocular surface. *Advances in Colloid and Interface Science*, *288*, 102342. https://doi.org/10.1016/J.CIS.2020.102342

Gratieri, T., Gelfuso, G. M., Rocha, E. M., Sarmento, V. H., de Freitas, O., & Lopez, R. F. V. (2010). A poloxamer/chitosan in situ forming gel with prolonged retention time for ocular delivery. *European Journal of Pharmaceutics and Biopharmaceutics*, *75*(2), 186–193. https://doi.org/https://doi.org/10.1016/j.ejpb.2010.02.011

Greaves, J. L., & Wilson, C. G. (1993a). Treatment of diseases of the eye with mucoadhesive delivery systems. *Advanced Drug Delivery Reviews*, *11*(3), 349–383. https://doi.org/10.1016/0169-409X(93)90016-W

Greaves, J. L., & Wilson, C. G. (1993b). Treatment of diseases of the eye with mucoadhesive delivery systems. *Advanced Drug Delivery Reviews*, *11*(3), 349–383. https://doi.org/10.1016/0169-409X(93)90016-W

Grimes, M. R., Scardino, M. A., & Martone, J. F. (1992). Worldwide blindness. *Nursing Clinics of North America*, *27*(3), 807–816. https://doi.org/10.1016/s0029-6465(22)02806-7

Grinninger, P., Verbruggen, A. M. J., Kraijer-Huver, I. M. G., Djajadiningrat-Laanen, S. C., Teske, E., & Boevé, M. H. (2015). Use of bandage contact lenses for treatment of spontaneous chronic corneal epithelial defects in dogs. *Journal of Small Animal Practice*, *56*(7), 446–449. https://doi.org/https://doi.org/10.1111/jsap.12360

Gulsen, D., & Chauhan, A. (2005). Dispersion of microemulsion drops in HEMA hydrogel: a potential ophthalmic drug delivery vehicle. *International Journal of Pharmaceutics*, *292*(1), 95–117. https://doi.org/https://doi.org/10.1016/j.ijpharm.2004.11.033

Han, H., Gao, Y., Chai, M., Zhang, X., Liu, S., Huang, Y., Jin, Q., Grzybowski, A., Ji, J., & Yao, K. (2020a). Biofilm microenvironment activated supramolecular nanoparticles for enhanced photodynamic therapy of bacterial keratitis. *Journal of Controlled Release*, *327*(May), 676–687. https://doi.org/10.1016/j.jconrel.2020.09.014

Han, H., Gao, Y., Chai, M., Zhang, X., Liu, S., Huang, Y., Jin, Q., Grzybowski, A., Ji, J., & Yao, K. (2020b). Biofilm microenvironment activated supramolecular nanoparticles for

enhanced photodynamic therapy of bacterial keratitis. *Journal of Controlled Release*, *327*(May), 676–687. https://doi.org/10.1016/j.jconrel.2020.09.014

Hanet, M. S., Jamart, J., & Chaves, A. P. (2012a). Fluoroquinolones or fortified antibiotics for treating bacterial keratitis: Systematic review and meta-analysis of comparative studies. *Canadian Journal of Ophthalmology*, *47*(6), 493–499. https://doi.org/10.1016/j.jcjo.2012.09.001

Hanet, M. S., Jamart, J., & Chaves, A. P. (2012b). Fluoroquinolones or fortified antibiotics for treating bacterial keratitis: Systematic review and meta-analysis of comparative studies. *Canadian Journal of Ophthalmology*, *47*(6), 493–499. https://doi.org/10.1016/j.jcjo.2012.09.001

Hanet, M.-S., Jamart, J., & Chaves, A. P. (2012). Fluoroquinolones or fortified antibiotics for treating bacterial keratitis: systematic review and meta-analysis of comparative studies. *Canadian Journal of Ophthalmology. Journal Canadien d'ophtalmologie*, *47*(6), 493–499. https://doi.org/10.1016/j.jcjo.2012.09.001

Haq, M. A., Su, Y., & Wang, D. (2016). Mechanical properties of PNIPAM based hydrogels: A review. *Materials Science & Engineering. C, Materials for Biological Applications*, *70*(Pt 1), 842–855. https://doi.org/10.1016/J.MSEC.2016.09.081

Hassan, E. E., & Gallo, J. M. (1990). A simple rheological method for the in vitro assessment of mucin-polymer bioadhesive bond strength. *Pharmaceutical Research*, *7*(5), 491–495. https://doi.org/10.1023/A:1015812615635

Henderson, E., Lee, B. H., Cui, Z., McLemore, R., Brandon, T. A., & Vernon, B. L. (2009). In vivo evaluation of injectable thermosensitive polymer with time-dependent LCST. *Journal of Biomedical Materials Research - Part A*, *90*(4), 1186–1197. https://doi.org/10.1002/jbm.a.32179

Hillery, A. M., Lloyd, A. W., & Swarbrick, J. (Eds.). (2016). *Drug Delivery and Targeting : For Pharmacists and Pharmaceutical Scientists*. https://doi.org/10.1201/B12801

Hilliam, Y., Kaye, S., & Winstanley, C. (2020). Pseudomonas aeruginosa and microbial keratitis. *Journal of Medical Microbiology*, *69*(1), 3–13. https://doi.org/10.1099/jmm.0.001110

Hosoya, K. I., Lee, V. H. L., & Kim, K. J. (2005). Roles of the conjunctiva in ocular drug delivery: a review of conjunctival transport mechanisms and their regulation. *European Journal of Pharmaceutics and Biopharmaceutics*, *60*(2), 227–240. https://doi.org/10.1016/J.EJPB.2004.12.007

Hot Topics in Bacterial Keratitis. (n.d.). Retrieved April 20, 2023, from https://www.reviewofcontactlenses.com/article/hot-topics-in-bacterial-keratitis

Hsiao, C. H., Sun, C. C., Yeh, L. K., Ma, D. K. H., Chen, P. Y. F., Lin, H. C., Tan, H. Y., Chen, H. C., Chen, S. Y., & Huang, Y. C. (2016). Shifting trends in bacterial keratitis in Taiwan: A 10-year review in a tertiary-care hospital. *Cornea*, *35*(3), 313–317. https://doi.org/10.1097/ICO.0000000000000734

Huang, A. J., Tseng, S. C., & Kenyon, K. R. (1989). Paracellular permeability of corneal and conjunctival epithelia. *Investigative Ophthalmology & Visual Science*, *30*(4), 684–689.

Hui, H. W., & Robinson, J. R. (1985). Ocular delivery of progesterone using a bioadhesive polymer. *International Journal of Pharmaceutics*, *26*(3), 203–213. https://doi.org/10.1016/0378-5173(85)90230-3

Ideta, R., Yanagi, Y., Tamaki, Y., Tasaka, F., Harada, A., & Kataoka, K. (2004). Effective accumulation of polyion complex micelle to experimental choroidal neovascularization in rats. *FEBS Letters*, *557*(1–3), 21–25. https://doi.org/10.1016/S0014-5793(03)01315-2

Inatomi, T., Spurr-Michaud, S., Tisdale, A. S., Zhan, Q., Feldman, S. T., & Gipson, I. K. (1996). Expression of secretory mucin genes by human conjunctival epithelia. *Investigative Ophthalmology & Visual Science*, *37*(8), 1684–1692.

Itoo, A. M., Paul, M., Ghosh, B., & Biswas, S. (2022a). Oxaliplatin delivery via chitosan/vitamin E conjugate micelles for improved efficacy and MDR-reversal in breast cancer. *Carbohydrate Polymers*, *282*, 119108. https://doi.org/https://doi.org/10.1016/j.carbpol.2022.119108

Itoo, A. M., Paul, M., Ghosh, B., & Biswas, S. (2022b). Oxaliplatin delivery via chitosan/vitamin E conjugate micelles for improved efficacy and MDR-reversal in breast cancer. *Carbohydrate Polymers*, *282*, 119108. https://doi.org/10.1016/J.CARBPOL.2022.119108

Jain, M. R. (1988). Drug delivery through soft contact lenses. *British Journal of Ophthalmology*, *72*(2), 150–154. https://doi.org/10.1136/BJO.72.2.150

Jalaja, K., Naskar, D., Kundu, S. C., & James, N. R. (2015). Fabrication of cationized gelatin nanofibers by electrospinning for tissue regeneration. *RSC Advances*, *5*(109), 89521–89530. https://doi.org/10.1039/C5RA10384C

Jeon, K. W. (2003). *International review of cytology. Volume 223 : a survey of cell biology*. https://books.google.com/books/about/International_Review_of_Cytology.html?id=777IETh2LNsC

Jeong, B., Bae, Y. H., Lee, D. S., & Kim, S. W. (1997). Biodegradable block copolymers as injectable drug-delivery systems. *Nature 1997 388:6645*, *388*(6645), 860–862. https://doi.org/10.1038/42218

Jett, B. D., & Gilmore, M. S. (2002). Host-parasite interactions in Staphylococcus aureus keratitis. *DNA and Cell Biology*, *21*(5–6), 397–404. https://doi.org/10.1089/10445490260099683

Jian, H. J., Wu, R. S., Lin, T. Y., Li, Y. J., Lin, H. J., Harroun, S. G., Lai, J. Y., & Huang, C. C. (2017). Super-Cationic Carbon Quantum Dots Synthesized from Spermidine as an Eye Drop Formulation for Topical Treatment of Bacterial Keratitis. *ACS Nano*, *11*(7), 6703–6716. https://doi.org/10.1021/acsnano.7b01023

Jones, D. B. (1981a). Decision-making in the Management of Microbial Keratitis. *Ophthalmology*, *88*(8), 814–820. https://doi.org/https://doi.org/10.1016/S0161-6420(81)34943-4

Jones, D. B. (1981b). Decision-making in the Management of Microbial Keratitis. *Ophthalmology*, *88*(8), 814–820. https://doi.org/10.1016/S0161-6420(81)34943-4

Joshi, P., Ahmed, M. S. U., Vig, K., Vega Erramuspe, I. B., & Auad, M. L. (2021). Synthesis and characterization of chemically crosslinked gelatin and chitosan to produce hydrogels for biomedical applications. *Polymers for Advanced Technologies*, *32*(5), 2229–2239. https://doi.org/https://doi.org/10.1002/pat.5257

Joshi, S. C., & Lam, Y. C. (2006). Modeling heat and degree of gelation for methyl cellulose hydrogels with NaCl additives. *Journal of Applied Polymer Science*, *101*(3), 1620–1629. https://doi.org/10.1002/APP.23565

Jung, H. J., Abou-Jaoude, M., Carbia, B. E., Plummer, C., & Chauhan, A. (2013a). Glaucoma therapy by extended release of timolol from nanoparticle loaded silicone-hydrogel contact lenses. *Journal of Controlled Release*, *165*(1), 82–89. https://doi.org/https://doi.org/10.1016/j.jconrel.2012.10.010

Jung, H. J., Abou-Jaoude, M., Carbia, B. E., Plummer, C., & Chauhan, A. (2013b). Glaucoma therapy by extended release of timolol from nanoparticle loaded silicone-hydrogel contact lenses. *Journal of Controlled Release*, *165*(1), 82–89. https://doi.org/https://doi.org/10.1016/j.jconrel.2012.10.010

Jung, J., Bae, Y., Kwan Cho, Y., Ren, X., & Sun, Y. (2020). Structural insights into conformation of amphiphilic quaternary ammonium chitosans to control fungicidal and anti-biofilm functions. *Carbohydrate Polymers*, *228*(September 2019), 115391. https://doi.org/10.1016/j.carbpol.2019.115391

Kakisu, K., Matsunaga, T., Kobayakawa, S., Sato, T., & Tochikubo, T. (2013). Development and Efficacy of a Drug-Releasing Soft Contact Lens. *Investigative Ophthalmology & Visual Science*, *54*(4), 2551–2561. https://doi.org/10.1167/iovs.12-10614

Karatas, A., Boluk, A., & Algan, H. A. (2014). Poloxamer/Chitosan In Situ Gelling System for Ocular Delivery of Ofloxacin. In *Current Drug Therapy* (Vol. 9, Issue 4, pp. 219–225). https://doi.org/http://dx.doi.org/10.2174/15748855109991505051715 15

Karp, C. L., Tuli, S. S., Yoo, S. H., Vroman, D. T., Alfonso, E. C., Huang, A. H., Pflugfelder, S. C., & Culbertson, W. W. (2003). Infectious keratitis after LASIK. *Ophthalmology*, *110*(3), 503–510. https://doi.org/10.1016/S0161-6420(02)01760-8

Katragadda, S., Gunda, S., Hariharan, S., & Mitra, A. K. (2008). Ocular Pharmacokinetics of Acyclovir Amino Acid Ester Prodrugs in the Anterior Chamber: Evaluation of Their Utility in Treating Ocular HSV Infections. *International Journal of Pharmaceutics*, *359*(1–2), 15. https://doi.org/10.1016/J.IJPHARM.2008.03.015

Kaur, N., Mathur, P., Yadav, P., Chakraborty, S., & Shanavas, A. (2020). Glycol chitosan in situ coating on PLGA nanoparticle curtails extraneous paclitaxel precipitates and imparts protein corona independent hemocompatibility. *Carbohydrate Polymers*, *237*, 116170. https://doi.org/https://doi.org/10.1016/j.carbpol.2020.116170

Kedar, U., Phutane, P., Shidhaye, S., & Kadam, V. (2010). Advances in polymeric micelles for drug delivery and tumor targeting. *Nanomedicine: Nanotechnology, Biology, and Medicine*, *6*(6), 714–729. https://doi.org/10.1016/J.NANO.2010.05.005

Keratitis, M., Keratitis, P. U., & Hamrah, P. (2000). Twenty-five – Year Panorama of Corneal Immunology Emerging Concepts in the Immunopathogenesis of. *Cornea*, *19*(5), 625–643.

Keratitis: Types, Symptoms & Treatment. (n.d.). Retrieved July 4, 2023, from https://my.clevelandclinic.org/health/diseases/24500-keratitis

Khalili, M., Asadi, M., Kahroba, H., Soleyman, M. R., Andre, H., & Alizadeh, E. (2021). Corneal endothelium tissue engineering: An evolution of signaling molecules, cells, and scaffolds toward 3D bioprinting and cell sheets. *Journal of Cellular Physiology*, *236*(5), 3275–3303. https://doi.org/10.1002/JCP.30085

Khanvilkar, K., Donovan, M. D., & Flanagan, D. R. (2001). Drug transfer through mucus. *Advanced Drug Delivery Reviews*, *48*(2–3), 173–193. https://doi.org/10.1016/S0169-409X(01)00115-6

Khiev, D., Mohamed, Z. A., Vichare, R., Paulson, R., Bhatia, S., Mohapatra, S., Lobo, G. P., Valapala, M., Kerur, N., Passaglia, C. L., Mohapatra, S. S., & Biswal, M. R. (2021). Emerging Nano-Formulations and Nanomedicines Applications for Ocular Drug Delivery. *Nanomaterials 2021, Vol. 11, Page 173*, *11*(1), 173. https://doi.org/10.3390/NANO11010173

Khutoryanskiy, V. V. (2011). Advances in Mucoadhesion and Mucoadhesive Polymers. *Macromolecular Bioscience*, *11*(6), 748–764. https://doi.org/10.1002/MABI.201000388

KING, D. E., MALONE, R., & LILLEY, S. H. (2000). New Classification and Update on the Quinolone Antibiotics. *American Family Physician*, *61*(9), 2741–2748. https://www.aafp.org/pubs/afp/issues/2000/0501/p2741.html

Kopeĉek, J. (2009). HYDROGELS FROM SOFT CONTACT LENSES AND IMPLANTS TO SELF-ASSEMBLED NANOMATERIALS. *Journal of Polymer Science. Part A, Polymer Chemistry*, *47*(22), 5929. https://doi.org/10.1002/POLA.23607

Kumari, P., Paul, M., Bhatt, H., Vishnu, S., Rompicharla, K., Sarkar, D., Ghosh, B., & Biswas, S. (2020). *Chlorin e6 Conjugated Methoxy-Poly (Ethylene Glycol) - Po l y (D , L-L a c t i d e) G l u t a t h i o n e S e n s i t i v e M i c e l l e s for Photodynamic Therapy*.

Kumari, P., Paul, M., Bobde, Y., Soniya, K., Kiran Rompicharla, S. V., Ghosh, B., & Biswas, S. (2020). Albumin-based lipoprotein nanoparticles for improved delivery and anticancer activity of curcumin for cancer treatment. *Nanomedicine*, *15*(29), 2851–2869. https://doi.org/10.2217/nnm-2020-0232

Kumbham, S., Paul, M., Bhatt, H., Ghosh, B., & Biswas, S. (2020). Oleanolic acid-conjugated poly (D, L-lactide)-based micelles for effective delivery of doxorubicin and combination chemotherapy in oral cancer. *Journal of Molecular Liquids*, *320*, 114389. https://doi.org/10.1016/j.molliq.2020.114389

Kumbham, S., Paul, M., Itoo, A., Ghosh, B., & Biswas, S. (2022). Oleanolic acid-conjugated human serum albumin nanoparticles encapsulating doxorubicin as synergistic combination chemotherapy in oropharyngeal carcinoma and melanoma. *International Journal of Pharmaceutics*, *614*, 121479. https://doi.org/10.1016/J.IJPHARM.2022.121479

Lakhundi, S., Siddiqui, R., & Khan, N. A. (2017). Pathogenesis of microbial keratitis. *Microbial Pathogenesis*, *104*, 97–109. https://doi.org/10.1016/J.MICPATH.2016.12.013

Lam, H. T., Zupančič, O., Laffleur, F., & Bernkop-Schnürch, A. (2021). Mucoadhesive properties of polyacrylates: Structure – Function relationship. *International Journal of Adhesion and Adhesives*, *107*, 102857. https://doi.org/10.1016/J.IJADHADH.2021.102857

Laulicht, B., Mancini, A., Geman, N., Cho, D., Estrellas, K., Furtado, S., Hopson, R., Tripathi, A., & Mathiowitz, E. (2012a). Bioinspired Bioadhesive Polymers: Dopa-Modified Poly(acrylic acid) Derivatives. *Macromolecular Bioscience*, *12*(11), 1555–1565. https://doi.org/10.1002/mabi.201200179

Laulicht, B., Mancini, A., Geman, N., Cho, D., Estrellas, K., Furtado, S., Hopson, R., Tripathi, A., & Mathiowitz, E. (2012b). Bioinspired Bioadhesive Polymers: Dopa-Modified Poly(acrylic acid) Derivatives. *Macromolecular Bioscience*, *12*(11), 1555–1565. https://doi.org/10.1002/mabi.201200179

Laurent, T. C. (1987). Biochemistry of hyaluronan. *Acta Oto-Laryngologica. Supplementum*, *442*(S442), 7–24. https://doi.org/10.3109/00016488709102833

Le Bourlais, C. A., Treupel-Acar, L., Rhodes, C. T., Sado, P. A., & Leverge, R. (2008). New Ophthalmic Drug Delivery Systems. *Http://Dx.Doi.Org/10.3109/03639049509048095*, *21*(1), 19–59. https://doi.org/10.3109/03639049509048095

Le Bourlais, C., Acar, L., Zia, H., Sado, P. A., Needham, T., & Leverge, R. (1998). Ophthalmic drug delivery systems - Recent advances. *Progress in Retinal and Eye Research*, *17*(1), 33–58. https://doi.org/10.1016/S1350-9462(97)00002-5

Lee, J. M., Suen, S. K. Q., Ng, W. L., Ma, W. C., & Yeong, W. Y. (2021). Bioprinting of Collagen: Considerations, Potentials, and Applications. *Macromolecular Bioscience*, *21*(1), 2000280. https://doi.org/10.1002/MABI.202000280

Lee, K. C., & Choo, H. S. (2014). Preparation of poly(BMA-co-MMA) particles by soap-free emulsion polymerization and its optical properties as photonic crystals. *Journal of Nanoscience and Nanotechnology*, *14*(11), 8279–8287. https://doi.org/10.1166/JNN.2014.9912

Lee, V. H. L., & Robinson, J. R. (1986a). Topical ocular drug delivery: recent developments and future challenges. *Journal of Ocular Pharmacology*, *2*(1), 67–108. https://doi.org/10.1089/JOP.1986.2.67

Lee, V. H. L., & Robinson, J. R. (1986b). Topical Ocular Drug Delivery: Recent Developments and Future Challenges. *Journal of Ocular Pharmacology*, *2*(1), 67–108. https://doi.org/10.1089/JOP.1986.2.67

Lehr, C. M., Bouwstra, J. A., Schacht, E. H., & Junginger, H. E. (1992). In vitro evaluation of mucoadhesive properties of chitosan and some other natural polymers. *International Journal of Pharmaceutics*, *78*(1–3), 43–48. https://doi.org/10.1016/0378-5173(92)90353-4

Leonardi, A., & Secchi, A. G. (2003). Vernal keratoconjunctivitis. *International Ophthalmology Clinics*, *43*(1), 41–58. https://doi.org/10.1097/00004397-200343010-00007

Levitt, A. E., Galor, A., Weiss, J. S., Felix, E. R., Martin, E. R., Patin, D. J., Sarantopoulos, K. D., & Levitt, R. C. (2015). Chronic dry eye symptoms after LASIK: Parallels and lessons to be learned from other persistent post-operative pain disorders. *Molecular Pain*, *11*(1), 1–12. https://doi.org/10.1186/s12990-015-0020-7

Li, C. C., & Chauhan, A. (2006). Modeling ophthalmic drug delivery by soaked contact lenses. *Industrial and Engineering Chemistry Research*, *45*(10), 3718–3734. https://doi.org/10.1021/IE0507934/ASSET/IMAGES/MEDIUM/IE0507934E00075.GIF

Li, J., & Zhuang, S. (2020). Antibacterial activity of chitosan and its derivatives and their interaction mechanism with bacteria: Current state and perspectives. *European Polymer Journal*, *138*, 109984. https://doi.org/10.1016/J.EURPOLYMJ.2020.109984

Li, L., Liang, N., Wang, D., Yan, P., Kawashima, Y., Cui, F., & Sun, S. (2018). Amphiphilic Polymeric Micelles Based on Deoxycholic Acid and Folic Acid Modified Chitosan for the Delivery of Paclitaxel. In *International Journal of Molecular Sciences* (Vol. 19, Issue 10). https://doi.org/10.3390/ijms19103132

Li, L.-H., Deng, J.-C., Deng, H.-R., Liu, Z.-L., & Li, X.-L. (2010). Preparation, characterization and antimicrobial activities of chitosan/Ag/ZnO blend films. *Chemical Engineering Journal*, *160*(1), 378–382. https://doi.org/https://doi.org/10.1016/j.cej.2010.03.051

Li, Y., Jia, H., Cheng, Q., Pan, F., & Jiang, Z. (2011). Sodium alginate–gelatin polyelectrolyte complex membranes with both high water vapor permeance and high permselectivity. *Journal of Membrane Science*, *375*(1–2), 304–312. https://doi.org/10.1016/J.MEMSCI.2011.03.058

Li, Y., Rodrigues, J., & Tomás, H. (2012). Injectable and biodegradable hydrogels: gelation, biodegradation and biomedical applications. *Chemical Society Reviews*, *41*(6), 2193–2221. https://doi.org/10.1039/C1CS15203C

Lillehoj, E. P., Hyun, S. W., Kim, B. T., Zhang, X. G., Lee, D. I., Rowland, S., & Kim, K. C. (2001a). Muc1 mucins on the cell surface are adhesion sites for Pseudomonas aeruginosa. *American Journal of Physiology - Lung Cellular and Molecular Physiology*, *280*(1 24-1). https://doi.org/10.1152/AJPLUNG.2001.280.1.L181/ASSET/IMAGES/LARGE/H5011023 3006.JPEG

Lillehoj, E. P., Hyun, S. W., Kim, B. T., Zhang, X. G., Lee, D. I., Rowland, S., & Kim, K. C. (2001b). Muc1 mucins on the cell surface are adhesion sites for Pseudomonas aeruginosa. *American Journal of Physiology - Lung Cellular and Molecular Physiology*, *280*(1 24-1). https://doi.org/10.1152/AJPLUNG.2001.280.1.L181/ASSET/IMAGES/LARGE/H5011023 3006.JPEG

Lim, C. H. L., Carnt, N. A., Farook, M., Lam, J., Tan, D. T., Mehta, J. S., & Stapleton, F. (2016). Risk factors for contact lens-related microbial keratitis in Singapore. *Eye*, *30*(3), 447–455. https://doi.org/10.1038/eye.2015.250

Limberg, M. B. (1991). A review of bacterial keratitis and bacterial conjunctivitis. *American Journal of Ophthalmology*, *112*(4 Suppl), 2S-9S. https://europepmc.org/article/med/1928269

Lin, D., Lei, L., Shi, S., Li, X., Lin, D., Lei, L., Shi, S., & Li, X. (2019). Stimulus-Responsive Hydrogel for Ophthalmic Drug Delivery. *Macromolecular Bioscience*, *19*(6), 1900001. https://doi.org/10.1002/MABI.201900001

Lin, H. Y., Wang, S. W., Mao, J. Y., Chang, H. T., Harroun, S. G., Lin, H. J., Huang, C. C., & Lai, J. Y. (2021). Carbonized nanogels for simultaneous antibacterial and antioxidant treatment of bacterial keratitis. *Chemical Engineering Journal*, *411*(October 2020), 128469. https://doi.org/10.1016/j.cej.2021.128469

Liu, Y., Shi, L., Su, L., Van der Mei, H. C., Jutte, P. C., Ren, Y., & Busscher, H. J. (2019). Nanotechnology-based antimicrobials and delivery systems for biofilm-infection control. *Chemical Society Reviews*, *48*(2), 428–446. https://doi.org/10.1039/C7CS00807D

Lu, Y., & Park, K. (2013). Polymeric micelles and alternative nanonized delivery vehicles for poorly soluble drugs. *International Journal of Pharmaceutics*, *453*(1), 198–214. https://doi.org/10.1016/J.IJPHARM.2012.08.042

Ludwig, A. (2005). The use of mucoadhesive polymers in ocular drug delivery. *Advanced Drug Delivery Reviews*, *57*(11), 1595–1639. https://doi.org/10.1016/J.ADDR.2005.07.005

Lundin, K. E. A., Molberg, O., & Sollid, L. M. (2005). Celiac disease. In *Mucosal Immunology, Two-Volume Set*. Elsevier Inc. https://doi.org/10.1016/B978-012491543-5/50078-4

Luo, L., Tam, J., Maysinger, D., & Eisenberg, A. (2002). Cellular internalization of poly(ethylene oxide)-b-poly(ε-caprolactone) diblock copolymer micelles. *Bioconjugate Chemistry*, *13*(6), 1259–1265. https://doi.org/10.1021/BC025524Y

Mah, T. F. C., & O'Toole, G. A. (2001). Mechanisms of biofilm resistance to antimicrobial agents. *Trends in Microbiology*, *9*(1), 34–39. https://doi.org/10.1016/S0966-842X(00)01913-2

Mahor, A., Prajapati, S. K., Verma, A., Gupta, R., Iyer, A. K., & Kesharwani, P. (2016). Moxifloxacin loaded gelatin nanoparticles for ocular delivery: Formulation and in-vitro, in-vivo evaluation. *Journal of Colloid and Interface Science*, *483*, 132–138. https://doi.org/10.1016/J.JCIS.2016.08.018

Malekinejad, H., Bazargani-Gilani, B., Tukmechi, A., & Ebrahimi, H. (2012). A cytotoxicity and comparative antibacterial study on the effect of Zataria multiflora Boiss, Trachyspermum copticum essential oils, and Enrofloxacin on Aeromonas hydrophila. *Avicenna Journal of Phytomedicine*, *2*(4), 188–195. https://doi.org/10.22038/ajp.2012.108

Malhotra, M., & Majumdar, D. (2001). *Permeation through cornea*. http://nopr.niscpr.res.in/handle/123456789/23624

Mandal, A., Bisht, R., Rupenthal, I. D., & Mitra, A. K. (2017a). Polymeric micelles for ocular drug delivery: From structural frameworks to recent preclinical studies. *Journal of Controlled Release*, *248*, 96–116. https://doi.org/10.1016/J.JCONREL.2017.01.012

Mandal, A., Bisht, R., Rupenthal, I. D., & Mitra, A. K. (2017b). Polymeric micelles for ocular drug delivery: From structural frameworks to recent preclinical studies. *Journal of Controlled Release*, *248*, 96–116. https://doi.org/10.1016/J.JCONREL.2017.01.012

Mandal, A., Bisht, R., Rupenthal, I. D., & Mitra, A. K. (2017c). Polymeric micelles for ocular drug delivery: From structural frameworks to recent preclinical studies. In *Journal of Controlled Release* (Vol. 248, pp. 96–116). Elsevier B.V. https://doi.org/10.1016/j.jconrel.2017.01.012

Mannermaa, E., Vellonen, K. S., & Urtti, A. (2006a). Drug transport in corneal epithelium and blood–retina barrier: Emerging role of transporters in ocular pharmacokinetics. *Advanced Drug Delivery Reviews*, *58*(11), 1136–1163. https://doi.org/10.1016/J.ADDR.2006.07.024

Mannermaa, E., Vellonen, K. S., & Urtti, A. (2006b). Drug transport in corneal epithelium and blood–retina barrier: Emerging role of transporters in ocular pharmacokinetics. *Advanced Drug Delivery Reviews*, *58*(11), 1136–1163. https://doi.org/10.1016/J.ADDR.2006.07.024

Marciano-Cabral, F., & Cabral, G. (2003). Acanthamoeba spp. as agents of disease in humans. *Clinical Microbiology Reviews*, *16*(2), 273–307. https://doi.org/10.1128/CMR.16.2.273-307.2003

Marquart, M. E., & O'Callaghan, R. J. (2013). Infectious keratitis: Secreted bacterial proteins that mediate corneal damage. *Journal of Ophthalmology*, *2013*. https://doi.org/10.1155/2013/369094

Mascarenhas, J., Lalitha, P., Prajna, N. V., Srinivasan, M., Das, M., D'Silva, S. S., Oldenburg, C. E., Borkar, D. S., Esterberg, E. J., Lietman, T. M., & Keenan, J. D. (2014). Acanthamoeba, fungal, and bacterial keratitis: A comparison of risk factors and clinical features. *American Journal of Ophthalmology*, *157*(1), 56–62. https://doi.org/10.1016/j.ajo.2013.08.032

Maulvi, F. A., Shetty, K. H., Desai, D. T., Shah, D. O., & Willcox, M. D. P. (2021). Recent advances in ophthalmic preparations: Ocular barriers, dosage forms and routes of administration. *International Journal of Pharmaceutics*, *608*, 121105. https://doi.org/10.1016/J.IJPHARM.2021.121105

Maulvi, F. A., Singhania, S. S., Desai, A. R., Shukla, M. R., Tannk, A. S., Ranch, K. M., Vyas, B. A., & Shah, D. O. (2018). Contact lenses with dual drug delivery for the treatment of bacterial conjunctivitis. *International Journal of Pharmaceutics*, *548*(1), 139–150. https://doi.org/10.1016/j.ijpharm.2018.06.059

Maulvi, F. A., Soni, T. G., & Shah, D. O. (2016a). A review on therapeutic contact lenses for ocular drug delivery. *Http://Dx.Doi.Org/10.3109/10717544.2016.1138342*, *23*(8), 3017–3026. https://doi.org/10.3109/10717544.2016.1138342

Maulvi, F. A., Soni, T. G., & Shah, D. O. (2016b). A review on therapeutic contact lenses for ocular drug delivery. *Http://Dx.Doi.Org/10.3109/10717544.2016.1138342*, *23*(8), 3017–3026. https://doi.org/10.3109/10717544.2016.1138342

M'Barki, A., Bocquet, L., & Stevenson, A. (2017). Linking Rheology and Printability for Dense and Strong Ceramics by Direct Ink Writing. *Scientific Reports*, *7*(1), 6017. https://doi.org/10.1038/s41598-017-06115-0

McKenzie, M., Betts, D., Suh, A., Bui, K., Kim, L. D., & Cho, H. (2015). Hydrogel-based drug delivery systems for poorly water-soluble drugs. *Molecules*, *20*(11), 20397–20408. https://doi.org/10.3390/molecules201119705

McLeod, S. D., LaBree, L. D., Tayyanipour, R., Flowers, C. W., Lee, P. P., & McDonnell, P. J. (1995). The Importance of Initial Management in the Treatment of Severe Infectious Corneal Ulcers. *Ophthalmology*, *102*(12), 1943–1948. https://doi.org/10.1016/S0161-6420(95)30771-3

Meng, T., Kulkarni, V., Simmers, R., Brar, V., & Xu, Q. (2019). Therapeutic implications of nanomedicine for ocular drug delivery. *Drug Discovery Today*, *24*(8), 1524–1538. https://doi.org/10.1016/j.drudis.2019.05.006

Miedziak, A. I., Miller, M. R., Rapuano, C. J., Laibson, P. R., & Cohen, E. J. (1999). Risk factors in microbial keratitis leading to penetrating keratoplasty. *Ophthalmology*, *106*(6), 1166–1171. https://doi.org/https://doi.org/10.1016/S0161-6420(99)90250-6

Mikos, A. G., & Peppas, N. A. (1990). Bioadhesive analysis of controlled-release systems. IV. An experimental method for testing the adhesion of microparticles with mucus. *Journal of Controlled Release*, *12*(1), 31–37. https://doi.org/10.1016/0168-3659(90)90180-2

Mishra, P., Ch, S., Hong, S. J., Biswas, S., & Roy, S. (2022). Antimicrobial peptide S100A12 (calgranulin C) inhibits growth, biofilm formation, pyoverdine secretion and suppresses type VI secretion system in Pseudomonas aeruginosa. *Microbial Pathogenesis*, *169*. https://doi.org/10.1016/j.micpath.2022.105654

Mizrahi, B., & Domb, A. (2008). Mucoadhesive Polymers for Delivery of Drugs to the Oral Cavity. *Recent Patents on Drug Delivery & Formulation*, *2*(2), 108–119. https://doi.org/10.2174/187221108784534126

Modaresifar, K., Hadjizadeh, A., & Niknejad, H. (2018). Design and fabrication of GelMA/chitosan nanoparticles composite hydrogel for angiogenic growth factor delivery. *Artificial Cells, Nanomedicine and Biotechnology*, *46*(8), 1799–1808. https://doi.org/10.1080/21691401.2017.1392970

Mortensen, K., & Pedersen, J. S. (1993). Structural study on the micelle formation of poly(ethylene oxide)-poly(propylene oxide)-poly(ethylene oxide) triblock copolymer in aqueous solution. *Macromolecules*, *26*(4), 805–812. https://doi.org/10.1021/ma00056a035

Muddineti, O. S., Kumari, P., Ghosh, B., Torchilin, V. P., & Biswas, S. (2017). D -α-Tocopheryl Succinate/Phosphatidyl Ethanolamine Conjugated Amphiphilic Polymer-Based Nanomicellar System for the Efficient Delivery of Curcumin and to Overcome Multiple Drug Resistance in Cancer. *ACS Applied Materials and Interfaces*, *9*(20), 16778–16792. https://doi.org/10.1021/acsami.7b01087

Nadagouda, M. N., & Varma, R. S. (2007). Synthesis of thermally stable carboxymethyl cellulose/metal biodegradable nanocomposites for potential biological applications. *Biomacromolecules*, *8*(9), 2762–2767. https://doi.org/10.1021/BM700446P

Nagpal, K., Singh, S. K., & Mishra, D. N. (2010). Chitosan Nanoparticles: A Promising System in Novel Drug Delivery. *Chemical and Pharmaceutical Bulletin*, *58*(11), 1423–1430. https://doi.org/10.1248/CPB.58.1423

Nath, R., Baruah, S., Saikia, L., Devi, B., Borthakur, A., & Mahanta, J. (2011). Mycotic corneal ulcers in upper Assam. *Indian Journal of Ophthalmology*, *59*(5), 367–371. https://doi.org/10.4103/0301-4738.83613

Ni, P. Y., Ding, Q. X., Fan, M., Liao, J. F., Qian, Z. Y., Luo, J. C., Li, X. Q., Luo, F., Yang, Z. M., & Wei, Y. Q. (2014). Injectable thermosensitive PEG-PCL-PEG hydrogel/acellular bone matrix composite for bone regeneration in cranial defects. *Biomaterials*, *35*(1), 236–248. https://doi.org/10.1016/J.BIOMATERIALS.2013.10.016

O'Brien, T. P. (2003). Management of bacterial keratitis: beyond exorcism towards consideration of organism and host factors. *Eye*, *17*(8), 957–974. https://doi.org/10.1038/sj.eye.6700635

Omerović, N., & Vranić, E. (2020). Application of nanoparticles in ocular drug delivery systems. *Health and Technology*, *10*(1), 61–78. https://doi.org/10.1007/s12553-019-00381-w

Ong, T. H., Chitra, E., Ramamurthy, S., Ling, C. C. S., Ambu, S. P., & Davamani, F. (2019). Cationic chitosan-propolis nanoparticles alter the zeta potential of S. epidermidis, inhibit biofilm formation by modulating gene expression and exhibit synergism with antibiotics. *PLOS ONE*, *14*(2), e0213079.

Onugwu, A. L., Nwagwu, C. S., Onugwu, O. S., Echezona, A. C., Agbo, C. P., Ihim, S. A., Emeh, P., Nnamani, P. O., Attama, A. A., & Khutoryanskiy, V. V. (2023). Nanotechnology based drug delivery systems for the treatment of anterior segment eye diseases. *Journal of Controlled Release*, *354*(December 2022), 465–488. https://doi.org/10.1016/j.jconrel.2023.01.018

Osidak, E. O., Karalkin, P. A., Osidak, M. S., Parfenov, V. A., Sivogrivov, D. E., Pereira, F. D. A. S., Gryadunova, A. A., Koudan, E. V., Khesuani, Y. D., Kasyanov, V. A., Belousov, S. I., Krasheninnikov, S. V., Grigoriev, T. E., Chvalun, S. N., Bulanova, E. A., Mironov, V. A., & Domogatsky, S. P. (2019). Viscoll collagen solution as a novel bioink for direct 3D bioprinting. *Journal of Materials Science: Materials in Medicine*, *30*(3), 1–12. https://doi.org/10.1007/S10856-019-6233-Y/FIGURES/6

Ou, F., McGoverin, C., Swift, S., & Vanholsbeeck, F. (2019). Rapid and cost-effective evaluation of bacterial viability using fluorescence spectroscopy. *Analytical and Bioanalytical Chemistry*, *411*(16), 3653–3663. https://doi.org/10.1007/s00216-019-01848-5

Özsoy, Y., Güngör, S., Kahraman, E., & Durgun, M. E. (2019). *Chapter 4 - Polymeric micelles as a novel carrier for ocular drug delivery* (A. M. B. T.-N. in B. Grumezescu, Ed.; pp. 85–117). William Andrew Publishing. https://doi.org/https://doi.org/10.1016/B978-0-12-816200-2.00005-0

Paradiso, P., Serro, A. P., Saramago, B., Colaço, R., & Chauhan, A. (2016). Controlled Release of Antibiotics From Vitamin E–Loaded Silicone-Hydrogel Contact Lenses. *Journal of Pharmaceutical Sciences*, *105*(3), 1164–1172. https://doi.org/https://doi.org/10.1016/S0022-3549(15)00193-8

Patel, A. (2013). Ocular drug delivery systems: An overview. *World Journal of Pharmacology*, *2*(2), 47. https://doi.org/10.5497/wjp.v2.i2.47

Patel, A., Cholkar, K., Agrahari, V., & Mitra, A. K. (2013). Ocular drug delivery systems: An overview. *World Journal of Pharmacology*, *2*(2), 47. https://doi.org/10.5497/WJP.V2.I2.47

Patel, P. B., Shastri, D. H., Shelat, P. K., & Shukla, A. K. (2010). Ophthalmic drug delivery system: Challenges and approaches. *Systematic Reviews in Pharmacy*, *1*(2), 113–120. https://doi.org/10.4103/0975-8453.75042

Paulsen, F. P., Corfield, A. P., Hinz, M., Hoffmann, W., Schaudig, U., Thale, A. B., & Berry, M. (2003). Characterization of Mucins in Human Lacrimal Sac and Nasolacrimal Duct. *Investigative Ophthalmology & Visual Science*, *44*(5), 1807–1813. https://doi.org/10.1167/IOVS.02-0744

Peppas, N. A., & Buri, P. A. (1985). Surface, interfacial and molecular aspects of polymer bioadhesion on soft tissues. *Journal of Controlled Release*, *2*(C), 257–275. https://doi.org/10.1016/0168-3659(85)90050-1

Peppas, N. A., & Sahlin, J. J. (1996). Hydrogels as mucoadhesive and bioadhesive materials: A review. *Biomaterials*, *17*(16), 1553–1561. https://doi.org/10.1016/0142-9612(95)00307-X

Peppas, N. A., Thomas, J. B., & McGinty, J. (2009). Molecular Aspects of Mucoadhesive Carrier Development for Drug Delivery and Improved Absorption. *Journal of Biomaterials Science. Polymer Edition*, *20*(1), 1. https://doi.org/10.1163/156856208X393464

Pestova, E., Millichap, J. J., Noskin, G. A., & Peterson, L. R. (2000). Intracellular targets of moxifloxacin: a comparison with other fluoroquinolones. *Journal of Antimicrobial Chemotherapy*, *45*(5), 583–590. https://doi.org/10.1093/JAC/45.5.583

Plotkowski, M. C., Chevillard, M., Pierrot, D., Altemayer, D., Zahm, J. M., & Colliot G/ Puchelle, E. (1991). Differential adhesion of Pseudomonas aeruginosa to human respiratory epithelial cells in primary culture. *The Journal of Clinical Investigation*, *87*(6), 2018–2028. https://doi.org/10.1172/JCI115231

Poggio, E. C., Glynn, R. J., Schein, O. D., Seddon, J. M., Shannon, M. J., Scardino, V. A., & Kenyon, K. R. (1989). The Incidence of Ulcerative Keratitis among Users of Daily-Wear and Extended-Wear Soft Contact Lenses. *New England Journal of Medicine*, *321*(12), 779–783. https://doi.org/10.1056/NEJM198909213211202

Popov, A. (2020). Mucus-Penetrating Particles and the Role of Ocular Mucus as a Barrier to Micro- and Nanosuspensions. *Journal of Ocular Pharmacology and Therapeutics : The Official Journal of the Association for Ocular Pharmacology and Therapeutics*, *36*(6), 366–375. https://doi.org/10.1089/JOP.2020.0022

Prada, D., Harris, A., Guidoboni, G., Rowe, L., Verticchio-Vercellin, A. C., & Mathew, S. (2019). Vascular Anatomy and Physiology of the Eye. *Modeling and Simulation in Science, Engineering and Technology*, 23–45. https://doi.org/10.1007/978-3-030-25886-3_2/COVER

R, S., ED, D., EJ, H., SH, Y., S, D., JL, G., FS, M., SV, S., & T, K. (2011). Microbial keratitis trends following refractive surgery: results of the ASCRS infectious keratitis survey and comparisons with prior ASCRS surveys of infectious keratitis following keratorefractive

procedures. *Journal of Cataract and Refractive Surgery*, *37*(7), 1343–1350. https://doi.org/10.1016/J.JCRS.2011.05.006

Račić, A., & Krajišnik, D. (2023). Biopolymers in Mucoadhesive Eye Drops for Treatment of Dry Eye and Allergic Conditions: Application and Perspectives. *Pharmaceutics 2023, Vol. 15, Page 470*, *15*(2), 470. https://doi.org/10.3390/PHARMACEUTICS15020470

Rahmani, S., Mohammadi Nia, M., Akbarzadeh Baghban, A., Nazari, M. R., & Ghassemi-Broumand, M. (2014). Spectral transmittance of UV-blocking soft contact lenses: A comparative study. *Contact Lens and Anterior Eye*, *37*(6), 451–454. https://doi.org/10.1016/j.clae.2014.07.011

Redgrave, L. S., Sutton, S. B., Webber, M. A., & Piddock, L. J. V. (2014). Fluoroquinolone resistance: mechanisms, impact on bacteria, and role in evolutionary success. *Trends in Microbiology*, *22*(8), 438–445. https://doi.org/10.1016/J.TIM.2014.04.007

Reichert, R., & Stern, G. (1984). Quantitative Adherence of Bacteria to Human Corneal Epithelial Cells. *Archives of Ophthalmology*, *102*(9), 1394–1395. https://doi.org/10.1001/archopht.1984.01040031136041

Reimondez-Troitiño, S., Csaba, N., Alonso, M. J., & De La Fuente, M. (2015). Nanotherapies for the treatment of ocular diseases. *European Journal of Pharmaceutics and Biopharmaceutics*, *95*, 279–293. https://doi.org/10.1016/j.ejpb.2015.02.019

Rizwan, M., Chan, S. W., Comeau, P. A., Willett, T. L., & Yim, E. K. F. (2020). Effect of sterilization treatment on mechanical properties, biodegradation, bioactivity and printability of GelMA hydrogels. *Biomedical Materials (Bristol, England)*, *15*(6). https://doi.org/10.1088/1748-605X/ABA40C

Robertson, D. M., Rogers, N. A., Petroll, W. M., & Zhu, M. (2017). Second harmonic generation imaging of corneal stroma after infection by Pseudomonas aeruginosa. *Scientific Reports*, *7*(1), 46116. https://doi.org/10.1038/srep46116

Rodríguez, I., Vázquez, J. A., Pastrana, L., & Khutoryanskiy, V. V. (2017). Enhancement and inhibition effects on the corneal permeability of timolol maleate: Polymers, cyclodextrins and chelating agents. *International Journal of Pharmaceutics*, *529*(1–2), 168–177. https://doi.org/10.1016/J.IJPHARM.2017.06.075

Rossi, S., Bonferoni, M. C., Ferrari, F., & Caramella, C. (2008). Drug Release and Washability of Mucoadhesive Gels Based on Sodium Carboxymethylcellulose and Polyacrylic Acid. *Http://Dx.Doi.Org/10.1080/10837459908984224*, *4*(1), 55–63. https://doi.org/10.1080/10837459908984224

Rossi, S., Ferrari, F., Bonferoni, M. C., & Caramella, C. (2001). Characterization of chitosan hydrochloride--mucin rheological interaction: influence of polymer concentration and polymer:mucin weight ratio. *European Journal of Pharmaceutical Sciences : Official Journal of the European Federation for Pharmaceutical Sciences*, *12*(4), 479–485. https://doi.org/10.1016/S0928-0987(00)00194-9

Roy, S., Pal, K., Anis, A., Pramanik, K., & Prabhakar, B. (2012). Polymers in Mucoadhesive Drug-Delivery Systems: A Brief Note.

Http://Dx.Doi.Org/10.1163/138577209X12478283327236, *12*(6), 483–495. https://doi.org/10.1163/138577209X12478283327236

Ruponen, M., & Urtti, A. (2015). Undefined role of mucus as a barrier in ocular drug delivery. *European Journal of Pharmaceutics and Biopharmaceutics : Official Journal of Arbeitsgemeinschaft Fur Pharmazeutische Verfahrenstechnik e.V*, *96*, 442–446. https://doi.org/10.1016/J.EJPB.2015.02.032

Rykowska, I., Nowak, I., & Nowak, R. (2021). Soft contact lenses as drug delivery systems: A review. In *Molecules* (Vol. 26, Issue 18). MDPI. https://doi.org/10.3390/molecules26185577

Sæther, H. V., Holme, H. K., Maurstad, G., Smidsrød, O., & Stokke, B. T. (2008). Polyelectrolyte complex formation using alginate and chitosan. *Carbohydrate Polymers*, *74*(4), 813–821. https://doi.org/10.1016/J.CARBPOL.2008.04.048

Santos, T. C. dos, Rescignano, N., Boff, L., Reginatto, F. H., Simões, C. M. O., de Campos, A. M., & Mijangos, C. U. (2017). Manufacture and characterization of chitosan/PLGA nanoparticles nanocomposite buccal films. *Carbohydrate Polymers*, *173*, 638–644. https://doi.org/https://doi.org/10.1016/j.carbpol.2017.06.014

Sarika, P. R., & James, N. R. (2016). Polyelectrolyte complex nanoparticles from cationised gelatin and sodium alginate for curcumin delivery. *Carbohydrate Polymers*, *148*, 354–361. https://doi.org/10.1016/J.CARBPOL.2016.04.073

Sarmento, B., Ribeiro, A., Veiga, F., Sampaio, P., Neufeld, R., & Ferreira, D. (2007). Alginate/chitosan nanoparticles are effective for oral insulin delivery. *Pharmaceutical Research*, *24*(12), 2198–2206. https://doi.org/10.1007/S11095-007-9367-4/FIGURES/5

Sarwat, S., Stapleton, F., Willcox, M., & Roy, M. (2019). Quantum Dots in Ophthalmology: A Literature Review. *Current Eye Research*, *44*(10), 1037–1046. https://doi.org/10.1080/02713683.2019.1660793

Sau-Hung Spence Leung, & Robinson, J. R. (1987). The contribution of anionic polymer structural features to mucoadhesion. *Journal of Controlled Release*, *5*(3), 223–231. https://doi.org/10.1016/0168-3659(88)90021-1

Schaefer, F., Bruttin, O., Zografos, L., & Guex-Crosier, Y. (2001a). Bacterial keratitis: a prospective clinical and microbiological study. *British Journal of Ophthalmology*, *85*(7), 842–847.

Schaefer, F., Bruttin, O., Zografos, L., & Guex-Crosier, Y. (2001b). Bacterial keratitis: a prospective clinical and microbiological study. *British Journal of Ophthalmology*, *85*(7), 842 LP – 847. https://doi.org/10.1136/bjo.85.7.842

Schlech, B. (2005). Ocular Pharmacokinetics of Moxifloxacin After Topical Treatment of Animals and Humans. *Survey of Ophthalmology*. https://www.academia.edu/21241515/Ocular_Pharmacokinetics_of_Moxifloxacin_After_Topical_Treatment_of_Animals_and_Humans

Shaikh, R., Raj Singh, T., Garland, M., Woolfson, A., & Donnelly, R. (2011a). Mucoadhesive drug delivery systems. *Journal of Pharmacy and Bioallied Sciences*, *3*(1), 89. https://doi.org/10.4103/0975-7406.76478

Shaikh, R., Raj Singh, T., Garland, M., Woolfson, A., & Donnelly, R. (2011b). Mucoadhesive drug delivery systems. *Journal of Pharmacy and Bioallied Sciences*, *3*(1), 89. https://doi.org/10.4103/0975-7406.76478

Shaikh, R., Raj Singh, T., Garland, M., Woolfson, A., & Donnelly, R. (2011c). Mucoadhesive drug delivery systems. *Journal of Pharmacy And Bioallied Sciences*, *3*(1), 89. https://doi.org/10.4103/0975-7406.76478

Shao, Y., You, D., Lou, Y., Li, J., Ying, B., Cheng, K., Weng, W., Wang, H., Yu, M., & Dong, L. (2019). Controlled Release of Naringin in GelMA-Incorporated Rutile Nanorod Films to Regulate Osteogenic Differentiation of Mesenchymal Stem Cells. *ACS Omega*, *4*(21), 19350–19357. https://doi.org/10.1021/acsomega.9b02751

Sharma, A., & Taniguchi, J. (2017). Review: Emerging strategies for antimicrobial drug delivery to the ocular surface: Implications for infectious keratitis. *The Ocular Surface*, *15*(4), 670–679. https://doi.org/10.1016/J.JTOS.2017.06.001

Shie, M. Y., Lee, J. J., Ho, C. C., Yen, S. Y., Ng, H. Y., & Chen, Y. W. (2020). Effects of gelatin methacrylate bio-ink concentration on mechano-physical properties and human dermal fibroblast behavior. *Polymers*, *12*(9). https://doi.org/10.3390/POLYM12091930

Shinde, U. A., & Nagarsenker, M. S. (2009). Characterization of Gelatin-Sodium Alginate Complex Coacervation System. *Indian Journal of Pharmaceutical Sciences*, *71*(3), 313. https://doi.org/10.4103/0250-474X.56033

Silhavy, T. J., Kahne, D., & Walker, S. (2010). The bacterial cell envelope. *Cold Spring Harbor Perspectives in Biology*, *2*(5). https://doi.org/10.1101/CSHPERSPECT.A000414

Silva, M. M., Calado, R., Marto, J., Bettencourt, A., Almeida, A. J., & Gonçalves, L. M. D. (2017). Chitosan nanoparticles as a mucoadhesive drug delivery system for ocular administration. *Marine Drugs*, *15*(12), 1–16. https://doi.org/10.3390/md15120370

Simões, S. M. N., Figueiras, A. R., Veiga, F., Concheiro, A., & Alvarez-Lorenzo, C. (2015). Polymeric micelles for oral drug administration enabling locoregional and systemic treatments. *Expert Opinion on Drug Delivery*, *12*(2), 297–318. https://doi.org/10.1517/17425247.2015.960841

Singh, N. K., & Lee, D. S. (2014). In situ gelling pH- and temperature-sensitive biodegradable block copolymer hydrogels for drug delivery. *Journal of Controlled Release : Official Journal of the Controlled Release Society*, *193*, 214–227. https://doi.org/10.1016/J.JCONREL.2014.04.056

Singh, P., Tyagi, M., Kumar, Y., Gupta, K. K., & Sharma, P. D. (2013). Ocular chemical injuries and their management. *Oman Journal of Ophthalmology*, *6*(2), 83.

Singh, S. B., Young, K., & Silver, L. L. (2017). What is an "ideal" antibiotic? Discovery challenges and path forward. *Biochemical Pharmacology*, *133*, 63–73. https://doi.org/10.1016/j.bcp.2017.01.003

Sintzel, M., Bernatchez, S. F., Tabatabay, C., & Gurny, R. (1996). Biomaterials in ophthalmic drug delivery. *European Journal of Pharmaceutics and Biopharmaceutics*.

Smith, J., Wood, E., & Dornish, M. (2004a). Effect of Chitosan on Epithelial Cell Tight Junctions. *Pharmaceutical Research*, *21*(1), 43–49. https://doi.org/10.1023/B:PHAM.0000012150.60180.e3

Smith, J., Wood, E., & Dornish, M. (2004b). Effect of Chitosan on Epithelial Cell Tight Junctions. *Pharmaceutical Research*, *21*(1), 43–49. https://doi.org/10.1023/B:PHAM.0000012150.60180.E3/METRICS

Smith, P. T., Basu, A., Saha, A., & Nelson, A. (2018). Chemical modification and printability of shear-thinning hydrogel inks for direct-write 3D printing. *Polymer*, *152*, 42–50. https://doi.org/https://doi.org/10.1016/j.polymer.2018.01.070

Sogias, I. A., Williams, A. C., & Khutoryanskiy, V. V. (2008a). Why is chitosan mucoadhesive? *Biomacromolecules*, *9*(7), 1837–1842. https://doi.org/10.1021/bm800276d

Sogias, I. A., Williams, A. C., & Khutoryanskiy, V. V. (2008b). Why is chitosan mucoadhesive? *Biomacromolecules*, *9*(7), 1837–1842. https://doi.org/10.1021/BM800276D/SUPPL_FILE/BM800276D-FILE002.PDF

Song, J. E., Kim, S., Kang, H. K., Chung, I., Kwak, Y. G., Um, T. H., Cho, C. R., & Chang, J. (2021). A case of bacterial keratitis caused by multi-drug-resistant Shewanella algae without marine exposure. *Oxford Medical Case Reports*, *2021*(11–12), 493–495. https://doi.org/10.1093/OMCR/OMAB131

Souto, E. B., Dias-Ferreira, J., López-Machado, A., Ettcheto, M., Cano, A., Espuny, A. C., Espina, M., Garcia, M. L., & Sánchez-López, E. (2019). Advanced Formulation Approaches for Ocular Drug Delivery: State-Of-The-Art and Recent Patents. *Pharmaceutics 2019, Vol. 11, Page 460*, *11*(9), 460. https://doi.org/10.3390/PHARMACEUTICS11090460

Šprincl, L., Vacík, J., & Kopeček, J. (1973). Biological tolerance of ionogenic hydrophilic gels. *Journal of Biomedical Materials Research*, *7*(1), 123–136. https://doi.org/10.1002/JBM.820070110

Šprincl, L., Vacík, J., Kopeček, J., & Lím, D. (1971). Biological tolerance of poly(N-substituted methacrylamides). *Journal of Biomedical Materials Research*, *5*(3), 197–205. https://doi.org/10.1002/JBM.820050307

Stapleton, F., Edwards, K., Keay, L., Naduvilath, T., Dart, J. K. G., Brian, G., & Holden, B. (2012). Risk Factors for Moderate and Severe Microbial Keratitis in Daily Wear Contact Lens Users. *Ophthalmology*, *119*(8), 1516–1521. https://doi.org/10.1016/J.OPHTHA.2012.01.052

Stapleton, F., Naduvilath, T., Keay, L., Radford, C., Dart, J., Edwards, K., Carnt, N., Minassian, D., & Holden, B. (2017). Risk factors and causative organisms in microbial keratitis in daily disposable contact lens wear. *PLOS ONE*, *12*(8), e0181343. https://doi.org/10.1371/JOURNAL.PONE.0181343

Štěpánek, M., Podhájecká, K., Tesařová, E., Procházka, K., Tuzar, Z., & Brown, W. (2001). Hybrid polymeric micelles with hydrophobic cores and mixed polyelectrolyte/nonelectrolyte

shells in aqueous media. 1. Preparation and basic characterization. *Langmuir*, *17*(14), 4240–4244. https://doi.org/10.1021/LA010246X

Stepanovska, J., Otahal, M., Hanzalek, K., Supova, M., & Matejka, R. (2021). pH Modification of High-Concentrated Collagen Bioinks as a Factor Affecting Cell Viability, Mechanical Properties, and Printability. *Gels 2021, Vol. 7, Page 252*, *7*(4), 252. https://doi.org/10.3390/GELS7040252

Stern, G. A., Lubniewski, A., & Allen, C. (1985). The interaction between Pseudomonas aeruginosa and the corneal epithelium. An electron microscopic study. *Archives of Ophthalmology (Chicago, Ill. : 1960)*, *103*(8), 1221–1225. https://doi.org/10.1001/ARCHOPHT.1985.01050080133033

SWAN, K. C. (1945). USE OF METHYL CELLULOSE IN OPHTHALMOLOGY. *Archives of Ophthalmology*, *33*(5), 378–380. https://doi.org/10.1001/ARCHOPHT.1945.00890170054004

Szekalska, M., Wróblewska, M., Czajkowska-Kośnik, A., Sosnowska, K., Misiak, P., Wilczewska, A. Z., & Winnicka, K. (2023). The Spray-Dried Alginate/Gelatin Microparticles with Luliconazole as Mucoadhesive Drug Delivery System. *Materials*, *16*(1). https://doi.org/10.3390/MA16010403/S1

Taylor, H. R., West, S. K., Rosenthal, F. S., Munoz, B., Newland, H. S., & Emmett, E. A. (1989). Corneal changes associated with chronic UV irradiation. *Archives of Ophthalmology*, *107*(10), 1481–1484.

Teweldemedhin, M., Gebreyesus, H., Atsbaha, A. H., Asgedom, S. W., & Saravanan, M. (2017a). Bacterial profile of ocular infections: A systematic review. *BMC Ophthalmology*, *17*(1), 1–9. https://doi.org/10.1186/S12886-017-0612-2/TABLES/3

Teweldemedhin, M., Gebreyesus, H., Atsbaha, A. H., Asgedom, S. W., & Saravanan, M. (2017b). Bacterial profile of ocular infections: a systematic review. *BMC Ophthalmology*, *17*(1), 212. https://doi.org/10.1186/s12886-017-0612-2

Thermosensitive polymeric hydrogels as drug delivery systems - PubMed. (n.d.). Retrieved April 21, 2023, from https://pubmed.ncbi.nlm.nih.gov/23092130/

Thibodeaux, B. A., Dajcs, J. J., Caballero, A. R., Marquart, M. E., Girgis, D. O., & O'Callaghan, R. J. (2004). Quantitative comparison of fluoroquinolone therapies of experimental Gram-negative bacterial keratitis. *Current Eye Research*, *28*(5), 337–342. https://doi.org/10.1076/ceyr.28.5.337.28676

Thomas, P. A. (2003). Current Perspectives on Ophthalmic Mycoses. *Clinical Microbiology Reviews*, *16*(4), 730–797. https://doi.org/10.1128/CMR.16.4.730-797.2003

Thomas, P. A., & Kaliamurthy, J. (2013). Mycotic keratitis: Epidemiology, diagnosis and management. *Clinical Microbiology and Infection*, *19*(3), 210–220. https://doi.org/10.1111/1469-0691.12126

Ting, D. S. J., Cairns, J., Gopal, B. P., Ho, C. S., Krstic, L., Elsahn, A., Lister, M., Said, D. G., & Dua, H. S. (2021). Risk Factors, Clinical Outcomes, and Prognostic Factors of

Bacterial Keratitis: The Nottingham Infectious Keratitis Study. *Frontiers in Medicine*, *8*. https://www.frontiersin.org/articles/10.3389/fmed.2021.715118

Ting, D. S. J., Ho, C. S., Deshmukh, R., Said, D. G., & Dua, H. S. (2021a). Infectious keratitis: an update on epidemiology, causative microorganisms, risk factors, and antimicrobial resistance. *Eye (London, England)*, *35*(4), 1084–1101. https://doi.org/10.1038/S41433-020-01339-3

Ting, D. S. J., Ho, C. S., Deshmukh, R., Said, D. G., & Dua, H. S. (2021b). Infectious keratitis: an update on epidemiology, causative microorganisms, risk factors, and antimicrobial resistance. *Eye 2021 35:4*, *35*(4), 1084–1101. https://doi.org/10.1038/s41433-020-01339-3

Ting, D. S. J., Ho, C. S., Deshmukh, R., Said, D. G., & Dua, H. S. (2021c). Infectious keratitis: an update on epidemiology, causative microorganisms, risk factors, and antimicrobial resistance. *Eye*, *35*(4), 1084–1101. https://doi.org/10.1038/s41433-020-01339-3

Tonda-Turo, C., Herva, M., Chiono, V., Ciardelli, G., & Spillantini, M. G. (2018). Influence of Drug-Carrier Polymers on Alpha-Synucleinopathies: A Neglected Aspect in New Therapies Development. *BioMed Research International*, *2018*. https://doi.org/10.1155/2018/4518060

Tsai, T. H., Chen, W. L., & Hu, F. R. (2010). Comparison of fluoroquinolones: Cytotoxicity on human corneal epithelial cells. *Eye*, *24*(5), 909–917. https://doi.org/10.1038/eye.2009.179

Tseng, C. L., Chen, K. H., Su, W. Y., Lee, Y. H., Wu, C. C., & Lin, F. H. (2013). Cationic gelatin nanoparticles for drug delivery to the ocular surface: In vitro and in vivo evaluation. *Journal of Nanomaterials*, *2013*. https://doi.org/10.1155/2013/238351

Ubani-Ukoma, U., Gibson, D., Schultz, G., Silva, B. O., & Chauhan, A. (2019). Evaluating the potential of drug eluting contact lenses for treatment of bacterial keratitis using an ex vivo corneal model. *International Journal of Pharmaceutics*, *565*, 499–508. https://doi.org/https://doi.org/10.1016/j.ijpharm.2019.05.031

Ulbrich, K., & Kopeček, J. (1976). Polymerization kinetics of N-ethylacrylamide. *Collection of Czechoslovak Chemical Communications*, *41*(1), 61–66. https://doi.org/10.1135/CCCC19760061

Ung, L., Acharya, N. R., Agarwal, T., Alfonso, E. C., Bagga, B., Bispo, P. J. M., Burton, M. J., Dart, J. K. G., Doan, T., Fleiszig, S. M. J., Garg, P., Gilmore, M. S., Gritz, D. C., Hazlett, L. D., Iovieno, A., Jhanji, V., Kempen, J. H., Lee, C. S., Lietman, T. M., … Chodosh, J. (2019). Infectious corneal ulceration: a proposal for neglected tropical disease status. *Bulletin of the World Health Organization*, *97*(12), 854–856. https://doi.org/10.2471/BLT.19.232660

Ung, L., Bispo, P. J. M., Shanbhag, S. S., Gilmore, M. S., & Chodosh, J. (2019). The persistent dilemma of microbial keratitis: Global burden, diagnosis, and antimicrobial resistance. *Survey of Ophthalmology*, *64*(3), 255–271. https://doi.org/10.1016/J.SURVOPHTHAL.2018.12.003

Vajpayee, R. B., Dada, T., Saxena, R., Vajpayee, M., Taylor, H. R., Venkatesh, P., & Sharma, N. (2000). Study of the First Contact Management Profile of Cases of Infectious Keratitis: A

Hospital-Based Study. *Cornea*, *19*(1). https://journals.lww.com/corneajrnl/Fulltext/2000/01000/Study_of_the_First_Contact_Management_Profile_of.11.aspx

Vaneev, A., Tikhomirova, V., Chesnokova, N., Popova, E., Beznos, O., Kost, O., & Klyachko, N. (2021). Nanotechnology for topical drug delivery to the anterior segment of the eye. *International Journal of Molecular Sciences*, *22*(22). https://doi.org/10.3390/ijms222212368

Varela-Fernández, R., Díaz-Tomé, V., Luaces-Rodríguez, A., Conde-Penedo, A., García-Otero, X., Luzardo-álvarez, A., Fernández-Ferreiro, A., & Otero-Espinar, F. J. (2020). Drug delivery to the posterior segment of the eye: Biopharmaceutic and pharmacokinetic considerations. *Pharmaceutics*, *12*(3), 1–39. https://doi.org/10.3390/pharmaceutics12030269

Vermeltfoort, P. B. J., Hooymans, J. M. M., Busscher, H. J., & Van Der Mei, H. C. (2008). Bacterial transmission from lens storage cases to contact lenses—Effects of lens care solutions and silver impregnation of cases. *Journal of Biomedical Materials Research Part B: Applied Biomaterials*, *87B*(1), 237–243. https://doi.org/10.1002/JBM.B.31102

Vysyaraju, N. R., Paul, M., Ch, S., Ghosh, B., & Biswas, S. (2022). Olaparib@human serum albumin nanoparticles as sustained drug-releasing tumour-targeting nanomedicine to inhibit growth and metastasis in the mouse model of triple-negative breast cancer. *Https://Doi.Org/10.1080/1061186X.2022.2092623*, *30*(10), 1088–1105. https://doi.org/10.1080/1061186X.2022.2092623

W, H. R. E., & S, C. D. (1999). Peptide Antibiotics. *Antimicrobial Agents and Chemotherapy*, *43*(6), 1317–1323. https://doi.org/10.1128/AAC.43.6.1317

Wadhwa, S., Paliwal, R., Rai Paliwal, S., & P. Vyas, S. (2010). Chitosan and its Role in Ocular Therapeutics. *Mini-Reviews in Medicinal Chemistry*, *9*(14), 1639–1647. https://doi.org/10.2174/138955709791012292

Wang, Q., Aleshintsev, A., Bolton, D., Zhuang, J., Brenowitz, M., & Gupta, R. (2019). Ca(II) and Zn(II) Cooperate to Modulate the Structure and Self-Assembly of S100A12. *Biochemistry*, *58*(17), 2269–2281. https://doi.org/10.1021/ACS.BIOCHEM.9B00123

Wang, X., Wang, S., & Zhang, Y. (2015). Advance of the application of nano-controlled release system in ophthalmic drug delivery. *Http://Dx.Doi.Org/10.3109/10717544.2015.1116025*, *23*(8), 2897–2901. https://doi.org/10.3109/10717544.2015.1116025

Wang, Y., Wang, J., Ji, Z., Yan, W., Zhao, H., Huang, W., & Liu, H. (2022). Application of Bioprinting in Ophthalmology. *International Journal of Bioprinting*, *8*(2), 147–158. https://doi.org/10.18063/IJB.V8I2.552

Wen, Y., Yu, B., Zhu, Z., Yang, Z., & Shao, W. (2020). Synthesis of Antibacterial Gelatin/Sodium Alginate Sponges and Their Antibacterial Activity. *Polymers*, *12*(9). https://doi.org/10.3390/POLYM12091926

Winfield, A. J., Jessiman, D., Williams, A., & Esakowitz, L. (1990). A study of the causes of non-compliance by patients prescribed eyedrops. *British Journal of Ophthalmology*, *74*(8), 477. https://doi.org/10.1136/bjo.74.8.477

Wong, R. L. M., Gangwani, R. A., Yu, L. W. H., & Lai, J. S. M. (2012a). New treatments for bacterial keratitis. *Journal of Ophthalmology*, *2012*. https://doi.org/10.1155/2012/831502

Wong, R. L. M., Gangwani, R. A., Yu, L. W. H., & Lai, J. S. M. (2012b). New treatments for bacterial keratitis. *Journal of Ophthalmology*, *2012*.

Wong, R. L. M., Gangwani, R. A., Yu, L. W. H., & Lai, J. S. M. (2012c). New treatments for bacterial keratitis. *Journal of Ophthalmology*, *2012*. https://doi.org/10.1155/2012/831502

Wu, Y., Wu, Y., Zhu, T., Han, H., Liu, H., Xu, T., Francois, P., Fischer, A., Bai, L., Götz, F., & Qu, D. (2015). Staphylococcus epidermidis SrrAB regulates bacterial growth and biofilm formation differently under oxic and microaerobic conditions. *Journal of Bacteriology*, *197*(3), 459–476. https://doi.org/10.1128/JB.02231-14

Xie, L., Zhong, W., Shi, W., & Sun, S. (2006). Spectrum of Fungal Keratitis in North China. *Ophthalmology*, *113*(11), 1943–1948. https://doi.org/10.1016/J.OPHTHA.2006.05.035

Xu, W., Ling, P., & Zhang, T. (2013). Polymeric Micelles, a Promising Drug Delivery System to Enhance Bioavailability of Poorly Water-Soluble Drugs. *Journal of Drug Delivery*, *2013*, 1–15. https://doi.org/10.1155/2013/340315

Yamamura, T., Hitomi, J., Nagasaki, K., … M. S.-B. and, & 1996, undefined. (n.d.). Human CAAF1 gene—molecular cloning, gene structure, and chromosome mapping. *Elsevier*. Retrieved July 3, 2023, from https://www.sciencedirect.com/science/article/pii/S0006291X96906002

Yermak, I. M., Davydova, V. N., & Volod'ko, A. V. (2022). Mucoadhesive Marine Polysaccharides. *Marine Drugs 2022, Vol. 20, Page 522*, *20*(8), 522. https://doi.org/10.3390/MD20080522

Zarrintaj, P., Ramsey, J. D., Samadi, A., Atoufi, Z., Khodadadi, M., Reza, M., Mohammadi, L., Zangene, E., Farokhi, M., Formela, K., Reza, M., Mozafari, M., & Thomas, S. (2020). Acta Biomaterialia Poloxamer : A versatile tri-block copolymer for biomedical applications. *Acta Biomaterialia*, *110*, 37–67. https://doi.org/10.1016/j.actbio.2020.04.028

Zeng, W., Hui, H., Liu, Z., Chang, Z., Wang, M., He, B., & Hao, D. (2021). TPP ionically cross-linked chitosan/PLGA microspheres for the delivery of NGF for peripheral nerve system repair. *Carbohydrate Polymers*, *258*, 117684. https://doi.org/https://doi.org/10.1016/j.carbpol.2021.117684

Zhang, X., Cao, X., & Qi, P. (2020). Therapeutic contact lenses for ophthalmic drug delivery: major challenges. *Https://Doi.Org/10.1080/09205063.2020.1712175*, *31*(4), 549–560. https://doi.org/10.1080/09205063.2020.1712175

Zheng, X. Y., Choy, B. N. K., Zhou, M. M., & Zhao, Z. Y. (2021). Antibiotic Resistance Pattern of Staphylococcus Aureus Isolated From Pediatrics With Ocular Infections: A 6-Year Hospital-Based Study in China. *Frontiers in Pediatrics*, *9*, 1294. https://doi.org/10.3389/FPED.2021.728634/BIBTEX

Zhu, M., Wang, Y., Ferracci, G., Zheng, J., Cho, N.-J., & Lee, B. H. (2019). Gelatin methacryloyl and its hydrogels with an exceptional degree of controllability and batch-to-batch consistency. *Scientific Reports*, *9*(1), 6863. https://doi.org/10.1038/s41598-019-42186-x

Zimmerman, A. B., Nixon, A. D., & Rueff, E. M. (2016). Contact lens associated microbial keratitis: practical considerations for the optometrist. *Clinical Optometry*, *8*, 1–12. https://doi.org/10.2147/OPTO.S66424

Abud, T. B., Di Zazzo, A. Di, Kheirkhah, A., & Dana, R. (2017). Systemic immunomodulatory strategies in high-risk corneal transplantation. *Journal of Ophthalmic and Vision Research*, *12*(1), 81–92. https://doi.org/10.4103/2008-322X.200156

Al-Mujaini, A., Al-Kharusi, N., Thakral, A., & Wali, U. K. (2009). Bacterial keratitis: Perspective on epidemiology, Clinico-Pathogenesis, diagnosis and treatment. *Sultan Qaboos University Medical Journal*, *9*(2), 184–195.

Al-Shehri, A., Jastaneiah, S., & Wagoner, M. D. (2009). Changing trends in the clinical course and outcome of bacterial keratitis at King Khaled Eye Specialist Hospital. *International Ophthalmology*, *29*(3), 143–152. https://doi.org/10.1007/s10792-008-9206-6

Austin, A., Lietman, T., & Rose-Nussbaumer, J. (2017). Update on the management of infectious keratitis. *Ophthalmology*, *124*(11), 1678–1689.

Baranowski, P., Karolewicz, B., Gajda, M., & Pluta, J. (2014). Ophthalmic drug dosage forms: Characterisation and research methods. *The Scientific World Journal*, *2014*. https://doi.org/10.1155/2014/861904

Bartimote, C., Foster, J., & Watson, S. (2020). The Spectrum of Microbial Keratitis: An Updated Review. In *The Open Ophthalmology Journal* (Vol. 13, Issue 1). https://doi.org/10.2174/1874364101913010100

Bharathi, M. J., Ramakrishnan, R., Meenakshi, R., Padmavathy, S., Shivakumar, C., & Srinivasan, M. (2007). Microbial keratitis in South India: Influence of risk factors, climate, and geographical variation. *Ophthalmic Epidemiology*, *14*(2), 61–69. https://doi.org/10.1080/09286580601001347

Bharathi, M. J., Ramakrishnan, R., Vasu, S., Meenakshi, R., Shivkumar, C., & Palaniappan, R. (2003). Epidemiology of bacterial keratitis in a referral centre in south India. *Indian Journal of Medical Microbiology*, *21*(4), 239.

Bhatt, H., Kiran Rompicharla, S. V., Ghosh, B., & Biswas, S. (2019). α-Tocopherol Succinate-Anchored PEGylated Poly(amidoamine) Dendrimer for the Delivery of Paclitaxel: Assessment of in Vitro and in Vivo Therapeutic Efficacy [Research-article]. *Molecular Pharmaceutics*, *16*(4), 1541–1554. https://doi.org/10.1021/acs.molpharmaceut.8b01232

Bobde, Y., Biswas, S., & Ghosh, B. (2020a). Current trends in the development of HPMA-based block copolymeric nanoparticles for their application in drug delivery. *European*

Polymer Journal, *139*(September), 110018. https://doi.org/10.1016/j.eurpolymj.2020.110018

Bobde, Y., Biswas, S., & Ghosh, B. (2020b). PEGylated N-(2 hydroxypropyl) methacrylamide-doxorubicin conjugate as pH-responsive polymeric nanoparticles for cancer therapy. *Reactive and Functional Polymers*, *151*(March), 104561. https://doi.org/10.1016/j.reactfunctpolym.2020.104561

Bobde, Y., Patel, T., Paul, M., Biswas, S., & Ghosh, B. (2021). PEGylated N-(2 hydroxypropyl) methacrylamide polymeric micelles as nanocarriers for the delivery of doxorubicin in breast cancer. *Colloids and Surfaces B: Biointerfaces*, *204*(May), 111833. https://doi.org/10.1016/j.colsurfb.2021.111833

Cholkar, K., Patel, A., Dutt Vadlapudi, A., & K Mitra, A. (2012). Novel nanomicellar formulation approaches for anterior and posterior segment ocular drug delivery. *Recent Patents on Nanomedicine*, *2*(2), 82–95.

Choy, Y. Bin, Park, J. H., & Prausnitz, M. R. (2008). Mucoadhesive microparticles engineered for ophthalmic drug delivery. *Journal of Physics and Chemistry of Solids*, *69*(5–6), 1533–1536. https://doi.org/10.1016/j.jpcs.2007.10.043

Cooper, R. C., & Yang, H. (2019). Hydrogel-based ocular drug delivery systems: Emerging fabrication strategies, applications, and bench-to-bedside manufacturing considerations. *Journal of Controlled Release*, *306*(May), 29–39. https://doi.org/10.1016/j.jconrel.2019.05.034

da Silva, S. B., Ferreira, D., Pintado, M., & Sarmento, B. (2016). Chitosan-based nanoparticles for rosmarinic acid ocular delivery-In vitro tests. *International Journal of Biological Macromolecules*, *84*, 112–120. https://doi.org/10.1016/j.ijbiomac.2015.11.070

Eltis, M. (2011). Contact-lens-related microbial keratitis: Case report and review. *Journal of Optometry*, *4*(4), 122–127. https://doi.org/10.1016/S1888-4296(11)70053-X

Fleiszig, S. M. J. (2006). The Glenn A. Fry award lecture 2005. The pathogenesis of contact lens-related keratitis. *Optometry and Vision Science : Official Publication of the American Academy of Optometry*, *83*(12), 866–873.

Goldstein, M. H., Kowalski, R. P., & Gordon, Y. J. (1999). Emerging fluoroquinolone resistance in bacterial keratitis: a 5-year review. *Ophthalmology*, *106*(7), 1213–1318.

Han, H., Gao, Y., Chai, M., Zhang, X., Liu, S., Huang, Y., Jin, Q., Grzybowski, A., Ji, J., & Yao, K. (2020). Biofilm microenvironment activated supramolecular nanoparticles for enhanced photodynamic therapy of bacterial keratitis. *Journal of Controlled Release*, *327*(May), 676–687. https://doi.org/10.1016/j.jconrel.2020.09.014

Hanet, M. S., Jamart, J., & Chaves, A. P. (2012). Fluoroquinolones or fortified antibiotics for treating bacterial keratitis: Systematic review and meta-analysis of comparative studies. *Canadian Journal of Ophthalmology*, *47*(6), 493–499. https://doi.org/10.1016/j.jcjo.2012.09.001

Henderson, E., Lee, B. H., Cui, Z., McLemore, R., Brandon, T. A., & Vernon, B. L. (2009). In vivo evaluation of injectable thermosensitive polymer with time-dependent LCST.

Journal of Biomedical Materials Research - Part A, *90*(4), 1186–1197. https://doi.org/10.1002/jbm.a.32179

Hsiao, C. H., Sun, C. C., Yeh, L. K., Ma, D. K. H., Chen, P. Y. F., Lin, H. C., Tan, H. Y., Chen, H. C., Chen, S. Y., & Huang, Y. C. (2016). Shifting trends in bacterial keratitis in Taiwan: A 10-year review in a tertiary-care hospital. *Cornea*, *35*(3), 313–317. https://doi.org/10.1097/ICO.0000000000000734

Keratitis, M., Keratitis, P. U., & Hamrah, P. (2000). Twenty-five – Year Panorama of Corneal Immunology Emerging Concepts in the Immunopathogenesis of. *Cornea*, *19*(5), 625–643.

Kumari, P., Muddineti, O. S., Rompicharla, S. V. K., Ghanta, P., Adithya, K. B. B. N., Ghosh, B., & Biswas, S. (2017). Cholesterol-conjugated poly(D, L-lactide)-based micelles as a nanocarrier system for effective delivery of curcumin in cancer therapy. *Drug Delivery*, *24*(1), 209–223. https://doi.org/10.1080/10717544.2016.1245365

Kumari, P., Paul, M., Bobde, Y., Soniya, K., Kiran Rompicharla, S. V., Ghosh, B., & Biswas, S. (2020). Albumin-based lipoprotein nanoparticles for improved delivery and anticancer activity of curcumin for cancer treatment. *Nanomedicine*, *15*(29), 2851–2869. https://doi.org/10.2217/nnm-2020-0232

Kumbham, S., Paul, M., Bhatt, H., Ghosh, B., & Biswas, S. (2020). Oleanolic acid-conjugated poly (D, L-lactide)-based micelles for effective delivery of doxorubicin and combination chemotherapy in oral cancer. *Journal of Molecular Liquids*, *320*, 114389. https://doi.org/10.1016/j.molliq.2020.114389

Laulicht, B., Mancini, A., Geman, N., Cho, D., Estrellas, K., Furtado, S., Hopson, R., Tripathi, A., & Mathiowitz, E. (2012). Bioinspired Bioadhesive Polymers: Dopa-Modified Poly(acrylic acid) Derivatives. *Macromolecular Bioscience*, *12*(11), 1555–1565. https://doi.org/10.1002/mabi.201200179

Levitt, A. E., Galor, A., Weiss, J. S., Felix, E. R., Martin, E. R., Patin, D. J., Sarantopoulos, K. D., & Levitt, R. C. (2015). Chronic dry eye symptoms after LASIK: Parallels and lessons to be learned from other persistent post-operative pain disorders. *Molecular Pain*, *11*(1), 1–12. https://doi.org/10.1186/s12990-015-0020-7

Malekinejad, H., Bazargani-Gilani, B., Tukmechi, A., & Ebrahimi, H. (2012). A cytotoxicity and comparative antibacterial study on the effect of Zataria multiflora Boiss, Trachyspermum copticum essential oils, and Enrofloxacin on Aeromonas hydrophila. *Avicenna Journal of Phytomedicine*, *2*(4), 188–195. https://doi.org/10.22038/ajp.2012.108

Marquart, M. E., & O'Callaghan, R. J. (2013). Infectious keratitis: Secreted bacterial proteins that mediate corneal damage. *Journal of Ophthalmology*, *2013*. https://doi.org/10.1155/2013/369094

Mascarenhas, J., Lalitha, P., Prajna, N. V., Srinivasan, M., Das, M., D'Silva, S. S., Oldenburg, C. E., Borkar, D. S., Esterberg, E. J., Lietman, T. M., & Keenan, J. D. (2014). Acanthamoeba, fungal, and bacterial keratitis: A comparison of risk factors and clinical features. *American Journal of Ophthalmology*, *157*(1), 56–62. https://doi.org/10.1016/j.ajo.2013.08.032

Meng, T., Kulkarni, V., Simmers, R., Brar, V., & Xu, Q. (2019). Therapeutic implications of nanomedicine for ocular drug delivery. *Drug Discovery Today*, *24*(8), 1524–1538. https://doi.org/10.1016/j.drudis.2019.05.006

Omerović, N., & Vranić, E. (2020). Application of nanoparticles in ocular drug delivery systems. *Health and Technology*, *10*(1), 61–78. https://doi.org/10.1007/s12553-019-00381-w

Ou, F., McGoverin, C., Swift, S., & Vanholsbeeck, F. (2019). Rapid and cost-effective evaluation of bacterial viability using fluorescence spectroscopy. *Analytical and Bioanalytical Chemistry*, *411*(16), 3653–3663. https://doi.org/10.1007/s00216-019-01848-5

Patel, P. B., Shastri, D. H., Shelat, P. K., & Shukla, A. K. (2010). Ophthalmic drug delivery system: Challenges and approaches. *Systematic Reviews in Pharmacy*, *1*(2), 113–120. https://doi.org/10.4103/0975-8453.75042

Reimondez-Troitiño, S., Csaba, N., Alonso, M. J., & De La Fuente, M. (2015). Nanotherapies for the treatment of ocular diseases. *European Journal of Pharmaceutics and Biopharmaceutics*, *95*, 279–293. https://doi.org/10.1016/j.ejpb.2015.02.019

Schaefer, F., Bruttin, O., Zografos, L., & Guex-Crosier, Y. (2001). Bacterial keratitis: a prospective clinical and microbiological study. *British Journal of Ophthalmology*, *85*(7), 842–847.

Sharma, P., Elofsson, M., & Roy, S. (2020). Attenuation of Pseudomonas aeruginosa infection by INP0341, a salicylidene acylhydrazide, in a murine model of keratitis. *Virulence*, *11*(1), 795–804. https://doi.org/10.1080/21505594.2020.1776979

Singh, P., Tyagi, M., Kumar, Y., Gupta, K. K., & Sharma, P. D. (2013). Ocular chemical injuries and their management. *Oman Journal of Ophthalmology*, *6*(2), 83.

Singh, S. B., Young, K., & Silver, L. L. (2017). What is an "ideal" antibiotic? Discovery challenges and path forward. *Biochemical Pharmacology*, *133*, 63–73. https://doi.org/10.1016/j.bcp.2017.01.003

Taylor, H. R., West, S. K., Rosenthal, F. S., Munoz, B., Newland, H. S., & Emmett, E. A. (1989). Corneal changes associated with chronic UV irradiation. *Archives of Ophthalmology*, *107*(10), 1481–1484.

Thibodeaux, B. A., Dajcs, J. J., Caballero, A. R., Marquart, M. E., Girgis, D. O., & O'Callaghan, R. J. (2004). Quantitative comparison of fluoroquinolone therapies of experimental Gram-negative bacterial keratitis. *Current Eye Research*, *28*(5), 337–342. https://doi.org/10.1076/ceyr.28.5.337.28676

Varela-Fernández, R., Díaz-Tomé, V., Luaces-Rodríguez, A., Conde-Penedo, A., García-Otero, X., Luzardo-álvarez, A., Fernández-Ferreiro, A., & Otero-Espinar, F. J. (2020). Drug delivery to the posterior segment of the eye: Biopharmaceutic and pharmacokinetic considerations. *Pharmaceutics*, *12*(3), 1–39. https://doi.org/10.3390/pharmaceutics12030269

Wong, R. L. M., Gangwani, R. A., Yu, L. W. H., & Lai, J. S. M. (2012). New treatments for bacterial keratitis. *Journal of Ophthalmology*, *2012*.

Abud, T. B., Di Zazzo, A. Di, Kheirkhah, A., & Dana, R. (2017). Systemic immunomodulatory strategies in high-risk corneal transplantation. *Journal of Ophthalmic and Vision Research*, *12*(1), 81–92. https://doi.org/10.4103/2008-322X.200156

Al-Mujaini, A., Al-Kharusi, N., Thakral, A., & Wali, U. K. (2009). Bacterial keratitis: Perspective on epidemiology, Clinico-Pathogenesis, diagnosis and treatment. *Sultan Qaboos University Medical Journal*, *9*(2), 184–195.

Al-Shehri, A., Jastaneiah, S., & Wagoner, M. D. (2009). Changing trends in the clinical course and outcome of bacterial keratitis at King Khaled Eye Specialist Hospital. *International Ophthalmology*, *29*(3), 143–152. https://doi.org/10.1007/s10792-008-9206-6

Austin, A., Lietman, T., & Rose-Nussbaumer, J. (2017). Update on the management of infectious keratitis. *Ophthalmology*, *124*(11), 1678–1689.

Baranowski, P., Karolewicz, B., Gajda, M., & Pluta, J. (2014). Ophthalmic drug dosage forms: Characterisation and research methods. *The Scientific World Journal*, *2014*. https://doi.org/10.1155/2014/861904

Bartimote, C., Foster, J., & Watson, S. (2020). The Spectrum of Microbial Keratitis: An Updated Review. In *The Open Ophthalmology Journal* (Vol. 13, Issue 1). https://doi.org/10.2174/1874364101913010100

Bharathi, M. J., Ramakrishnan, R., Meenakshi, R., Padmavathy, S., Shivakumar, C., & Srinivasan, M. (2007). Microbial keratitis in South India: Influence of risk factors, climate, and geographical variation. *Ophthalmic Epidemiology*, *14*(2), 61–69. https://doi.org/10.1080/09286580601001347

Bharathi, M. J., Ramakrishnan, R., Vasu, S., Meenakshi, R., Shivkumar, C., & Palaniappan, R. (2003). Epidemiology of bacterial keratitis in a referral centre in south India. *Indian Journal of Medical Microbiology*, *21*(4), 239.

Bhatt, H., Kiran Rompicharla, S. V., Ghosh, B., & Biswas, S. (2019). α-Tocopherol Succinate-Anchored PEGylated Poly(amidoamine) Dendrimer for the Delivery of Paclitaxel: Assessment of in Vitro and in Vivo Therapeutic Efficacy [Research-article]. *Molecular Pharmaceutics*, *16*(4), 1541–1554. https://doi.org/10.1021/acs.molpharmaceut.8b01232

Bobde, Y., Biswas, S., & Ghosh, B. (2020a). Current trends in the development of HPMA-based block copolymeric nanoparticles for their application in drug delivery. *European Polymer Journal*, *139*(September), 110018. https://doi.org/10.1016/j.eurpolymj.2020.110018

Bobde, Y., Biswas, S., & Ghosh, B. (2020b). PEGylated N-(2 hydroxypropyl) methacrylamide-doxorubicin conjugate as pH-responsive polymeric nanoparticles for cancer therapy. *Reactive and Functional Polymers*, *151*(March), 104561. https://doi.org/10.1016/j.reactfunctpolym.2020.104561

Bobde, Y., Patel, T., Paul, M., Biswas, S., & Ghosh, B. (2021). PEGylated N-(2 hydroxypropyl) methacrylamide polymeric micelles as nanocarriers for the delivery of doxorubicin in breast cancer. *Colloids and Surfaces B: Biointerfaces*, *204*(May), 111833. https://doi.org/10.1016/j.colsurfb.2021.111833

Cholkar, K., Patel, A., Dutt Vadlapudi, A., & K Mitra, A. (2012). Novel nanomicellar formulation approaches for anterior and posterior segment ocular drug delivery. *Recent Patents on Nanomedicine*, *2*(2), 82–95.

Choy, Y. Bin, Park, J. H., & Prausnitz, M. R. (2008). Mucoadhesive microparticles engineered for ophthalmic drug delivery. *Journal of Physics and Chemistry of Solids*, *69*(5–6), 1533–1536. https://doi.org/10.1016/j.jpcs.2007.10.043

Cooper, R. C., & Yang, H. (2019). Hydrogel-based ocular drug delivery systems: Emerging fabrication strategies, applications, and bench-to-bedside manufacturing considerations. *Journal of Controlled Release*, *306*(May), 29–39. https://doi.org/10.1016/j.jconrel.2019.05.034

da Silva, S. B., Ferreira, D., Pintado, M., & Sarmento, B. (2016). Chitosan-based nanoparticles for rosmarinic acid ocular delivery-In vitro tests. *International Journal of Biological Macromolecules*, *84*, 112–120. https://doi.org/10.1016/j.ijbiomac.2015.11.070

Eltis, M. (2011). Contact-lens-related microbial keratitis: Case report and review. *Journal of Optometry*, *4*(4), 122–127. https://doi.org/10.1016/S1888-4296(11)70053-X

Fleiszig, S. M. J. (2006). The Glenn A. Fry award lecture 2005. The pathogenesis of contact lens-related keratitis. *Optometry and Vision Science : Official Publication of the American Academy of Optometry*, *83*(12), 866–873.

Goldstein, M. H., Kowalski, R. P., & Gordon, Y. J. (1999). Emerging fluoroquinolone resistance in bacterial keratitis: a 5-year review. *Ophthalmology*, *106*(7), 1213–1318.

Han, H., Gao, Y., Chai, M., Zhang, X., Liu, S., Huang, Y., Jin, Q., Grzybowski, A., Ji, J., & Yao, K. (2020). Biofilm microenvironment activated supramolecular nanoparticles for enhanced photodynamic therapy of bacterial keratitis. *Journal of Controlled Release*, *327*(May), 676–687. https://doi.org/10.1016/j.jconrel.2020.09.014

Hanet, M. S., Jamart, J., & Chaves, A. P. (2012). Fluoroquinolones or fortified antibiotics for treating bacterial keratitis: Systematic review and meta-analysis of comparative studies. *Canadian Journal of Ophthalmology*, *47*(6), 493–499. https://doi.org/10.1016/j.jcjo.2012.09.001

Henderson, E., Lee, B. H., Cui, Z., McLemore, R., Brandon, T. A., & Vernon, B. L. (2009). In vivo evaluation of injectable thermosensitive polymer with time-dependent LCST. *Journal of Biomedical Materials Research - Part A*, *90*(4), 1186–1197. https://doi.org/10.1002/jbm.a.32179

Hsiao, C. H., Sun, C. C., Yeh, L. K., Ma, D. K. H., Chen, P. Y. F., Lin, H. C., Tan, H. Y., Chen, H. C., Chen, S. Y., & Huang, Y. C. (2016). Shifting trends in bacterial keratitis in Taiwan: A 10-year review in a tertiary-care hospital. *Cornea*, *35*(3), 313–317. https://doi.org/10.1097/ICO.0000000000000734

Keratitis, M., Keratitis, P. U., & Hamrah, P. (2000). Twenty-five – Year Panorama of Corneal Immunology Emerging Concepts in the Immunopathogenesis of. *Cornea*, *19*(5), 625–643.

Kumari, P., Muddineti, O. S., Rompicharla, S. V. K., Ghanta, P., Adithya, K. B. B. N., Ghosh, B., & Biswas, S. (2017). Cholesterol-conjugated poly(D, L-lactide)-based micelles as a nanocarrier system for effective delivery of curcumin in cancer therapy. *Drug Delivery*, *24*(1), 209–223. https://doi.org/10.1080/10717544.2016.1245365

Kumari, P., Paul, M., Bobde, Y., Soniya, K., Kiran Rompicharla, S. V., Ghosh, B., & Biswas, S. (2020). Albumin-based lipoprotein nanoparticles for improved delivery and anticancer activity of curcumin for cancer treatment. *Nanomedicine*, *15*(29), 2851–2869. https://doi.org/10.2217/nnm-2020-0232

Kumbham, S., Paul, M., Bhatt, H., Ghosh, B., & Biswas, S. (2020). Oleanolic acid-conjugated poly (D, L-lactide)-based micelles for effective delivery of doxorubicin and combination chemotherapy in oral cancer. *Journal of Molecular Liquids*, *320*, 114389. https://doi.org/10.1016/j.molliq.2020.114389

Laulicht, B., Mancini, A., Geman, N., Cho, D., Estrellas, K., Furtado, S., Hopson, R., Tripathi, A., & Mathiowitz, E. (2012). Bioinspired Bioadhesive Polymers: Dopa-Modified Poly(acrylic acid) Derivatives. *Macromolecular Bioscience*, *12*(11), 1555–1565. https://doi.org/10.1002/mabi.201200179

Levitt, A. E., Galor, A., Weiss, J. S., Felix, E. R., Martin, E. R., Patin, D. J., Sarantopoulos, K. D., & Levitt, R. C. (2015). Chronic dry eye symptoms after LASIK: Parallels and lessons to be learned from other persistent post-operative pain disorders. *Molecular Pain*, *11*(1), 1–12. https://doi.org/10.1186/s12990-015-0020-7

Malekinejad, H., Bazargani-Gilani, B., Tukmechi, A., & Ebrahimi, H. (2012). A cytotoxicity and comparative antibacterial study on the effect of Zataria multiflora Boiss, Trachyspermum copticum essential oils, and Enrofloxacin on Aeromonas hydrophila. *Avicenna Journal of Phytomedicine*, *2*(4), 188–195. https://doi.org/10.22038/ajp.2012.108

Marquart, M. E., & O'Callaghan, R. J. (2013). Infectious keratitis: Secreted bacterial proteins that mediate corneal damage. *Journal of Ophthalmology*, *2013*. https://doi.org/10.1155/2013/369094

Mascarenhas, J., Lalitha, P., Prajna, N. V., Srinivasan, M., Das, M., D'Silva, S. S., Oldenburg, C. E., Borkar, D. S., Esterberg, E. J., Lietman, T. M., & Keenan, J. D. (2014). Acanthamoeba, fungal, and bacterial keratitis: A comparison of risk factors and clinical features. *American Journal of Ophthalmology*, *157*(1), 56–62. https://doi.org/10.1016/j.ajo.2013.08.032

Meng, T., Kulkarni, V., Simmers, R., Brar, V., & Xu, Q. (2019). Therapeutic implications of nanomedicine for ocular drug delivery. *Drug Discovery Today*, *24*(8), 1524–1538. https://doi.org/10.1016/j.drudis.2019.05.006

Omerović, N., & Vranić, E. (2020). Application of nanoparticles in ocular drug delivery systems. *Health and Technology*, *10*(1), 61–78. https://doi.org/10.1007/s12553-019-00381-w

Ou, F., McGoverin, C., Swift, S., & Vanholsbeeck, F. (2019). Rapid and cost-effective evaluation of bacterial viability using fluorescence spectroscopy. *Analytical and Bioanalytical Chemistry*, *411*(16), 3653–3663. https://doi.org/10.1007/s00216-019-01848-5

Patel, P. B., Shastri, D. H., Shelat, P. K., & Shukla, A. K. (2010). Ophthalmic drug delivery system: Challenges and approaches. *Systematic Reviews in Pharmacy*, *1*(2), 113–120. https://doi.org/10.4103/0975-8453.75042

Reimondez-Troitiño, S., Csaba, N., Alonso, M. J., & De La Fuente, M. (2015). Nanotherapies for the treatment of ocular diseases. *European Journal of Pharmaceutics and Biopharmaceutics*, *95*, 279–293. https://doi.org/10.1016/j.ejpb.2015.02.019

Schaefer, F., Bruttin, O., Zografos, L., & Guex-Crosier, Y. (2001). Bacterial keratitis: a prospective clinical and microbiological study. *British Journal of Ophthalmology*, *85*(7), 842–847.

Sharma, P., Elofsson, M., & Roy, S. (2020). Attenuation of Pseudomonas aeruginosa infection by INP0341, a salicylidene acylhydrazide, in a murine model of keratitis. *Virulence*, *11*(1), 795–804. https://doi.org/10.1080/21505594.2020.1776979

Singh, P., Tyagi, M., Kumar, Y., Gupta, K. K., & Sharma, P. D. (2013). Ocular chemical injuries and their management. *Oman Journal of Ophthalmology*, *6*(2), 83.

Singh, S. B., Young, K., & Silver, L. L. (2017). What is an "ideal" antibiotic? Discovery challenges and path forward. *Biochemical Pharmacology*, *133*, 63–73. https://doi.org/10.1016/j.bcp.2017.01.003

Taylor, H. R., West, S. K., Rosenthal, F. S., Munoz, B., Newland, H. S., & Emmett, E. A. (1989). Corneal changes associated with chronic UV irradiation. *Archives of Ophthalmology*, *107*(10), 1481–1484.

Thibodeaux, B. A., Dajcs, J. J., Caballero, A. R., Marquart, M. E., Girgis, D. O., & O'Callaghan, R. J. (2004). Quantitative comparison of fluoroquinolone therapies of experimental Gram-negative bacterial keratitis. *Current Eye Research*, *28*(5), 337–342. https://doi.org/10.1076/ceyr.28.5.337.28676

Varela-Fernández, R., Díaz-Tomé, V., Luaces-Rodríguez, A., Conde-Penedo, A., García-Otero, X., Luzardo-álvarez, A., Fernández-Ferreiro, A., & Otero-Espinar, F. J. (2020). Drug delivery to the posterior segment of the eye: Biopharmaceutic and pharmacokinetic considerations. *Pharmaceutics*, *12*(3), 1–39. https://doi.org/10.3390/pharmaceutics12030269

Wong, R. L. M., Gangwani, R. A., Yu, L. W. H., & Lai, J. S. M. (2012). New treatments for bacterial keratitis. *Journal of Ophthalmology*, *2012*.

Ahmed, S., Amin, M. M., El-Korany, S. M., & Sayed, S. (2022). Corneal targeted fenticonazole nitrate-loaded novasomes for the management of ocular candidiasis: Preparation, in vitro characterization, ex vivo and in vivo assessments.

Https://Doi.Org/10.1080/10717544.2022.2103600, *29*(1), 2428–2441. https://doi.org/10.1080/10717544.2022.2103600

Ahn, M., Yoon, K. C., Ryu, S. K., Cho, N. C., & You, I. C. (2011). Clinical aspects and prognosis of mixed microbial (bacterial and fungal) keratitis. *Cornea*, *30*(4), 409–413. https://doi.org/10.1097/ICO.0B013E3181F23704

Alexandrakis, G., Alfonso, E. C., & Miller, D. (2000). Shifting trends in bacterial keratitis in South Florida and emerging resistance to fluoroquinolones. *Ophthalmology*, *107*(8), 1497–1502. https://doi.org/10.1016/S0161-6420(00)00179-2

Analysis of the risk factors predisposing to fungal, bacteri... : Indian Journal of Medical Research. (n.d.). Retrieved April 17, 2023, from https://journals.lww.com/ijmr/Abstract/2009/30060/Analysis_of_the_risk_factors_predisposing_to.15.aspx

Blondeau, J. M. (2004). Fluoroquinolones: mechanism of action, classification, and development of resistance. *Survey of Ophthalmology*, *49*(2), S73–S78. https://doi.org/10.1016/J.SURVOPHTHAL.2004.01.005

Cafaggi, S., Russo, E., Stefani, R., Leardi, R., Caviglioli, G., Parodi, B., Bignardi, G., De Totero, D., Aiello, C., & Viale, M. (2007). Preparation and evaluation of nanoparticles made of chitosan or N-trimethyl chitosan and a cisplatin–alginate complex. *Journal of Controlled Release*, *121*(1–2), 110–123. https://doi.org/10.1016/J.JCONREL.2007.05.037

Ch, S., Mishra, P., Bhatt, H., Ghosh, B., Roy, S., & Biswas, S. (2021). Hydroxypropyl methacrylamide-based copolymeric nanoparticles loaded with moxifloxacin as a mucoadhesive, cornea-penetrating nanomedicine eye drop with enhanced therapeutic benefits in bacterial keratitis. *Colloids and Surfaces B: Biointerfaces*, *208*, 112113. https://doi.org/10.1016/J.COLSURFB.2021.112113

Ch, S., Padaga, S. G., Ghosh, B., Roy, S., & Biswas, S. (2023). Chitosan-poly(lactide-co-glycolide)/poloxamer mixed micelles as a mucoadhesive thermo-responsive moxifloxacin eye drop to improve treatment efficacy in bacterial keratitis. *Carbohydrate Polymers*, *312*, 120822. https://doi.org/10.1016/J.CARBPOL.2023.120822

Desai, A., Shukla, M., Maulvi, F., & Ranch, K. (2020). Ophthalmic and otic drug administration: Novel approaches and challenges. *Novel Drug Delivery Technologies: Innovative Strategies for Drug Re-Positioning*, 335–381. https://doi.org/10.1007/978-981-13-3642-3_10/COVER

Doi, R., & Kokufuta, E. (2011). Conductometric and light scattering studies on the complexation between cationic polyelectrolyte nanogel and anionic polyion. *Langmuir*, *27*(1), 392–398. https://doi.org/10.1021/LA1037519/ASSET/IMAGES/LARGE/LA-2010-037519_0007.JPEG

Dubashynskaya, N., Poshina, D., Raik, S., Urtti, A., & Skorik, Y. A. (2019). Polysaccharides in Ocular Drug Delivery. *Pharmaceutics 2020, Vol. 12, Page 22*, *12*(1), 22. https://doi.org/10.3390/PHARMACEUTICS12010022

Elsayed, I., & Sayed, S. (2017). Tailored nanostructured platforms for boosting transcorneal permeation: Box–Behnken statistical optimization, comprehensive in vitro, ex vivo

and in vivo characterization. *International Journal of Nanomedicine*, *12*, 7947–7962. https://doi.org/10.2147/IJN.S150366

Fisher, L. M., Heaton, V. J., Smith, H. J., Nichol, K. A., Hoban, D. J., & Zhanel, G. G. (2003). Dual activity of fluoroquinolones against Streptococcus pneumoniae. *Journal of Antimicrobial Chemotherapy*, *51*(2), 463–464. https://doi.org/10.1093/JAC/DKG059

Fleiszig, S. M. J., & Evans, D. J. (2021). The pathogenesis of bacterial keratitis: studies with Pseudomonas aeruginosa. *Https://Doi.Org/10.1111/j.1444-0938.2002.Tb03082.x*, *85*(5), 271–278. https://doi.org/10.1111/J.1444-0938.2002.TB03082.X

Friess, W. (1998). Collagen – biomaterial for drug delivery. *European Journal of Pharmaceutics and Biopharmaceutics*, *45*(2), 113–136. https://doi.org/10.1016/S0939-6411(98)00017-4

Goldstein, M. H., Kowalski, R. P., & Gordon, Y. J. (1999). Emerging fluoroquinolone resistance in bacterial keratitis: A 5-year review. *Ophthalmology*, *106*(7), 1213–1318. https://doi.org/10.1016/S0161-6420(99)00716-2

Grassiri, B., Zambito, Y., & Bernkop-Schnürch, A. (2021). Strategies to prolong the residence time of drug delivery systems on ocular surface. *Advances in Colloid and Interface Science*, *288*, 102342. https://doi.org/10.1016/J.CIS.2020.102342

Itoo, A. M., Paul, M., Ghosh, B., & Biswas, S. (2022). Oxaliplatin delivery via chitosan/vitamin E conjugate micelles for improved efficacy and MDR-reversal in breast cancer. *Carbohydrate Polymers*, *282*, 119108. https://doi.org/10.1016/J.CARBPOL.2022.119108

Jalaja, K., Naskar, D., Kundu, S. C., & James, N. R. (2015). Fabrication of cationized gelatin nanofibers by electrospinning for tissue regeneration. *RSC Advances*, *5*(109), 89521–89530. https://doi.org/10.1039/C5RA10384C

Jones, D. B. (1981). Decision-making in the Management of Microbial Keratitis. *Ophthalmology*, *88*(8), 814–820. https://doi.org/10.1016/S0161-6420(81)34943-4

Kumbham, S., Paul, M., Itoo, A., Ghosh, B., & Biswas, S. (2022). Oleanolic acid-conjugated human serum albumin nanoparticles encapsulating doxorubicin as synergistic combination chemotherapy in oropharyngeal carcinoma and melanoma. *International Journal of Pharmaceutics*, *614*, 121479. https://doi.org/10.1016/J.IJPHARM.2022.121479

Li, Y., Jia, H., Cheng, Q., Pan, F., & Jiang, Z. (2011). Sodium alginate–gelatin polyelectrolyte complex membranes with both high water vapor permeance and high permselectivity. *Journal of Membrane Science*, *375*(1–2), 304–312. https://doi.org/10.1016/J.MEMSCI.2011.03.058

Limberg, M. B. (1991). A review of bacterial keratitis and bacterial conjunctivitis. *American Journal of Ophthalmology*, *112*(4 Suppl), 2S-9S. https://europepmc.org/article/med/1928269

Mahor, A., Prajapati, S. K., Verma, A., Gupta, R., Iyer, A. K., & Kesharwani, P. (2016). Moxifloxacin loaded gelatin nanoparticles for ocular delivery: Formulation and in-vitro, in-

vivo evaluation. *Journal of Colloid and Interface Science*, *483*, 132–138. https://doi.org/10.1016/J.JCIS.2016.08.018

Maulvi, F. A., Shetty, K. H., Desai, D. T., Shah, D. O., & Willcox, M. D. P. (2021). Recent advances in ophthalmic preparations: Ocular barriers, dosage forms and routes of administration. *International Journal of Pharmaceutics*, *608*, 121105. https://doi.org/10.1016/J.IJPHARM.2021.121105

Pestova, E., Millichap, J. J., Noskin, G. A., & Peterson, L. R. (2000). Intracellular targets of moxifloxacin: a comparison with other fluoroquinolones. *Journal of Antimicrobial Chemotherapy*, *45*(5), 583–590. https://doi.org/10.1093/JAC/45.5.583

Račić, A., & Krajišnik, D. (2023). Biopolymers in Mucoadhesive Eye Drops for Treatment of Dry Eye and Allergic Conditions: Application and Perspectives. *Pharmaceutics 2023, Vol. 15, Page 470*, *15*(2), 470. https://doi.org/10.3390/PHARMACEUTICS15020470

Rodríguez, I., Vázquez, J. A., Pastrana, L., & Khutoryanskiy, V. V. (2017). Enhancement and inhibition effects on the corneal permeability of timolol maleate: Polymers, cyclodextrins and chelating agents. *International Journal of Pharmaceutics*, *529*(1–2), 168–177. https://doi.org/10.1016/J.IJPHARM.2017.06.075

Sæther, H. V., Holme, H. K., Maurstad, G., Smidsrød, O., & Stokke, B. T. (2008). Polyelectrolyte complex formation using alginate and chitosan. *Carbohydrate Polymers*, *74*(4), 813–821. https://doi.org/10.1016/J.CARBPOL.2008.04.048

Sarika, P. R., & James, N. R. (2016). Polyelectrolyte complex nanoparticles from cationised gelatin and sodium alginate for curcumin delivery. *Carbohydrate Polymers*, *148*, 354–361. https://doi.org/10.1016/J.CARBPOL.2016.04.073

Sarmento, B., Ribeiro, A., Veiga, F., Sampaio, P., Neufeld, R., & Ferreira, D. (2007). Alginate/chitosan nanoparticles are effective for oral insulin delivery. *Pharmaceutical Research*, *24*(12), 2198–2206. https://doi.org/10.1007/S11095-007-9367-4/FIGURES/5

Shinde, U. A., & Nagarsenker, M. S. (2009). Characterization of Gelatin-Sodium Alginate Complex Coacervation System. *Indian Journal of Pharmaceutical Sciences*, *71*(3), 313. https://doi.org/10.4103/0250-474X.56033

Souto, E. B., Dias-Ferreira, J., López-Machado, A., Ettcheto, M., Cano, A., Espuny, A. C., Espina, M., Garcia, M. L., & Sánchez-López, E. (2019). Advanced Formulation Approaches for Ocular Drug Delivery: State-Of-The-Art and Recent Patents. *Pharmaceutics 2019, Vol. 11, Page 460*, *11*(9), 460. https://doi.org/10.3390/PHARMACEUTICS11090460

Stapleton, F., Edwards, K., Keay, L., Naduvilath, T., Dart, J. K. G., Brian, G., & Holden, B. (2012). Risk Factors for Moderate and Severe Microbial Keratitis in Daily Wear Contact Lens Users. *Ophthalmology*, *119*(8), 1516–1521. https://doi.org/10.1016/J.OPHTHA.2012.01.052

Szekalska, M., Wróblewska, M., Czajkowska-Kośnik, A., Sosnowska, K., Misiak, P., Wilczewska, A. Z., & Winnicka, K. (2023). The Spray-Dried Alginate/Gelatin Microparticles with Luliconazole as Mucoadhesive Drug Delivery System. *Materials*, *16*(1). https://doi.org/10.3390/MA16010403/S1

Tseng, C. L., Chen, K. H., Su, W. Y., Lee, Y. H., Wu, C. C., & Lin, F. H. (2013). Cationic gelatin nanoparticles for drug delivery to the ocular surface: In vitro and in vivo evaluation. *Journal of Nanomaterials*, *2013*. https://doi.org/10.1155/2013/238351

Vysyaraju, N. R., Paul, M., Ch, S., Ghosh, B., & Biswas, S. (2022). Olaparib@human serum albumin nanoparticles as sustained drug-releasing tumour-targeting nanomedicine to inhibit growth and metastasis in the mouse model of triple-negative breast cancer. *Https://Doi.Org/10.1080/1061186X.2022.2092623*, *30*(10), 1088–1105. https://doi.org/10.1080/1061186X.2022.2092623

Wen, Y., Yu, B., Zhu, Z., Yang, Z., & Shao, W. (2020). Synthesis of Antibacterial Gelatin/Sodium Alginate Sponges and Their Antibacterial Activity. *Polymers*, *12*(9). https://doi.org/10.3390/POLYM12091926

Wong, R. L. M., Gangwani, R. A., Yu, L. W. H., & Lai, J. S. M. (2012). New treatments for bacterial keratitis. *Journal of Ophthalmology*, *2012*. https://doi.org/10.1155/2012/831502

Yermak, I. M., Davydova, V. N., & Volod'ko, A. V. (2022). Mucoadhesive Marine Polysaccharides. *Marine Drugs 2022, Vol. 20, Page 522*, *20*(8), 522. https://doi.org/10.3390/MD20080522

Ajdary, R., Tardy, B. L., Mattos, B. D., Bai, L., & Rojas, O. J. (2021). Plant Nanomaterials and Inspiration from Nature: Water Interactions and Hierarchically Structured Hydrogels. *Advanced Materials*, *33*(28), 2001085. https://doi.org/https://doi.org/10.1002/adma.202001085

Al-Mujaini, A., Al-Kharusi, N., Thakral, A., & Wali, U. K. (2009). *Bacterial Keratitis: Perspective on Epidemiology, Clinico-Pathogenesis, Diagnosis and Treatment* *ية، ا لتشخيصية ،اخلروصي أركانا ،ثاكرال أوبيندار والي وا لعالجية ا لتهاب ا لقر نية اجلرثومي: أألبعاد ا لوبا ،ئية املرضية ا لسر ير* .(Vol. 9, Issue 2). Epub *نادية ،اجمليني اهلل عبد*

An, J., Yuan, X., Luo, Q., & Wang, D. (2010). Preparation of chitosan-graft-(methyl methacrylate)/Ag nanocomposite with antimicrobial activity. *Polymer International*, *59*(1), 62–70. https://doi.org/https://doi.org/10.1002/pi.2689

Austin, A., Lietman, T., & Rose-Nussbaumer, J. (2017). Update on the Management of Infectious Keratitis. *Ophthalmology*, *124*(11), 1678–1689. https://doi.org/https://doi.org/10.1016/j.ophtha.2017.05.012

Baniasadi, H., Madani, Z., Ajdary, R., Rojas, O. J., & Seppälä, J. (2021). Ascorbic acid-loaded polyvinyl alcohol/cellulose nanofibril hydrogels as precursors for 3D printed materials. *Materials Science and Engineering C*, *130*. https://doi.org/10.1016/j.msec.2021.112424

Baniasadi, H., Polez, R. T., Kimiaei, E., Madani, Z., Rojas, O. J., Österberg, M., & Seppälä, J. (2021). 3D printing and properties of cellulose nanofibrils-reinforced quince seed mucilage bio-inks. *International Journal of Biological Macromolecules*, *192*, 1098–1107. https://doi.org/https://doi.org/10.1016/j.ijbiomac.2021.10.078

Baranowski, P., Karolewicz, B., Gajda, M., & Pluta, J. (2014). Ophthalmic Drug Dosage Forms: Characterisation and Research Methods. *The Scientific World Journal*, *2014*, 861904. https://doi.org/10.1155/2014/861904

Bialasiewicz, A., Shenoy, R., Thakral, A., Al-Muniri, A. A., Shenoy, U., & Al-Mughairi, Z. (2006). Mikrobielle Keratitis. *Der Ophthalmologe*, *103*(8), 682–687. https://doi.org/10.1007/s00347-006-1363-2

Bourcier, T., Thomas, F., Borderie, V., Chaumeil, C., & Laroche, L. (2003). Bacterial keratitis: predisposing factors, clinical and microbiological review of 300 cases. *British Journal of Ophthalmology*, *87*(7), 834. https://doi.org/10.1136/bjo.87.7.834

Carvalho, I. M., Marques, C. S., Oliveira, R. S., Coelho, P. B., Costa, P. C., & Ferreira, D. C. (2015a). Sustained drug release by contact lenses for glaucoma treatment—A review. *Journal of Controlled Release*, *202*, 76–82. https://doi.org/https://doi.org/10.1016/j.jconrel.2015.01.023

Carvalho, I. M., Marques, C. S., Oliveira, R. S., Coelho, P. B., Costa, P. C., & Ferreira, D. C. (2015b). Sustained drug release by contact lenses for glaucoma treatment—A review. *Journal of Controlled Release*, *202*, 76–82. https://doi.org/https://doi.org/10.1016/j.jconrel.2015.01.023

Ch, S., Mishra, P., Bhatt, H., Ghosh, B., Roy, S., & Biswas, S. (2021). Hydroxypropyl methacrylamide-based copolymeric nanoparticles loaded with moxifloxacin as a mucoadhesive, cornea-penetrating nanomedicine eye drop with enhanced therapeutic benefits in bacterial keratitis. *Colloids and Surfaces B: Biointerfaces*, *208*, 112113. https://doi.org/https://doi.org/10.1016/j.colsurfb.2021.112113

Ch, S., Padaga, S. G., Ghosh, B., Roy, S., & Biswas, S. (2023). Chitosan-poly(lactide-co-glycolide)/poloxamer mixed micelles as a mucoadhesive thermo-responsive moxifloxacin eye drop to improve treatment efficacy in bacterial keratitis. *Carbohydrate Polymers*, *312*, 120822. https://doi.org/10.1016/J.CARBPOL.2023.120822

Cometta, S., Jones, R. T., Juárez-Saldivar, A., Donose, B. C., Yasir, M., Bock, N., Dargaville, T. R., Bertling, K., Brünig, M., Rakić, A. D., Willcox, M., & Hutmacher, D. W. (2022). Melimine-Modified 3D-Printed Polycaprolactone Scaffolds for the Prevention of Biofilm-Related Biomaterial Infections. *ACS Nano*, *16*(10), 16497–16512. https://doi.org/10.1021/acsnano.2c05812

Daniell, M., Mills, R., & Morlet, N. (2003). Microbial keratitis: what's the preferred initial therapy? *British Journal of Ophthalmology*, *87*(9), 1167. https://doi.org/10.1136/bjo.87.9.1167

Egrilmez, S., & Yildirim-Theveny, Ş. (2020). Treatment-resistant bacterial keratitis: Challenges and solutions. In *Clinical Ophthalmology* (Vol. 14, pp. 287–297). Dove Medical Press Ltd. https://doi.org/10.2147/OPTH.S181997

Gade, S. K., Nirmal, J., Garg, P., & Venuganti, V. V. K. (2020). Corneal delivery of moxifloxacin and dexamethasone combination using drug-eluting mucoadhesive contact lens to treat ocular infections. *International Journal of Pharmaceutics*, *591*, 120023. https://doi.org/https://doi.org/10.1016/j.ijpharm.2020.120023

Gangopadhyay, N., Daniell, M., Weih, L., & Taylor, H. R. (2000). Fluoroquinolone and fortified antibiotics for treating bacterial corneal ulcers. *British Journal of Ophthalmology*, *84*(4), 378. https://doi.org/10.1136/bjo.84.4.378

Grinninger, P., Verbruggen, A. M. J., Kraijer-Huver, I. M. G., Djajadiningrat-Laanen, S. C., Teske, E., & Boevé, M. H. (2015). Use of bandage contact lenses for treatment of spontaneous chronic corneal epithelial defects in dogs. *Journal of Small Animal Practice*, *56*(7), 446–449. https://doi.org/https://doi.org/10.1111/jsap.12360

Gulsen, D., & Chauhan, A. (2005). Dispersion of microemulsion drops in HEMA hydrogel: a potential ophthalmic drug delivery vehicle. *International Journal of Pharmaceutics*, *292*(1), 95–117. https://doi.org/https://doi.org/10.1016/j.ijpharm.2004.11.033

Jian, H. J., Wu, R. S., Lin, T. Y., Li, Y. J., Lin, H. J., Harroun, S. G., Lai, J. Y., & Huang, C. C. (2017). Super-Cationic Carbon Quantum Dots Synthesized from Spermidine as an Eye Drop Formulation for Topical Treatment of Bacterial Keratitis. *ACS Nano*, *11*(7), 6703–6716. https://doi.org/10.1021/acsnano.7b01023

Joshi, P., Ahmed, M. S. U., Vig, K., Vega Erramuspe, I. B., & Auad, M. L. (2021). Synthesis and characterization of chemically crosslinked gelatin and chitosan to produce hydrogels for biomedical applications. *Polymers for Advanced Technologies*, *32*(5), 2229–2239. https://doi.org/https://doi.org/10.1002/pat.5257

Jung, H. J., Abou-Jaoude, M., Carbia, B. E., Plummer, C., & Chauhan, A. (2013a). Glaucoma therapy by extended release of timolol from nanoparticle loaded silicone-hydrogel contact lenses. *Journal of Controlled Release*, *165*(1), 82–89. https://doi.org/https://doi.org/10.1016/j.jconrel.2012.10.010

Jung, H. J., Abou-Jaoude, M., Carbia, B. E., Plummer, C., & Chauhan, A. (2013b). Glaucoma therapy by extended release of timolol from nanoparticle loaded silicone-hydrogel contact lenses. *Journal of Controlled Release*, *165*(1), 82–89. https://doi.org/https://doi.org/10.1016/j.jconrel.2012.10.010

Kakisu, K., Matsunaga, T., Kobayakawa, S., Sato, T., & Tochikubo, T. (2013). Development and Efficacy of a Drug-Releasing Soft Contact Lens. *Investigative Ophthalmology & Visual Science*, *54*(4), 2551–2561. https://doi.org/10.1167/iovs.12-10614

Kumari, P., Paul, M., Bobde, Y., Soniya, K., Kiran Rompicharla, S. V., Ghosh, B., & Biswas, S. (2020). Albumin-based lipoprotein nanoparticles for improved delivery and anticancer activity of curcumin for cancer treatment. *Nanomedicine*, *15*(29), 2851–2869. https://doi.org/10.2217/nnm-2020-0232

Li, J., & Zhuang, S. (2020). Antibacterial activity of chitosan and its derivatives and their interaction mechanism with bacteria: Current state and perspectives. *European Polymer Journal*, *138*, 109984. https://doi.org/10.1016/J.EURPOLYMJ.2020.109984

Lim, C. H. L., Carnt, N. A., Farook, M., Lam, J., Tan, D. T., Mehta, J. S., & Stapleton, F. (2016). Risk factors for contact lens-related microbial keratitis in Singapore. *Eye*, *30*(3), 447–455. https://doi.org/10.1038/eye.2015.250

Mannermaa, E., Vellonen, K. S., & Urtti, A. (2006). Drug transport in corneal epithelium and blood–retina barrier: Emerging role of transporters in ocular pharmacokinetics.

Advanced Drug Delivery Reviews, *58*(11), 1136–1163. https://doi.org/10.1016/J.ADDR.2006.07.024

Maulvi, F. A., Singhania, S. S., Desai, A. R., Shukla, M. R., Tannk, A. S., Ranch, K. M., Vyas, B. A., & Shah, D. O. (2018). Contact lenses with dual drug delivery for the treatment of bacterial conjunctivitis. *International Journal of Pharmaceutics*, *548*(1), 139–150. https://doi.org/10.1016/j.ijpharm.2018.06.059

M'Barki, A., Bocquet, L., & Stevenson, A. (2017). Linking Rheology and Printability for Dense and Strong Ceramics by Direct Ink Writing. *Scientific Reports*, *7*(1), 6017. https://doi.org/10.1038/s41598-017-06115-0

Miedziak, A. I., Miller, M. R., Rapuano, C. J., Laibson, P. R., & Cohen, E. J. (1999). Risk factors in microbial keratitis leading to penetrating keratoplasty. *Ophthalmology*, *106*(6), 1166–1171. https://doi.org/https://doi.org/10.1016/S0161-6420(99)90250-6

Mishra, P., Ch, S., Hong, S. J., Biswas, S., & Roy, S. (2022). Antimicrobial peptide S100A12 (calgranulin C) inhibits growth, biofilm formation, pyoverdine secretion and suppresses type VI secretion system in Pseudomonas aeruginosa. *Microbial Pathogenesis*, *169*. https://doi.org/10.1016/j.micpath.2022.105654

Modaresifar, K., Hadjizadeh, A., & Niknejad, H. (2018). Design and fabrication of GelMA/chitosan nanoparticles composite hydrogel for angiogenic growth factor delivery. *Artificial Cells, Nanomedicine and Biotechnology*, *46*(8), 1799–1808. https://doi.org/10.1080/21691401.2017.1392970

O'Brien, T. P. (2003). Management of bacterial keratitis: beyond exorcism towards consideration of organism and host factors. *Eye*, *17*(8), 957–974. https://doi.org/10.1038/sj.eye.6700635

Paradiso, P., Serro, A. P., Saramago, B., Colaço, R., & Chauhan, A. (2016). Controlled Release of Antibiotics From Vitamin E–Loaded Silicone-Hydrogel Contact Lenses. *Journal of Pharmaceutical Sciences*, *105*(3), 1164–1172. https://doi.org/https://doi.org/10.1016/S0022-3549(15)00193-8

Patel, A. (2013). Ocular drug delivery systems: An overview. *World Journal of Pharmacology*, *2*(2), 47. https://doi.org/10.5497/wjp.v2.i2.47

Poggio, E. C., Glynn, R. J., Schein, O. D., Seddon, J. M., Shannon, M. J., Scardino, V. A., & Kenyon, K. R. (1989). The Incidence of Ulcerative Keratitis among Users of Daily-Wear and Extended-Wear Soft Contact Lenses. *New England Journal of Medicine*, *321*(12), 779–783. https://doi.org/10.1056/NEJM198909213211202

Rahmani, S., Mohammadi Nia, M., Akbarzadeh Baghban, A., Nazari, M. R., & Ghassemi-Broumand, M. (2014). Spectral transmittance of UV-blocking soft contact lenses: A comparative study. *Contact Lens and Anterior Eye*, *37*(6), 451–454. https://doi.org/10.1016/j.clae.2014.07.011

Rizwan, M., Chan, S. W., Comeau, P. A., Willett, T. L., & Yim, E. K. F. (2020). Effect of sterilization treatment on mechanical properties, biodegradation, bioactivity and printability of GelMA hydrogels. *Biomedical Materials (Bristol, England)*, *15*(6). https://doi.org/10.1088/1748-605X/ABA40C

Robertson, D. M., Rogers, N. A., Petroll, W. M., & Zhu, M. (2017). Second harmonic generation imaging of corneal stroma after infection by Pseudomonas aeruginosa. *Scientific Reports*, *7*(1), 46116. https://doi.org/10.1038/srep46116

Rykowska, I., Nowak, I., & Nowak, R. (2021). Soft contact lenses as drug delivery systems: A review. In *Molecules* (Vol. 26, Issue 18). MDPI. https://doi.org/10.3390/molecules26185577

Shao, Y., You, D., Lou, Y., Li, J., Ying, B., Cheng, K., Weng, W., Wang, H., Yu, M., & Dong, L. (2019). Controlled Release of Naringin in GelMA-Incorporated Rutile Nanorod Films to Regulate Osteogenic Differentiation of Mesenchymal Stem Cells. *ACS Omega*, *4*(21), 19350–19357. https://doi.org/10.1021/acsomega.9b02751

Shie, M. Y., Lee, J. J., Ho, C. C., Yen, S. Y., Ng, H. Y., & Chen, Y. W. (2020). Effects of gelatin methacrylate bio-ink concentration on mechano-physical properties and human dermal fibroblast behavior. *Polymers*, *12*(9). https://doi.org/10.3390/POLYM12091930

Smith, J., Wood, E., & Dornish, M. (2004). Effect of Chitosan on Epithelial Cell Tight Junctions. *Pharmaceutical Research*, *21*(1), 43–49. https://doi.org/10.1023/B:PHAM.0000012150.60180.E3/METRICS

Smith, P. T., Basu, A., Saha, A., & Nelson, A. (2018). Chemical modification and printability of shear-thinning hydrogel inks for direct-write 3D printing. *Polymer*, *152*, 42–50. https://doi.org/https://doi.org/10.1016/j.polymer.2018.01.070

Sogias, I. A., Williams, A. C., & Khutoryanskiy, V. V. (2008). Why is chitosan mucoadhesive? *Biomacromolecules*, *9*(7), 1837–1842. https://doi.org/10.1021/BM800276D/SUPPL_FILE/BM800276D-FILE002.PDF

Ting, D. S. J., Cairns, J., Gopal, B. P., Ho, C. S., Krstic, L., Elsahn, A., Lister, M., Said, D. G., & Dua, H. S. (2021). Risk Factors, Clinical Outcomes, and Prognostic Factors of Bacterial Keratitis: The Nottingham Infectious Keratitis Study. *Frontiers in Medicine*, *8*. https://www.frontiersin.org/articles/10.3389/fmed.2021.715118

Ubani-Ukoma, U., Gibson, D., Schultz, G., Silva, B. O., & Chauhan, A. (2019). Evaluating the potential of drug eluting contact lenses for treatment of bacterial keratitis using an ex vivo corneal model. *International Journal of Pharmaceutics*, *565*, 499–508. https://doi.org/https://doi.org/10.1016/j.ijpharm.2019.05.031

Vajpayee, R. B., Dada, T., Saxena, R., Vajpayee, M., Taylor, H. R., Venkatesh, P., & Sharma, N. (2000). Study of the First Contact Management Profile of Cases of Infectious Keratitis: A Hospital-Based Study. *Cornea*, *19*(1). https://journals.lww.com/corneajrnl/Fulltext/2000/01000/Study_of_the_First_Contact_Management_Profile_of.11.aspx

W, H. R. E., & S, C. D. (1999). Peptide Antibiotics. *Antimicrobial Agents and Chemotherapy*, *43*(6), 1317–1323. https://doi.org/10.1128/AAC.43.6.1317

Wang, Q., Aleshintsev, A., Bolton, D., Zhuang, J., Brenowitz, M., & Gupta, R. (2019). Ca(II) and Zn(II) Cooperate to Modulate the Structure and Self-Assembly of S100A12. *Biochemistry*, *58*(17), 2269–2281. https://doi.org/10.1021/ACS.BIOCHEM.9B00123

Winfield, A. J., Jessiman, D., Williams, A., & Esakowitz, L. (1990). A study of the causes of non-compliance by patients prescribed eyedrops. *British Journal of Ophthalmology*, *74*(8), 477. https://doi.org/10.1136/bjo.74.8.477

Yamamura, T., Hitomi, J., Nagasaki, K., … M. S.-B. and, & 1996, undefined. (n.d.). Human CAAF1 gene—molecular cloning, gene structure, and chromosome mapping. *Elsevier*. Retrieved July 3, 2023, from https://www.sciencedirect.com/science/article/pii/S0006291X96906002

Zhu, M., Wang, Y., Ferracci, G., Zheng, J., Cho, N.-J., & Lee, B. H. (2019). Gelatin methacryloyl and its hydrogels with an exceptional degree of controllability and batch-to-batch consistency. *Scientific Reports*, *9*(1), 6863. https://doi.org/10.1038/s41598-019-42186-x

Appendix

Publications and Presentations

Publications

1. Ch S, Mishra P, Bhatt H, Ghosh B, Roy S, Biswas S. Hydroxypropyl methacrylamide-based copolymeric nanoparticles loaded with moxifloxacin as a mucoadhesive, cornea-penetrating nanomedicine eye drop with enhanced therapeutic benefits in bacterial keratitis. Colloids and Surfaces B: Biointerfaces. 2021 Dec 1;208:112113.
2. Mishra P, Ch S, Hong SJ, Biswas S, Roy S. Antimicrobial peptide S100A12 (calgranulin C) inhibits growth, biofilm formation, pyoverdine secretion and suppresses type VI secretion system in Pseudomonas aeruginosa. Microbial Pathogenesis. 2022 Aug 1;169:105654.
3. Vysyaraju NR, Paul M, Ch S, Ghosh B, Biswas S. Olaparib@ human serum albumin nanoparticles as sustained drug-releasing tumor-targeting nanomedicine to inhibit growth and metastasis in the mouse model of triple-negative breast cancer. Journal of Drug Targeting. 2022 Jun 21:1-8.
4. Ch S, Padaga SG, Ghosh B, Roy S, Biswas S. Chitosan-poly (lactide-co-glycolide)/poloxamer mixed micelles as a mucoadhesive thermo-responsive moxifloxacin eye drop to improve treatment efficacy in bacterial keratitis. Carbohydrate Polymers. 2023 Mar 21:120822.
5. Sidhartha PN, Ch S, Ghosh B, Chappanda KN. The Quality by Design approach for optimization of slayer exciter based Low Power Portable Atmospheric Plasma jet on bactericidal efficacy of Pseudomonas Aeruginosa. Journal of Biophotonics. 2023 Mar 8:e202200333.

Manuscripts under process

1. Anti-Biofilm, Anti-Quorum sensing activity of Chitosan oligosaccharide lactate conjugated Pluronic F127 micelles loaded with Gatifloxacin for the treatment of Bacterial Keratitis. Manuscript submitted.
2. Glycol chitosan-poly (lactic acid) (1:1) conjugate nanoparticles encapsulating ciprofloxacin: A mucoadhesive anti-quorum-sensing biofilm-disrupting treatment modality for bacterial keratitis. Manuscript submitted.

3. Cationic Gelatin-Sodium Alginate Polyelectrolyte Complex Nanoparticles loaded with Moxifloxacin Optimized by Quality by Design approach for treating Bacterial Keratitis. Manuscript submitted.

Book chapters

1. Micelles based drug delivery for pancreatic cancer: **Sanjay ch**, Tarun Kumar Patel, Swati Biswas, and **Balaram Ghosh***: Book entitles "Recent advancement in nanocarriers for pancreatic cancer therapy": *Elsevier*, 2022 (submitted 15.10.2022)
2. Codelivery of curcumin and siRNA as anticancer therapeutics: Milan Paul, Ch Sanjay, Sri Ganga Padaga, **Balaram Ghosh**, Swati Biswas: Book titled "Curcumin-based nanomedicines as cancer therapeutics": *Elsevier*, 2022 (submitted in Nov 2022)

Patent

1. Patent filed on "**3D-Bioprinted Inherently Antibacterial Contact Lens Carrying Antimicrobial Peptide Payload for Ocular Infections"** Date created – 04-03-2023, Application number- **202311005942** status- **Not yet Granted.**

Presentations

1. **Title:** 3D-Bioprinted Inherently Antibacterial Contact Lens Carrying Antimicrobial Peptide Payload for Ocular Infections. Authors: Sanjay Ch, Priyasha Mishra, Padaga Sri Ganga, Balaram Ghosh, Sanhita Roy and Swati Biswas. Poster presented in "21st International Symposium on Advances in Technology and Business Potential of New Drug Delivery Systems" Feb 24 - 25, 2023; Mumbai-400047, India.
2. **Title**: Chitosan/poloxamer-based mixed micelles for ocular moxifloxacin delivery in bacterial keratitis. Authors: Sanjay ch, Milan Paul, Sri ganga Padaga, Balaram Ghosh, and Swati Biswas. Poster presented in 20th International e-Symposium on Advances in Technology and Business Potential of New Drug Delivery Systems from 24-26th February 2022.
3. **Title:** Development of polymeric nanoparticles for the efficient delivery of a fluoroquinolone antibiotic for the treatment of bacterial keratitis. Authors: Sanjay ch, Priyasha Mishra, Sanhitha Roy, Balaram Ghosh, and Swati Biswas. Poster presented in International Chemical Biology Society-8th Annual conference on "Navigating Translational Discoveries" November 2-4,2019; CSIR-ICT, Hyderabad, India.

4. **Title:** Moxifloxacin HCl loaded chitosan-PLGA, Poloxamer based mixed micelles as a mucoadhesive, thermoresponsive polymer for the treatment of bacterial keratitis induced in mice models. Authors: Sanjay ch, Milan Paul, Sri ganga Padaga, Balaram Ghosh, and Swati Biswas. Poster presented in International Virtual Conference on Biomaterial-Based Therapeutics, Engineering and Medicine (BIOTEM-2021) on "31st ANNUAL SBAOI MEETING AND 14th STERMI ANNUAL MEETING AND INTERNATIONAL CONFERENCE ON BIOMATERIAL - BASED THERAPEUTICS, ENGINEERING & MEDICINE (BIOTEM-2021)" from 17-21 December 2021.

Biography

Biography of Sanjay Ch

Mr. Sanjay Ch completed his Bachelor of Pharmacy from Gokaraju Rangaraju College of Pharmacy, Osmania University, Hyderabad, Telangana, India 2016. He pursued his Master of Pharmacy in Pharmaceutics from Manipal College of Pharmaceutical Sciences, Manipal Academy of Higher Education, Manipal, Karnataka, India 2018. Post twelve months of experience at Hetero Labs Ltd as a Research Associate, Mr. Sanjay Ch joined Prof. Swati Biswas's lab at BITS Pilani Hyderabad Campus to pursue his doctoral research. Mr. Sanjay Ch worked on "Development of Nanoparticles-formulations of fluoroquinolone antibiotics for the treatment of bacterial keratitis**."** Moreover, Mr. Sanjay Ch has received a senior research fellowship (SRF) from the Indian Council of Medical Research (ICMR) to carry out research work on the "Development of Nanoparticles- formulations of fluoroquinolone antibiotics for the treatment of bacterial keratitis." Further, he received an international travel grant from the Council for Scientific and Industrial Research, India, for a Poster presentation, at the CRS 2022 Annual Meeting and Expo on Advanced delivery science by the Controlled Release Society – held in Montreal, Canada, from July 11-15, 2022. He has published 12 peer-reviewed scientific publications in reputed international journals and one Indian Patent application and presented papers at various international conferences.

Biography of Prof. Swati Biswas

Prof. Swati Biswas is an Associate Professor in the Department of Pharmacy, Birla Institute of Technology and Science, Pilani, Hyderabad Campus. She received her B. Pharm degree (1998) and M.Pharmacy (2000) from Jadavpur University, India. She was awarded her Ph.D. in Pharmaceutical Sciences in 2008 from Wayne State University, USA. After completing doctoral studies, she pursued her postdoctoral studies at Northeastern University, USA (2013). She has been involved in research for the last 15 years. She is the editorial advisory board member for the journal ACS Publications, molecular pharmaceutics for 2021-2023, and associate editor for Frontiers in Biomaterials Sciences in the specialty section of delivery systems and controlled release (since 2021). She has been featured among the world's top 2 % scientists in the single year 2019 in pharmacology and pharmacy/nanoscience & nanotechnology/ clinical medicine. She has over 90 research publications, two US patents, and three Indian Patents. She has authored 4 book chapters in "Dendrimers: Synthesis, Applications, and Role in Nanotechnology," "Drug Delivery Strategies for Poorly Water-Soluble Drugs," "Handbook of Polymers for Pharmaceutical Technologies, Volume 2: Processing and Applications" and "**RNA Imaging."** She has completed many sponsored projects and currently handling projects sponsored by DST and ICMR. She has guided five Ph.D. students; currently, four are pursuing their Ph.D. work under her guidance.